FUNDAMENTAL STUDIES OF THIONOCARBAMATE INTERACTIONS WITH SULFIDE MINERALS

by

Cesar Indiongco Basilio

Dissertation submitted to the Faculty of the

Virginia Polytechnic Institute and State University

in partial fulfillment of the requirements for the degree of

Doctor of Philosophy

in

Mining and Minerals Engineering

APPROVED:

Roe-Hoan Yoon, Chairman	Gregory T. Adel
Gerald H. Luttrell	Jerzy A. Mielczarski
D. R. Nagaraj	Michael E. Karmis

April, 1989

Blacksburg, Virginia

FUNDAMENTAL STUDIES OF THIONOCARBAMATE INTERACTIONS WITH SULFIDE MINERALS

by

Cesar Indiongco Basilio

Roe-Hoan Yoon, Chairman

Mining and Minerals Engineering

(ABSTRACT)

The interactions of O-isopropyl-N-ethylthionocarbamate (IPETC) and O-isobutyl-N-ethoxycarbonylthionocarbamate (IBECTC) with Cu_2S, $CuFeS_2$ and FeS_2 have been characterized using thermodynamic calculations, electrochemistry, microflotation tests, contact angle measurements, FTIR and UV spectroscopy. Pearson's theory of hard and soft acids and bases (HSAB) has also been applied to these flotation systems, through the use of Drago's acid-base concept and flow microcalorimetry.

The results of the thermodynamic calculations and electrochemical measurements suggest that IPETC and IBECTC adsorption on copper and chalcocite are dependent on potential. This has been verified by contact angle and in-situ spectroelectrochemical measurements. Microflotation tests with these thionocarbamates show that the floatability of Cu_2S and $CuFeS_2$ is dependent on pH. The floatability of FeS_2 only becomes significant at acidic conditions and high collector additions.

Spectroscopic measurements also show that thionocarbamate adsorption is dependent on pH and is most favored on Cu_2S followed by $CuFeS_2$and FeS_2. FTIR results indicate that IPETC is adsorbed on Cu^0, Cu_2S and $CuFeS_2$ through a coordination of the sulfur atom with the surface Cu. IBECTC adsorption on these substrates involves the coordination of Cu with both sulfur and oxygen atoms to form

a six-membered chelate ring. Adsorption of these collectors cannot remove or prevent the formation of sulfoxy oxidation products on the FeS_2 surface, unlike the case with the xanthate-pyrite system. This may explain the improved selectivity of IPETC and IBECTC over xanthates. Infrared reflection-absorption spectroscopic studies show that KEX is preferentially adsorbed on Cu^0 over IPETC and IBECTC. Between IPETC and IBECTC, the latter is more favorably adsorbed than the former.

Kinetic studies using UV spectroscopy show that the rate of thionocarbamate adsorption is highest on Cu_2S followed by $CuFeS_2$ and FeS_2. IBECTC adsorption on each sulfide mineral is relatively faster than IPETC, indicating the higher collecting power of IBECTC.

The HSAB concept suggests that the interaction of thionocarbamates (soft bases) with sulfide minerals that are classified as soft acids should be favored. The C/E ratios of Cu_2S and FeS_2 were determined to be 0.86 and 0.52, respectively. This indicates that FeS_2 is a harder acid than Cu_2S, thus providing an explanation for the observed selectivity of both IPETC and IBECTC against FeS_2.

Acknowledgements

The author wishes to express his sincere appreciation of the guidance, inspiration, patience and support that Professor R. H. Yoon has given throughout the course of this study. The author is also grateful to his committee members - Dr. G. T. Adel, Dr. G. H. Luttrell, Dr. D. R. Nagaraj and Dr. M. E. Karmis, for their suggestions and time.

Special thanks is given to Dr. J. O. Leppinen for his invaluable suggestions and assistance, particularly in the FTIR measurements. The author is also grateful to Dr. R. Woods, Dr. J. Mielczarski and Dr. M. Celik for their suggestions and discussions. Sincere gratitude is also expressed to , and for their technical assistance, and to the graduate students in the coal and mineral processing research group, particularly, , , and for their friendship, support and willing assistance at all times.

The author acknowledges the American Cyanamid Company for their financial support and for supplying the reagents. He is also grateful to the Department of Geological Sciences for doing the surface area analysis of the mineral samples.

The friendship of the Filipino community that the author met in Blacksburg, Virginia is also appreciated. Finally, the author wishes to express his deepest appreciation to his family, particularly, and , for their support, and

specially to his wife, , for her continuing love, patience, support and enthusiasm, as well as for typing and reading the manuscript.

Table of Contents

List of Illustrations

List of Tables

1.0 INTRODUCTION

1.1 General

Froth flotation was first introduced commercially at Broken Hill, Australia, in 1904 (Sutherland and Wark, 1955) and started in the United States in 1911 at Basin, Montana (Rickard, 1932). Today, it is one of the most widely used and economical means of processing mineral raw materials. Worldwide, about two billion tons of materials are treated annually by froth flotation with the majority being metal sulfides and oxides (Kitchener, 1984).

In the last two decades, the mineral industry has faced a variety of problems such as higher energy costs, depletion of high grade simple ores, increasing environmental constraints and other economic pressures like higher interest rates (Crozier, 1984). These and other problems challenged the minerals industry to seek for more efficient and productive means of processing minerals. Recent advances made as a result of this effort include flotation reagent development, new flotation machines and application of process control to plant operations. However, the development of flotation collectors has not kept pace with the present needs of the industry (Glembotskii et al., 1988; Nagaraj et al., 1988). The demand for new efficient flotation collectors rises annually.

Present industrial needs include lowering reagent costs, improving collector efficiency in the treatment of complex and low-grade ores under a wider range of conditions and achieving higher recoveries of precious metals (Nagaraj et al, 1986). It is interesting to note that about 98% of all flotation reagents used presently were known and patented before 1955 (Crozier, 1984). This clearly indicates that little change has occurred in this field.

Thio-collectors have been used widely for the flotation of sulfide minerals since 1923. This collector group includes xanthates, dithiophosphates, dithiocarbamates, dialkyl thionocarbamates, mercaptobenzothiazole, etc. Xanthates are still the dominant sulfide collector and account for about 60% of the total thio-collector consumption in the United States (USBM, 1987). It is believed that the situation is similar worldwide.

Xanthates are the most commonly used sulfide mineral collector because of their strong collecting power and relatively low cost. They have very general use with the majority of sulfide minerals, and are used in alkaline circuits due to their instability in acid pH environments. However, these properties have now limited their application in industry. In many sulfide plants, lime consumption often accounts for over 50% of the total reagent cost, as most plants have to operate at pH $\geq$ 10 (USBM, 1987). With the attention shifted towards beneficiating large tonnages of low-grade complex ores containing sulfides and precious metals, numerous plants are operating in the pH range of 3-10 (Nagaraj et al., 1988). However, good recovery, selectivity, and plant profitability are not attained with the use of xanthates at acidic conditions. Consequently, there is a need to develop new collectors capable of satisfying the present requirements of the sulfide industry.

A number of sulfide collectors developed recently satisfy the major requirements of current plant practice mentioned above. These include : MIG-4E (Glembotskii et al., 1984); F1 and F2 collectors from the Dow Chemical Company (Klimpel et al., 1988);

alkoxycarbonyl alkyl thionocarbamates and thioureas, and dialkyl monothiophosphates and monothiophosphinates from the American Cyanamid Company (Nagaraj et al., 1985; 1986; 1987; Nagaraj and Wang, 1986; 1987; Fu et al., 1987a; 1987b). The MIG-4E collector ($HC{\equiv}CH\text{-}CH{=}CH\text{-}O\text{-}C_4H_9$) developed in the USSR, has acetylene and ethylene groups instead of the traditional electron donor atoms (i.e., O, N, S, P). This collector has a high selectivity in recovering silver and gold minerals. It is also effective in the flotation of copper, lead, molybdenum and bismuth sulfides from complex ores containing pyrite and non-activated sphalerite.

The main components of F1 and F2 are 2-hexylthioethylamine hydrochloride and 2-hexylthioethyl propionamide, respectively (Klimpel et al., 1988). F1 is a very strong chelation collector for Zn, Ni, Pt, Pd, Au and Co-containing minerals with moderate ability to collect Cu-minerals. Its strength and selectivity are very sensitive to collector dosage. On the other hand, F2 is an effective collector for copper ores with good selectivity over pyrite and pyrrhotite. In addition, it is also a good collector for precious metals.

The modified thionocarbamates and thioureas developed by the American Cyanamid Company are stable and effective in acidic pH range and have excellent selectivity against pyrite and pyrrhotite (Nagaraj et al., 1988). They are more powerful than their dialkyl counterparts and give good precious metals recovery. The monothiophosphates and monothiophosphinates are obtained by replacing one of the sulfur donors in the functional group of their respective dithio derivatives with oxygen. They are stronger, more stable collectors and are stronger acids than their dithio analogues. The monothiophosphates are true acid circuit collectors, while the monothiophosphinates are effective in neutral and mildly alkaline conditions. All of these collectors have been proven to be effective and some are already being used in industry.

However, relatively little fundamental information is available about these reagents and their reaction mechanisms. A better understanding of the reaction mechanism can lead to improvements and better control of the flotation process. For example, if the collector adsorption process is known to occur via an electrochemical mechanism, potential control could result in process improvements. Interactions between sulfide minerals and thiol collectors occur through a corrosion-type mixed potential mechanism. In this mechanism, simultaneous anodic and cathodic electrochemical reactions occur on the mineral surface. The anodic reaction involves the oxidation of the collector, while the cathodic reaction is oxygen reduction. The potential across the solid-solution interface would then determine the reactions that are possible on the mineral surface. Thus, the potential of the system is an important parameter in sulfide flotation with thiol collectors. However, some non-ionic sulfide collectors may not be as sensitive to potential as the thiol collectors. Therefore, factors other than electrochemical mechanisms must also be considered.

1.2 Literature Review

Xanthate was first discovered in 1822 (Zeise, 1822), but did not find commercial application in sulfide flotation until 1923 (Keller, 1925). The use of dithiophosphate compounds and their free acids as flotation collectors was patented a year after Keller had patented xanthate for the same usage (Whitworth, 1926). The patent for dithiophosphates was subsequently assigned to the American Cyanamid Company and sold commercially starting in 1930 as Aerofloat and Aero Promoters (Mingione, 1984).

O-isopropyl-N-thionocarbamate (IPETC) was first introduced only in 1954 and sold commercially as Z-200 by Dow Chemical Company (Harris and Fishback, 1954). This reagent can be produced by a multistep process involving the formation of xanthate,

$$ROH + CS_2 + NaOH \rightarrow ROCS_2Na + H_2O, \qquad [1.1]$$

followed by reacting the xanthate solution with methyl chloride,

$$ROCS_2Na + CH_3Cl \rightarrow ROCS_2CH_3 + NaCl. \qquad [1.2]$$

The product is then reacted with ethylamine,

$$ROCS_2CH_3 + C_2H_5NH_2 \rightarrow ROCSNHC_2H_5 + CH_3HS \qquad [1.3]$$

to obtain the dialkyl thionocarbamate. The reaction product is purified by a steam distillation process. A catalytic process has recently been developed, in which xanthate is directly reacted with an amine using soluble salts of nickel or palladium as catalysts (Bolth et al., 1975),

$$R_1OCS_2Na + R_2NH_2 \xrightarrow{Ni,Pd} R_1OCSNHR_2 + NaHS. \qquad [1.4]$$

This process, developed by Minerec Corporation, produces a higher purity product but is more expensive. The Dow multistep process is not currently being used due to a mercaptan by-product disposal problem.

Applications of dialkyl thionocarbamates have been popular for the flotation of copper sulfides and copper-activated sulfide minerals (Dow, 1968). There have also been reports from the USSR that thionocarbamates are good collectors for precious metals flotation and can also selectively extract copper from Cu-Ni Bessemer matte (Livshits et al., 1974). Flotation tests on Cu-Ni-pyrrhotite ores have shown good separation of the copper and nickel from the pyrrhotite (Scherbakov and Perepechin, 1983). In spite of the considerable commercial acceptance of the thionocarbamates (i.e. Z-200, Minerec

1661 and 1331), it is surprising that very little fundamental studies have been made to date.

The good selectivity of thionocarbamates against pyrite was noted by Glembotskii and his co-workers at USSR Academy of Science (Glembotskii et al., 1968). They found that isopropyl methylthionocarbamates (IPMTC) are more effective collectors for chalcopyrite and molybdenite than corresponding xanthates and dithiophosphates, but are weaker collectors for pyrite. Their adsorption studies showed that the adsorbability of IPMTC on pyrite is about 4-5 times less than that of xanthate and that it can be readily washed off by water.

Glembotskii and Livshits (1969) carried out further studies on the adsorption of IPMTC on chalcopyrite, pyrite and molybdenite. Using methanol and pyridine to wash off physically-adsorbed IPMTC, they found that a constant amount of the collector remains chemisorbed on the chalcopyrite surface, independent of the amount of collector initially added. The same observation was made for molybdenite but not for pyrite, where the collector coating was completely washed off. These results indicate that IPMTC is stongly bound to chalcopyrite and molybdenite but not to pyrite, which accounts for its good selectivity against pyrite.

Glembotskii and Frolov (1978) studied the adsorption mechanism for neutral oily collectors, such as thionocarbamates and thiourea, containing heteroatoms with an unshared pair of electrons. They proposed that these reagents donate an unshared pair of electrons to the metal cations exposed on the surface of the mineral and form surface chelates. The nature of the bonding is that of a donor-acceptor with the collector being the electron-donor and the mineral is the acceptor.

Using Pearson's concept of hard and soft acids and bases, Glembotskii (1977) suggested that thionocarbamates, being soft bases, should react preferentially with those metal ions which are soft acids. These include Cu(I, II), Ag, Hg(II), Au(III), Tl(III) and

Se(IV,VI). On the other hand, their reactions with hard acids, such as Fe, Zn, Co and Ni, should not be as favored. This concept was proven in a series of solvent extraction experiments using various metal ions (Seryakova et al., 1975). The results showed that IPETC is a selective extractant for Ag, Hg, Cu, Au, Tl and Se. However, Zn, Fe, Ga, In, Bi, W and Co were practically not extracted. The reaction products were suggested to have the general formula MX_mS_p, in which M is a metal ion with m^+ charge and X is the inorganic anion. The sulfur-containing extractant is given by S with a M:S ratio of p.

Glembotskii suggested that the collecting power of thio collectors is directly proportional to the electron density of the reactive center of the molecule, (i.e., sulfur) (Glembotskii, 1977). He showed that electron-donating substituents increase the electron density at the reactive center, thereby making the collector stronger, while electron-accepting substituents act in the opposite manner. By extending the same concept to neutral thio collectors, the reactivity of thionocarbamates would be dependent on the substituent groups.

Bogdanov et al. (1976 and 1977) explained the reactivity of thionocarbamates using the molecular orbital theory. It was suggested that during the interaction between chalcopyrite and thionocarbamate, the d-orbitals of the copper atom overlap with the empty d-orbitals of the sulfur in thionocarbamate, forming a dative π-bond. The nitrogen and sulfur atoms are also shown to form covalent σ-bonds with copper. When the electron density at nitrogen increases due to the presence of an electron-donating substituent, the σ-bonding between the copper and nitrogen is intensified. This would reduce the degree of overlapping by the copper and sulfur d-orbitals, thereby reducing the total bond strength.

According to Bogdanov, O-butyl-N-benzoylthionocarbamate (BBTC) is a stronger collector than O-butyl-N-ethylthionocarbamate (BETC) since the benzoyl group is

electron-withdrawing, while the ethyl group is weakly electron-donating. However, the opposite conclusion should be obtained according to Glembotskii, because the electron density at the reactive center (i.e., sulfur) is lower in the benzoyl derivative. The fact that O-butyl-N-benzoylthionocarbamate is the stronger collector has been attributed by Glembotskii to the presence of the double-bonded oxygen as another reactive center.

By using infrared spectroscopy, Bogdanov et al. (1976) also studied the nature of surface compounds formed by BBTC and BETC on a copper film, chalcopyrite and pyrite. The IR spectra for the adsorbed species were compared with those of the reagent and their respective copper salts, $Cu(BBTC)_2$ and Cu(BETC). In all cases, it was concluded that the reagents were chemisorbed on the samples through the formation of surface coordination compounds.

The effect of alkyl substituent groups on the collecting properties of thionocarbamates was also studied by Ackerman et al. (1984). Their flotation tests indicated that the collector strength increased in direct relationship to the total number of carbon groups present in both the O-alkyl and N-alkyl groupings. They suggested that the O-alkyl group affects hydrophobicity, while the N-alkyl group controls the accessibility of the reactive group to the mineral surface. It was concluded that a balance of the O- and the N-alkyl groupings is needed for an effective collector.

Substituting the N-alkyl group in IPETC with an allyl group resulted in better flotation performance of sulfide ores containing Cu, Mo, Pb and Zn minerals (Lewellyn and Wang, 1985). This substitution was based on the concept that incorporation of an olefinic double bond in IPETC would improve the collector activity. Olefins are known to form complexes with Pt, Pd and copper (Cotton and Wilkinson, 1980).

The purity of the reagent was found to affect the collector performance of thionocarbamates (Ackerman et al., 1986). In this study, commercial grade Z-200, purified Z-200 and freshly synthesized IPETC were used. There was no significant

change in chalcopyrite recovery in the presence of collector impurities at acidic and neutral conditions. However, for chalcocite, the purified and freshly synthesized reagents gave better recoveries than the commercial grade Z-200. Pyrite showed the greatest difference in floatability with the use of the three different grades of reagents. The commercial grade Z-200 gave the poorest pyrite recovery, suggesting that the impurities assist in the selectivity of the collector against pyrite.

There has been an increasing interest in the development of new selective flotation reagents over the past 20 years (Crozier, 1984; Klimpel, 1988). A majority of the different approaches used in searching for new reagents with specific applications are based on the theoretical concepts of coordination and chelation mechanisms of chemisorption (Glembotskii, 1970; Somasundaran and Nagaraj, 1984; Nagaraj et al., 1988; Glembotskii et al., 1988). It is interesting to note that in most of the work dealing with selective reagent design, thionocarbamate was always used as an example.

1.3 Chemistry of Thionocarbamates

1.3.1 Dialkyl Thionocarbamates

The simple dialkyl thionocarbamates are neutral, oily collectors belonging to the thionocarbamate group -O-C(S)-NH-. The most popular example is O-isopropyl-N-ethylthionocarbamate,

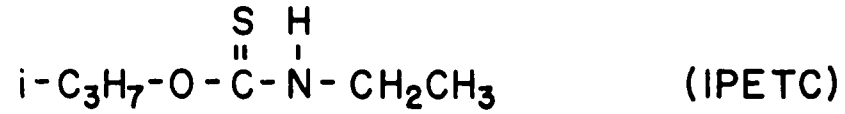

(IPETC)

The pKa for IPETC is > 12 (Lewellyn, 1983) and is a popular collector for copper sulfides and copper-activated sulfides. It is stable in both alkaline and acidic conditions (Dow, 1968). IPETC has the advantage of higher selectivity and long-term storage stability over xanthates and dithiophosphates. However, it is not considered a powerful collector and it is not very effective at low pH values (Nagaraj et al., 1986). The process of making IPETC has already been discussed in the previous section.

1.3.2 Alkoxycarbonyl alkyl thionocarbamates

The N-alkyl group in the simple diakyl thionocarbamate is replaced with an alkoxycarbonyl group to form the modified thionocarbamate. The use of the strongly electron-withdrawing ethoxycarbonyl subsituent introduces an additional active center, oxygen, to the O-isobutyl-N-ethoxycarbonyl thionocarbamate molecule (Nagaraj et al., 1988),

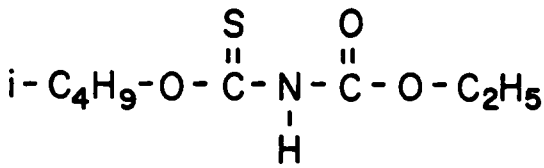

(IBECTC)

The functional grouping of this reagent is now more complex and has quite different properties from the simple thionocarbamates. The pKa of the molecule is 10.5 and it is stable in the pH range of 3-10.5 (Lewellyn, 1983). At pH ≥ 11, IBECTC is observed to ionize into the following two forms:

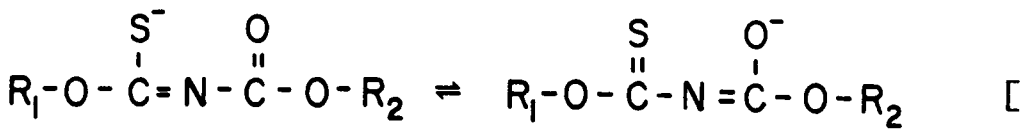

[1.5]

IBECTC is also an oily neutral collector, but is easily dispersible in water. It is a powerful collector for certain sulfide minerals and has all of the advantages of IPETC.

This modified thionocarbamate is prepared by reacting alkyl chloroformate with sodium thiocyanate to form an isothiocyanate intermediate. This is then reacted with isobutanol to give IBECTC (Nagaraj et al., 1985; 1986).

1.4 Objectives of the Study

The main objective of this study is to investigate the reaction mechanisms of copper-specific collectors, specifically IPETC and IBECTC, on chalcocite and chalcopyrite. Since these two reagents have known selectivity against pyrite, their interaction with pyrite are also studied in order to find possible explanations for the selective behavior. It is also the objective of this work to determine the flotation characteristics of chalcocite, chalcopyrite and pyrite using IPETC and IBECTC. The results are useful in identifying process variables and establishing optimum flotation conditions. The fundamental research on IPETC and IBECTC include: 1) thermodynamic calculations, 2)electrochemical studies, 3) flotation and contact angle measurements, 4) Fourier Transform Infrared (FTIR) spectroscopic characterization, 5) adsorption studies and 6) surface acidity measurements.

Thermodynamic calculations for the copper- and chalcocite-water systems in the presence of IPETC and IBECTC are carried out using the SOLGASWATER computer program. The emphasis of these calculations is on constructing E_h-pH diagrams and determining the regions where Cu-thionocarbamate compounds are stable.

Cyclic voltammetry is conducted to investigate the electrochemical behavior of IPETC and IBECTC on platinum, copper and sulfide mineral electrodes. Microflotation tests of chalcocite, chalcopyrite and pyrite with IPETC and IBECTC are also carried

out. The principal objective of these tests is to determine flotation recovery as a function of pH and collector concentration. The flotation characteristics of each sulfide mineral for different collectors are correlated with the mechanisms inferred from the FTIR characterization and electrochemical studies. The results also help to establish the conditions that could be applied in practice. In addition, a modified electrochemical cell is used for determining contact angles as a function of applied potentials. This helps explain some of the observations made from the electrochemical studies.

Using an in-situ FTIR technique, the adsorption of IPETC and IBECTC on sulfide minerals is studied. A modified attenuated total reflectance (ATR) cell is used for these experiments. The effects of pH and concentration are monitored and the results compared with the flotation behavior. In-situ spectroelectrochemical studies are carried out to verify the electrochemical behavior of the thionocarbamates observed in the voltammetric and contact angle measurements. Using copper foil samples, the structure and orientation of the adsorbed thionocarbamate layers are determined by infrared reflection-absorption spectroscopy (IRAS). The results are helpful in better understanding the adsorption mechanisms of these reagents. Since adsorbed species give distinct characteristic IRAS spectra, the preferential adsorption of different collectors on copper can be monitored. In these preferential adsorption studies, combinations of collectors involving IPETC, IBECTC and KEX, are used. The objective is to determine the relative strength and adsorption kinetics of these three collectors.

The adsorption of IPETC and IBECTC on the sulfide mineral surfaces are also studied by monitoring the solution chemistry using a fast-scan UV spectrophotometer. This can provide information regarding the kinetics of collector adsorption. As a complement to the in-situ ATR measurements, UV spectroscopy is used to monitor the amount of collector remaining in solution. The effect of pH and concentration on collector adsorption can then be expressed in a more direct quantitative manner.

Pearson's concept of hard and soft acids and bases is theoretically applied to the flotation systems being studied here. Using Drago's theory and flow microcalorimetry, the Drago E and C parameters of chalcocite and pyrite are determined. These parameters give an indication of the acidity of the two minerals. The selectivity of the collectors can then be explained in terms of their acid-base characteristics.

2.0 SOLUTION AND FLOTATION CHEMISTRY

2.1 Introduction

The most important chemical process in sulfide flotation is the interaction of the mineral surface with the collector that renders the mineral hydrophobic. Most of the studies concerning basic mechanisms of this interaction process have involved only xanthate collectors. With most thiol collectors, specifically xanthates, the adsorption takes place through an anodic oxidation reaction, involving the collector and the mineral. The anodic reaction is coupled with a cathodic reduction, which is usually the reduction of oxygen. This knowledge is useful in developing improved methods for the separation of sulfide minerals.

Thionocarbamates differ from most thiol collectors since they remain neutral molecules in solution rather than ions. It may be possible to exploit this difference in designing new strategies for selective flotation. Thus, it is important to elucidate the mode of action of thionocarbamates for the flotation of sulfides.

Thermodynamics have been shown to be useful in explaining the solution and flotation chemistry of sulfide minerals. Numerous investigators have utilized extensive thermodynamic calculations in studying different flotation systems (Forssberg et al.,

1984; Pritzker and Yoon, 1984a, 1984b; Basilio, 1985; Basilio et al., 1985; Pritzker et al., 1985; Woods et al., 1987; Young, 1987; Palsson and Forssberg, 1988). Similar calculations have been carried out for the Cu^0- and Cu_2S-thionocarbamate systems. The results can serve as a guide in predicting the conditions under which flotation is possible.

Electrochemical techniques, such as voltammetry, can be applied to obtain kinetic information that allows determination of the reaction mechanisms on sulfide surfaces. This has been done by this author and numerous other investigators for xanthate-sulfide mineral systems. Investigation of the reaction of collectors at noble metal electrodes, as well as sulfide mineral electrodes, has provided an understanding of the oxidation and reduction of the collector species. Cyclic voltammetry has been conducted using platinum, copper, and sulfide mineral electrodes to study the electrochemical behavior of IPETC and IBECTC. This will be useful in understanding the interaction of these collectors with sulfide minerals.

Flotation tests on sulfides have been used to help identify the reactions that are important in inducing flotation, as well as establish the conditions that could be applied in practice. Since IPETC and IBECTC are copper-specific collectors, microflotation tests with chalcocite and chalcopyrite have been carried out. In addition, the tests have also been extended to include pyrite so that the selectivity of these collectors can be defined more clearly. Contact angle measurements, using a modified electrochemical cell, were used to study the effect of potential on floatability. This is a better technique for studying potential effect than by using electrochemical flotation. The problem of varying and inaccurate potential for each particle, that has been observed with the use of either chemical or potentiostatic control of mineral potential in electrochemical flotation, is avoided here.

2.2 Experimental

2.2.1 Outline of the Calculations

The SOLGASWATER computer program was utilized in the construction of the E_h-pH diagrams. This program was developed by the Department of Inorganic Chemistry, University of Umea, Sweden and is based on a free-energy minimization method (Eriksson, 1979). SOLGASWATER is a flexible program that can be applied to study the chemistry of multi-component, multi-phase aqueous systems. The version of the computer program used in these calculations can handle systems that contain up to 80 species, including a maximum of 48 solid phases. Details of the theory and algorithm used in the program have been described elsewhere (Eriksson, 1979; Forssberg et al., 1984; Young, 1987; Palsson and Forssberg, 1988).

The amount of chalcocite considered in the calculations for the Cu_2S-H_2O system is equivalent to an ore, with a specific gravity of 3.0, assaying 2% Cu in a flotation pulp that is 30% solids by weight. A similar amount of copper was used for the Cu-H_2O system. The calculations were done with the addition of 10^{-3} M IPETC or IBECTC and 10^{-5} M Cl^-. Only the case where the oxidation of sulfide is allowed to proceed as far as sulfate was considered in the calculations.

The thermodynamic data that have been considered in this study is the same as those used previously (Basilio, 1985; Young, 1987). Potentiometric titration was used to determine the solubility product of the two Cu-thionocarbamate compounds. In this method, a solution containing 10^{-6} M Cu(I) and 10^{-5} M Cl^- were titrated with 10^{-7} M IPETC or IBECTC solution. The Cu(I) solution was produced by reducing Cu(II) with hydroxylamine hydrochloride. The potential of the solution was monitored using a Keithley 642 Electrometer attached to a saturated calomel reference electrode and

platinum wire. The experimental endpoint volume was determined through a graphical method with the E_{cell} plotted against the volume of the titrant (x-axis).

The precipitates were identified by complete elemental analysis to be $Cu(IPETC)_2Cl$ and $Cu(IBECTC)_2Cl$. The K_{sp} for $Cu(IPETC)_2Cl$ and $Cu(IBECTC)_2Cl$ were determined to be $10^{-28.73}$ and $10^{-29.89}$, respectively.

2.2.2 Materials

The mineral samples used for the experiments were acquired from Ward's Natural Science Establishment. The chalcocite and chalcopyrite samples were both from Transvaal, Messina, South Africa, while the pyrite samples were from Leadville, Colorado.

The collector reagents used were O-isopropyl-N-ethyl thionocarbamate (IPETC) and O-isobutyl-N-ethoxycarbonyl thionocarbamate (IBECTC). They were obtained from the American Cyanamid Company. The thionocarbamates used were both over 95% pure (by volume), as measured by gas chromatography. The impurities were reported to be mostly short chain alcohols. The structure and purity of the reagents were also checked by ^1H NMR and ^{13}C NMR spectroscopy.

The cyclic voltammetry experiments were conducted at pH 9.2 (0.05 M $Na_2B_4O_7$ solution) and pH 4.6 (0.5 M CH_3COOH/0.5 M $NaCH_3COO$ solution). For the microflotation and contact angle measurements, no buffer solution was used. Instead, 0.1 M NaCl solutions were used for the microflotation and contact angle experiments with the pH controlled by the addition of NaOH or HCl solutions. All the reagents used were of analytical grade and all the solutions were prepared with double distilled water. Prior to each series of electrochemical experiments, the 75 ml solution was deoxygenated by purging with low-oxygen nitrogen gas (< 0.05 ppm O_2) for at least one hour.

2.2.3 Cyclic Voltammetry

The sulfide mineral electrodes were prepared from pure mineral specimens with a rectangular cross section. The cut mineral sample was then permanently attached to a copper wire with Electrodag 199, a carbon-based conducting cement. This assembly was sealed in a glass holder with Buehler epoxy resin. The electrode surface was then ground and polished. The resulting geometric area exposed to the solution was 0.30 cm^2. Prior to each test run, the electrode was polished with 600-grit silicon carbide paper.

The voltammetry experiments were conducted using a conventional three-electrode circuit (Figure 2.1). This consisted of the sulfide mineral electrode (working electrode), a saturated calomel electrode (reference electrode) and an isolated platinum wire electrode (counter electrode). The electrode potential was controlled with a PAR Model 371 Potentiostat/Galvanostat and a PAR Model 175 Universal Programmer. The voltammograms were recorded on a Linseis Model LY18100 X-Y_1Y_2 recorder. Although a calomel electrode was used as the reference electrode, the potentials reported here and in other experiments, are all expressed on the standard hydrogen electrode (SHE) scale.

2.2.4 Microflotation Tests

The pure mineral sample was crushed and ground using an agate mortar and pestle. The ground sample was then hand-screened to obtain a -65 + 100 mesh size fraction (150-212 μm). To minimize oxidation, this step, which took no more than five minutes, was done just before each experiment. In each test, a 1-gm finely-ground sample was added to 100 ml of 0.01 M NaCl solution. The pH of the solution was controlled

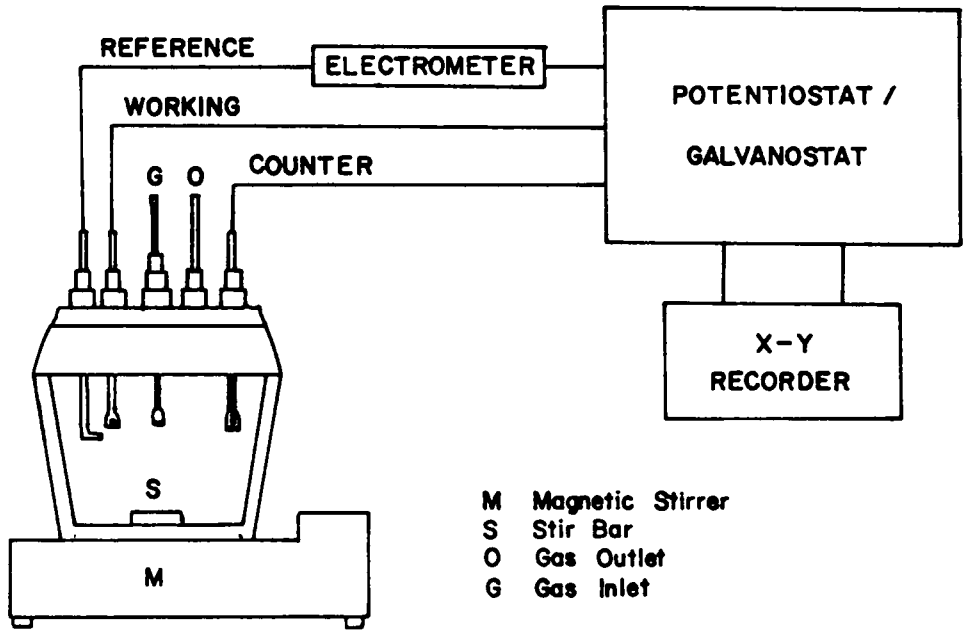

Figure 2.1. Schematic diagram showing the experimental set-up used for the linear sweep voltammetry.

automatically by a Fisher Computer-Aided Titrimetry system before and during conditioning. The collector was then added to the mineral slurry and conditioned for 5 minutes. For the collectorless flotation measurements, the mineral slurry was conditioned in 0.01 M NaCl solution for 5 minutes.

After conditioning, the slurry was transferred completely to the microflotation cell. Detailed description of the cell has been shown previously (Basilio, 1985). A 1-minute flotation time was employed for all the experiments. The concentrate and tailings were then recovered, dried and weighed to obtain the flotation recovery for each test.

2.2.5 Contact Angle Measurements

The sulfide mineral electrodes for the contact angle measurements were prepared in the same manner as that for the voltammetry experiments. However, the electrodes used here have an exposed geometric area of 1 cm^2. Prior to each test, the electrode was fine polished with 1000-grit silicon carbide paper and then with Buehler polishing cloth. After polishing, the electrode was cleaned in an ultrasonic cleaner and rinsed with double distilled water.

The modified electrochemical cell used for the contact angle study utilizes a three-electrode system (Figure 2.2). The cell has parallel plate windows made of optical glass to facilitate contact angle measurements. The potential of the working electrode was controlled using a PAR Model 371 Potentiostat/Galvanostat. Except for the cell, the electrochemical set-up is similar to the one used for the voltammetric experiments. Before each experiment, the buffer solution containing 10^{-3} M thionocarbamate was deoxygenated in the cell by purging with low oxygen N_2 gas for at least one hour. Afterwards, the purging gas was continously introduced above the solution. The freshly fine-polished electrode was then positioned in the center of the cell with the exposed

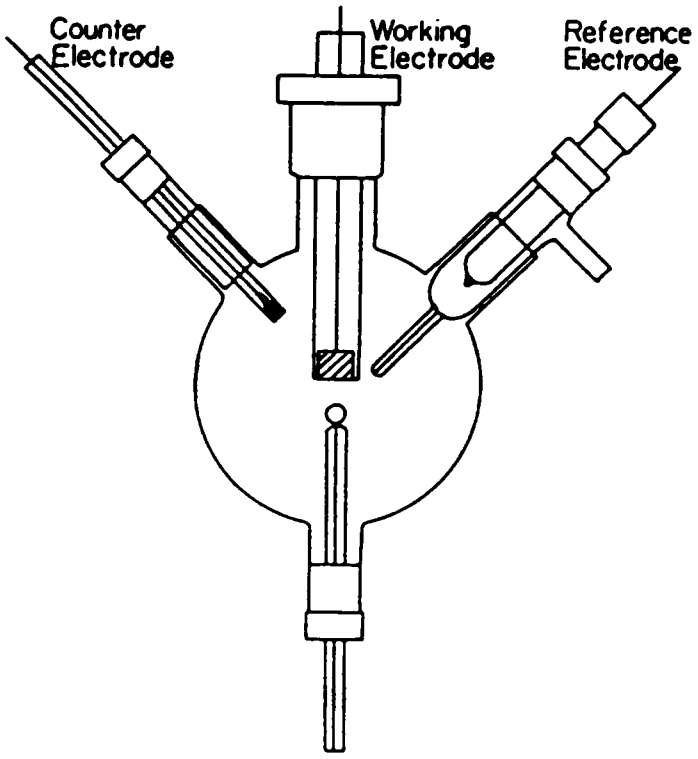

Figure 2.2. Schematic diagram of the modified electrochemical cell used for the contact angle measurements.

mineral surface facing down. The nitrogen bubble was deposited on the electrode surface using a capillary glass tube with a Gilson Micrometer syringe attached to it. The contact angles were measured using a Rame Hart Model 100 Goniometer. Measurements of the contact angles were made under different potentiostatic conditions. At each potential, the contact angles on four different sides of the electrode surface were measured and the average was reported as the final value.

2.3 Results and Discussions

2.3.1 Thermodynamic Calculations

a. E_h-pH diagrams in the presence of IPETC

Figure 2.3 shows the E_h- pH diagram constructed for the Cu^0-H_2O system in the presence of 10^{-3} M IPETC and 10^{-5} M Cl^-. It shows the E_h-pH region in which $Cu(IPETC)_2Cl$ can be formed along with other co-existing solid phases. Assuming that $Cu(IPETC)_2Cl$ is the species responsible for making the Cu^0 surface hydrophobic, flotation will be possible in these regions. $Cu(IPETC)_2Cl$ is found to co-exist with Cu^0, Cu_2O and CuO in a large region starting at E_h = -520 mv. The thermodynamic calculations indicate that the lower flotation edge at pH $\geq$ 1 may be attributed to the following reaction :

$$Cu^0 + 2IPETC + Cl^- \rightarrow Cu(IPETC)_2Cl + e^- . \qquad [2.1]$$

However, at pH < 1, the formation of $Cu(IPETC)_2Cl$ is defined by :

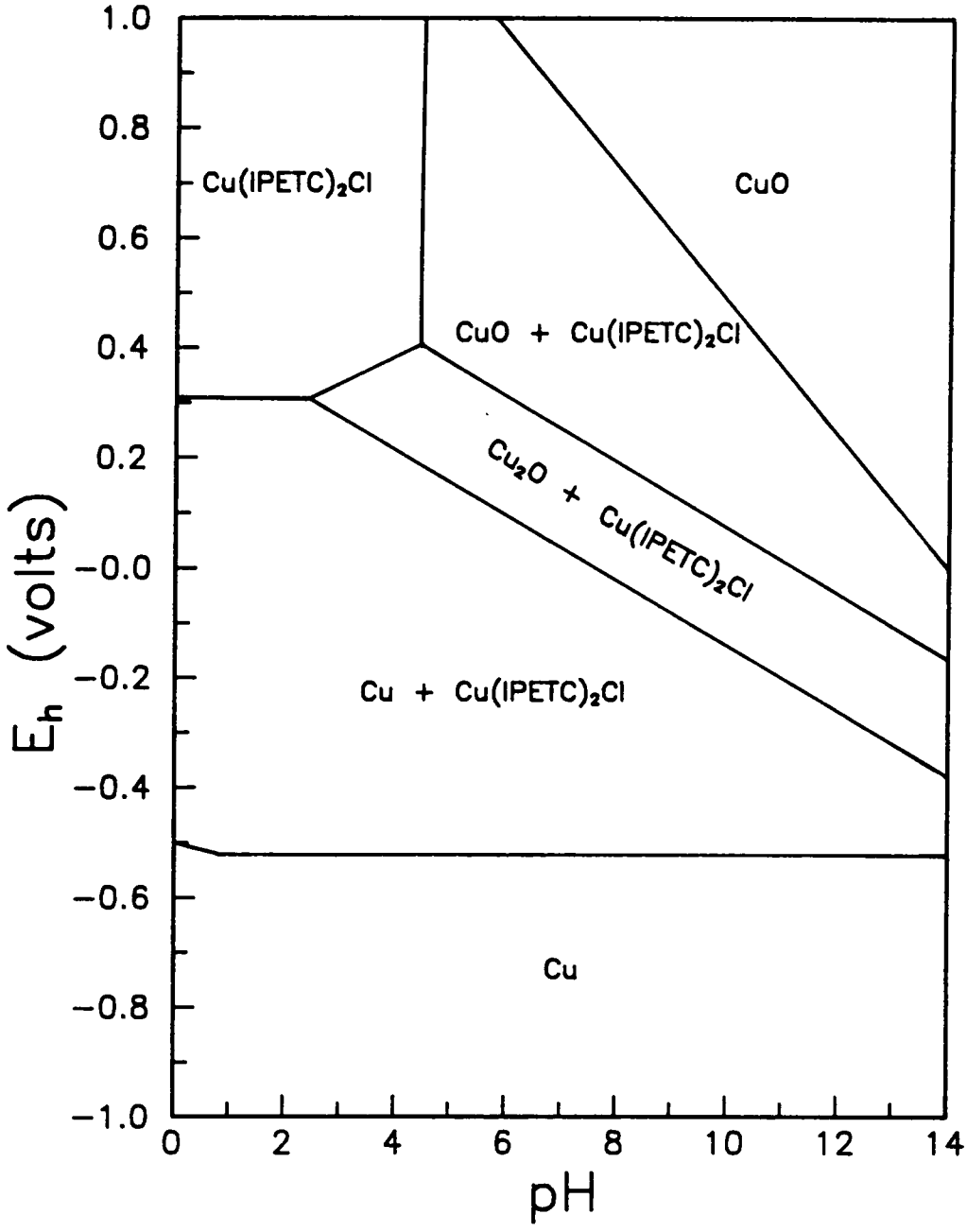

Figure 2.3. E_h-pH diagram of the Cu^0-H_2O system in the presence of 10^{-3} M IPETC and 10^{-5} M Cl^- at T = 298°K and P = 1 atm.

$$Cu^0 + 2IPETC + HCl \rightarrow Cu(IPETC)_2Cl + H^+ + e^- . \qquad [2.2]$$

At acidic and oxidizing conditions, $Cu(IPETC)_2Cl$ is the only stable solid species present. It is stable up to the highest potential considered in the computation. However, this Cu-thionocarbamate compound disappears at alkaline conditions according to this pH-dependent reaction :

$$Cu(IPETC)_2Cl + H_2O \rightarrow CuO + 2IPETC + Cl^- + 2H^+ + e^- . \qquad [2.3]$$

The general shape of this stability diagram is similar to that constructed for the Cu^0-H_2O system in the presence of xanthate (Young, 1987). However, the $Cu(IPETC)_2Cl$ stability region is larger than that for CuX. This is due to the lower solubility product of $Cu(IPETC)_2Cl$.

The stability diagram for the Cu_2S-H_2O system in the presence of 10^{-3} M IPETC and 10^{-5} M Cl^- is shown in Figure 2.4. It can be predicted that Cu_2S flotation is possible in the E_h-pH region where $Cu(IPETC)_2Cl$ is stable. $Cu(IPETC)_2Cl$ co-exists with Cu^0, Cu_2S, CuS, Cu_2O and CuO in a large region. It is interesting to note that the boundaries of this region are the same as those observed for the Cu^0-H_2O system.

Based on the thermodynamic calculations, the lower boundary may also be attributed to reactions [2.1] and [2.2]. This explains why the lower boundary for the $Cu(IPETC)_2Cl$ stability region is similar to that observed in Figure 2.3. The upper region of the stability diagram for Cu_2S is also similar to the one for the Cu^0 This is expected since there are no reactions involving sulfur occurring at high potentials.

Only the region between approximately -500 mv and the Cu^0/Cu_2O line is different from the previous diagram. The oxidation of Cu_2S is observed to be both E_h- and pH-dependent. The stability diagram changes considerably if the non-stoichiometric

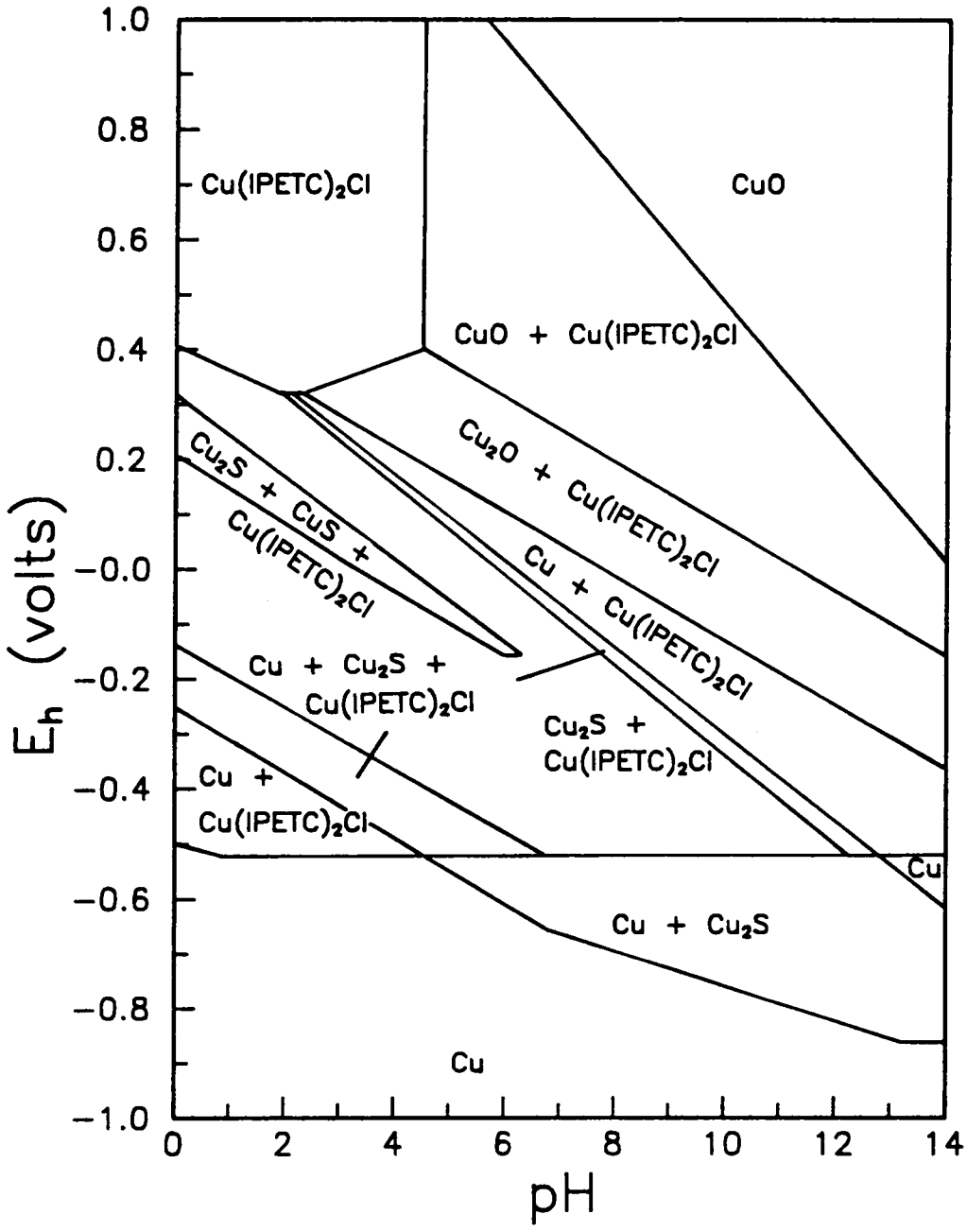

Figure 2.4. E_h-pH diagram of the Cu_2S-H_20 system in the presence of 10^{-3} M IPETC and 10^{-5} M Cl^- at T = 298°K and P = 1 atm.

copper sulfides were considered in the calculations. This was shown in the calculations for the Cu_2S-KEX-H_2O system (Young, 1987).

b. E_h-pH diagrams in the presence of IBECTC

The E_h-pH diagram for the Cu^0-H_2O system with the addition of 10^{-3} M IBECTC and 10^{-5} M Cl^- (Figure 2.5) is similar to that constructed in the presence of IPETC. The specie that was considered as being responsible for making the surface hydrophobic is $Cu(IBECTC)_2Cl$. The stability region of $Cu(IBECTC)_2Cl$ is larger than that of $Cu(IPETC)_2Cl$ due to its lower K_{sp} value. $Cu(IBECTC)_2Cl$ co-exists with Cu^0, Cu_2O and CuO at potentials > -600 mv. Only the Cu-IBECTC compound is stable at acidic and oxidizing conditions since Cu^0 dissolves above 310 mv. At pH > 4.4, the stability of $Cu(IBECTC)_2Cl$ is dependent on the following oxidation reaction :

$$Cu(IBECTC)_2Cl + H_2O \rightarrow CuO + 2IBECTC + Cl^- + 2H^+ + e^- . \quad [2.4]$$

The region where the Cu-IBECTC compound co-exists with CuO is larger than those observed in the two previous stability diagrams.

Based on the computations, the lower $Cu(IBECTC)_2Cl$ boundary may be attributed to the reaction involving Cu^0,

$$Cu^0 + 2IBECTC + Cl^- \rightarrow Cu(IBECTC)_2Cl + e^- . \quad [2.5]$$

A reaction similar to reaction [2.2], which involves IBECTC instead of IPETC, is responsible for the pH-dependent line at pH < 1.

Figure 2.6 shows the stability diagram for the Cu_2S-H_2O system in the presence of 10^{-3} M IBECTC and 10^{-5} M Cl^-. Chalcocite floatability is anticipated in the E_h-pH

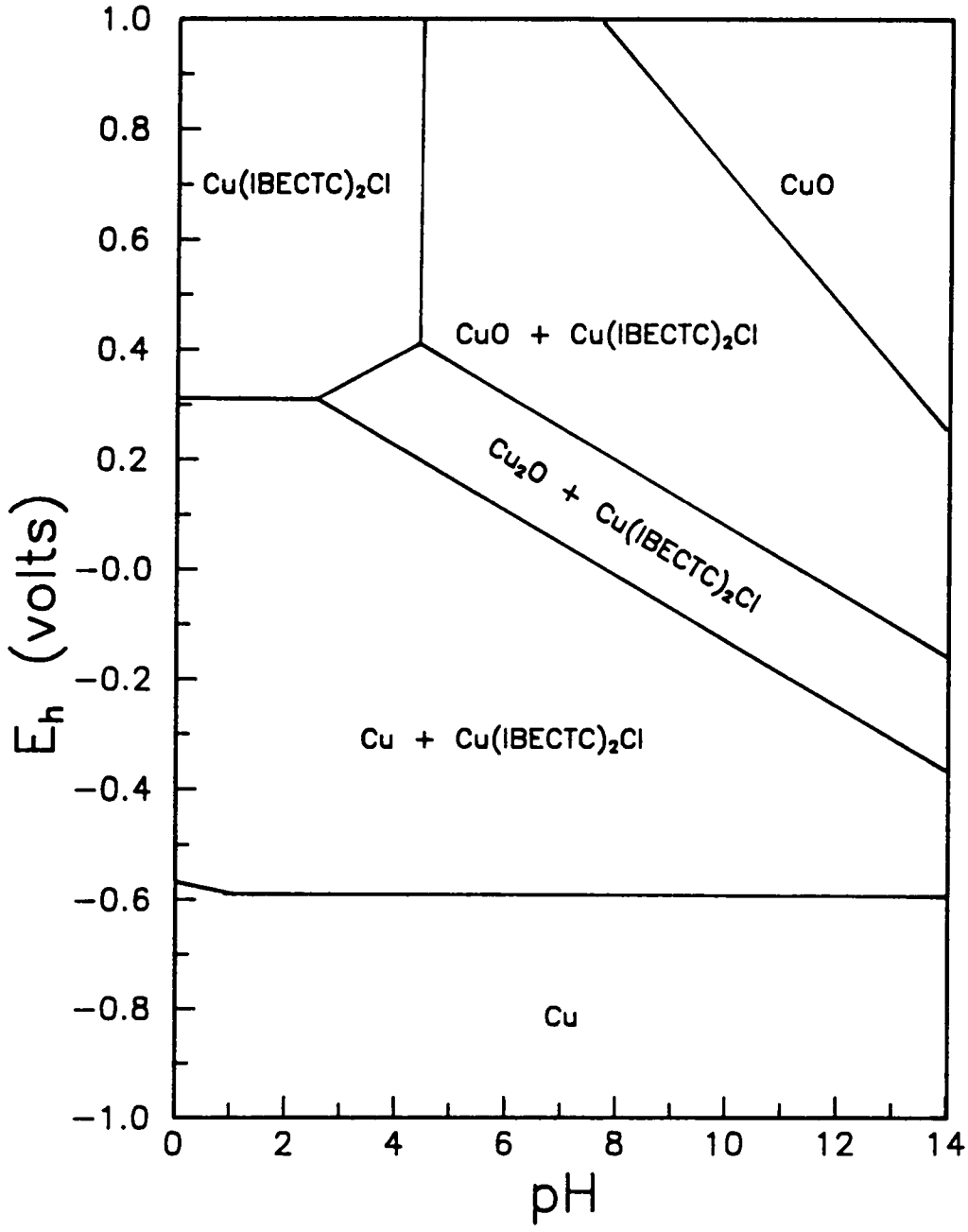

Figure 2.5. E_h-pH diagram of the Cu^0-H_2O system in the presence of 10^{-3} M IBECTC and 10^{-5} M Cl^- at T = 298°K and P = 1 atm.

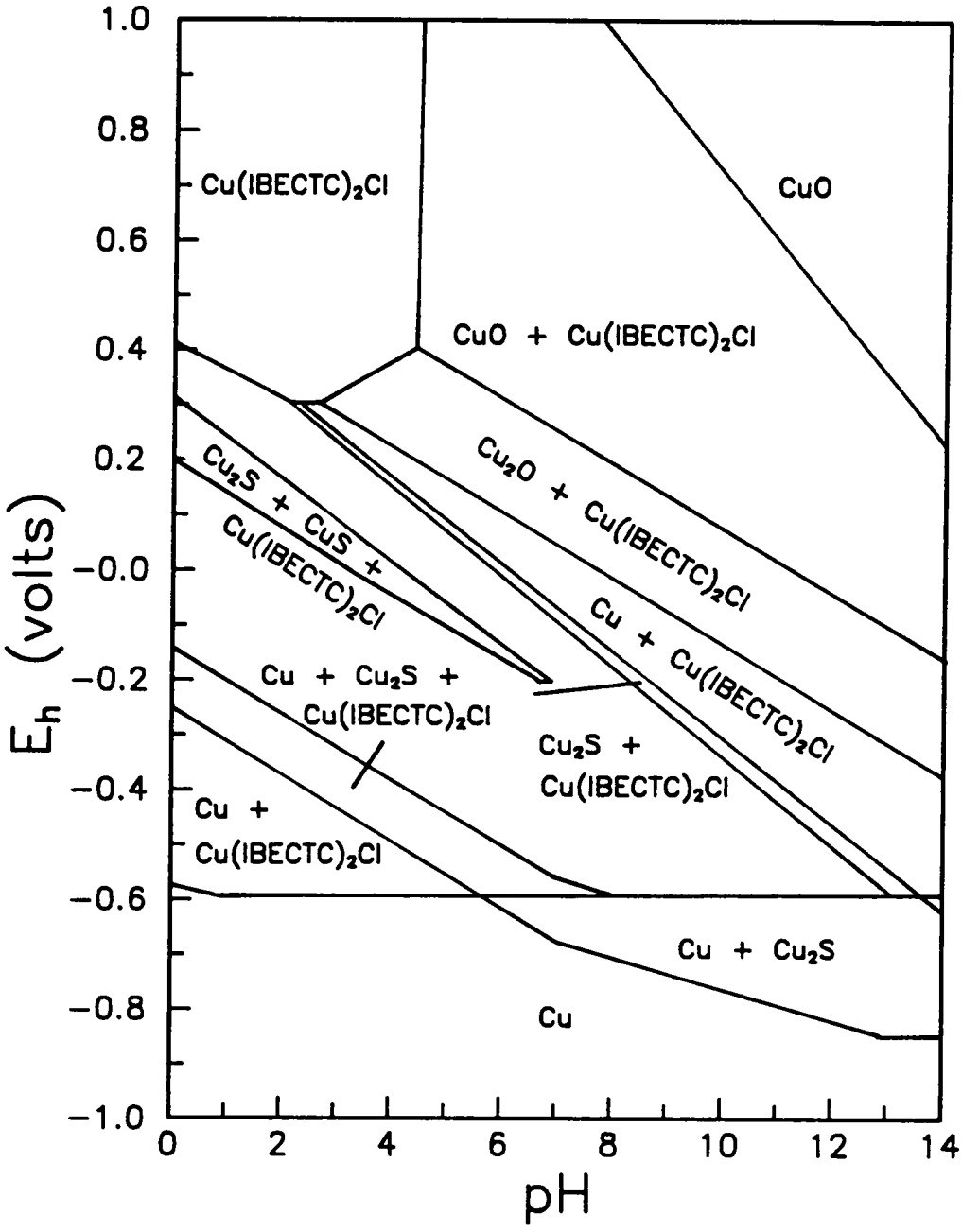

Figure 2.6. E_h-pH diagram of the Cu_2S-H_20 system in the presence of 10^{-3} M IBECTC and 10^{-5} M Cl^- at T = 298°K and P = 1 atm.

region where $Cu(IBECTC)_2Cl$ is stable. This region starts at E_h > -600 mv and is bounded by the (CuO + $Cu(IBECTC)_2Cl$)/CuO line at alkaline conditions. This diagram is similar to that obtained for the Cu_2S-IPETC-H_2O system, except for the larger stability region for $Cu(IBECTC)_2Cl$. This is, as explained previously, due to the lower K_{sp} value for $Cu(IBECTC)_2Cl$.

It should be pointed out that the size of the $Cu(IBECTC)_2Cl$ region is the same as that found for the Cu^0-H_2O system. This is due to the fact that the reactions responsible for the lower and upper boundaries are the same. The reactions involving sulfur occur only at the middle portion of this region.

c. Effect of E_h and pH on the formation of Cu-thionocarbamate compounds

In the calculations, the quantity of solid stable in a given region has also been determined since the solid phases are included in the mass balances. The effect of E_h and pH on the percentage of thionocarbamate initially added that ends up as $Cu(IPETC)_2Cl$ or $Cu(IBECTC)_2Cl$ can be studied using these calculated values. This quantity is hereupon referred to as % $Cu(IPETC)_2Cl$ or % $Cu(IBECTC)_2Cl$ and is used to correlate with the experimental data.

Figure 2.7 shows the effect of E_h on % $Cu(IPETC)_2Cl$ at pH 6 and an IPETC addition of 10^{-3} M. These values were taken from the results of the calculations for the Cu^0- and Cu_2S-H_2O systems. An initial Cl^- concentration of 10^{-5} M is used for this and subsequent calculations. The % $Cu(IPETC)_2Cl$ increases sharply above -520 mv and reaches a maximum at around -450 mv. The curve stays at this value up to approximately 850 mv before dropping down to 0. This is a wide potential region where flotation is possible.

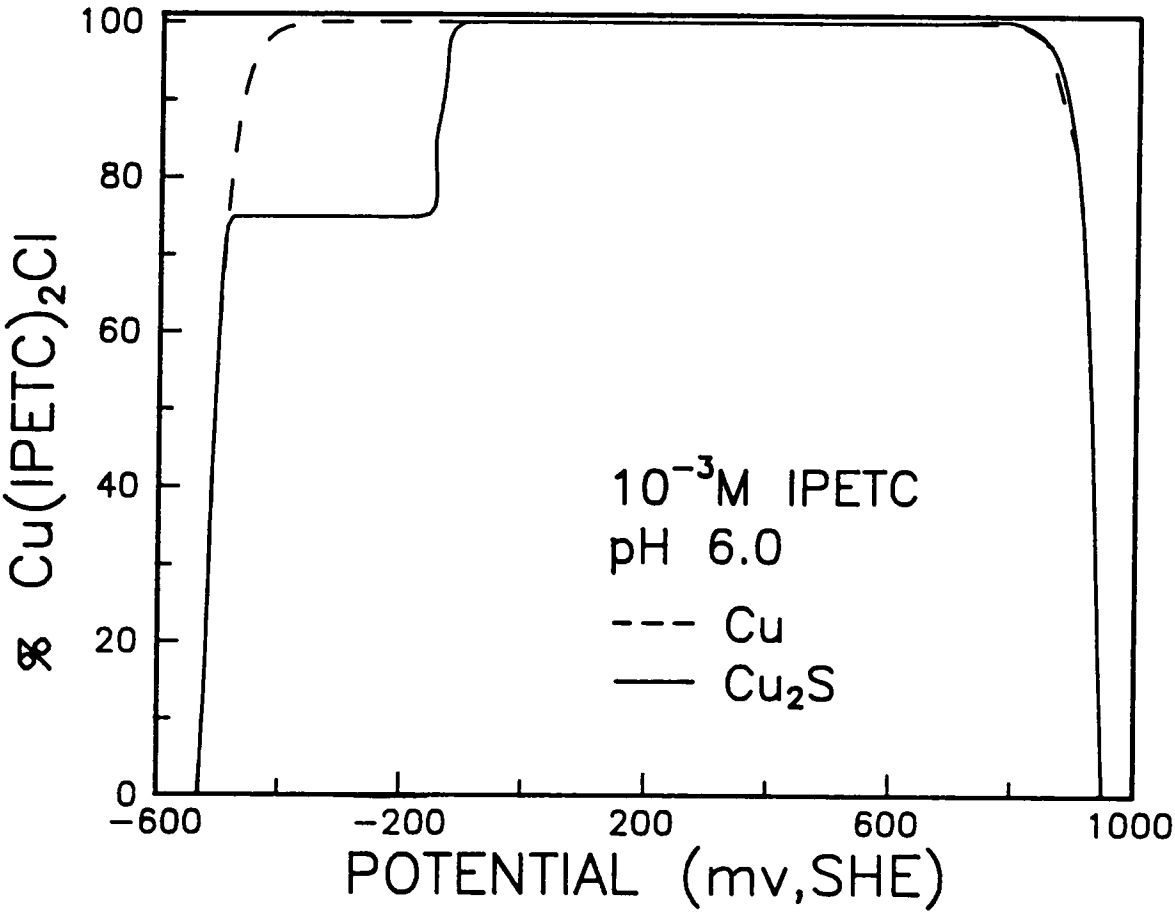

Figure 2.7. Effect E_h on % $Cu(IPETC)_2Cl$ for a collector addition of 10^{-3} M IPETC at pH 6.0 for the Cu^0- and Cu_2S-H_2O sytems.

As indicated in the E_h-pH diagrams, the % $Cu(IPETC)_2Cl$ curves for both systems are similar. The only significant difference is the plateau observed between -480 and -180 mv for the Cu_2S-H_2O system. This is due to the stability of Cu_2S at this potential region, which directly affects the amount of copper available to form $Cu(IPETC)_2Cl$. From these curves, Cu^0 and Cu_2S flotation is feasible in the potential region between -500 and 900 mv. However, maximum floatability for Cu_2S would only be possible in a narrower E_h range.

Similar curves are found in Figure 2.8 which shows the effect of E_h on % $Cu(IBECTC)_2Cl$ for the Cu^0- and Cu_2S-H_2O systems. These were calculated using an IBECTC concentration of 10^{-3} M at pH 6. The lower flotation edge is observed at a lower E_h when IBECTC is used as the collector. This is probably due to the lower solubility product of $Cu(IBECTC)_2Cl$. On the other hand, the upper flotation edge is shifted to a higher E_h for both systems involving the addition of IBECTC. The curves for both Cu^0 and Cu_2S coincide almost over the entire E_h range except for the region between -500 and 100 mv. The amount of $Cu(IBECTC)_2$ produced in this region is slightly less in the Cu_2S-H_2O system, due to the stability of Cu_2S. The thermodynamically predicted flotation range with the use of IPETC or IBECTC is larger than that found for the Cu_2S-KEX-H_2O system (Basilio, 1985).

The effect of pH on % $Cu(IPETC)_2Cl$ and % $Cu(IBECTC)_2Cl$ at E_h = 200 mv are shown in Figures 2.9 and 2.10, respectively. The calculations were all done in the presence of 10^{-3} M collector and 10^{-5} M Cl^-. Only the results at 200 mv are shown since this potential correspond to the average open-circuit potential observed in the experiments. The curve for % $Cu(IPETC)_2Cl$ starts and remains at the maximum value before decreasing sharply above pH 11.5 for both Cu^0 and Cu_2S. At lower potentials, the amount of $Cu(IPETC)_2Cl$ produced is maximum over the entire pH range. The % $Cu(IBECTC)_2Cl$ curve follows a similar behavior except that it starts to decrease at pH

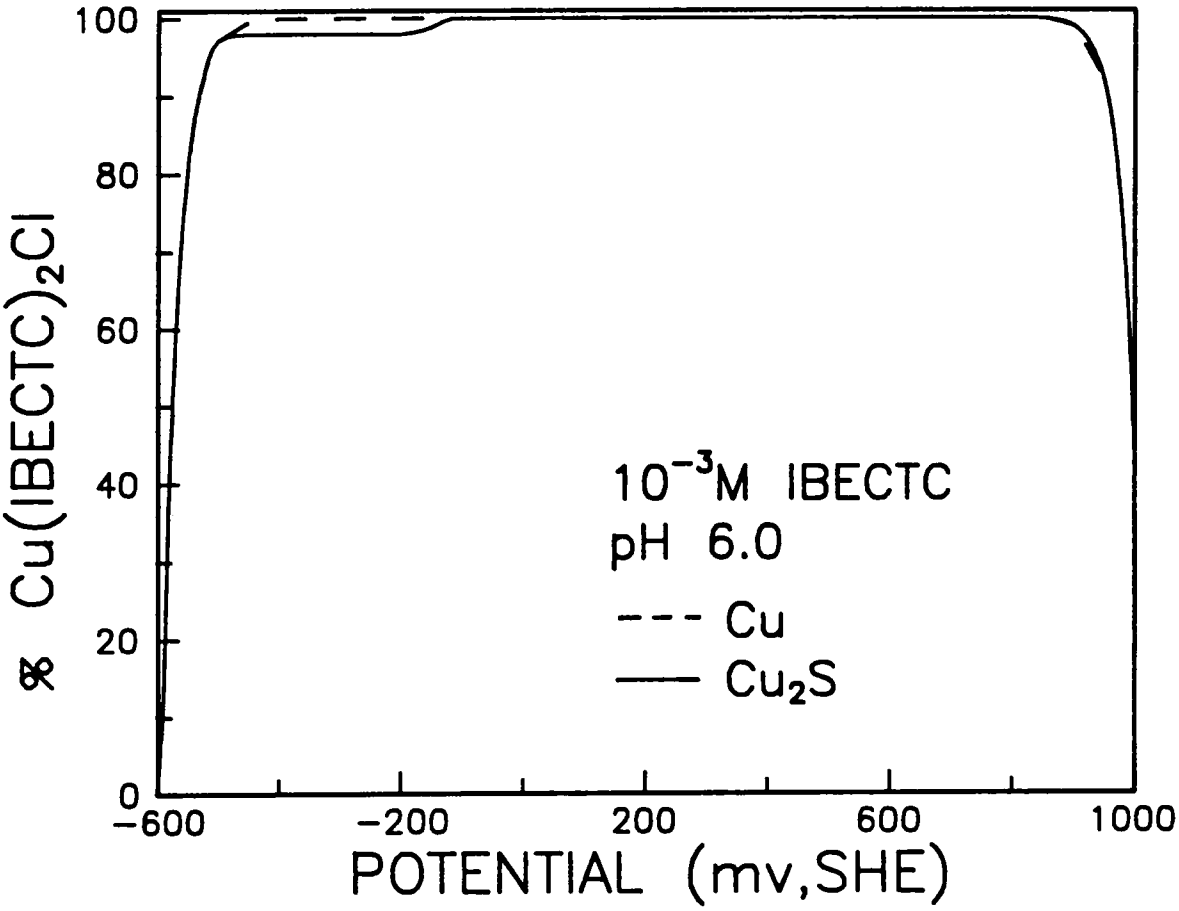

Figure 2.8. Effect E_h on % $Cu(IBECTC)_2Cl$ for a collector addition of 10^{-3} M IBECTC at pH 6.0 for the Cu^0- and Cu_2S-H_2O sytems.

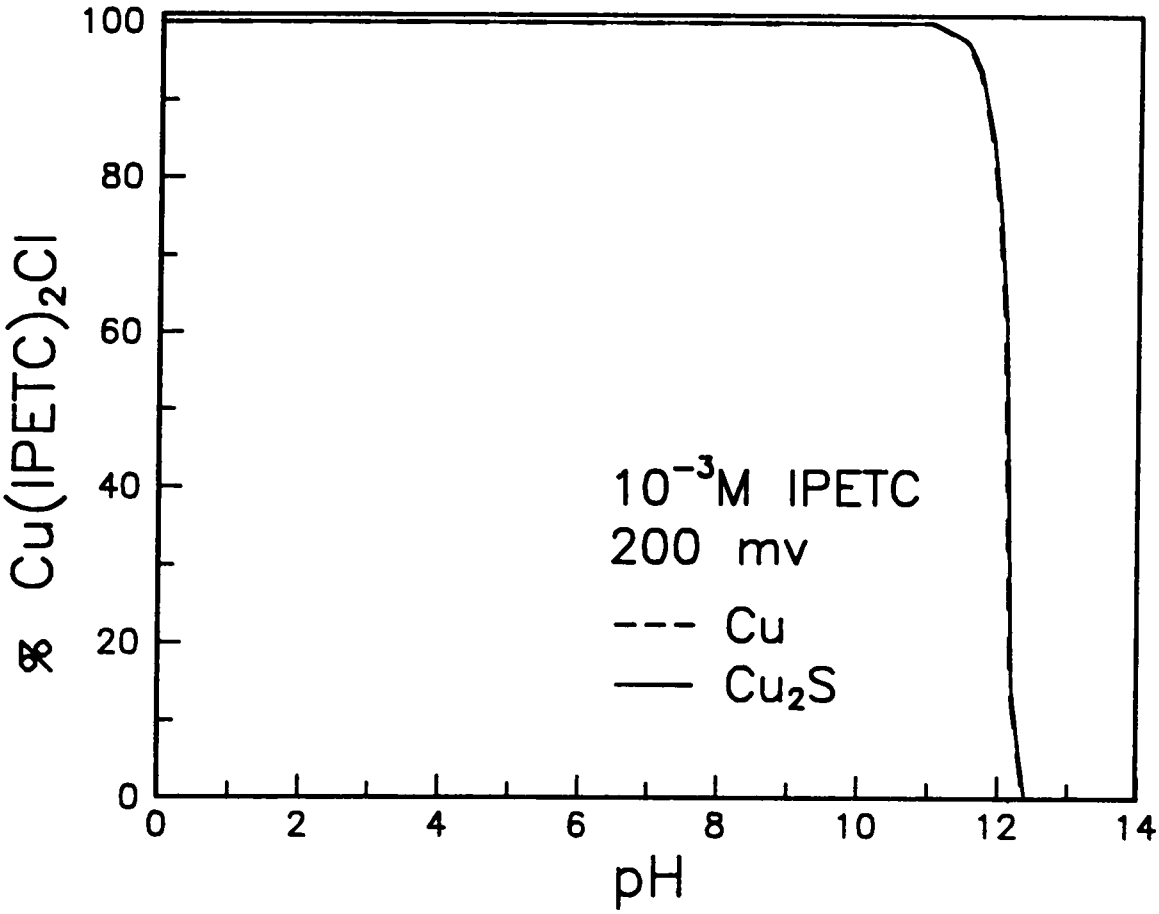

Figure 2.9. Effect of pH on % $Cu(IPETC)_2Cl$ for a collector addition of 10^{-3} M IPETC at an E_h of 200 mv for the Cu^0- and Cu_2S-H_2O sytems.

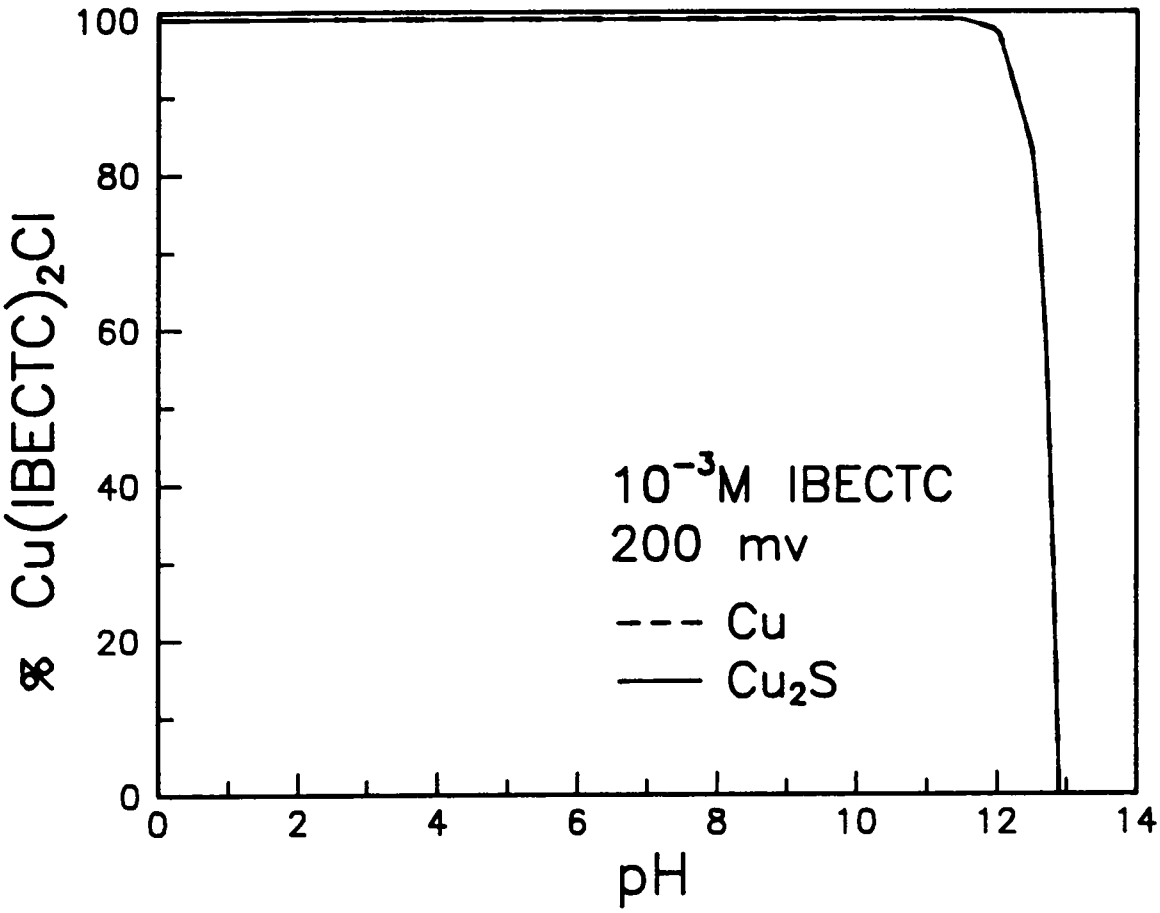

Figure 2.10. Effect of pH on % $Cu(IBECTC)_2Cl$ for a collector addition of 10^{-3} M IBECTC at an E_h of 200 mv for the Cu^0- and Cu_2S-H_2O sytems.

12. Both curves indicate a wide pH range for Cu^0 and Cu_2S flotation. However, the flotation range is expected to decrease with lower collector addition.

2.3.2 Cyclic Voltammetry

a. In the absence and presence of IPETC at pH 9.2

Platinum: Voltammetry experiments were carried out on a platinum wire electrode in unstirred 0.05 M $Na_2B_4O_7$ solution (pH 9.2). The scan was started at a potential of -450 mv and proceeded in the anodic direction at a sweep rate of 50 mv/sec. The upper and lower potential limits were set at 1000 and -450 mv, respectively. The voltammograms for platinum in the absence and presence of 10^{-4} M IPETC are both shown in Figure 2.11. The current in the region between -450 and -50 mv is associated with the adsorption and desorption of hydrogen. At potentials higher than -50 mv, the observed current is attributed to the adsorption and desorption of oxygen. The adsorption of oxygen and hydrogen are both obtained by charge-transfer processes from water (Bald and Breiter, 1961; Woods, 1971).

In the presence of 10^{-4}M IPETC, a slight change in the voltammetric behavior of platinum is observed. The current at the start of the scan is lower, which is due to the inhibition of the hydrogen adsorption reactions. This may be brought about by the adsorption of IPETC without electron-transfer. The effects of xanthate (Woods, 1971), dithiophosphate (Chander and Fuerstenau, 1974) and halides (Frumkin, 1963; Breiter, 1963) adsorption on platinum have also been observed to inhibit these hydrogen adsorption reactions. At higher potentials, the passivation of platinum by IPETC occurs, inhibiting the adsorption and desorption of oxygen on platinum. However, unlike that found for xanthate and dithiophosphate, there is no oxidation of the reagent

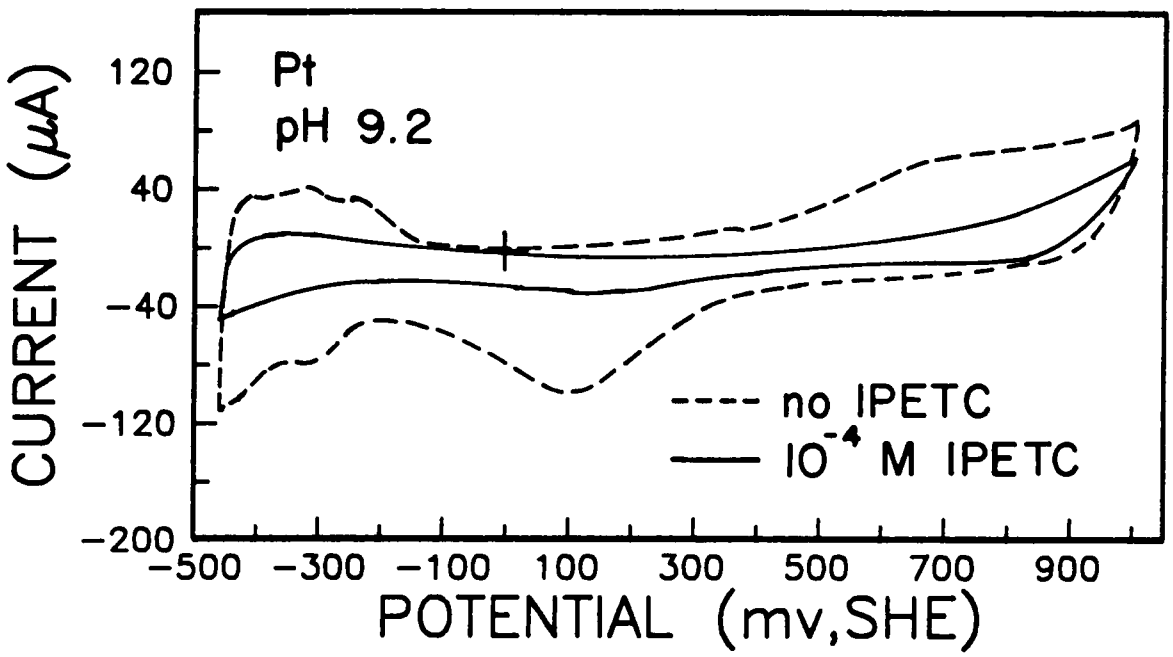

Figure 2.11. Voltammograms of platinum in unstirred 0.05 M $Na_2B_4O_7$ solution (pH 9.2) with and without 10^{-4} M IPETC. Scan rate = 50 mv/sec.

observed at these potentials, indicating the non-electroactivity of IPETC on platinum over this potential region.

Copper: The voltammograms of copper in the absence and presence of 10^{-4}M IPETC are shown in Figure 2.12. The potential was cycled between -500 and 450 mv at 50 mv/sec from a starting potential of -500 mv. In the absence of IPETC, the voltammogram shows the oxidation and reduction of Cu^0 at alkaline conditions. The current starting above -50 mv, A_2, is attributed to the oxidation of Cu^0 to Cu_2O and CuO. On the return scan, cathodic peaks, C_1 and C_2, are observed near 25 and -275 mv, respectively. These correspond to the reduction of CuO to Cu_2O and Cu_2O to metallic copper, respectively.

The addition of 10^{-4}M IPETC results in the formation of a new anodic peak, A_1. At a potential near 0 mv, anodic currents start to flow, due probably to the interaction of IPETC with the electrode surface. This is similar to the prewave observed for the electrochemical adsorption of xanthate on Cu^0 (Woods, 1971). The adsorption may be represented by the following reaction:

$$Cu^0 + IPETC \rightarrow Cu(IPETC)^+ + e^-, \qquad [2.6]$$

where the product is a copper thionocarbamate complex. This reaction may also involve an anion, A, to form Cu(IPETC)A, instead of $Cu(IPETC)^+$:

$$nCu^0 + nIPETC + A^{n-} \rightarrow [Cu(IPETC)]_nA + ne^-. \qquad [2.7]$$

Another possible reaction might involve the release of H^+ from the breaking of the N-H bond in IPETC during adsorption,

$$Cu^0 + IPETC \rightarrow Cu(IPETC)' + H^+ + e^-. \qquad [2.8]$$

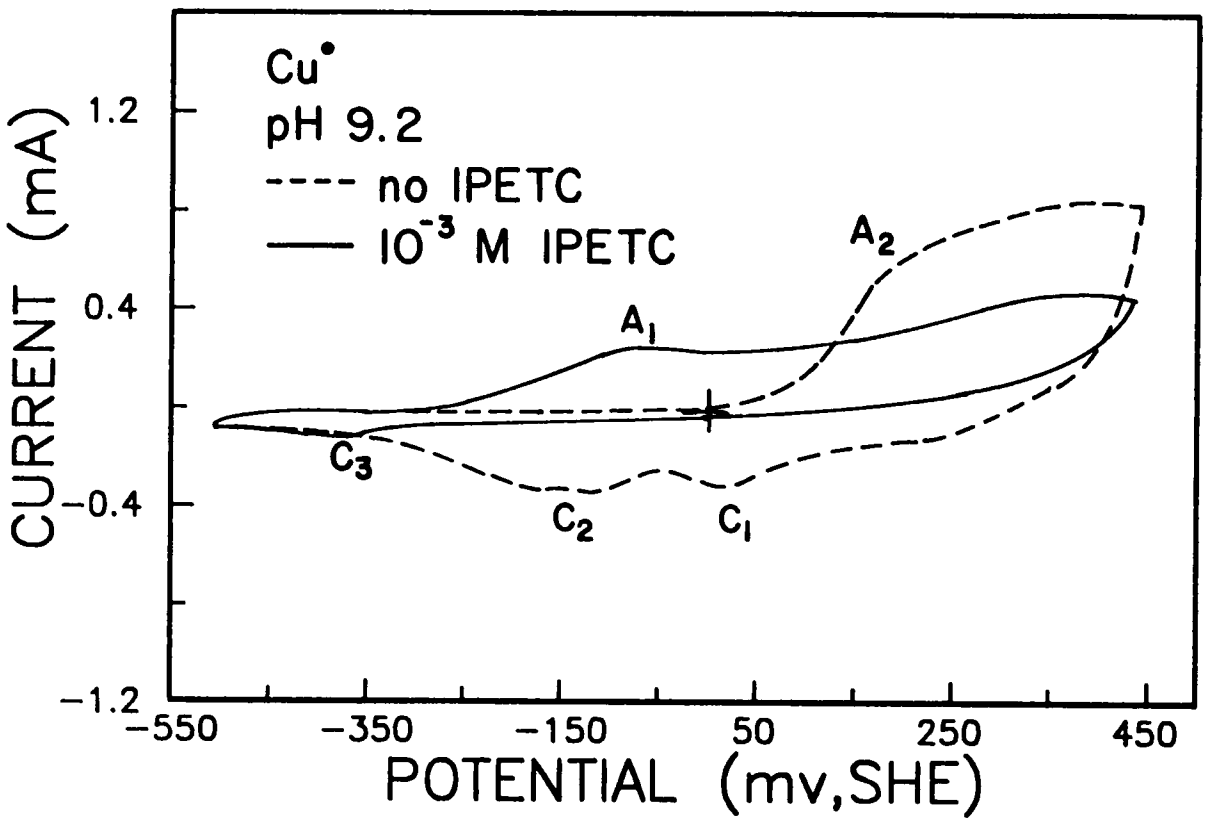

Figure 2.12. Voltammograms of copper in unstirred 0.05 M $Na_2B_4O_7$ (pH 9.2) with and without 10^{-3} M IPETC. Scan rate = 50 mv/sec.

where (IPETC)′ = (C_3H_7-OCSN$^-$-C_2H_5).

The adsorption reaction given above would probably be a result of coupled chemical reactions. In organic electrochemistry, coupled chemical reactions of the EC type are very common (Southampton Electrochemistry Group, 1985). The EC mechanism involves an initial electron transfer step (E), followed by a chemical reaction (C). This mechanism may be applicable to the interaction observed here. The first step presumably involves the electrochemical reaction:

$$Cu^0 \rightarrow Cu^+ + e^-, \qquad [2.9]$$

followed immediately, depending on the IPETC complex formed, by the non-electrochemical interaction with IPETC :

$$Cu^+ + IPETC \rightarrow Cu(IPETC)^+, \qquad [2.10]$$

$$nCu^+ + nIPETC + A^{n-} \rightarrow [Cu(IPETC)]_nA, \qquad [2.11]$$

or

$$Cu^+ + IPETC \rightarrow Cu(IPETC)' + H^+. \qquad [2.12]$$

The chemical reaction is presumably irreversible, as suggested by the absence of a reverse peak in the voltammogram.

The stability of Cu(I) produced in reaction [2.9] may be attributed to the presence of IPETC. Cu(I) has been found to form a complex with IPETC (Seryakova et al., 1975; Basilio et al., 1988). Studies with ring-disc electrodes in borate buffer solutions have also established that Cu(I) is formed as an intermediate with a measurable lifetime in Cu^0 oxidation (Albery and Hitchman, 1971).

In the presence of IPETC, A_2 has a lower magnitude, while C_1 and C_2 have been replaced by a single peak, C_3, near -350 mv. This indicates that IPETC adsorption has inhibited the oxidation and reduction reactions involving Cu^0 and the copper oxides. Although not shown by the voltammogram, there is a possibility that IPETC is already adsorbed, without any apparent electron-transfer, on the electrode at the starting potential. This has also been seen for the Pt electrode. The thermodynamic calculations also predict the adsorption of IPETC at this potential. The FTIR measurements (to be discussed later in Chapter 3.0) would help show whether IPETC adsorption has occurred before the start of A_1.

Chalcocite: The next series of voltammetry experiments at pH 9.2 were carried out on different sulfide mineral electrodes. The electrochemical behavior of chalcocite with and without IPETC is shown by the voltammograms in Figure 2.13. When the anodic scan began at a starting potential of -400 mv, the oxidation of chalcocite in the absence of the collector is initially observed above 175 mv. The resulting anodic peak, A_2, is attributed to the oxidation of chalcocite to CuO and non-stoichiometric copper sulfide (Basilio, 1985; Young et al., 1988). On the return scan, the reduction of the oxidation products is observed at cathodic peak, C_1. At a slower scan rate, C_1 is found to separate into three peaks at around the same potential region (Young et al., 1988). This has been attributed to reduction reactions involving non-stoichiometric copper sulfides. The cathodic current found below -400 mv, C_3, may be attributed to Cu_2S and HS^- formation (Walker et al., 1984; Basilio, 1985; Young, 1987). The anodic peak, A_3, is due to the reverse of C_3.

An additional peak, A_1, is observed starting above 0 mv with the addition of 10^{-3}M IPETC. This may correspond to the adsorption of IPETC on chalcocite that is accompanied by an electron-transfer, which was also observed on copper. The adsorption of IPETC results in the inhibition of chalcocite oxidation (A_2) and reduction

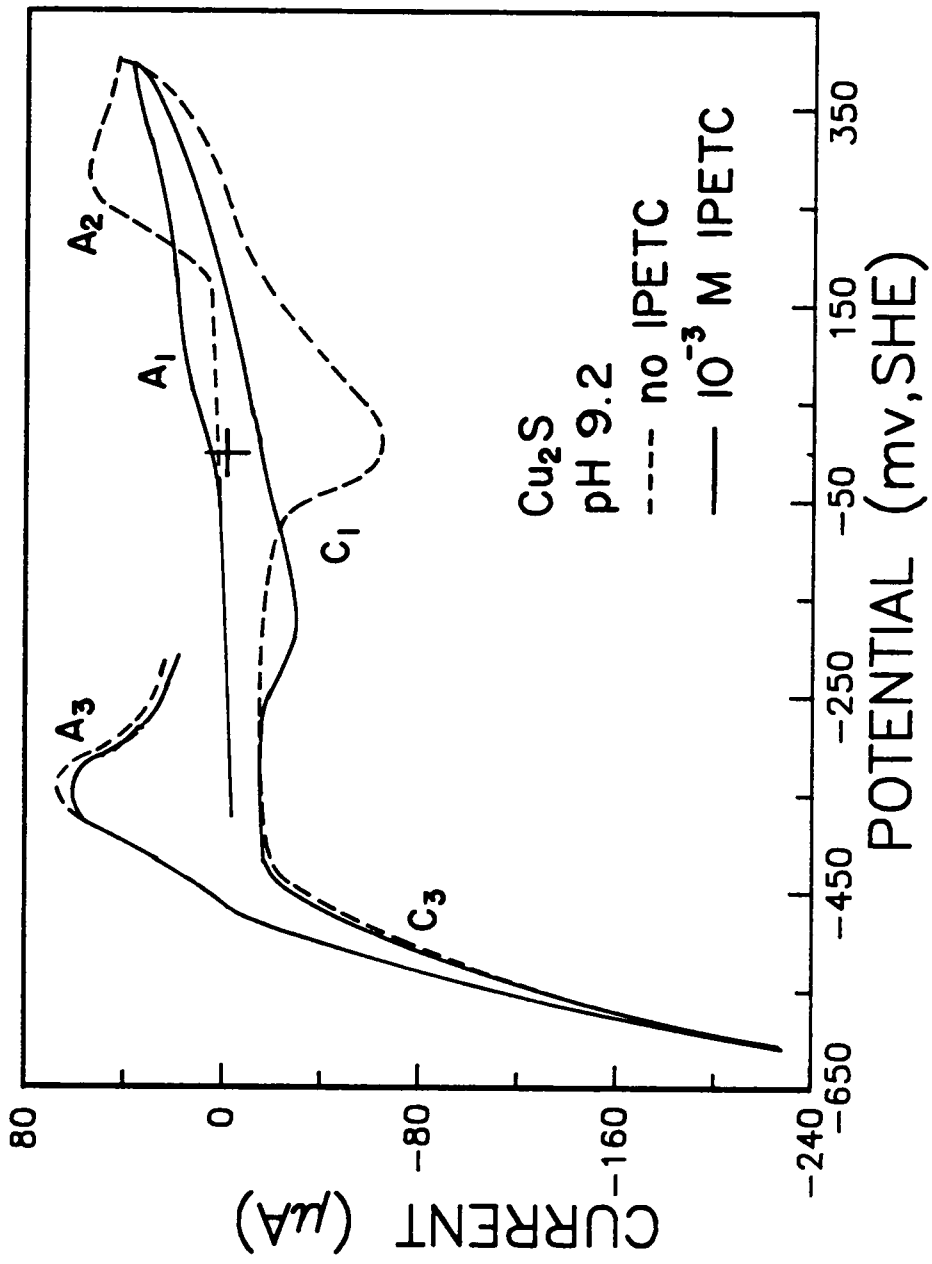

Figure 2.13. Voltammograms of chalcocite in unstirred 0.05 M $Na_2B_4O_7$ (pH 9.2) with and without 10^{-3} M IPETC. Scan rate = 50 mv/sec.

(C_1). On the return scan, C_1 is now observed near -150 mv. This shifting is typical of passivated electrodes. The rest of the voltammogram does not show any significant change with the addition of IPETC. It is interesting to note that there are no signs of IPETC adsorbing before the start of A_1. However, the E_h-pH diagrams indicate that the Cu-IPETC compound is already stable below this potential. The results of the contact angle and FTIR measurements would help clarify this discrepancy.

If the mechanism of IPETC adsorption on copper and chalcocite are similar, then A_1 would correspond to the reaction between IPETC and copper ions brought about by chalcocite oxidation. The possible reactions for this EC mechanism may be given by the following :

$$Cu_2S + xIPETC \rightarrow xCu(IPETC)^+ + Cu_{2-x}S + xe^-, \qquad [2.13]$$

$$nCu_2S + nxIPETC + xA^{n-} \rightarrow x[Cu(IPETC)]_nA + nCu_{2-x}S + nxe^-, \qquad [2.14]$$

or

$$Cu_2S + xIPETC \rightarrow xCu(IPETC)' + Cu_{2-x}S + xH^+ + xe^-. \qquad [2.15]$$

The first step involve in all three reactions is given by the following electrochemical reaction :

$$Cu_2S \rightarrow xCu^+ + Cu_{2-x}S + xe^-. \qquad [2.16]$$

The Cu(I) then reacts with IPETC according to either reactions [2.10], [2.11] or [2.12]. It should be pointed out that the reversibility of these reactions are not indicated in the voltammogram.

Chalcopyrite: The voltammograms for $CuFeS_2$ in unstirred 0 and 10^{-3}M IPETC solutions are shown in Figure 2.14. These were obtained by scanning the potential between -250 mv and 450 mv at 20 mv/sec. It can be seen that anodic current flows at potentials above -25 mv and gives rise to a peak at about 275 mv. This has been attributed by Gardner and Woods (1979) to the following reaction:

$$CuFeS_2 + 3H_2O \rightarrow CuS + Fe(OH)_3 + S^0 + 3H^+ + 3e^-. \qquad [2.17]$$

The continued increase in current above 350 mv (A_2) is attributed to the further oxidation of CuS to copper oxide. On the return scan, the reduction of the oxidation products is seen starting below 0 mv (C_1). Addition of 10^{-3}M IPETC does not considerably change the shape of the voltammograms of $CuFeS_2$. The major difference is seen in the change in the magnitude of the current flow. This is probably due to the non-electrochemical adsorption of IPETC on $CuFeS_2$, resulting in the passivation of the oxidation reactions. There is no evidence here of any IPETC adsorption reactions that are accompanied by an electron-transfer. The absence of any soluble copper species in the oxidation products of chalcopyrite at these conditions is probably responsible for this observation.

Pyrite: The last set of voltammograms obtained at pH 9.2 show the voltammetric behavior of FeS_2 in the absence and presence of 10^{-3}M IPETC (Figure 2.15). From a starting potential of -450 mv, the potential was scanned anodically to 450 mv at 50 mv/sec. The oxidation of pyrite is shown by the anodic peak, A_1, at around -50 mv and additional current flow starting above 150 mv (A_2). Anodic peak, A_1, corresponds to the formation of $Fe(OH)_3$ and elemental sulfur (Janetski et al., 1977; Hamilton and Woods, 1981). The steady increase in current at A_2 is associated with the further oxidation of pyrite to form $Fe(OH)_3$ and sulfate. On the return scan, a single cathodic peak, C_1, appears at around -250 mv corresponding to the reduction of both $Fe(OH)_3$

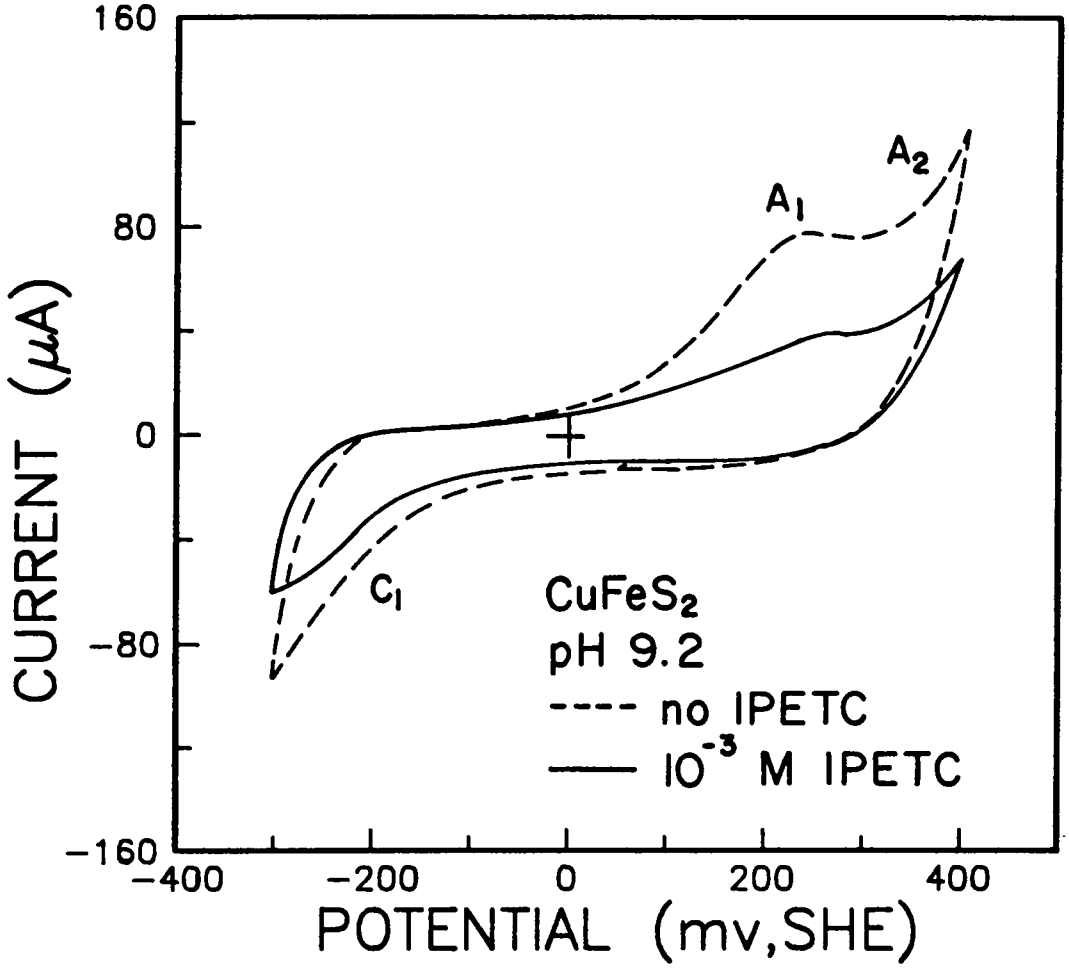

Figure 2.14. Voltammograms of chalcopyrite in unstirred 0.05 M $Na_2B_4O_7$ solution (pH 9.2) with and without 10^{-3} M IPETC. Scan rate = 50 mv/sec.

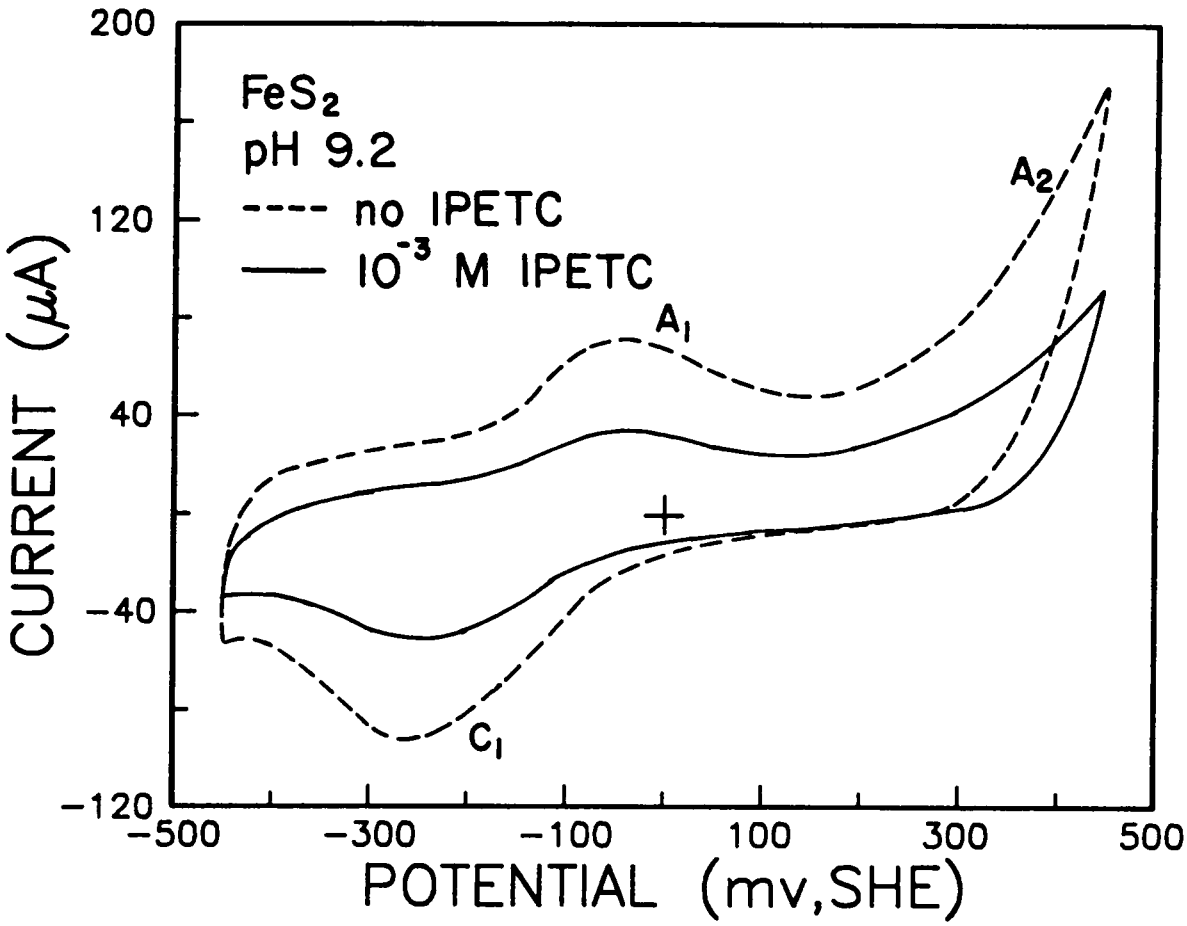

Figure 2.15. Voltammograms of pyrite in unstirred 0.05 M $Na_2B_4O_7$ solution (pH 9.2) with and without 10^{-3} M IPETC. Scan rate = 50 mv/sec.

and S^0 to iron sulfide. The likely product of sulfur reduction in the presence of iron oxide is FeS (Hamilton and Woods, 1981) , as shown by the following reaction:

$$Fe(OH)_3 + S^0 + 3e^- \rightarrow FeS + 3OH^-. \qquad [2.18]$$

The addition of 10^{-3}M IPETC does not considerably alter the shape of the voltammograms. Similar to what is observed for $CuFeS_2$, only a decrease in the current flow is found here. There is no apparent shift in the anodic and cathodic peaks. Again, the decrease in current may be attributed to the passivation of the electrode by non-electrochemical IPETC adsorption. IPETC, which is known to be selective against pyrite, would most probably be physisorbed on the electrode surface. It is interesting to note that the rest potential of pyrite in 100 ppm IPETC solution is 545 mv, while that of chalcopyrite is 195 mv (Goold and Finkelstein, 1972). Based on these investigators' measured E° of 195 mv for IPETC solution, the formation of an Fe-thionocarbamate complex is not feasible. The FTIR and contact angle data will help clarify this matter.

b. In the absence and presence of IPETC at pH 4.6

Platinum: To see the effect of pH, the voltammetric measurements were conducted in unstirred 0.5 M CH_3COOH/0.5 M $NaCH_3COO$ buffer solution (pH 4.6). The voltammograms for platinum were obtained by scanning the potential between -200 and 1000 mv at a sweep rate of 50 mv/sec. Figure 2.16 shows that the general electrochemical behavior of the platinum electrode is not affected by lowering the pH. The only difference, when compared to the voltammogram obtained at pH 9.2, is in the shift of the hydrogen and oxygen desorption/adsorption region to higher potentials. This shift of about 270 mv, agrees with theoretical calculations. Addition of 10^{-3}M IPETC solution results in the inhibition of the reactions involving hydrogen and oxygen.

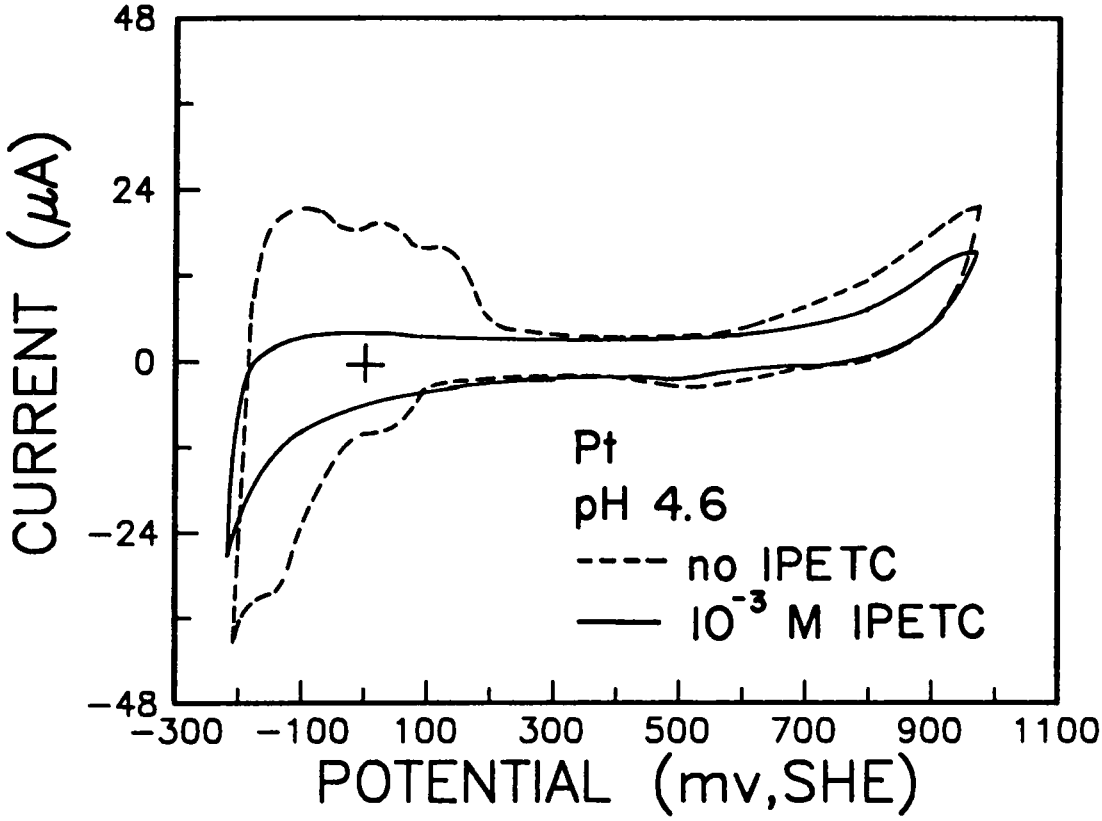

Figure 2.16. Voltammograms of platinum in unstirred 0.05 M CH_3COOH/0.05 M $NaCH_3COO$ solution (pH 4.6) with and without 10^{-3} M IPETC. Scan rate = 50 mv/sec.

This is similar to the observations found from the voltammograms obtained at pH 9.2. There is also no indication that the IPETC adsorption, which presumably caused the electrode passivation, involved any electron-transfer.

Copper: Voltammetry experiments were conducted on copper in the absence and presence of 10^{-3}M IPETC (Figure 2.17). At a scan rate of 50 mv/sec, the potential was cycled between -600 and 1350 mv. The oxidation of copper is observed to be shifted towards a higher potential at pH 4.6, which is expected since the oxidation of Cu^0 to copper oxides are pH-dependent reactions. The magnitude of this potential shift should be equal to 59 mv per pH unit. On the return scan, only a single cathodic peak, C_1', is found, instead of C_1 and C_2. This probably indicates that only a single oxidation product was produced. The other cathodic peaks, observed at pH 9.2, would appear here if the anodic limit were increased.

In the presence of 10^{-3}M IPETC, anodic peak, A_1, is observed before the start of the copper oxidation peak. This prewave has been associated with the electrochemical reaction involving IPETC and copper (reactions [2.6], [2.7] or [2.8]). It is interesting to note that A_1 has also been shifted by about 220 mv at pH 4.6, indicating the pH dependence of IPETC adsorption. This supports the pH dependent reaction [2.8] over reactions [2.6] or [2.7].

On the return scan, C_1' is smaller and shifted to a lower potential. The lower magnitudes of the current peak indicates the passivation of the electrode. Similar observations were also found for the adsorption of IPETC at pH 9.2.

Chalcocite: The voltammograms obtained for chalcocite without stirring at pH 4.6 are shown in Figure 2.18. At the starting potential of -500 mv, cathodic current is observed. This indicates the reduction of chalcocite by the following reaction:

$$Cu_2S + 2H^+ + 2e^- \rightarrow 2Cu^0 + H_2S_{(aq)}. \qquad [2.19]$$

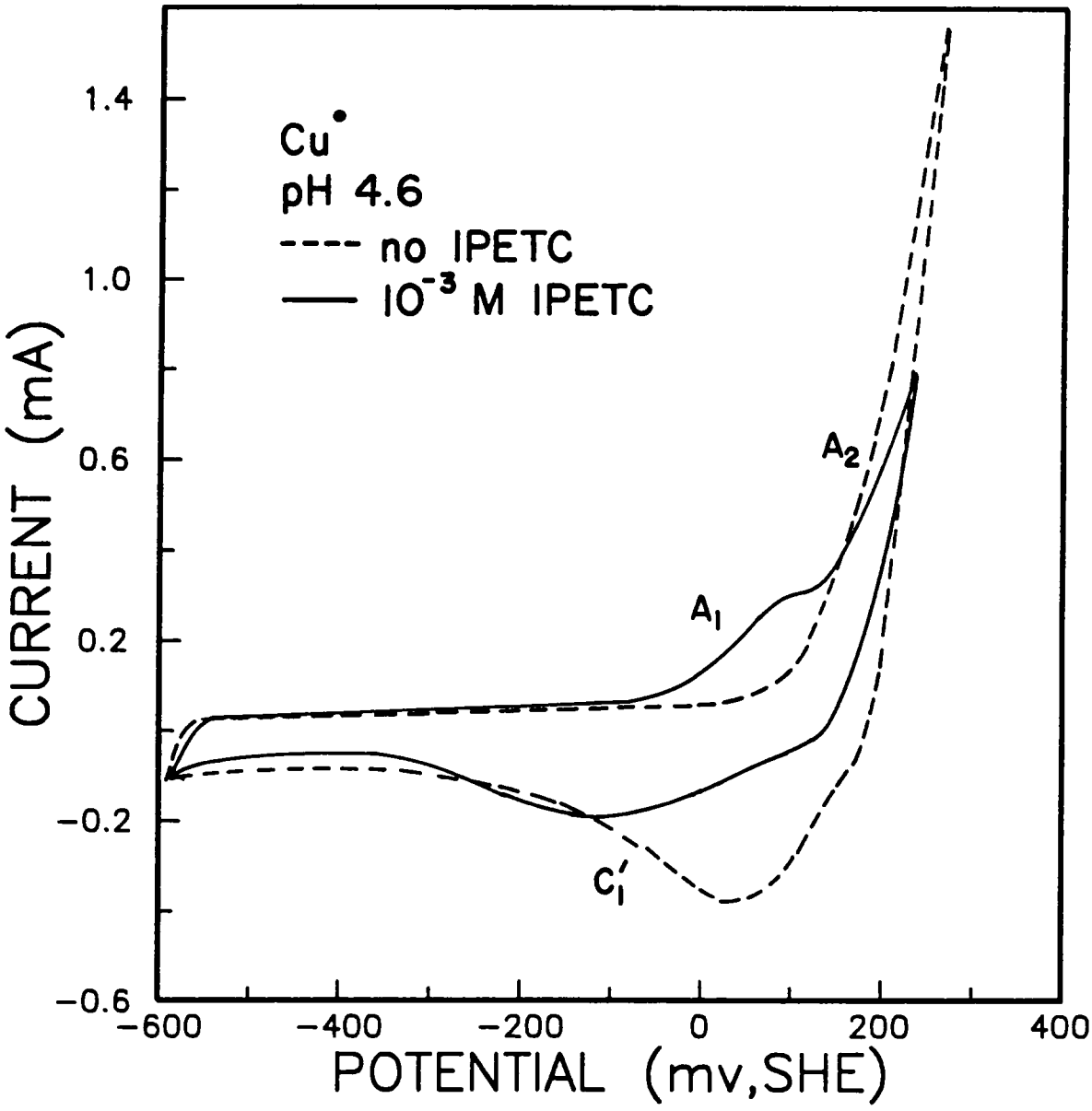

Figure 2.17. Voltammograms of copper in unstirred 0.05 M CH_3COOH/0.05 M $NaCH_3COO$ solution (pH 4.6) with and without 10^{-3} M IPETC. Scan rate = 50 mv/sec.

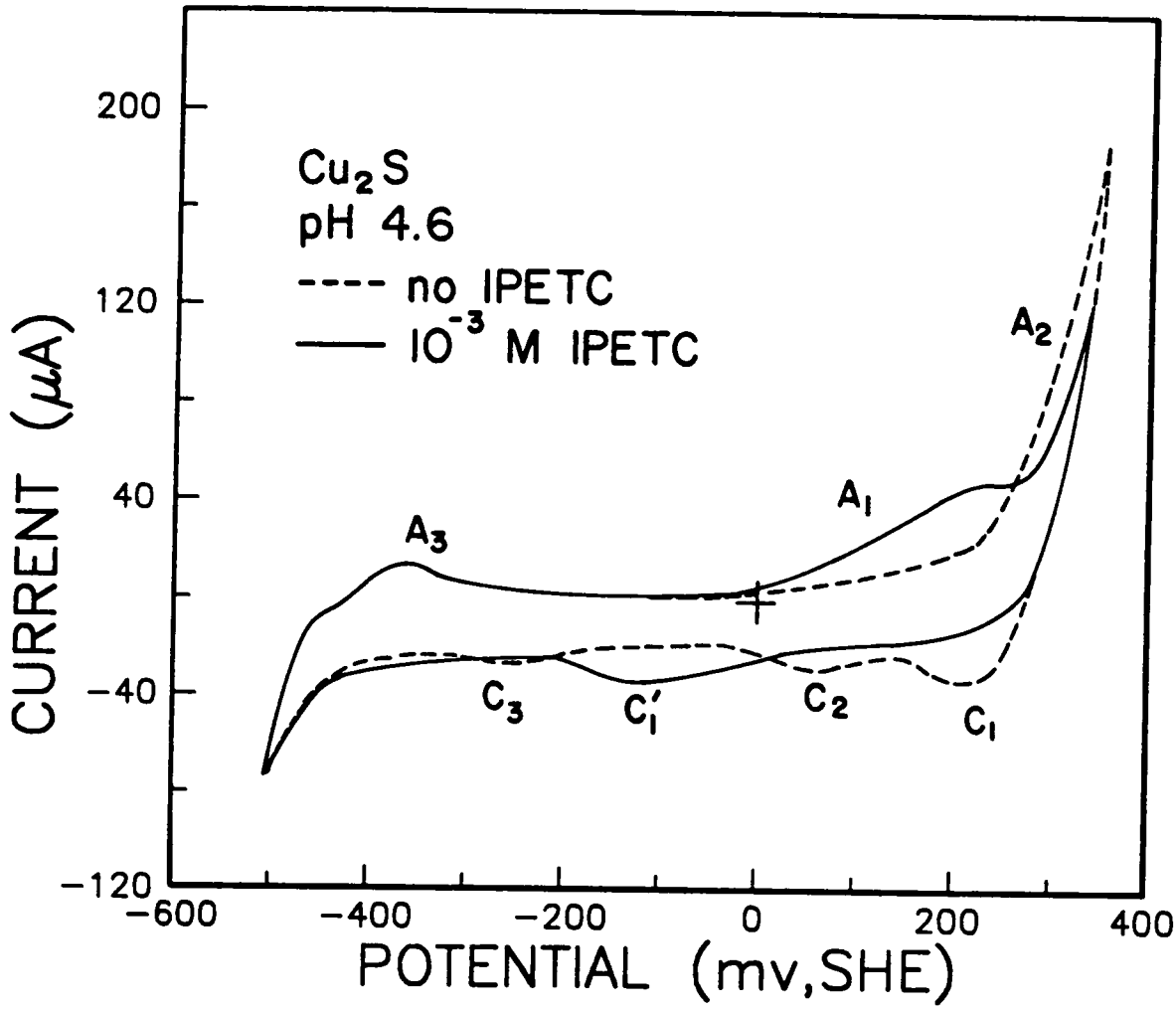

Figure 2.18. Voltammograms of chalcocite in unstirred 0.05 M CH_3COOH/0.05 M $NaCH_3COO$ solution (pH 4.6) with and without 10^{-3} M IPETC. Scan rate = 50 mv/sec.

As the potential is scanned anodically at 50 mv/sec, anodic peak, A_3, is observed above -425 mv. This is associated with the reverse of reaction [2.19]. Further oxidation of chalcocite is shown by the anodic peak, A_2, at higher potentials. A_2 would correspond to the formation of non-stoichiometric copper sulfide. It should be noted that A_2 is not shifted to higher potentials by the change in pH. This agrees with the pH-independent reaction [2.16] suggested for this anodic peak. Cathodic peaks, C_1 and C_2, correspond to the reverse of the oxidation reactions (Young et al., 1988).

The voltammogram for chalcocite in the presence of IPETC is also shown in Figure 2.18. On the initial scan and up to a potential below 0 mv, IPETC does not seem to affect the voltammogram. Above 0 mv, anodic current, A_1, starts to flow. This corresponds to the adsorption of IPETC according to either reactions [2.13], [2.14] or [2.15]. However, this peak has shifted at this pH, thus favoring reaction [2.15]. Similar to the adsorption on copper, this reaction is also pH-dependent. The current associated with A_2 decreases due to the passivation of the electrode surface by IPETC. On the return scan, a new peak, C_1', is observed below 0 mv, which presumably has replaced C_1 and C_2. As is shown in the voltammogram at pH 9.2, the passivation of the electrode surface prevented the further oxidation of chalcocite. The reduction peaks are shifted as a result of this behavior.

Chalcopyrite: Figure 2.19 shows the voltammetric behavior of chalcopyrite without stirring at pH 4.6. The voltammograms have an upper and lower potential limit of 600 and -530 mv, respectively, with a starting potential of -550 mv. Chalcopyrite oxidation starts at about -100 mv and has been explained by the following reaction (Gardner and Woods, 1979):

$$CuFeS_2 \rightarrow CuS + Fe^{2+} + S^0 + 2e^-. \qquad [2.20]$$

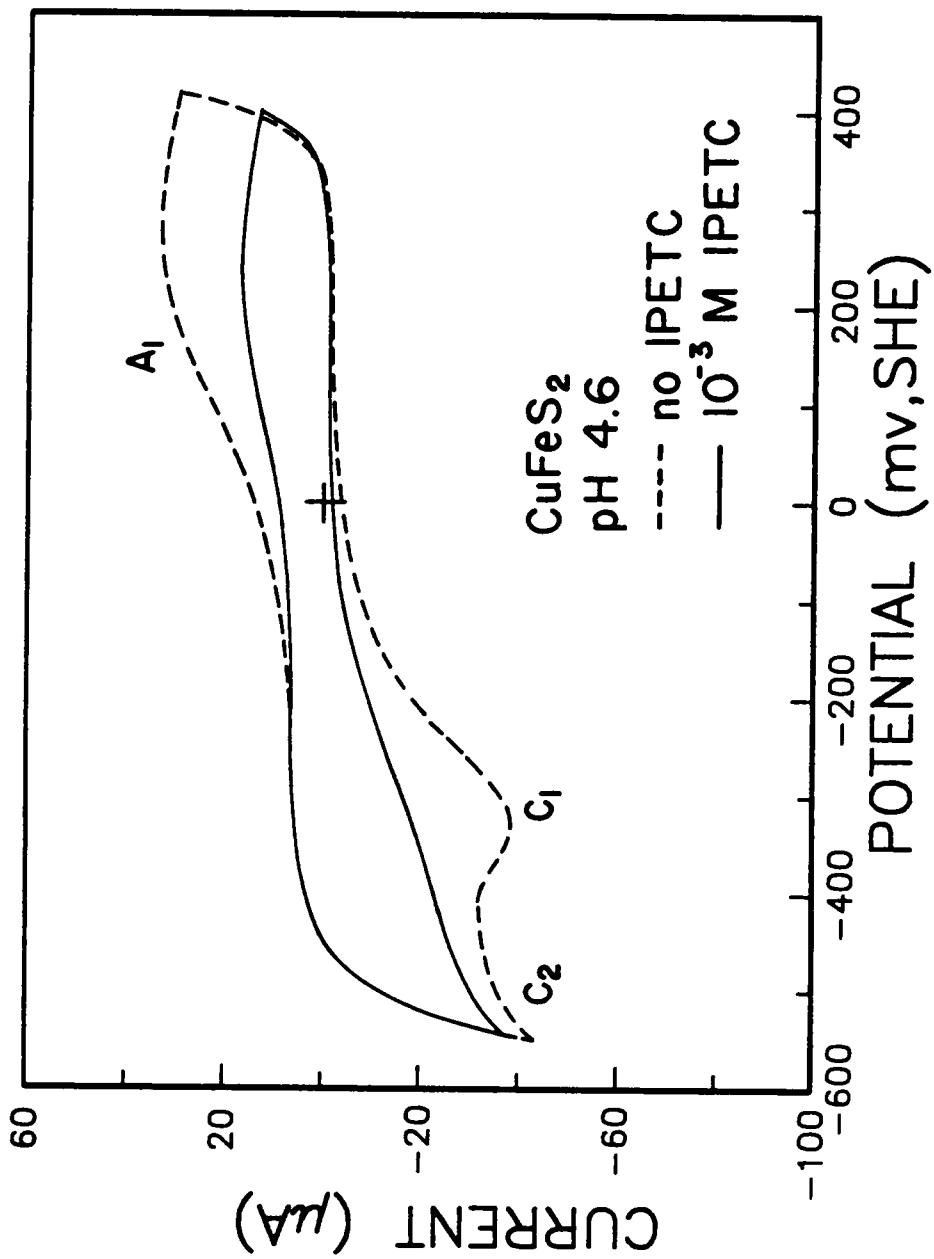

Figure 2.19. Voltammograms of chalcopyrite in unstirred 0.05 M CH_3COOH/0.05 M $NaCH_3COO$ solution (pH 4.6) with and without 10^{-3} M IPETC. Scan rate = 50 mv/sec.

This reaction is different from reaction [2.17] because oxidation of iron proceeds only as far as Fe(II) at acidic conditions. The reverse of reaction [2.20] is shown by the cathodic current on the reverse sweep. However, in stirred solutions, the reverse of this reaction would not be expected.

The addition of 10^{-3}M IPETC does not considerably alter the shape of the voltammogram. Passivation of the electrode occurs over the entire scan range as it does at pH 9.2. This has been previously attributed to potential-independent adsorption of IPETC. It is interesting to note that even though soluble iron species are produced by chalcopyrite oxidation, no apparent electrochemical reaction with IPETC was observed. This is consistent with the solvent extraction studies of Seryakova et al. (1975) , who found that IPETC does not extract Fe-ions. Experiments involving the precipitation of thionocarbamate compounds (discussed later in Chapter 3.0) also show that IPETC does not seem to form a precipitate with Fe-ions. This is an indication of the selectivity of the reagent against iron sulfides.

Pyrite: The voltammograms for pyrite at pH 4.6 are shown in Figure 2.20. The potential sweeps started at -450 mv and proceeded in the anodic direction at a scan rate of 50 mv/sec. In the absence of any collector, the reducing currents are observed at the starting potential. This may be attributed to the reduction of pyrite to produce FeS and H_2S. On the initial scan, anodic currents at A_1 are observed. This is due to the reverse of the initial reduction reaction. However, the difference in the charge associated with A_1 and C_1 suggests that not all of the H_2S is reacted with FeS to form FeS_2. The anodic peak, A_2, observed above 0 mv, therefore, may be represented by the following reaction:

$$H_2S \rightarrow S^0 + 2H^+ + 2e^-. \qquad [2.21]$$

Similar observations were also made by Hamilton and Woods (1981).

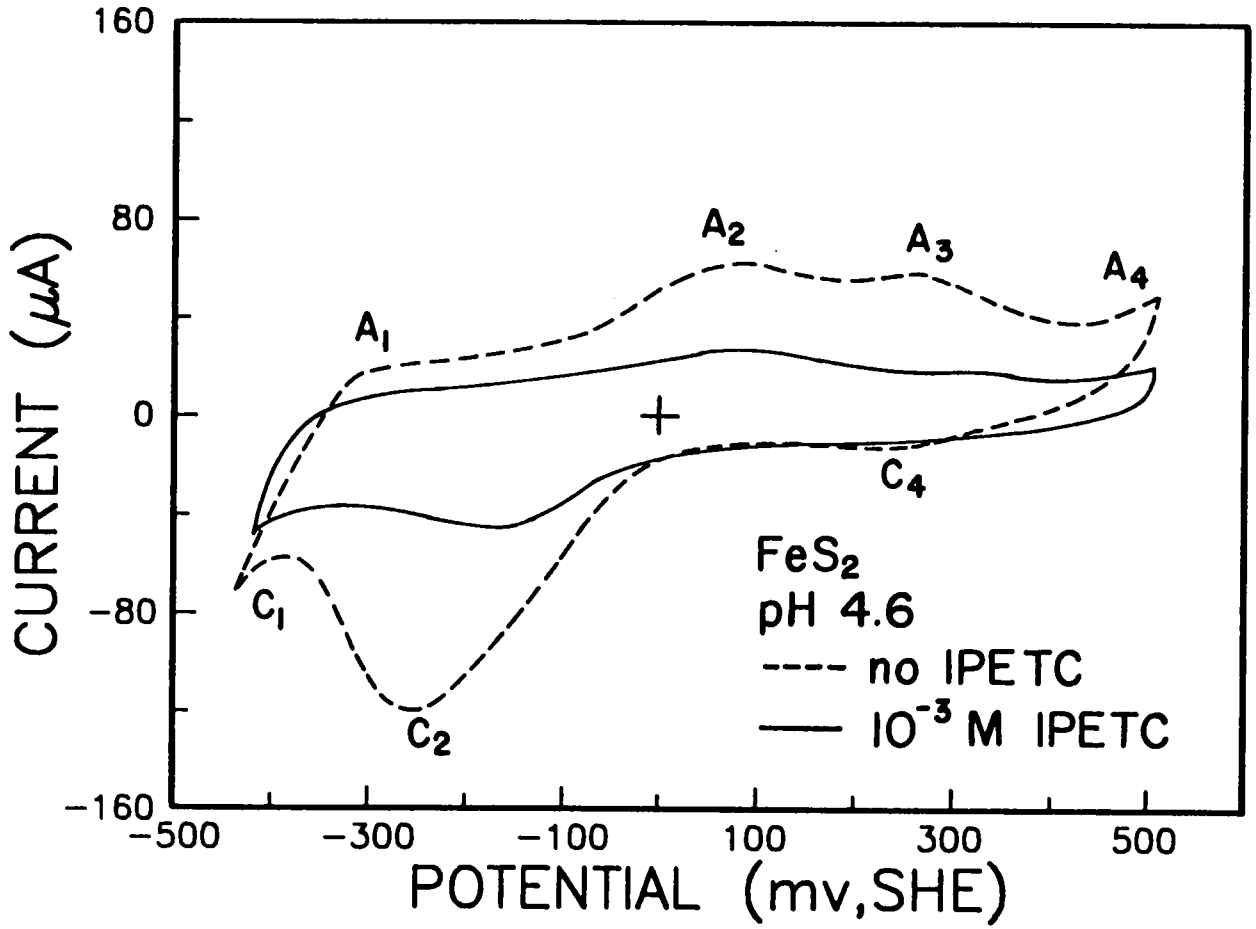

Figure 2.20. Voltammograms of pyrite in unstirred 0.05 M CH_3COOH/0.05 M $NaCH_3COO$ solution (pH 46) with and without 10^{-3} M IPETC. Scan rate = 50 mv/sec.

The oxidation of pyrite is shown by the anodic peak, A_3, which corresponds to pyrite oxidation to either elemental sulfur,

$$FeS_2 \rightarrow Fe^{2+} + 2S^0 + 2e^- \qquad [2.22]$$

or sulfate,

$$FeS_2 + 8H_2O \rightarrow Fe^{2+} + 2SO_4^{2-} + 16H^+ + 14e^-. \qquad [2.23]$$

The continued increase in anodic current, A_4, above 400 mv, may be attributed to the oxidation of Fe(II) to $Fe(OH)_3$. On the return scan, the reverse of this reaction is shown by cathodic peak, C_4, near 250 mv. The reduction of sulfur is shown by the large cathodic current at C_2.

Inhibition of the oxidation and reduction reactions is observed when 10^{-3}M IPETC is added. This may also be attributed to the non-electrochemical adsorption of IPETC. Again, there is no evidence here to suggest the oxidation or reduction of IPETC on the pyrite electrode.

c. In the absence and presence of IBECTC at pH 4.6

The effect of IBECTC on the voltammetric behavior of Pt^0, Cu^0, Cu_2S, $CuFeS_2$ and FeS_2 electrodes are shown by the next series of voltammograms obtained at a scan rate of 50 mv/sec. All of the measurements were carried out in unstirred 0.5 M CH_3COOH/0.5 M $NaCH_3COO$ solutions (pH 4.6). Since there is no apparent effect of pH on the electrochemistry of thionocarbamates, except on copper and chalcocite, experiments were limited to this pH only. It should also be pointed out that the applicability of IBECTC is at neutral to acidic conditions.

Platinum: The addition of 10^{-3}M IBECTC results in the same effect as that of IPETC addition on platinum over the potential range of -200 to 1200 mv (Figure 2.21). The inhibition of the hydrogen and oxygen adsorption/desorption reactions is probably due to non-electrochemical adsorption of IBECTC. The voltammogram also does not show any evidence of IBECTC oxidation or reduction on the platinum surface, strongly suggesting that IBECTC is also electrochemically inactive at these experimental conditions.

Copper: The voltammogram for Cu^0 in 10^{-3}M IBECTC is shown in Figure 2.22. This was obtained by scanning the potential between -750 and 300 mv. The voltammogram for Cu^0 when no collector is added, is also shown for comparison. The electrode is observed to be passivated by the adsorption of IBECTC on the Cu^0 surface. However, a new anodic peak, A_1, is observed above 0 mv when IBECTC is added. This may be associated with the electrochemical reaction between copper and IBECTC. Similar to the observations made for the IPETC-Cu^0 system, A_1 may be due to the formation of a complex between copper and IBECTC. Assuming an EC mechanism, the initial electrochemical step would be reaction [2.9] followed by, depending on the Cu-IBECTC complex formed, the chemical reaction with IBECTC :

$$Cu^+ + IBECTC \rightarrow Cu(IBECTC)^+, \qquad [2.24]$$

$$nCu^+ + nIBECTC + A^{n-} \rightarrow [Cu(IBECTC)]_nA, \qquad [2.25]$$

$$Cu^+ + IBECTC \rightarrow Cu(IBECTC)' + H^+, \qquad [2.26]$$

where (IBECTC)′ = (C_4H_9-OCSN$^-$OCO-C_2H_5).

The cathodic peak, C_1, observed in the return scan is shifted to lower potentials by the addition of IBECTC. The passivation of the electrode brought about by the formation of the Cu-IBECTC complex would probably be responsible for this shift in

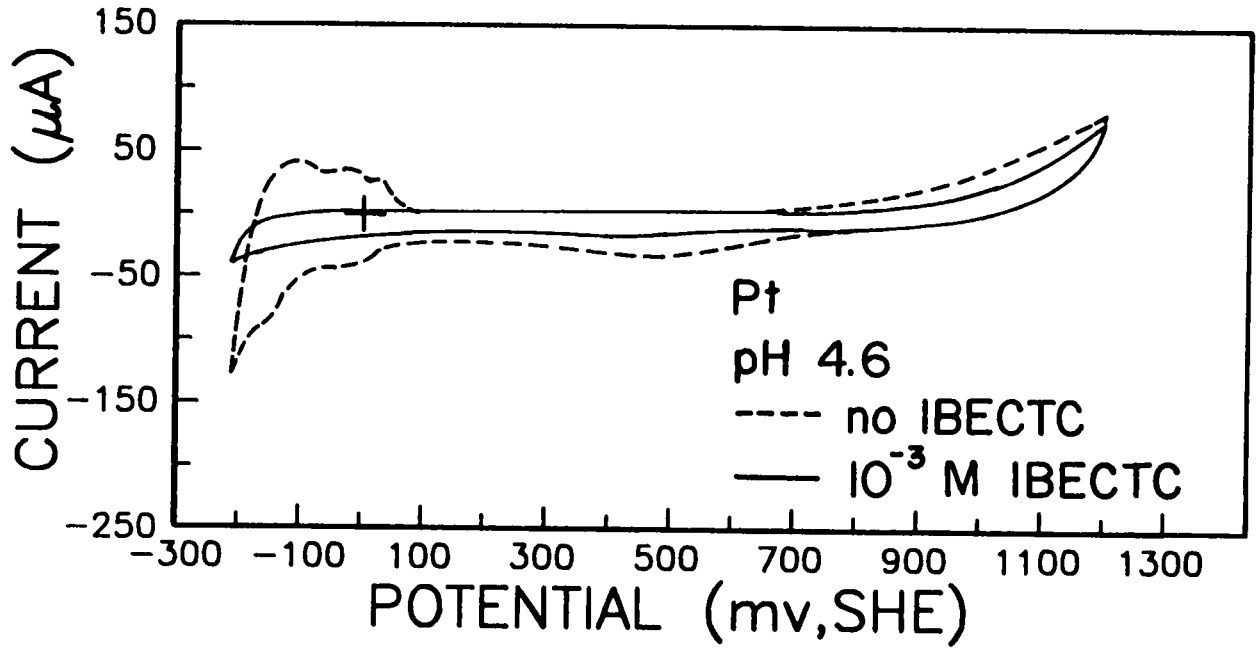

Figure 2.21. Voltammograms of platinum in unstirred 0.05 M CH_3COOH/0.05 M $NaCH_3COO$ solution (pH 4.6) with and without 10^{-3} M IBECTC. Scan rate = 50 mv/sec.

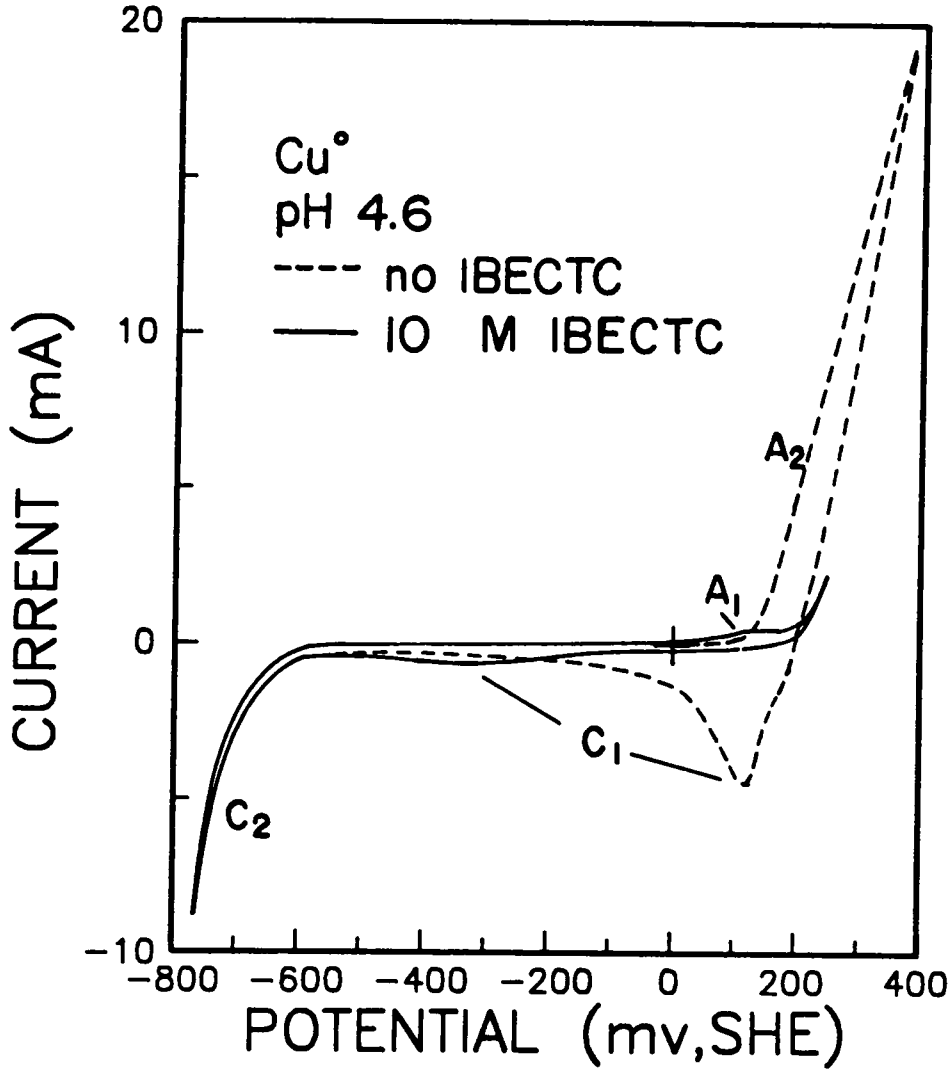

Figure 2.22. Voltammograms of copper in unstirred 0.05 M CH_3COOH/0.05 M $NaCH_3COO$ solution (pH 4.6) with and without 10^{-3} M IBECTC. Scan rate = 50 mv/sec.

potential. The sharp decrease in currents at much lower potentials, C_2, is due to the reduction of oxidized copper to Cu^0. There seems to be no evidence in the voltammogram of the reverse of the anodic reaction associated with A_1. For coupled chemical reactions of this type, a reverse peak may become apparent at higher sweep rates. Unfortunately, the slew rate of the X-Y recorder used here is insufficient to record the voltammogram at the required high scan rates (> 0.5 V/sec) without distorting it.

Chalcocite: The effect of IBECTC on the voltammetric behavior of chalcocite is shown in Figure 2.23. The scan was started at -750 mv with upper and lower limits of 400 and -750 mv, respectively. In the presence of IBECTC, the shape of the voltammogram is similar to the one obtained with IPETC (Figure 2.18). The interaction of IBECTC with chalcocite is shown by the anodic peak, A_2, which occurs above 0 mv. A_2 probably corresponds to a reaction similar to those given previously for the Cu_2S-IPETC system :

$$Cu_2S + xIBECTC \rightarrow xCu(IBECTC)^+ + Cu_{2-x}S + xe^- , \qquad [2.27]$$

$$nCu_2S + nxIBECTC + A^{n-} \rightarrow x[Cu(IBECTC)]_nA + nCu_{2-x}S + nxe^- , \qquad [2.28]$$

$$Cu_2S + xIBECTC \rightarrow xCu(IBECTC)' + Cu_{2-x}S + xH^+ + xe^- . \qquad [2.29]$$

This is the overall reaction for the EC mechanism which involves reaction [2.16] followed by the chemical reaction with IBECTC. After the adsorption of IBECTC, the oxidation of chalcocite is observed to be inhibited. The lower current at A_3 suggests passivation of the electrode surface. On the return cathodic scan, the reduction peaks have decreased drastically. There seems to be no evidence in the voltammogram suggesting the reversibility of the reaction corresponding to A_2. However, as mentioned previously, an increase in scan rate may show the reverse peak in the voltammogram. It is also not

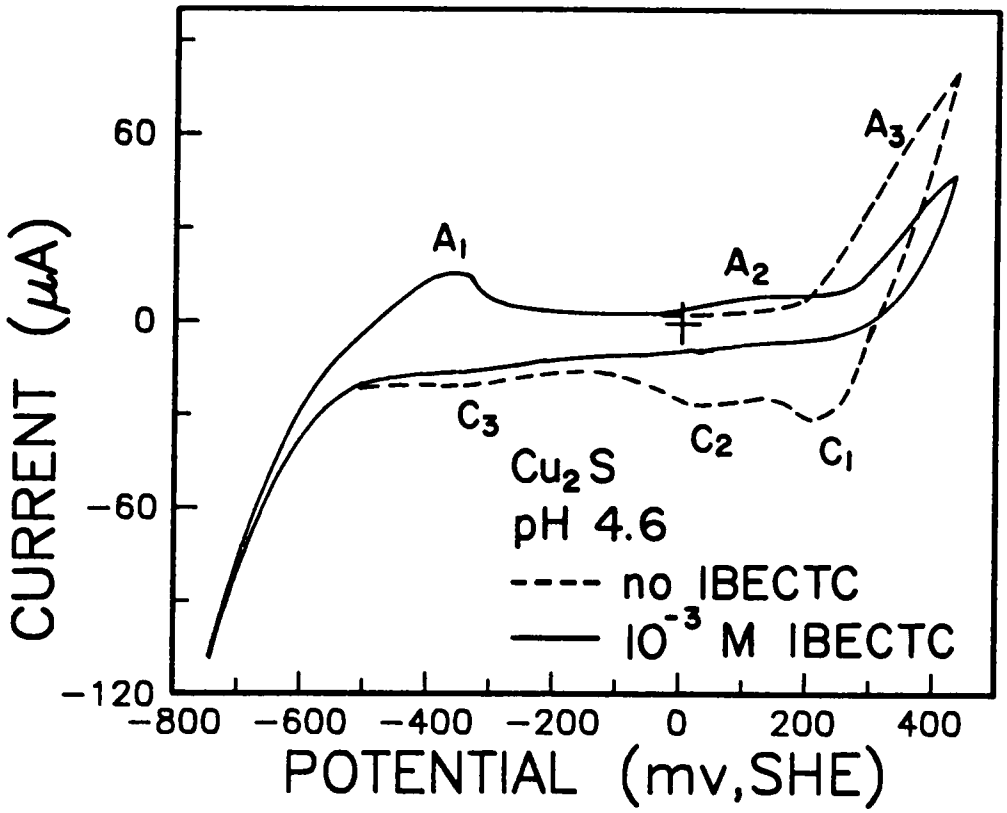

Figure 2.23. Voltammograms of chalcocite in unstirred 0.05 M CH_3COOH/0.05 M $NaCH_3COO$ solution (pH 4.6) with and without 10^{-3} M IBECTC. Scan rate = 50 mv/sec.

clear whether there is non-electrochemical IBECTC adsorption occurring at the starting potential.

Chalcopyrite: Figure 2.24 shows the voltammograms for chalcopyrite in the absence and presence of 10^{-3}M IBECTC. The scan was carried out between -400 and 400 mv. The shapes of the voltammograms are similar to the ones obtained for the $CuFeS_2$-IPETC system. The only apparent effect of IBECTC addition is the passivation of the electrode surface over the entire scan range. This may also be attributed to the non-electrochemical adsorption of IBECTC. The absence of any chalcopyrite-IBECTC interaction is probably due to the oxidation of $CuFeS_2$ to CuS, instead of soluble copper species. It is the formation of soluble copper species that is responsible for the thionocarbamate interaction with copper and chalcocite. Also, the soluble iron species produced during the oxidation does not apparently cause any electrochemical reaction between IBECTC and the electrode. Precipitation reactions show that IBECTC does not form any visible precipitate with Fe ions (discussed later in Chapter 3.0.). Both IPETC and IBECTC exhibit this behavior, which indicates the good selectivity of these reagents against iron sulfides.

Pyrite: The last set of voltammograms show the effect of IBECTC on pyrite oxidation and reduction at pH 4.6 (Figure 2.25). These were obtained by scanning the potential from an initial potential of -450 mv to an upper limit of 500 mv. The addition of 10^{-3}M IBECTC does not alter the general shape of the voltammogram. The only difference lies in the lower magnitude of the current. Passivation of the electrode is responsible for the inhibition of the electrochemical reactions. Again, there is no apparent electron-transfer involved in the adsorption of IBECTC on pyrite.

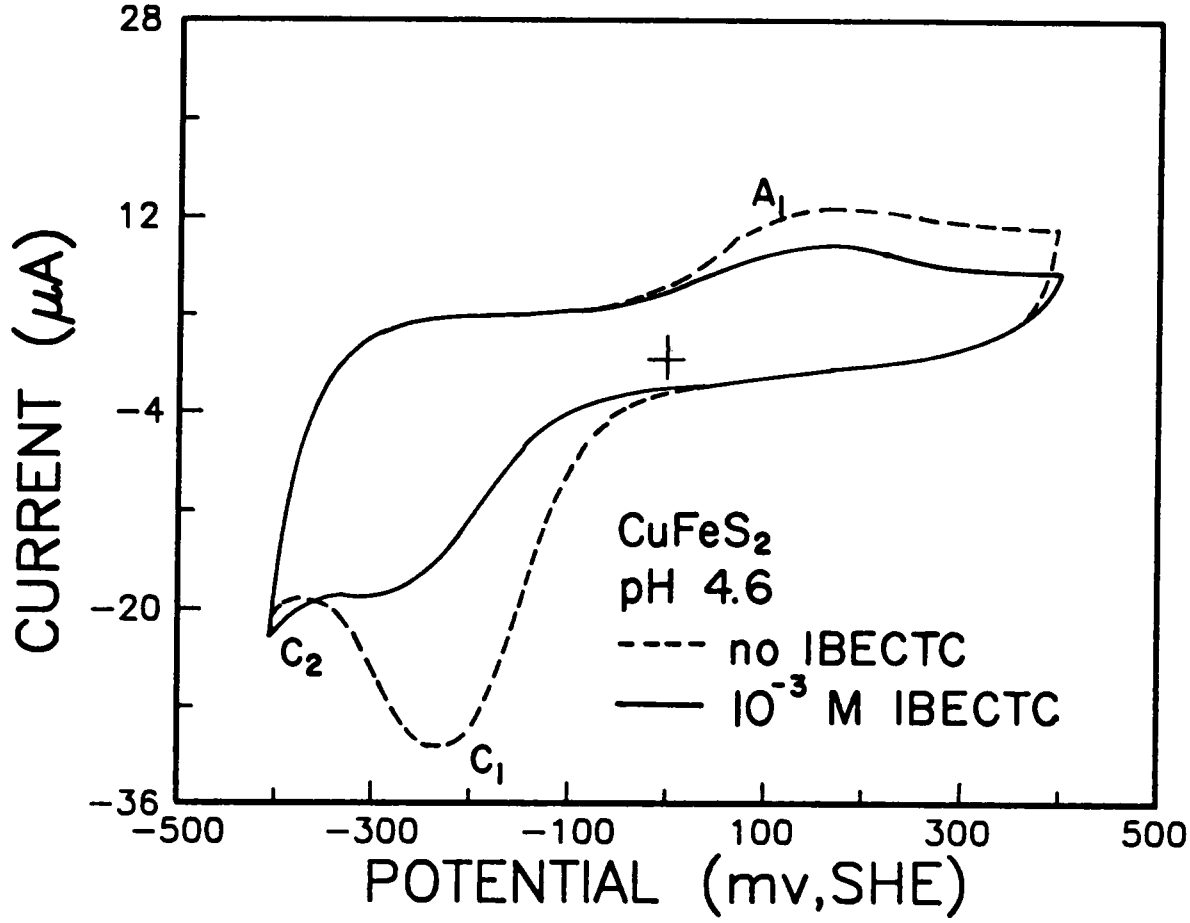

Figure 2.24. Voltammograms of chalcopyrite in unstirred 0.05 M CH_3COOH/0.05 M $NaCH_3COO$ solution (pH 4.6) with and without 10^{-3} M IBECTC. Scan rate = 50 mv/sec.

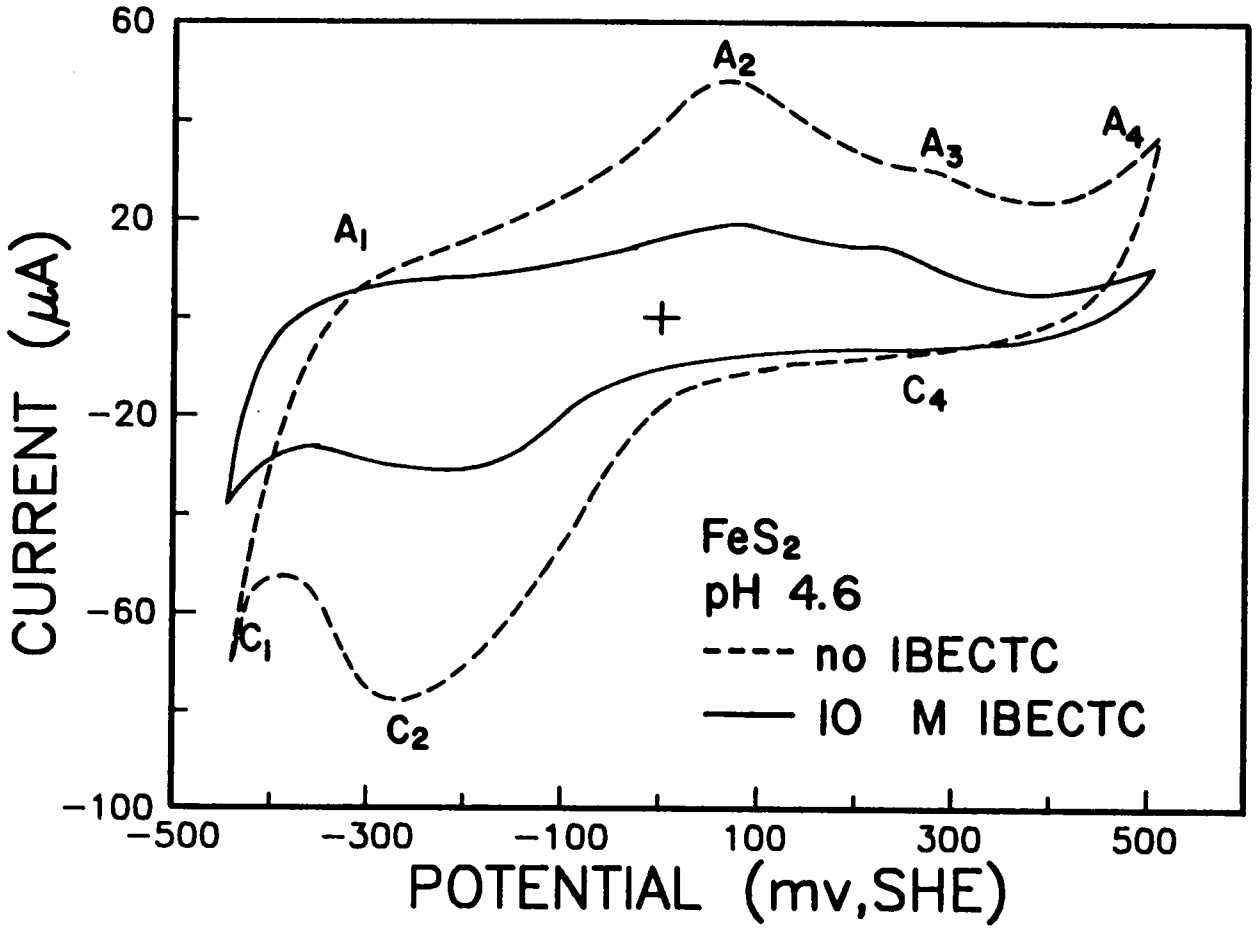

Figure 2.25. Voltammograms of pyrite in unstirred 0.05 M CH_3COOH/0.05 M $NaCH_3COO$ solution (pH 4.6) with and without 10^{-3} M IBECTC. Scan rate = 50 mv/sec.

2.3.3 Microflotation

Microflotation tests have been conducted to study the effect of pH on the floatability of chalcocite, chalcopyrite and pyrite using IPETC and IBECTC. These tests were carried out at collector additions of 10^{-6} and 10^{-7}M. The pH was adjusted by using either HCl or NaOH solutions. Flotation behavior of chalcocite using IPETC and IBECTC were also studied at different thionocarbamate concentrations.

a. Effect of pH

The natural floatabilities of chalcocite, chalcopyrite and pyrite were studied by doing the flotation experiments in the absence of a collector at different pH conditions. The results are given as a function of pH in Figure 2.26. Chalcocite shows almost negligible natural floatability over the entire pH range except at pH 6. Chalcopyrite, which is known to have natural floatability at certain conditions, shows good floatability in acidic solutions. The flotation recovery for chalcopyrite decreases with increasing pH. On the other hand, the pyrite samples used here are almost completely hydrophilic over the entire pH range. In general, it is only chalcopyrite which shows significant natural floatability.

The addition of 10^{-7}M IPETC increased the recovery of all three sulfide minerals. Figure 2.27 shows the flotation behavior of chalcocite, chalcopyrite and pyrite as a function of pH. The recovery of chalcocite decreases sharply below pH 8. For chalcopyrite, the recovery decreases continuously with increasing pH. Floatability is good up to pH 6 and drops significantly at pH 10 and 12. Probably because of its natural floatability, chalcopyrite recovery is greater when compared to chalcocite. Pyrite remains hydrophilic over the entire pH range studied in these experiments. It does not

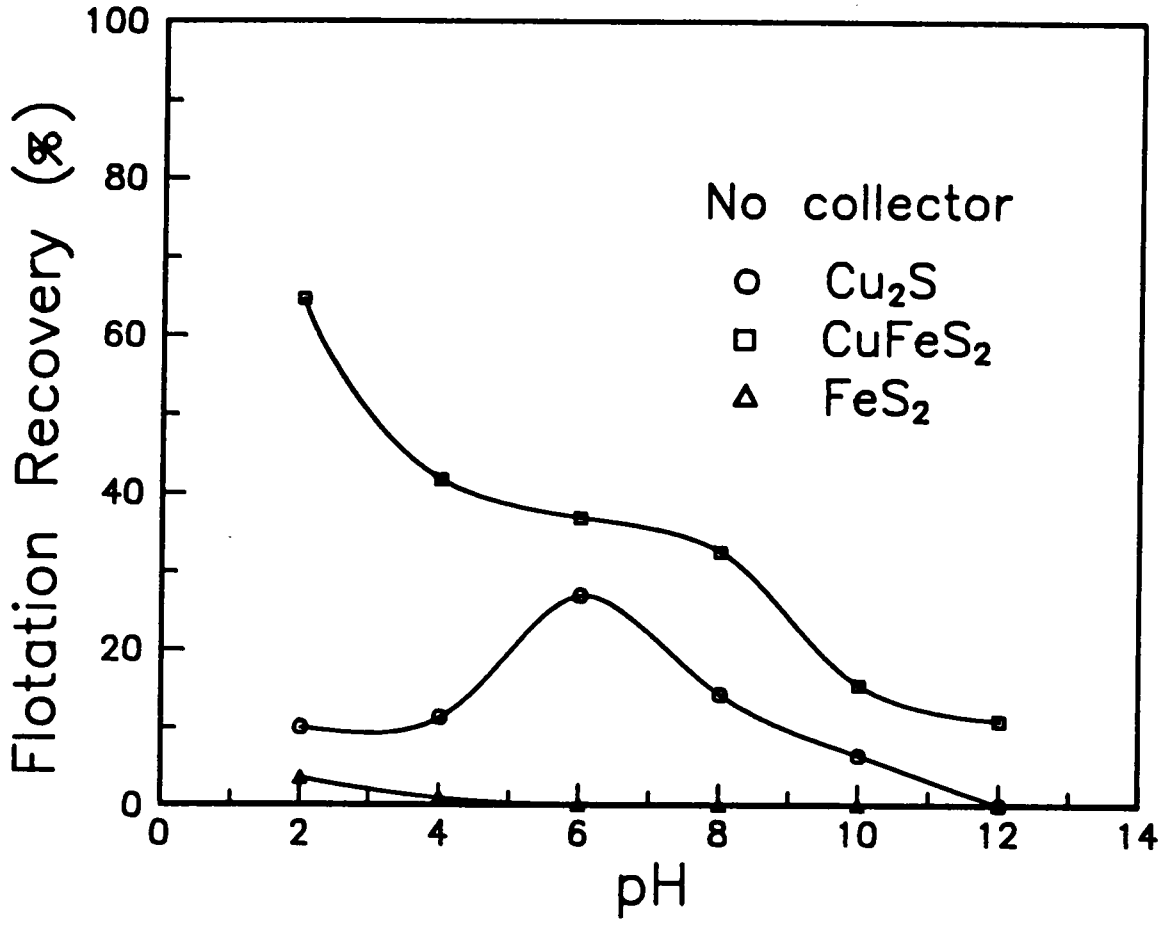

Figure 2.26. The effect of pH on the flotation recovery of chalcocite, chalcopyrite and pyrite in the absence of any collector.

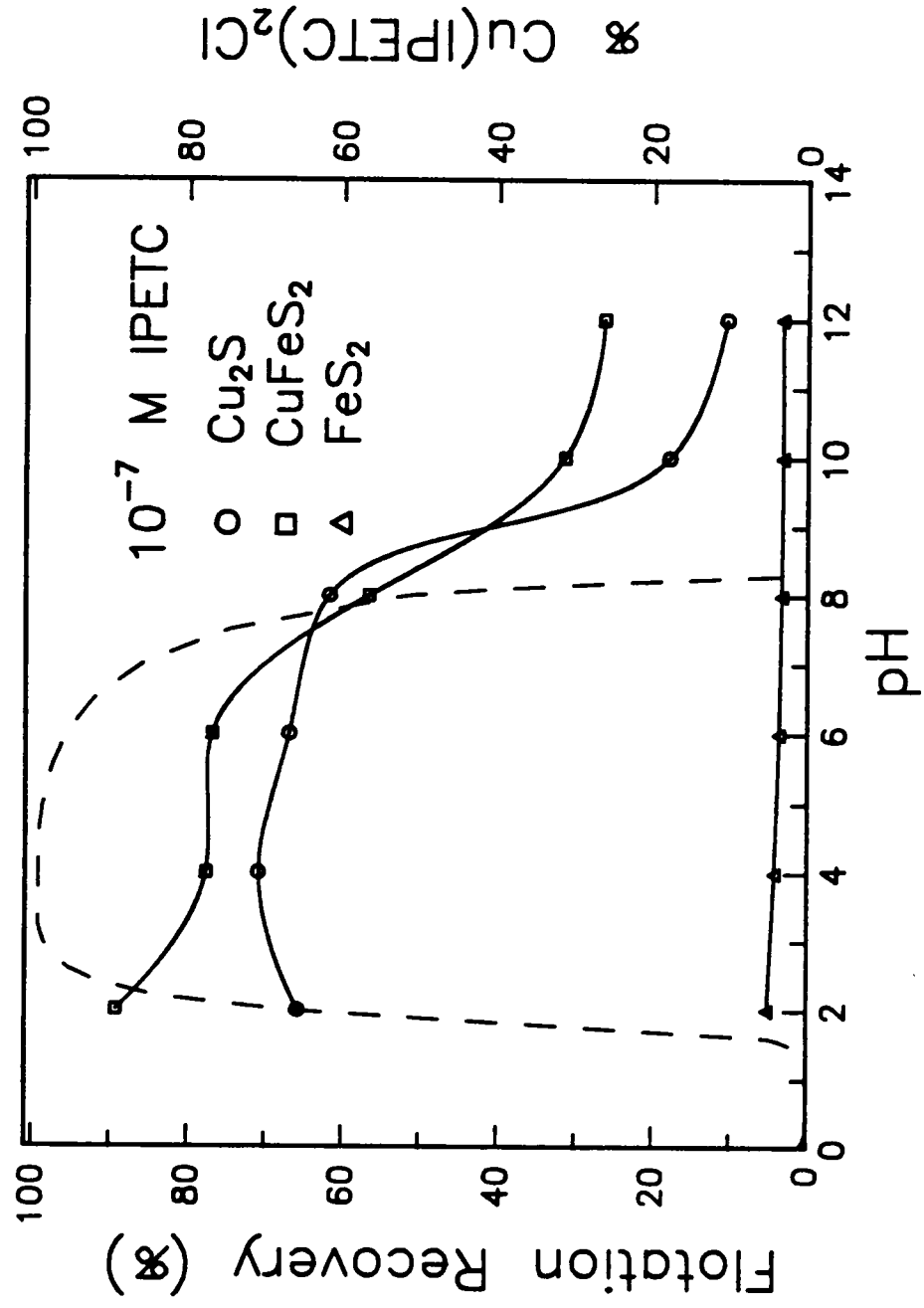

Figure 2.27. Effect of pH on the flotation recovery of chalcocite, chalcocpyrite and pyrite in the presence of 10^{-7} M IPETC and on % $Cu(IPETC)_2Cl$ calculated for Cu_2S at 200 mv.

show any significant floatability even at acidic conditions, providing an evidence for the good selectivity of IPETC against pyrite flotation. The results shown in Figure 2.27 suggest that the copper sulfides can be separated from pyrite using this low IPETC concentration at pH $\leq$ 8.

Also shown in Figure 2.27 is the effect of pH on % $Cu(IPETC)_2Cl$ as determined by the thermodynamic calculations for the Cu_2S-H_2O systems. The computations have been carried out in the presence of the same amount of IPETC and at an E_h of 200 mv. This potential is near the average open-circuit potential measured in the flotation experiments. The thermodynamic predictions are in reasonable agreement with the flotation results for Cu_2S.

When the IPETC addition was increased to 10^{-6}M, an increase in the recovery of the three sulfide minerals was observed (Figure 2.28). The flotation results show that chalcocite recovery is now about 100% at pH $\leq$ 8. The thermodynamic calculations for Cu_2S also show a similar response to pH at this concentration. However, there is some discrepancy observed at alkaline conditions. Flotation recovery decreases slightly at pH > 8, while % $Cu(IPETC)_2Cl$ drops to zero at pH 9.4. It is interesting to note that the calculations agree better with the chalcopyrite flotation data. For chalcopyrite, flotation recovery was good up to pH 8 and then decreases substantially at pH 10 and 12. The floatability of pyrite is affected by IPETC only at very acidic conditions. It shows good flotation recovery at pH 2 and 4, but remains hydrophilic at pH $\geq$ 6. Collectorless flotation studies for pyrite using MIBC as a frother showed a similar behavior (Leppinen, 1986; Celik, 1988). It should be noted that IPETC has been found to have slight frothing properties (Dow, 1968). Therefore, the floatability at acidic conditions may possibly be brought about by the frothing property of IPETC. It can be inferred from these results that selective flotation of copper sulfides from an ore that also contains pyrite may be feasible with 10^{-6}M IPETC at pH $\geq$ 6.

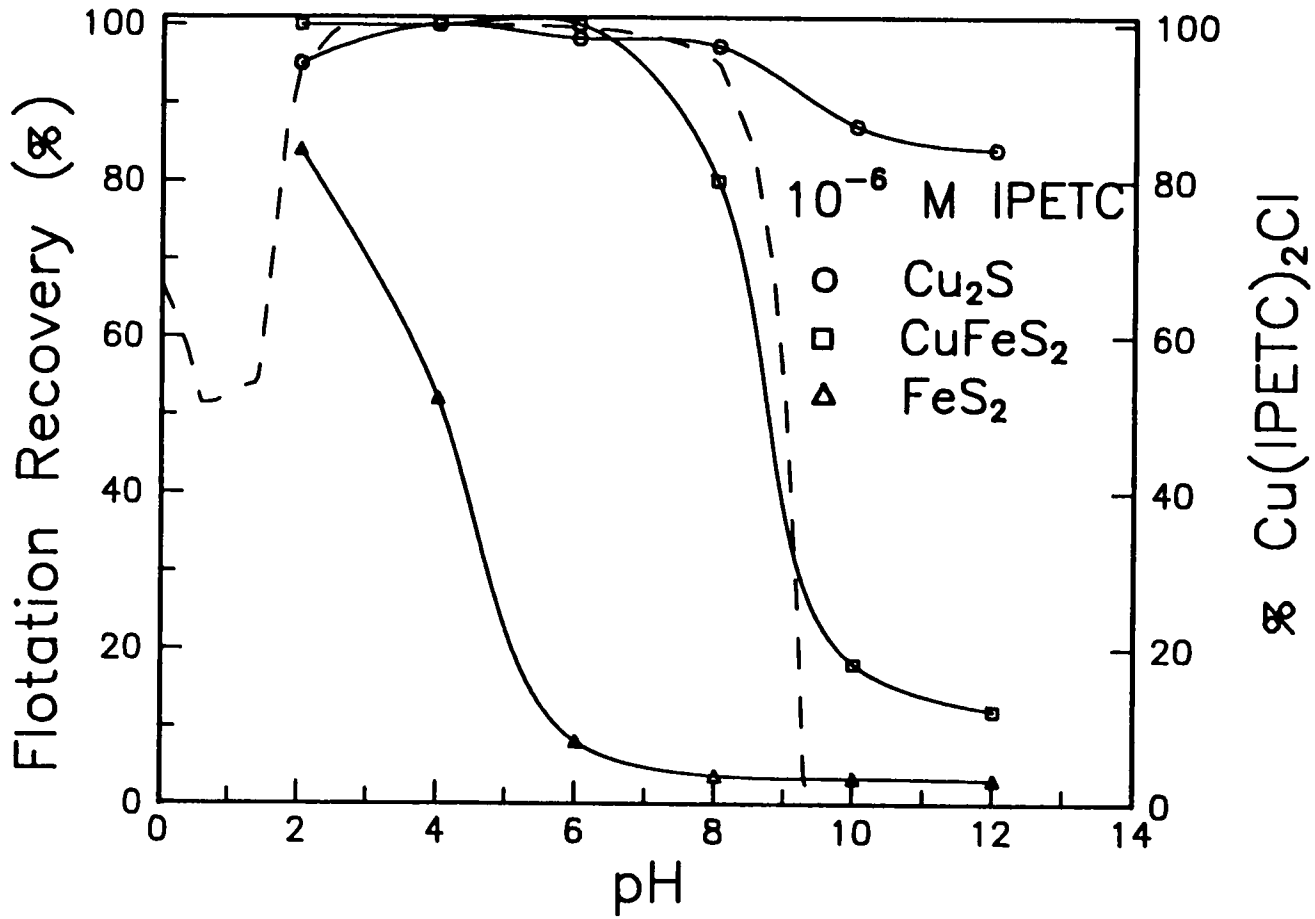

Figure 2.28. Effect of pH on the flotation recovery of chalcocite, chalcocpyrite and pyrite in the presence of 10^{-6} M IPETC and on % $Cu(IPETC)_2Cl$ calculated for Cu_2S at 200 mv.

Figure 2.29 shows the flotation results obtained using 10^{-7}M IBECTC at different pH conditions. Compared to collectorless flotation, there is an increase in the flotation recovery for all three sulfide minerals. Chalcocite recovery is good up to pH 6 and it decreases at higher pH. % $Cu((IBECTC)_2Cl$ is also maximum at around this pH range. The curve shows an interesting decrease starting above pH 0 and reaches a minimum value at about pH 1.2. At higher pH, however, the curve increases again. This correponds to the equilibrium between Cu_2S and CuS in the calculations.

The floatability of chalcopyrite decreases continuously with increasing alkalinity but has higher recoveries when compared to chalcocite. This has been previously attributed to the natural floatability of chalcopyrite. The flotation recovery of pyrite over the entire pH range is almost negligible. The two copper sulfides can therefore be separated from pyrite by flotation with 10^{-7}M IBECTC at pH $\leq$ 6.

The flotation response of chalcocite, chalcopyrite and pyrite in the presence of 10^{-6}M IBECTC is shown in Figure 2.30. It can be seen that the floatability of these sulfide minerals are pH-dependent. Chalcocite recovery is good up to pH 8 and shows a slight decrease in recovery at very alkaline conditions. This decrease may be brought about by IBECTC being unstable at alkaline conditions. IBECTC has a pKa of 10.5 and is known to ionize at pH $\geq$ 11 (Nagaraj et al., 1988). The thermodynamic predictions for Cu_2S at this concentration agrees well with the actual flotation data. The minimum previously observed in the calculations at acidic pH and lower collector concentration is less pronounced in this figure. At alkaline conditions, the amount of $Cu(IBECTC)_2Cl$ produced also decreased slightly.

The flotation recovery of chalcopyrite is 100% at acidic conditions and decreases continuously at neutral to alkaline conditions. Like the flotation behavior of chalcocite at pH $\geq$ 10, chalcopyrite flotation may also be affected by the instability of IBECTC at these alkaline conditions. Pyrite shows good flotation recovery at pH 2 and decreases

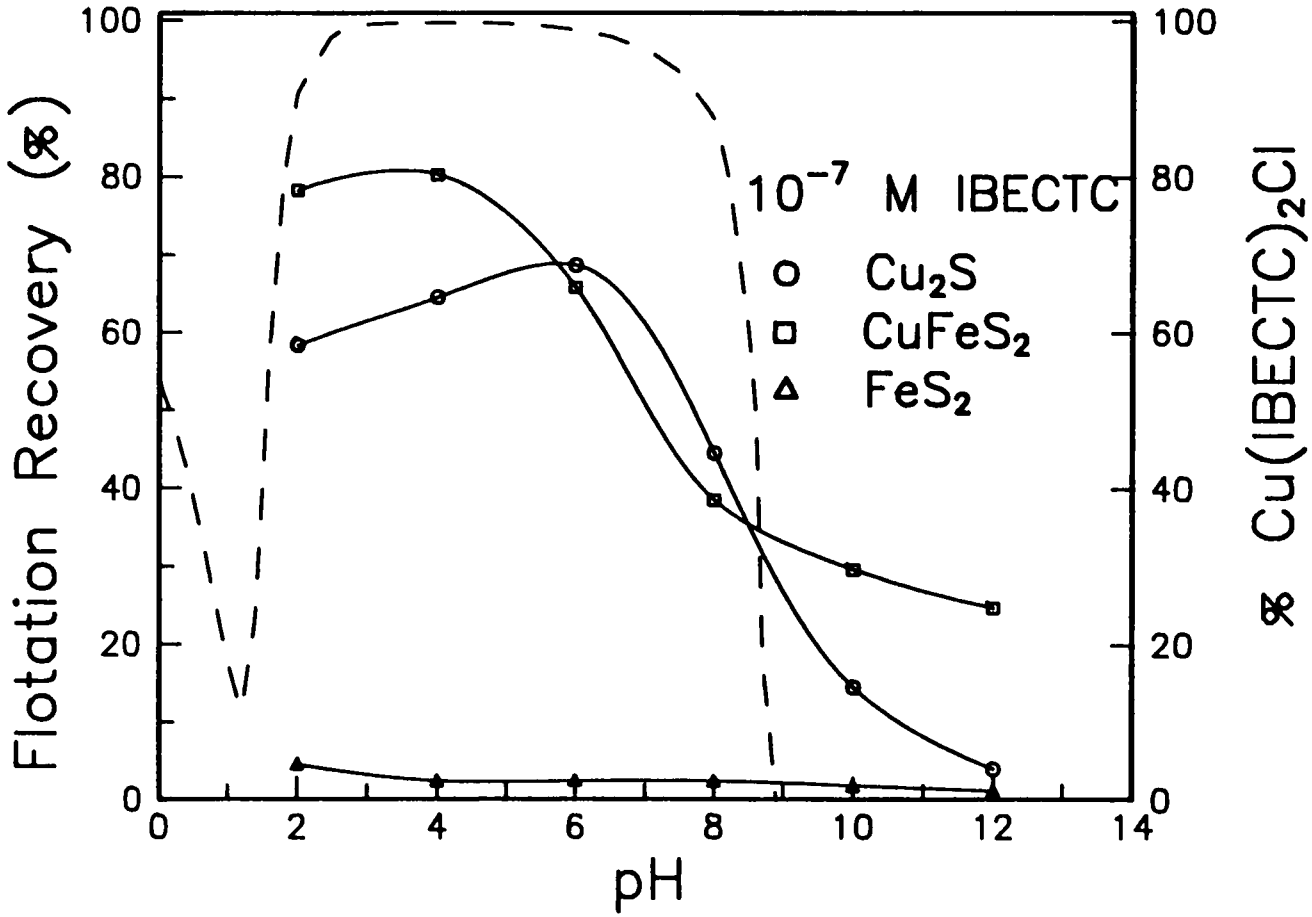

Figure 2.29. Effect of pH on the flotation recovery of chalcocite, chalcocpyrite and pyrite in the presence of 10^{-7} M IBECTC and on % $Cu(IBECTC)_2Cl$ calculated for Cu_2S at 200 mv.

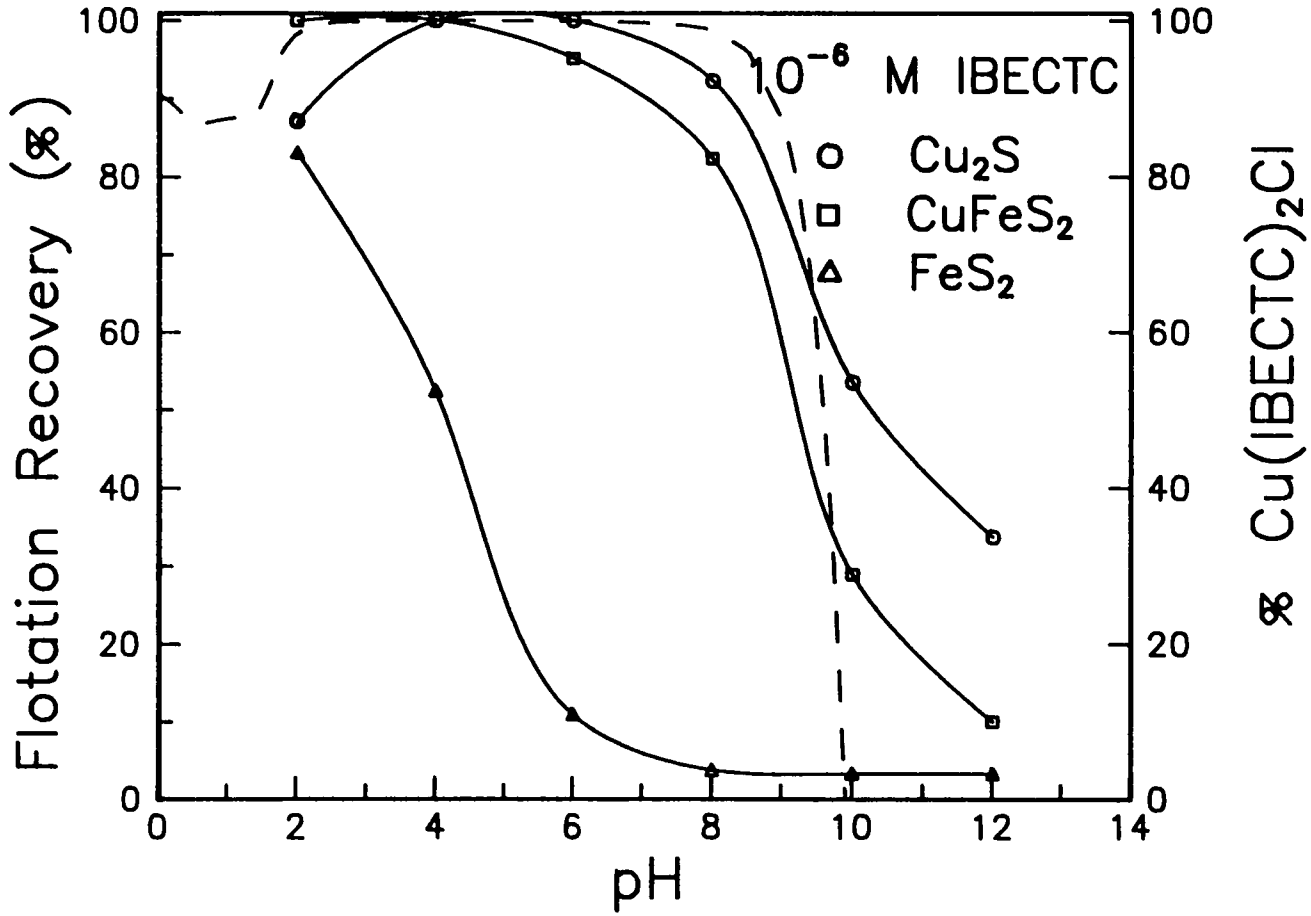

Figure 2.30. Effect of pH on the flotation recovery of chalcocite, chalcocpyrite and pyrite in the presence of 10^{-6} M IBECTC and on % $Cu(IBECTC)_2Cl$ calculated for Cu_2S at 200 mv

sharply with increasing pH. This is similar to the results obtained from pyrite with 10^{-6}M IPETC; therefore, the higher recovery at pH 2 may also be attributed to some frothing properties of thionocarbamates. In general, the results also indicate the good selectivity of IBECTC against pyrite flotation. Pyrite separation should be effective with 10^{-6}M IBECTC at pH $\geq$ 6.

b. Effect of Concentration

Microflotation tests on chalcocite have been carried out at different concentrations to determine the minimum amount of thionocarbamate that is required for good recovery. The experiments were done at pH 6 for different concentrations of IPETC and IBECTC. Figure 2.31 shows that the recovery of chalcocite is high even at collector concentrations as low as 10^{-7}M. In contrast, chalcocite microflotation with 10^{-7}M KEX at pH 8 resulted in almost negligible recovery (Basilio, 1985). This would illustrate the relative collecting power of thionocarbamate collectors at acidic conditions, as compared to xanthates. However, it should be noted that chalcocite flotation with KEX used a finer particle size (106-150 μm). The minimum amount of IPETC required for 80% flotation recovery would be about 3 x 10^{-7}M, while for IBECTC, it would require about 1.8 x 10^{-7}M. Although the difference is small, IBECTC appears to be stronger. The flotation test with KEX indicates that around 3 x 10^{-6}M will be needed for 80% recovery. However, thermodynamic calculations show that this minimum value is expected to decrease at lower pH and larger particle size (Basilio, 1985). Nevertheless, the collecting power of thionocarbamates for chalcocite is as good as that of xanthates and it has the advantage of better selectivity against pyrite. It should also be pointed out that xanthate flotation at acidic conditions is not practical due to its instability at these conditions.

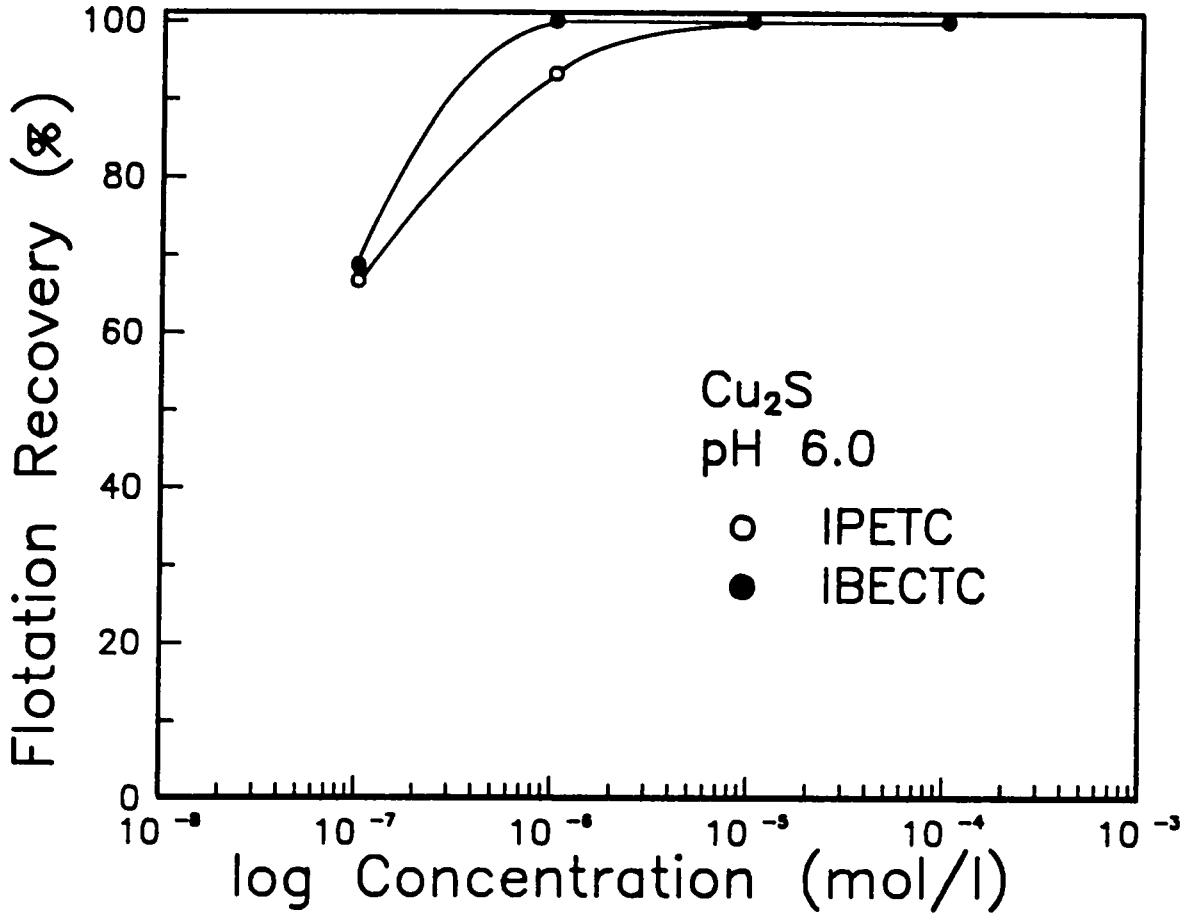

Figure 2.31. Effect of collector concentration on the flotation recovery of chalcocite at pH 6.0.

2.3.4 Contact Angle Measurements

The effects of potential on the floatability of sulfide minerals have been studied previously using microflotation, where the potential is controlled either chemically or electrochemically (Heyes and Trahar, 1979; Basilio et al., 1985; Richardson and Walker, 1985). However, there are some questions about the efficiency and accuracy of the potential control. To overcome this problem, the effect of potential on floatability was studied by using contact angle measurements. The contact angle developed between the gas bubble and the mineral surface was used to measure hydrophobicity, which is directly related to floatability. Using a modified electrochemical cell, the contact angle was measured for different sulfide-thionocarbamate systems at different potentials.

a. In the absence of a collector

The effect of potential on the natural hydrophobicity of chalcocite, chalcopyrite and pyrite was studied at pH 6 (Figure 2.32). The contact angle measured for chalcocite in the absence of a collector did not change with increasing potentials. Chalcocite has low contact angles which remained constant from -500 to 400 mv. This would be indicative of the lack of natural hydrophobicity of chalcocite. On the other hand, the hydrophobicity of chalcopyrite showed a dependence on potential. There is an increase in contact angle above -200 mv and it is hydrophobic at potentials $\geq$ -100 mv. This is in agreement with the collectorless flotation test results for chalcopyrite (Luttrell and Yoon, 1984). The gas bubble did not stick to the surface of pyrite over the entire E_h range studied. Pyrite was completely hydrophilic even at reducing conditions.

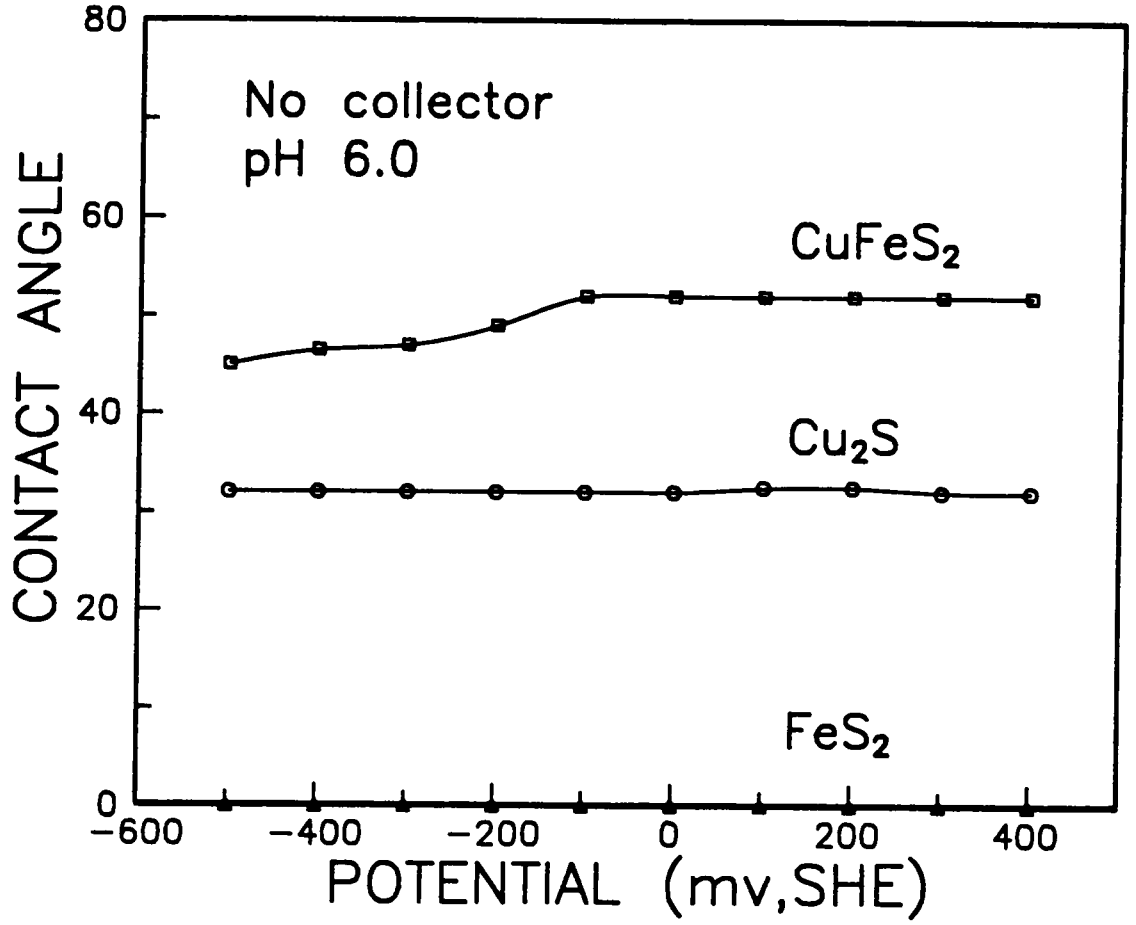

Figure 2.32. Effect of potential on the contact angle of chalcocite, chalcopyrite and pyrite in the absence of a collector at pH 6.0.

b. In the presence of IPETC

Contact angles were measured for the three sulfide minerals in the presence of 10^{-4}M IPETC at pH 6 and different potentials (Figure 2.33). Compared to Figure 2.32, the hydrophobicity of all three sulfide minerals increased with the addition of IPETC. The contact angle measured for chalcocite increases sharply from the starting potential of -500 mv and levels off at -200 mv. Flotation recovery of chalcocite would then be expected to be good at potentials $\geq$ -400 mv. This would indicate that IPETC is already adsorbed before the start of the IPETC adsorption peak that is observed in the voltammogram (Figures 2.13 and 2.18). Non-electrochemical IPETC adsorption was not clearly evident in the voltammograms for copper and chalcocite, but was observed for the other electrodes. It should be noted that the contact angle on chalcocite does not decrease even at oxidizing potentials (> 200 mv). This would presumably indicate that the adsorbed IPETC species are not oxidized at these potentials.

Figure 2.33 also shows the effect of E_h on % $Cu(IPETC)_2Cl$ calculated for Cu^0 and Cu_2S at pH 6 and an IPETC addition of 10^{-4} M. The curve for % $Cu(IPETC)_2Cl$ in the Cu_2S-IPETC system shows a plateau between -400 and -150 mv before increasing sharply at higher potentials. These results are different from the contact angle data for Cu_2S at low potentials. However, the calculated lower flotation edge for Cu^0 agrees with the experimental results. This may be attributed to the reduction of the chalcocite surface at the starting potential.

Chalcopyrite shows similar behavior but has slightly higher contact angles when compared to chalcocite. Its effective flotation range would start at $E_h \geq$ -300 mv. The data also verify the voltammetry results regarding the potential-independent adsorption of IPETC. Pyrite does not show high contact angles in the presence of 10^{-4}M IPETC. Its slight hydrophobicity almost remains constant over the entire potential range. Even

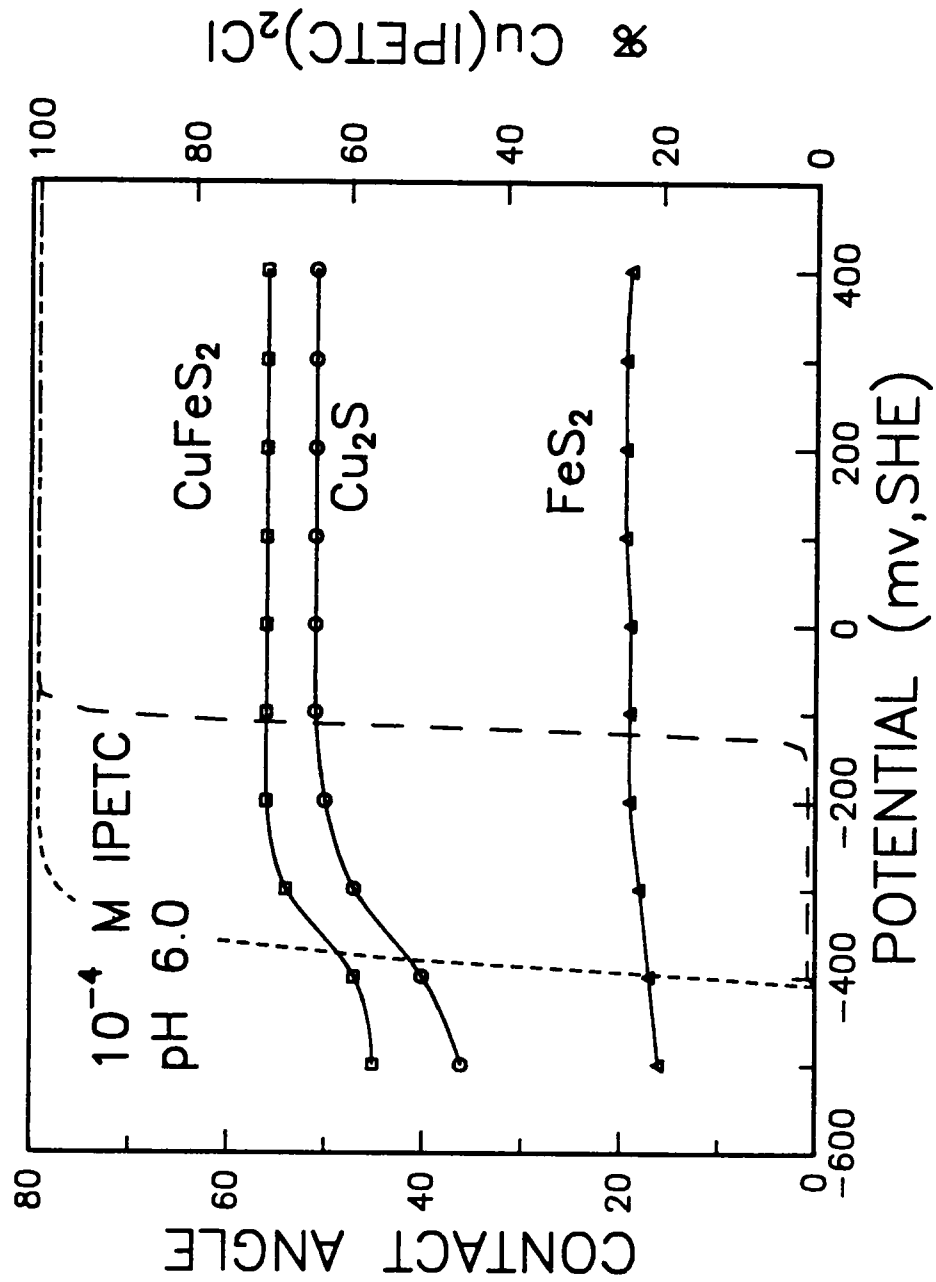

Figure 2.33. Effect of potential on the contact angle of chalcocite, chalcocpyrite and pyrite in the presence of 10^{-4} M IPETC and on % $Cu(IPETC)_2Cl$ calculated for for Cu^0 (----) and Cu_2S (——) at pH 6.

though the contact angles are higher with the addition of IPETC, they do not seem to be high enough to induce flotation. However, the results do indicate the non-electrochemical adsorption of IPETC on pyrite.

c. In the presence of IBECTC

The effect of potential on the floatability of chalcocite, chalcopyrite and pyrite with the addition of 10^{-4}M IBECTC at pH 6 is shown in Figure 2.34. The contact angles measured for chalcocite showed a response similar to that observed in IPETC solutions. Chalcocite would be expected to have good floatability at $E_h \geq$ -200 mv. However, when compared to IPETC, higher contact angles on chalcocite and chalcopyrite are obtained with IBECTC, indicating further the greater strength of IBECTC. Chalcopyrite also shows good floatability above -400 mv and this increases continuously with increasing potential up to -200 mv. At more oxidizing potentials, the contact angle of chalcopyrite remains constant. On the other hand, low contact angles are found for pyrite over the entire E_h range. There is no apparent potential dependence and pyrite remains relatively hydropilic over the entire potential range. Also, the contact angles measured on pyrite are lower than those with IPETC. All three minerals show adsorption of IBECTC even at the starting potential, thus supporting the conclusions from voltammetry.

The results of the thermodynamic calculations for Cu^0 and Cu_2S in the presence of 10^{-4} M IBECTC at pH 6 are also compared to the contact angle data in Figure 2.34. The % $Cu(IBECTC)_2Cl$ curve calculated for Cu_2S shows a plateau similar to that observed for the Cu_2S-IPETC system. There is also some discrepancy between the contact angle and calculated data for Cu_2S. However, the calculated % $Cu(IBECTC)_2Cl$ curve for Cu^0 is in excellent agreement with the measured lower

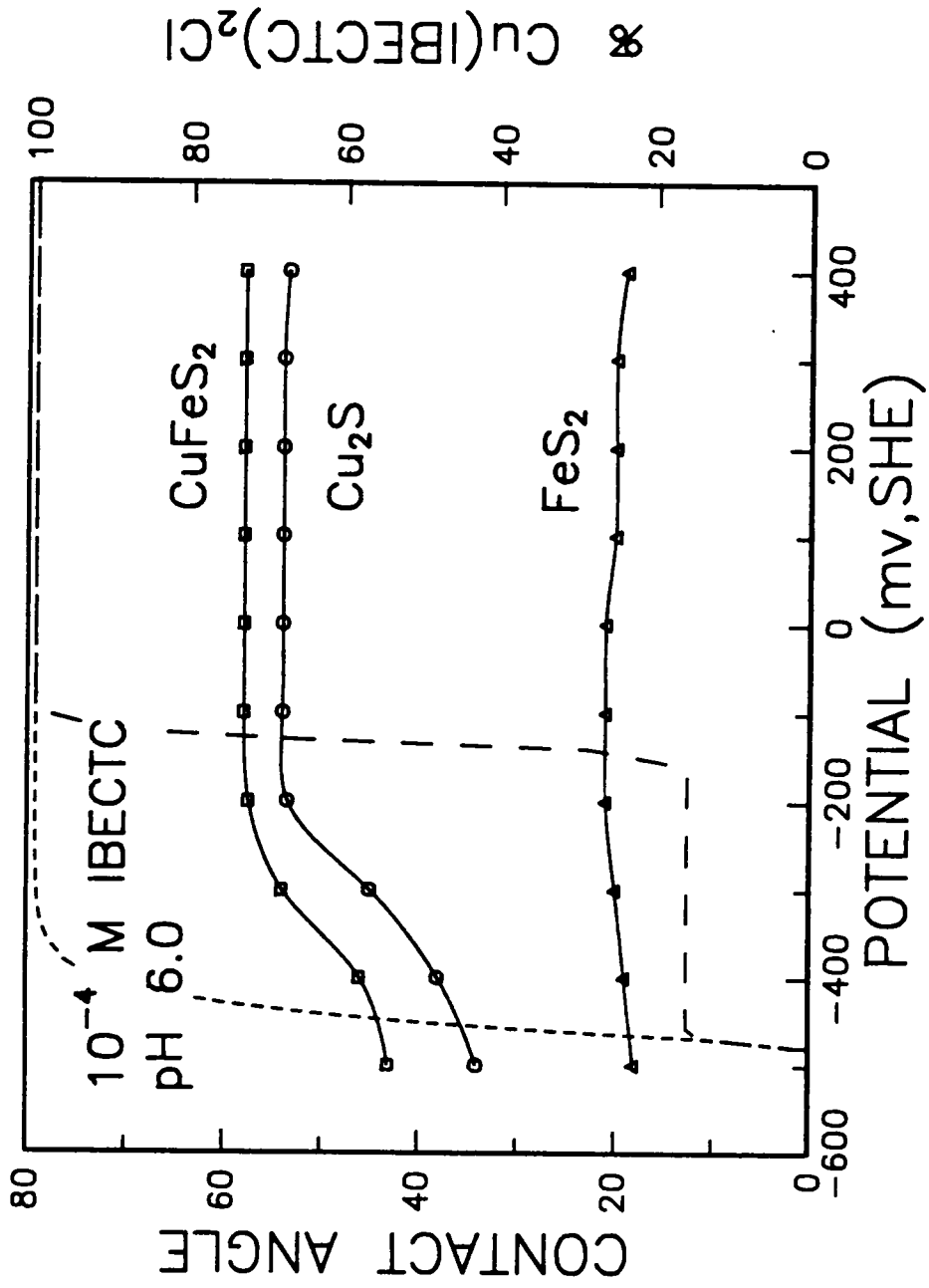

Figure 2.34. Effect of potential on the contact angle of chalcocite, chalcocpyrite and pyrite in the presence of 10^{-4} M IBECTC and on % $Cu(IBECTC)_2Cl$ calculated for Cu^0 (----) and Cu_2S (— —) at pH 6.

flotation edge. This has been attributed previously in the Cu_2S-IPETC system to the reduction of the electrode at the starting potential.

2.4 Summary

Mass-balanced thermodynamic calculations have been carried out to construct E_h-pH diagrams for metallic copper and chalcocite in the presence of 10^{-3} M IPETC and 10^{-5} M Cl^-. Similar computations have also been done involving the addition of 10^{-3} M IBECTC. The E_h-pH regions where $Cu(IPETC)_2Cl$ or $Cu(IBECTC)_2Cl$ are stable have been determined from these calculations. The boundaries of the stability region for the two Cu-thionocarbamate compounds are the same for both Cu^0 and Cu_2S systems, respectively. This is due to the independence of the upper and lower boundaries on reactions involving sulfur. However, there are some differences between the two systems in the middle section of the stability regions due to the oxidation of Cu_2S.

The stability of $Cu(IBECTC)_2Cl$ occurs over a wider E_h-pH region than that of $Cu(IPETC)_2Cl$. However, both thionocarbamate collectors showed larger stability regions than those observed for the Cu_2S-KEX system. The lower solubility products of these two Cu-thionocarbamate compounds are responsible for this difference. The effect of E_h and pH on % $Cu(IPETC)_2Cl$ or % $Cu(IBECTC)_2Cl$ for the Cu^0 and Cu_2S systems have also been determined and compared with the experimental data.

Voltammetry experiments for platinum at pH 9.2 and 4.6 did not show any anodic oxidation of IPETC. However, passivation of the electrode was observed for the entire voltammogram, suggesting that IPETC adsorption occurred without any electron-transfer. The voltammogram obtained for copper in the presence of 10^{-3}M IPETC at pH 9.2 showed an anodic oxidation peak near 0 mv. This was attributed to

the interaction of copper with IPETC during the oxidation of the electrode. At pH 4.6, a shift of the anodic adsorption peak was observed, strongly suggesting that the reaction is pH dependent. This interaction probably corresponds to a coupled chemical reaction of the EC type involving oxidation of Cu^0 to Cu(I), followed by the formation of Cu(IPETC)′ with H^+ ions being released by the breaking of the N-H bond in the collector (reactions [2.9] and [2.12]).

The interaction of IPETC with chalcocite resulted in the appearance of an oxidation peak starting near 0 mv. This peak was assigned to the electrochemical adsorption of IPETC on chalcocite. The probable reaction mechanism is probably analogous to the EC mechanism proposed for IPETC adsorption on copper. This may be represented by reactions [2.16] and [2.12]. Decreasing the pH results in a shift of the IPETC adsorption peaks to a higher potential. This supports the suggestion that IPETC interaction involves H^+ ions, which are presumably produced by the breakage of the N-H bond in IPETC. FTIR measurements will be used in the next chapter to help verify this conclusion.

The electrochemical behavior of IPETC on chalcopyrite and pyrite are similar. The adsorption of IPETC on both electrodes are apparently non-electrochemical. This was manifested in the decrease in current for the entire voltammogram when IPETC was added, without any apparent IPETC adsorption peak observed. It should be noted that there was no direct evidence of non-electrochemical IPETC adsorption on copper and chalcocite prior to the appearance of the anodic adsorption peaks.

The electrochemical data obtained for IBECTC with the different electrodes were similar to those observed for IPETC. There was no anodic oxidation of IBECTC on the platinum, chalcopyrite and pyrite electrodes at pH 4.6. However, IBECTC adsorbed non-electrochemically on these electrode surfaces. At the starting potential, IBECTC

was already adsorbed on these electrodes, as indicated by the inhibition of the oxidation and reduction reactions.

On copper, anodic currents associated with IBECTC adsorption were observed above 0 mv. The shape of the voltammogram is also similar to that obtained in IPETC solution. The mechanism involved in this anodic peak is probably similar to the one suggested for IPETC, except that the adsorption product is Cu(IBECTC)'. The coupled chemical reaction may be given by reactions [2.9] and [2.26]. For chalcocite, anodic currents attributed to the interaction of IBECTC with chalcocite started to flow above 0 mv. Adsorption probably occurs through an EC mechanism similar to that proposed for IPETC. Reaction [2.16] followed by reaction [2.26] probably best describe this mechanism.

The flotation recoveries of chalcocite, chalcopyrite and pyrite with IPETC are dependent on pH. The microflotation data obtained at a collector addition of 10^{-7}M indicate that the effective flotation range for chalcocite and chalcopyrite are below pH 8. Chalcopyrite is observed to give better floatability than chalcocite at this collector level. This is probably enhanced by the collectorless flotation of chalcopyrite. The floatability of pyrite, on the other hand, is very low for the entire pH range, demonstrating IPETC's excellent potential for selectivity.

When the IPETC concentration is increased to 10^{-6}M, pyrite flotation becomes significant below pH 4. The recovery of chalcocite increases and is excellent over a wider pH range. At pH $\leq$ 6, 100% recovery is obtained for chalcopyrite and recovery decreases slightly at pH 8. Efficient separation of copper sulfides from pyrite is feasible a pH $\geq$ 6. The results of the thermodynamic calculations for chalcocite in the presence of 10^{-7} and 10^{-6} M IPETC are in reasonable agreement with the flotation test results.

The floatability of the three sulfide minerals were also found to be pH-dependent when IBECTC was used as the collector. The recovery of chalcocite is maximum at pH

6 and decreases with increasing pH. Similar observations were also made from the calculated % $Cu(IBECTC)_2Cl$ vs. pH curve. Chalcopyrite shows decreasing floatability with increasing pH. As is the case with IPETC, IBECTC floats chalcopyrite more readily than chalcocite. This has been attributed to the collectorless flotation of chalcopyrite. Pyrite flotation is negligible throughout the pH range studied, indicating the collector's good selectivity.

Increasing the collector concentration to 10^{-6}M results in good pyrite recovery at pH < 4. The recovery of chalcocite and chalcopyrite also increases with the higher collector addition. The effective flotation range for chalcocite is extended to pH 8, while chalcopyrite shows good recovery up to pH 6. Chalcocite and chalcopyrite can be separated easily from pyrite by flotation at pH $\geq$ 6.

Microflotation tests on chalcocite at pH 6 and different thionocarbamate concentrations show good recovery even at low collector concentrations. For 80% recovery, the minimum amount of IPETC and IBECTC required would be about 3 x 10^{-7}M and 1.8 x 10^{-7}M per gram of mineral, repectively. This is comparable to the results obtained using xanthate, indicating that the collecting strength of IPETC and IBECTC for chalcocite is as good as that of xanthate. Between the two thionocarbamates, IBECTC gives slightly better recoveries than IPETC at low collector concentrations.

The results obtained from the contact angle measurements indicate that the hydrophobicity of the three sulfide minerals increased with the addition of IPETC. The contact angles of chalcocite and chalcopyrite increase sharply from the starting potential of -500 mv up to -200 mv for chalcocite, and -300 mv for chalcopyrite. At higher potentials, the contact angles remain at the maximum value. It should be pointed out that IPETC adsorption is observed below the potential where the interaction is found in the voltammogram. Thermodynamic calculations also show that $Cu(IPETC)_2Cl$ is

stable at these low potentials. This has been attributed to the low K_{sp} value for this compound, thus requiring only a small amount of copper ions. A similar situation probably exist on the chalcocite electrode surface which results in the adsorption of IPETC and the corresponding hydrophobicity observed at this conditions. Chalcopyrite shows slightly better hydrophobicity than chalcocite, which has also been observed in the microflotation data. On the other hand, pyrite shows low contact angles over the entire E_h range.

In the case of IBECTC, the effects of E_h are almost the same. The only significant difference is that the contact angles measured are relatively higher in IBECTC solutions, implying that IBECTC has a higher collecting power. It should be noted that a higher collecting power is associated with lower selectivity. However, the increase in contact angle for pyrite is relatively small. The results of the measurements for IBECTC indicate that there is adsorption of the collector even at the starting potential of -500 mv. There is already good hydrophobicity shown by chalcocite at potentials lower than where thionocarbamate interaction is indicated in the voltammogram. This suggests that the initial IPETC or IBECTC adsorption is independent of potential. It is also possible that the electrode surface has oxidized slightly, but enough to produce the amount of copper ions required for thionocarbamate adsorption. The computations have already shown that only a small amount of copper ions is required for the formation of Cu-thionocarbamate compounds.

3.0 SPECTROSCOPIC STUDY OF THE THIONOCARBAMATE-SULFIDE SYSTEM

3.1 Introduction

Spectroscopic techniques have been vastly improved in recent years. The use of infrared spectroscopy has become popular due to the rapid commercial development of Fourier Transform Infrared (FTIR) spectrometers. IR spectroscopic analysis provides a powerful tool for investigating the mode of bonding of organic ligands in complexes with metal ions. Recently, more work employing IR spectroscopy have been carried out to study the interactions that occur between flotation reagents and mineral surfaces.

Various experimental techniques are available for IR study of adsorbed species. In-situ techniques are probably the most useful since they allow surface analysis without having to remove the sample from its aqueous environment. One technique capable of in-situ analysis is attenuated total reflectance (ATR) spectroscopy. In this technique (Fahrenfort, 1961; Harrick, 1963; 1965; 1967), a radiation beam traverses a dense medium (reflecting element) in contact with a rare medium (absorbing sample), and depending on the incident angle, is totally internal reflected. During this reflection, the beam penetrates beyond the interface of the two media into the rare medium. Since the

beam is capable of interacting with the absorbing sample, this leads to an attenuation or reduction of the totally reflected radiation. Therefore, the sample layer very close to the interface can be examined spectroscopically. ATR spectroscopy has been very useful in investigating solid-liquid and solid-gas interfaces (Strojek and Mielczarski, 1983; Mirabella, 1985).

In the present work, an in-situ ATR technique has been employed to study the adsorption of IPETC and IBECTC on chalcocite, chalcopyrite and pyrite. A modified ATR cell was used to analyze the sulfide mineral samples without completely removing the sample from the solution. The results would help explain the observations made in the previous chapter.

Voltammetric techniques have been shown to provide useful information regarding the adsorption of thionocarbamates on sulfide minerals. However, a more direct examination of the surface is necessary to identify the species that are formed during the electrochemical reactions. Consequently, an in-situ spectroelectrochemical technique was used to study the adsorption of thionocarbamates on copper and chalcocite under potentiostatic control. In this technique, an electrochemical ATR (ECATR) cell was specially developed that allows in-situ analysis of the electrode surface. The ECATR cell has been previously used by the author to study the electrochemical adsorption of xanthates on different sulfide minerals (Leppinen et al., 1988). The results from these experiments will provide an excellent complement to the voltammetric and contact angle data obtained in Chapter 2.0.

Infrared reflection-absorption spectroscopy (IRAS), first suggested by Greenler (1966), is a method of obtaining the IR spectrum of adsorbed molecules or thin films on a highly reflective (typically metallic) surface. This is different from specular reflectance, which is the measurement of the reflectance spectrum of a flat, clear surface of an absorbing material (Griffiths and de Haseth, 1986). The IRAS method involves

using the appropriate angle of incidence and state of polarization in reflecting radiation from the sample-covered substrate (Greenler et al., 1971). In IRAS, the parallel, but not the perpendicular, component is absorbed, giving rise to the so-called surface selection rule (Golden et al., 1981; 1984). Determination of the orientation and geometric structure of the adsorbed molecules can be obtained using these rules. This technique has been applied in the investigations of solid-metal, gas-metal and liquid-metal interfaces (Tompkins, 1975; Swalen and Rabolt, 1985; Golden, 1985).

IRAS has been applied in the study of xanthate adsorption on copper (Mielczarski and Leppinen, 1987) and chalcocite (Mielczarski and Yoon, 1988). It has also been used here to study the structure and orientation of the adsorbed layer to help in the understanding of thionocarbamate adsorption mechanisms. Since different adsorbed collector molecules give distinct characteristic spectra, IRAS was also used to study the preferential adsorption of IPETC, IBECTC and KEX on copper. Copper samples were exposed to different combinations of these collectors in order to determine which is preferentially adsorbed. This would give an indication of the relative strengths and kinetics of the three different collectors.

UV spectroscopy has been shown to be effective in the analysis of thionocarbamates (Jones and Woodcock, 1969; Goold, 1972). As a complement to the ATR measurements, UV spectroscopic analysis was used to measure the amount of thionocarbamate that was adsorbed by the sulfide minerals. Using a packed bed flow-through cell, the kinetics of thionocarbamate adsorption has also been studied. The data obtained would also be useful in explaining the selectivity of IPETC and IBECTC against pyrite.

From all of these spectroscopic work, the author hopes to obtain a clearer picture of the adsorption of IPETC and IBECTC on chalcocite, chalcopyrite and pyrite. The

data collected would help explain the flotation and voltammetric behavior of these minerals with thionocarbamates.

3.2 Experimental

3.2.1 Materials

The mineral samples that were used for the experiments have been described in the previous chapter. The specific surface area of the -500 mesh fraction used for the experiments was typically in the range of 0.7 - 0.8 m^2/g, as analyzed by BET (courtesy of the Department of Geological Sciences). The sample used for the IRAS measurements was electrolytic copper foil (99.9% pure) that had a thickness of 0.002 inch. The thionocarbamates were of the same type and purity as those previously described. Potassium ethyl xanthate (KEX) was prepared by dissolving it in acetone and recrystallizing in petroleum ether. The dissolution and recrystallization process was done three times to ensure purity. All the experiments were conducted in 10^{-2}M NaCl solution to maintain a constant ionic strength, unless stated otherwise. Buffer solutions were not used in order to avoid further complications of the IR spectra. The pH was adjusted by using HCl or NaOH solutions. All the reagents were of analytical grade and double-distilled water was used to prepare the solutions. In the spectroelectrochemical experiments, the solution was purged with low-O_2 nitrogen gas prior to each measurement.

3.2.2 FTIR Spectroscopy

The FTIR spectra were recorded using a Perkin Elmer Model 1710 FTIR Spectrometer equipped with a deuterated triglycine sulfate (DTGS) and mercury cadmium telluride (MCT) detector. In each measurement, a total of 100 spectra were recorded and signal-averaged in the 4000-400 cm^{-1} region. The spectral resolution was set at 4 cm^{-1}. For the attenuated total reflectance (ATR) and in-situ spectroelectrochemical measurements, a Barne's Model 302 Continuously Variable ATR accessory was used. The infrared reflectance-absorption spectroscopic (IRAS) measurements were done using a Barne's Model 501 Variable Angle Specular Reflectance accessory with a Harrick Wire Grid Polarizer.

a. Attenuated total reflectance spectroscopy

Typically, 1 gm of freshly-ground mineral ($< 25\ \mu m$) was conditioned with a thionocarbamate solution for 15 minutes. It was adjusted prior to the addition of the mineral by using HCl or NaOH solutions. The pH was monitored and controlled during conditioning by a Fisher Scientific Computer Aided Titrimeter System. After conditioning, the slurry was transferred into a specially designed ATR cell to record the spectra of the adsorbed species.

The ATR cell shown in Figure 3.1 is equipped with a thumbscrew. It allows most of the water to be filtered out of the sample and to pass through a porous plate. However, the sample still contains a sufficient amount of the solution, so that the chemistry of the system does not change appreciably during the measurement. The thumb screw also allows the wet filter cake to be pressed against the reflection element. This cell has the advantage of being very close to an in-situ technique since the sample

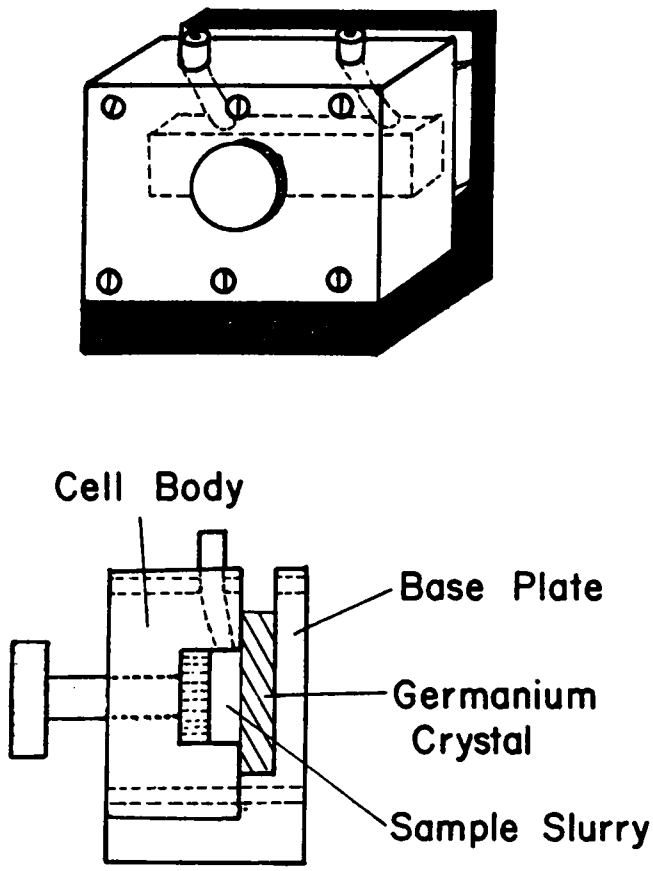

Figure 3.1. Schematic representation of the ATR cell used for the in-situ FTIR measurements.

is measured in the same conditioning solution. The reflection element is a 45°-germanium plate with dimensions of 50 x 20 x 3 mm. The entire cell was mounted on the ATR accessory.

The spectral manipulation included subtraction of solution and water vapor spectra, baseline correction and smoothing. These operations were observed to cause slight changes in the peak positions and intensities. For this reason, spectral interpretations were limited to significant shifts in peak positions. Quantitative (or at least, semi-quantitative) determination of the surface products was possible as long as the particle size of the sample was uniform and the contact area on the germanium reflection element was constant.

The Cu(I) compounds of IPETC and IBECTC were precipitated using two methods. The first precipitate was obtained by mixing a solution of Cu(I)-chloride complex, saturated with NaCl, with the thionocarbamate solution. The second method involved the reduction of Cu_2SO_4 solution with 10% (by weight) ascorbic acid to produce Cu(I) ions. Ascorbic acid is a preferred reductant for copper because it does not introduce extraneous metal ions (Handley and Dean, 1961). One ml of the 10% ascorbic acid solution was added for each 20-mg of copper in solution. The resulting Cu(I) ions were then reacted with the thionocarbamate solution. The precipitates were filtered and dried in a vacuum dessicator. It should be noted that the second set of precipitates was prepared using a different batch of thionocarbamates. Although the purities of the reagents are the same, as determined by gas chromatography, this does not discount the possibility of some differences between the two batches of reagents. Cu(II), Fe(II) or Fe(III) did not form any precipitates with either IPETC or IBECTC. Extraction stuides with IPETC have also shown similar results (Seryakova et al., 1975). For example, no precipitation was observed when mixing Cu_2SO_4 and thionocarbamate solutions. Only

when Cu(II) was reduced to Cu(I), by addition of a reducing agent, did the precipitate start to form.

b. Infrared reflection-adsorption spectroscopy

The surface of the copper sample was prepared by fine polishing with Buehler Metadi II diamond polishing compound (0.25 μm) initially, and then with Buehler gamma alumina powder (0.05 μm). After each step of polishing, the copper foil was rinsed thoroughly with ethanol and ultrasonically cleaned in an ethanol bath. The sample was then washed with 10% HCl solution to remove any pre-adsorbed products, and finally with double-distilled water. The freshly cleaned copper samples were conditioned in 10^{-4}M thionocarbamate solutions (pH 4 and 6) at different periods of time to get different degrees of surface coverages. After the adsorption of the collector, the samples were removed quickly from the solution and placed directly into the IRAS accessory for measurements. The surface of each sample after collector adsorption was hydrophobic enough not to require drying.

For the preferential adsorption studies, the copper sample was prepared in a similar manner. The sample was conditioned in a solution of different collector combinations. This was done at different periods of time to see various degrees of coverage. Another set of experiments were done where the copper sample was conditioned using one collector at a time. The sample was first conditioned in one collector solution and then in another. The spectra were recorded after each conditioning. A constant conditioning time of 15 minutes was used for these experiments.

The incoming infrared beam was polarized and had an angle of incidence of 85°. All of the recorded IRAS spectra were referenced to a freshly cleaned copper surface. The IR signal intensity of the spectra was expressed as $(R^0 - R)/R^0$, where R^0 and R

are the reflectivities of the sample in the absence and presence of adsorbed collector, respectively.

The IRAS technique has also been used to verify the results of the in-situ spectroelectrochemical measurements. The effect of potential on thionocarbamate adsorption on copper was studied by conditioning the sample in the three-electrode electrochemical cell and recording the spectra externally. The copper surface was prepared as described previously and used as the working electrode in the electrochemical cell. Its potential was then controlled for 15 minutes before the electrode was removed quickly for spectral recording. The sample was rinsed with water after removal from potential control to prevent any collector adsorption at open circuit potentials.

c. In-situ spectroelectrochemical spectroscopy

A modified electrochemical attenuated total reflectance (ECATR) cell was used for the in-situ spectroelectrochemical measurements. The ECATR cell was specially constructed utilizing the existing optical system of the Barne's ATR accessory. Figure 3.2 shows the ECATR cell which consists of a teflon cell body and a movable working electrode holder. The chalcocite bed or copper electrode is attached to the end of this movable holder. The platinum counter electrode is placed in a cavity along the inner wall of the cell near the working electrode. The capillary tip for the reference electrode is placed close to the working electrode. The entire cell body is attached to a stainless steel holder, which is on the other side of the reflection element. The electrolyte solution is circulated to the ECATR cell through a purging vessel where the solution is continuously purged with low-oxygen nitrogen gas (Figure 3.3).

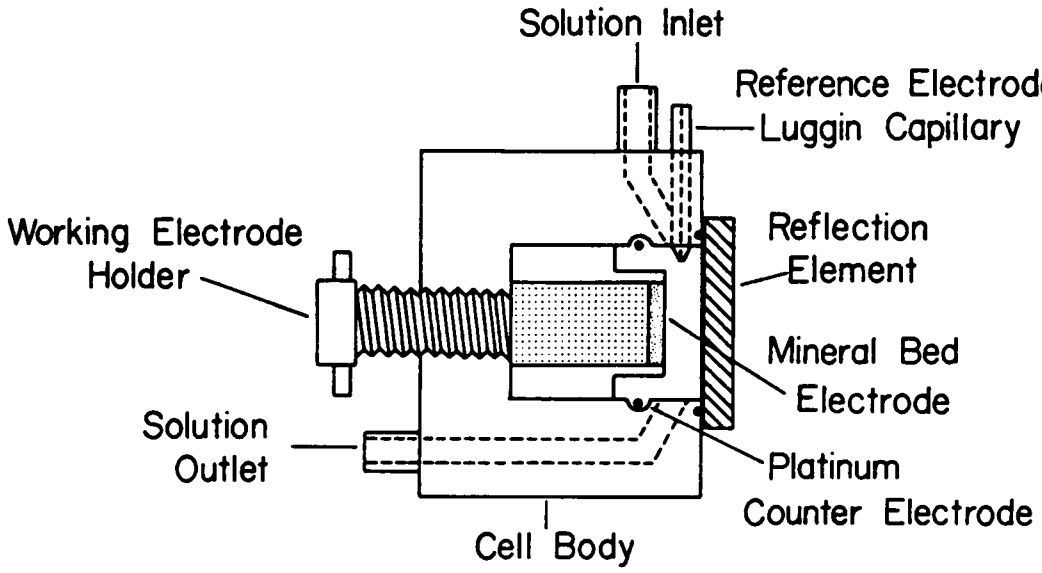

Figure 3.2. Schematic diagram of the ECATR cell constructed for the the in-situ FTIR measurements under controlled potential conditions.

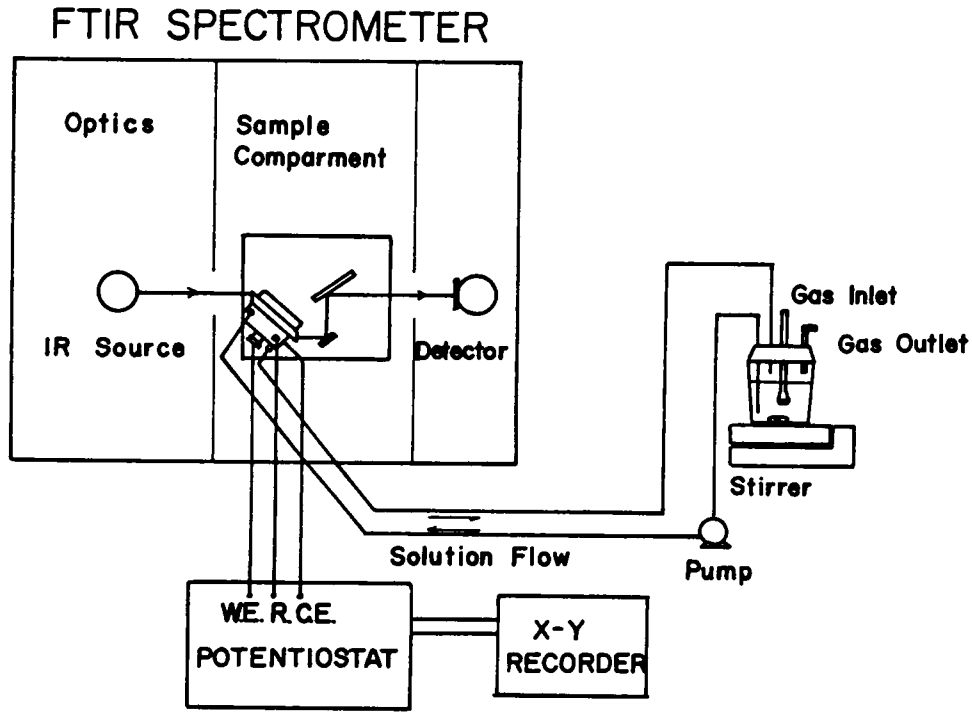

Figure 3.3. Schematic diagram of the experimental set-up for the in-situ spectroelectrochemistry.

The chalcocite working electrode was made of finely-ground powder (<25μm) embedded in carbon paste. In the experiments involving copper, a freshly cleaned copper foil was used. The working electrode was held at constant potential with a PAR Model 371 Potentiostat/Galvanostat. A saturated calomel electrode was used as the reference electrode, although all the potentials reported here are expressed on the SHE scale. The electrolyte solution was circulated through the cell during the polarization period of 15 minutes. Afterwards, the solution flow was stopped and the working electrode was pressed against the germanium reflecting element to record the spectra. In order to eliminate background effects, a reference spectrum (i.e., the spectrum taken with the working electrode not in contact with the reflecting element), was taken prior to each measurement.

3.2.3 UV/VIS Spectroscopy

The remaining slurry from the ATR experimental sample was used for the adsorption studies. This slurry was decanted and centrifuged to recover a clear solution. The supernatant solution was analyzed for IPETC or IBECTC using a Perkin-Elmer Lambda Array 3840 UV/VIS Spectrophotometer. A 1-cm pathlength quartz cell was used for the measurements. The absorbance for IPETC and IBECTC were measured at 244 nm and 256 nm, respectively.

Figure 3.4 shows the set-up used for the kinetic studies. The experiments were carried out using 1 gm of freshly-ground sulfide mineral (75-106 μm) in 100 ml of 10^{-5}M thionocarbamate solution at pH 6. The solution is initially circulated through the flow UV cell by a Masterflex tubing pump system. After the circulation of the solution has reached equilibrium and the UV absorbance reading has remained constant, the solid is introduced into the flow-through conditioning cell. During the measurements, the

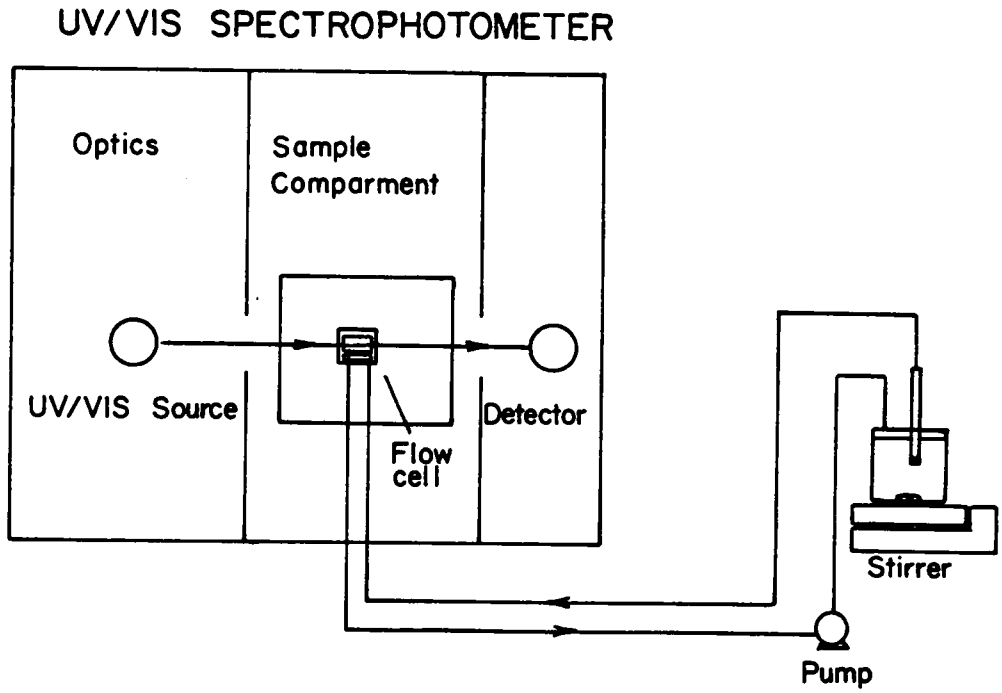

Figure 3.4. Schematic representation of the experimental set-up for the UV adsorption kinetic studies.

UV/VIS spectrophotometer recorded the absorbance at a fixed wavelength every 12 seconds. The wavelength was set at 244 and 256 nm for IPETC and IBECTC, respectively. Absorbance readings of blank samples (without a collector) were taken for the three sulfide minerals and subtracted from the actual values. This was done to ensure that the changes in the UV absorbance readings were not affected by any soluble species being produced by the sulfide minerals.

Calibration curves were constructed by measuring the absorbance of different solutions of known IPETC and IBECTC concentrations at 244 and 256 nm, respectively. Beer's Law was obeyed up to about 8 x 10^{-4}M. The standard solution used in constructing the calibration curve was also prepared in 10^{-2}M NaCl solution with the pH adjusted to 6.0.

Due to this limitation, the UV data reported for the study on the effect of pH were obtained from ATR measurements done at an initial collector concentration of 10^{-4}M. However, even though the ATR measurements were done at two different concentrations, only the results for tests done at 10^{-3}M collector concentrations are shown in the next section.

3.3 Results and Discussions

3.3.1 IR Characterization of Thionocarbamates

IPETC and IBECTC, as well as related Cu-thionocarbamate compounds, were characterized by their respective IR spectra using ATR spectroscopy.

a. IPETC and copper-IPETC compounds

The ATR spectra of liquid IPETC, solid Cu-IPETC(I) and Cu-IPETC(II) are presented in Figure 3.5. Cu-IPETC(I) and Cu-IPETC(II) refer to the two compounds precipitated using the two different methods described in section 3.2.2. In molecules having a nitrogen atom adjacent to the thiocarbonyl group, strong vibrational coupling occurs, causing mixed vibrations and making the spectral interpretation more complex (Rao et al., 1964). The broad bands at 1500-1600 cm^{-1} are usually attributed to C-N stretching, N-H deformation and C-H deformation. It is suggested that the bands at 1090-1100 cm^{-1} have contributions from C-N, C=S and C-H vibrations. The strong absorption bands at 1210-1230cm^{-1} are most likely due to the antisymmetric O-C=S stretching vibration (Tarantelli and Furlani, 1971), while those at 1130-1150 cm^{-1} are due to the symmetric O-C=S vibration (Solozhenkin et al., 1982). The minor bands near 1050 cm^{-1} are probably due to C=S vibration. At higher wavenumber regions, the N-H stretching vibration is most probably responsible for the band at 3262 cm^{-1}. The sharp peaks at 2979 and 2935 cm^{-1} may be attributed to C-H stretching vibrations associated with CH_3 and CH_2 groups.

The C-N stretching band in the IR spectrum of IPETC shifts from 1522 to 1575 cm^{-1} in Cu-IPETC(I). Also, the antisymmetric O-C=S stretching vibration shifts by about 15 cm^{-1} to 1228 cm^{-1}. These chemical shifts can be attributed to the resonance forms I and III, shown below, of IPETC ligand bonded to Cu(I):

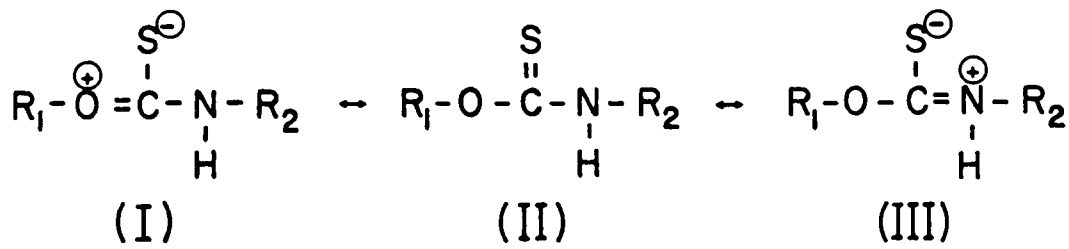

(I) (II) (III)

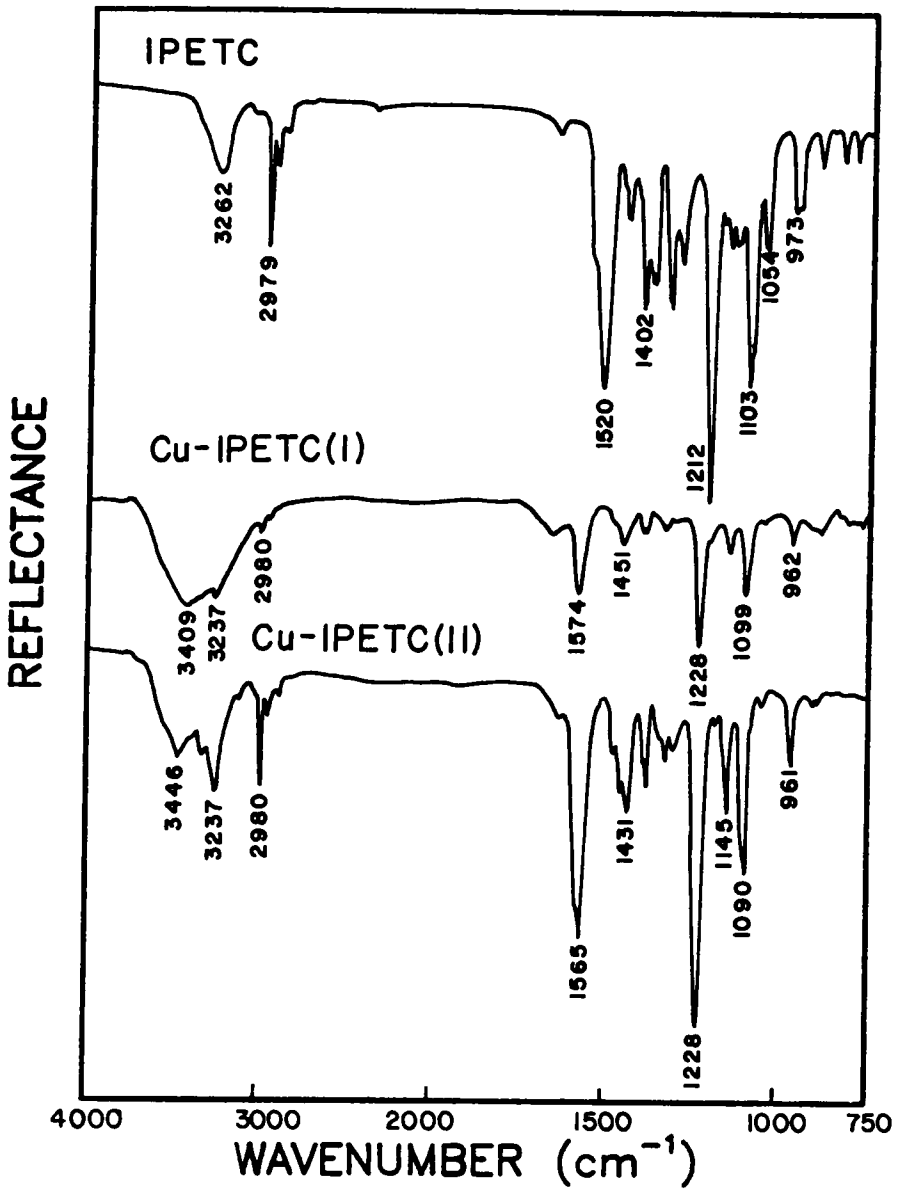

Figure 3.5. FTIR reflection spectra of IPETC, Cu-IPETC(I) and Cu-IPETC(II).

In view of these resonance forms, IPETC is likely to be bonded to Cu(I) through its sulfur atom. The N-H stretching band is shifted from 3262 to 3237 cm^{-1} in the precipitate. This shift, which is related to the shift in the C-N stretching band, may also be attributed to the resonance of the IPETC ligand bonded to Cu(I). It also indicates that the hydrogen bonding of the N-H group in IPETC has not been broken. Whether the bonding is aided by coordination through nitrogen, as suggested by Bogdanov et al. (1976), is not clearly shown by the IR spectra.

The IR spectrum of Cu-IPETC(II) does not show any significant difference from that of Cu-IPETC(I). The only noticeable shift is in the band for the C-N stretching vibrations. The band at 1574 cm^{-1} is shifted to 1565 cm^{-1}. This may be due to a lower degree of resonance as compared to that observed for Cu-IPETC(I). However, the bonding of the IPETC to Cu(I) is still likely to be through its sulfur atom.

b. IBECTC and copper-IBECTC compounds

Figure 3.6 shows the IR spectra of IBECTC, Cu-IBECTC(I) and Cu-IBECTC(II). The designations given for Cu-IBECTC(I) and Cu-IBECTC(II) are the same as those given for Cu-IPETC compounds. Compared to those of IPETC, the spectra are more complicated because the C-O vibrations of the alkoxycarbonyl group are most probably mixed with other vibrations. The strong band at 1170 cm^{-1} in the IBECTC spectrum is probably due to the combination of O-C=O and N-C=S group vibrations. The band at 1245-1270 cm^{-1} is most likely due to C-O stretching vibrations (Silverstein et al., 1980), while the C=O bond has a broad absorption band at 1717-1770 cm^{-1}. The 1515 cm^{-1} band is due to a combination of C-N stretching and N-H deformation vibrations. The band at 2975-2965 cm^{-1} is due to CH_3 and CH_2 group vibrations. The hydrogen bonding of the N-H group is probably responsible for the band at 3255 cm^{-1}.

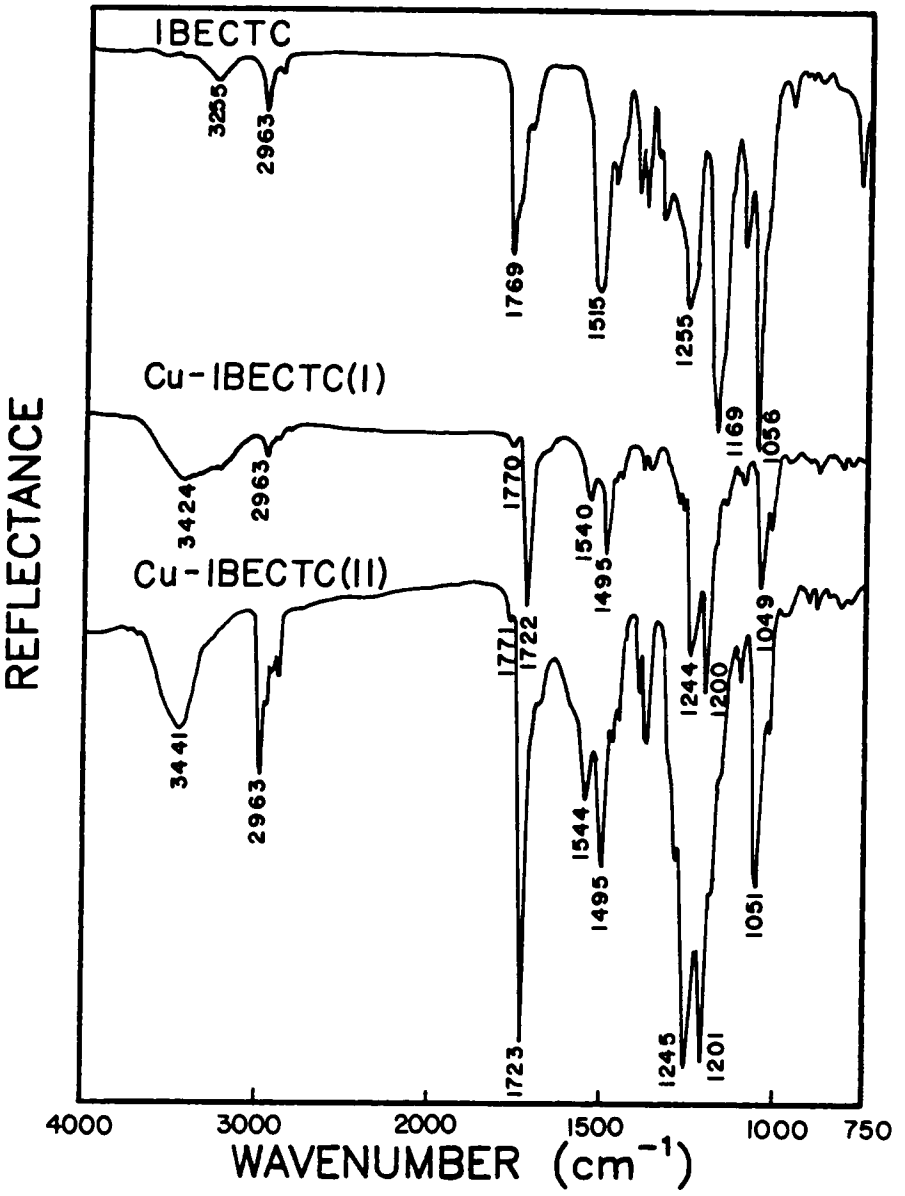

Figure 3.6. FTIR reflection spectra of IBECTC, Cu-IBECTC(I) and Cu-IBECTC(II).

In the spectra of Cu-IBECTC(I) and Cu-IBECTC(II), the stretching vibration of the ester group, O-C=O, occurs at 1201 cm^{-1}, showing a significant chemical shift from the corresponding vibration observed at 1170 cm^{-1} with IBECTC. However, the most significant shift occurs in the C=O stretching vibration, as the peak appearing at 1722 cm^{-1} exhibits a shift of 48 cm^{-1} toward a lower frequency. The N-H stretching vibration found at 3255 cm^{-1} is not evident here, probably because the broad band at 3424 cm^{-1}, attributed to water, covers it. Note that the C-N vibration shows a split at 1543 and 1495 cm^{-1}, which can be explained by the resonance structures of the molecule coordinated to Cu(I):

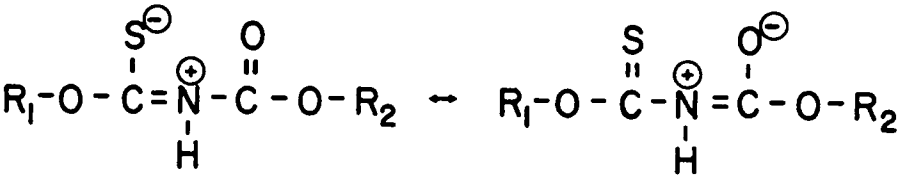

It is evident, therefore, that the bonding of IBECTC to Cu(I) involves both sulfur and oxygen, resulting in the formation of a six-membered ring compound. The stability of thionocarbamate-metal compounds is known to increase due to a chelate-ring formation (Tarantelli and Furlani,1971). A six-membered ring, as in the case of the copper-IBECTC compounds, is expected to have an enhanced stability over that of an unchelated molecule. It should be noted that there is no significant difference between the IR spectra of the two Cu-IBECTC compounds.

3.3.2 Effect of pH

Using the in-situ ATR cell, the effect of pH on the adsorption of thionocarbamates on sulfide minerals was studied. The ATR spectra of IPETC and IBECTC on chalcocite,

chalcopyrite and pyrite were recorded at different pH conditions. Although the spectra were recorded in the 4000-400 cm^{-1} region, the spectral regions shown in this section have been limited to 1600-1000 cm^{-1} and 1800-1000 cm^{-1} for IPETC and IBECTC, respectively.

a. IPETC adsorption on chalcocite

The IR spectra obtained for chalcocite in the presence of 10^{-3}M IPETC at different pH are shown in Figure 3.7. It can be seen that the IR spectrum of IPETC adsorbed on chalcocite is significantly different from those of IPETC and bulk Cu-IPETC compounds. The characteristic bands occur at intermediate positions between those of the reference compounds. However, the shifts are in the same direction from IPETC as Cu-IPETC compounds. It can therefore be concluded that on the surface of chalcocite, IPETC is bonded through its sulfur atom even though the interaction may be weaker than that in the bulk compound. Surprisingly, Bogdanov et al. (1976), in their studies of the adsorption of O-butyl-N-ethylthionocarbamate (BETC) on chalcopyrite, found that the shifts occurred in exactly the opposite direction. This finding led them to conclude that the coordination also takes place through nitrogen. However, there is no evidence from the IR spectra that would support this conclusion. Electron density calculations and the minimum energy steric conformation suggest that the NH group in IPETC is not sterically accessible to enable it form a bond with Cu (Nagaraj et al., 1989).

It is interesting to note that the IR spectra of the adsorbed species change significantly with pH. The spectra obtained at pH 2 and 4 are similar except for the magnitude of the IR signal intensity. At pH 4, the IR signal intensities are higher, which would suggest an increase in adsorption of IPETC. When the pH is increased to 6, the

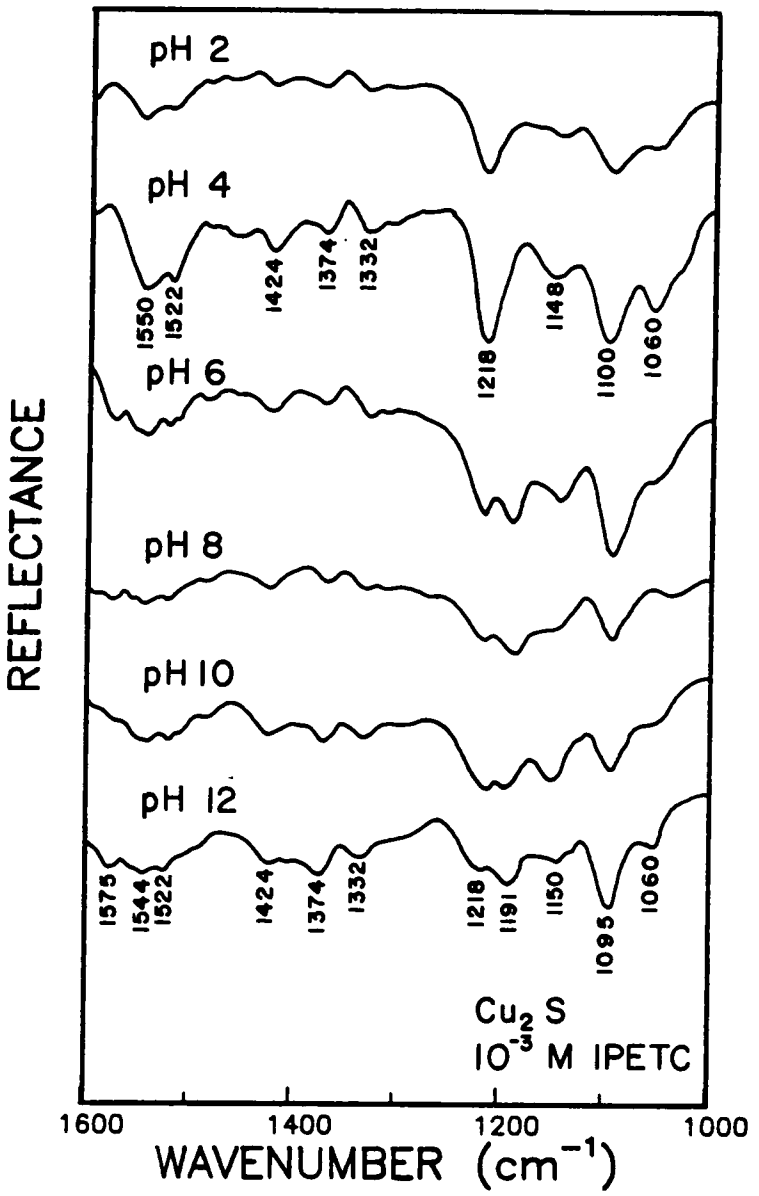

Figure 3.7. FTIR reflection spectra of IPETC adsorbed on chalcocite conditioned in 10^{-3} M IPETC solution at different pH.

IR spectrum shows new bands that appear at 1576 and 1192 cm^{-1}, while those at 1545-1549 cm^{-1} and 1218-1220 cm^{-1} get weaker. The strong signal at 1095 cm^{-1} may also represent a new band because there is a slight shoulder near 1100 cm^{-1} and the intensity of the band is significantly stronger than at pH 4. The new absorption bands that appear at pH 6 do not seem to indicate the presence of bulk precipitate because while the band at 1576 cm^{-1} is very close to that of Cu-IPETC compound, the band at 1192 cm^{-1} is not. It is likely that at low pH values, IPETC coordinates with the surface copper through its sulfur, while at high pH values, the coordination might involve both sulfur and oxygen. The shifts in C-O stretching vibrations may explain the weakening of the carbon-oxygen bond due to the coordination. Considerations of steric accessibility and electron density warrant coordination through oxygen rather than nitrogen (Glembotskii, 1977).

A further increase in pH does not show any new shifts or appearances of new peaks. The IR spectra obtained at pH 8 to 12 are similar to that obtained at pH 6. The only noticeable difference is in the decrease in the IR signal intensity. Based on the IR measurements, it would seem that the adsorption of IPETC on chalcocite is favored at acidic conditions.

b. IPETC adsorption on chalcopyrite

Figure 3.8 shows the effect of pH on the FTIR spectra of IPETC adsorbed on chalcopyrite at a collector concentration of 10^{-3}M. As shown, the characteristic bands of IPETC adsorbed on chalcopyrite occur at nearly the same frequencies as those observed on chalcocite at pH $\leq$ 4.0. This would suggest that IPETC adsorption on chalcopyrite probably also involves the coordination of surface copper with sulfur. The only noticeable difference is in the shift of the band at 1550 cm^{-1} to 1540 cm^{-1}. This

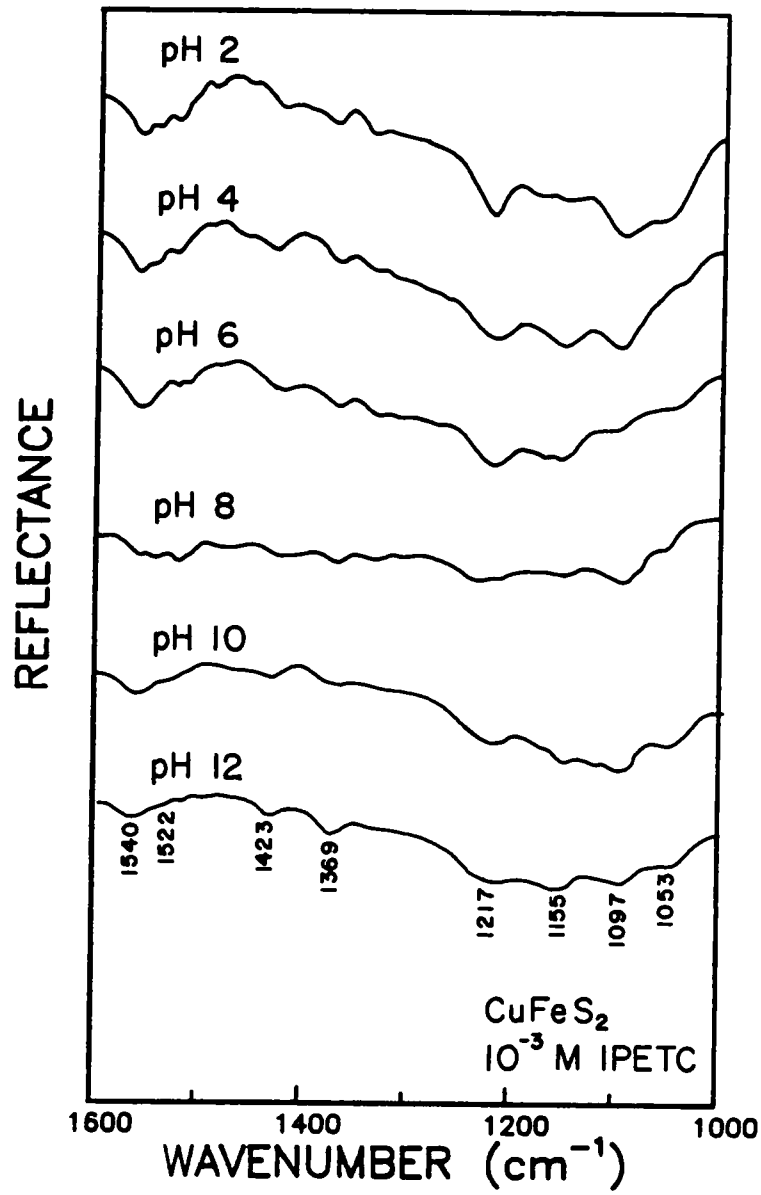

Figure 3.8. FTIR reflection spectra of IPETC adsorbed on chalcopyrite conditioned in 10^{-3} M IPETC solution at different pH.

shift is more in the direction of pure IPETC than the copper thionocarbamate compounds, probably indicating weaker chemisorption.

At higher pH conditions, the FTIR spectra obtained for chalcopyrite do not show any significant shift in band frequency or appearance of a new peak. This would suggest that IPETC adsorption on chalcopyrite does not change over the pH range of this study. However, the IR signal intensities were observed to decrease with increasing pH. This is in excellent agreement with the microflotation test results discussed in the previous chapter, even though there is a big difference in amount of collector used.

c. IPETC adsorption on pyrite

The effect of pH on the adsorpion of IPETC on pyrite was also investigated. The FTIR spectra for pyrite conditioned in 10^{-3}M IPETC solution at different pH is shown in Figure 3.9. At pH $\leq$ 8, there is a large peak found at 1090 cm^{-1} which may be attributed to the sulfoxy oxidation products present on the surface of pyrite (Miller and Wilkins, 1952). The band associated with the sulfoxy oxidation products is shifted to a higher wavenumber at pH 10 and 12. This might be due to the formation of a different oxidation product (Bellamy, 1975).

The amount of sulfoxy oxidation products present on pyrite far exceeds those on chalcocite and chalcopyrite. On the basis of their voltammetry experiments, Hamilton and Woods (1981) showed that pyrite oxidizes largely to sulfate and a small amount of elemental sulfur. Chalcocite and chalcopyrite, on the other hand, are not readily oxidized beyond the formation of elemental sulfur, according to the voltammetric studies reported by many investigators (Gardner and Woods, 1979; Walker et al., 1984; Basilio et al., 1985). It is interesting to note that the IPETC adsorption on pyrite does not remove the sulfoxy oxidation products or prevent their formation. The oxidation

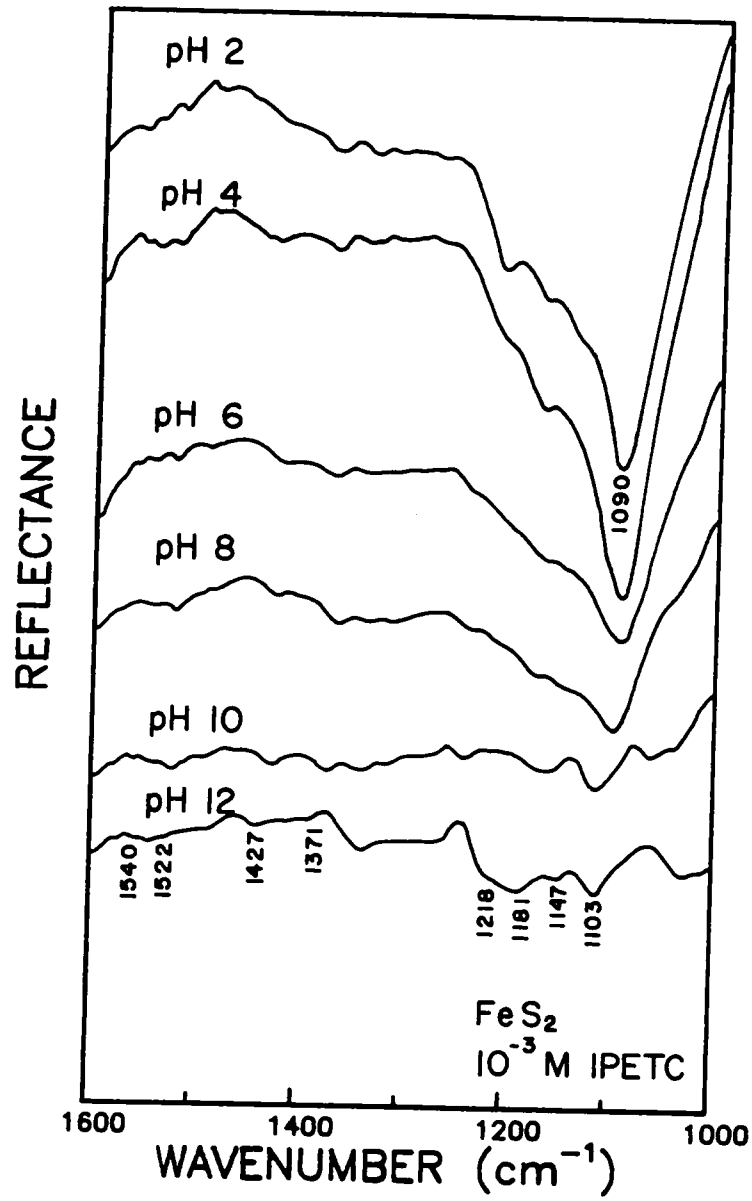

Figure 3.9. FTIR reflection spectra of IPETC adsorbed on pyrite conditioned in 10^{-3} M IPETC solution at different pH.

products are probably responsible for making the mineral surface hydrophilic. Figure 3.10 shows that the amount of the oxidation products, as determined at the 1090 cm^{-1} band, is maximum at pH 4 and decreases sharply afterwards. At pH values greater than 10, there are practically no sulfoxy oxidation products on pyrite.

The fact that IPETC is not capable of removing the oxidation products from pyrite surfaces or of preventing their formation may account for the observed selectivity against pyrite in flotation. On the contrary, when pyrite is contacted by ethyl xanthate, the oxidation products are almost completely replaced by the dixanthogen-like adsorption products, as shown in Figure 3.11. It is interesting to note that pyrite flotation is observed at pH < 4 and high IPETC concentration, where the IR spectra also show the presence of these hydrophilic oxidation products. However, the amount of IPETC adsorbed at this condition is maximum. As a result, the surface presumably is able to overcome the hydrophilic effect of the oxidation products.

Due to the large amounts of the sulfoxy oxidation products present on the pyrite surface, the IR spectrum of the oxidation products was subtracted from the original spectrum (Figure 3.9) and the resulting spectra at different pH are shown in Figure 3.12. The characteristic adsorption bands for IPETC adsorbed on pyrite show some similarity to those observed on chalcopyrite. The adsorption bands, compared to that for chalcopyrite, are shifted more toward the direction of pure IPETC, an indication of a weaker chemisorption. At higher pH values, the shift becomes more significant and the IR signal intensity decreases. This would suggest that the chemisorption of IPETC on pyrite becomes weaker with increasing pH. It may also be possible that IPETC starts to physisorb at alkaline conditions. This would be in line with the findings of Bogdanov et al. (1976) that BETC physisorbs on pyrite at high pH values.

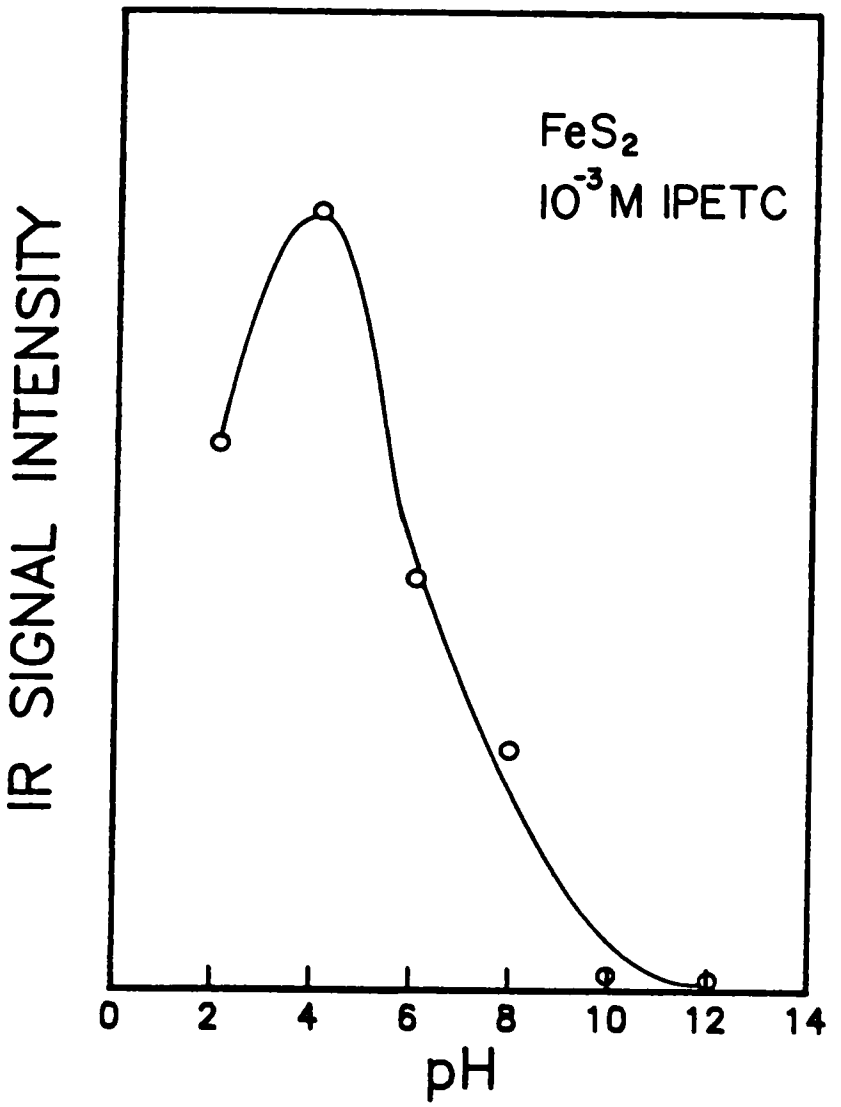

Figure 3.10. Effect of pH on the IR signal intensity of sulfoxy oxidation products detected on pyrite conditioned in 10^{-3} M IPETC solution at different pH.

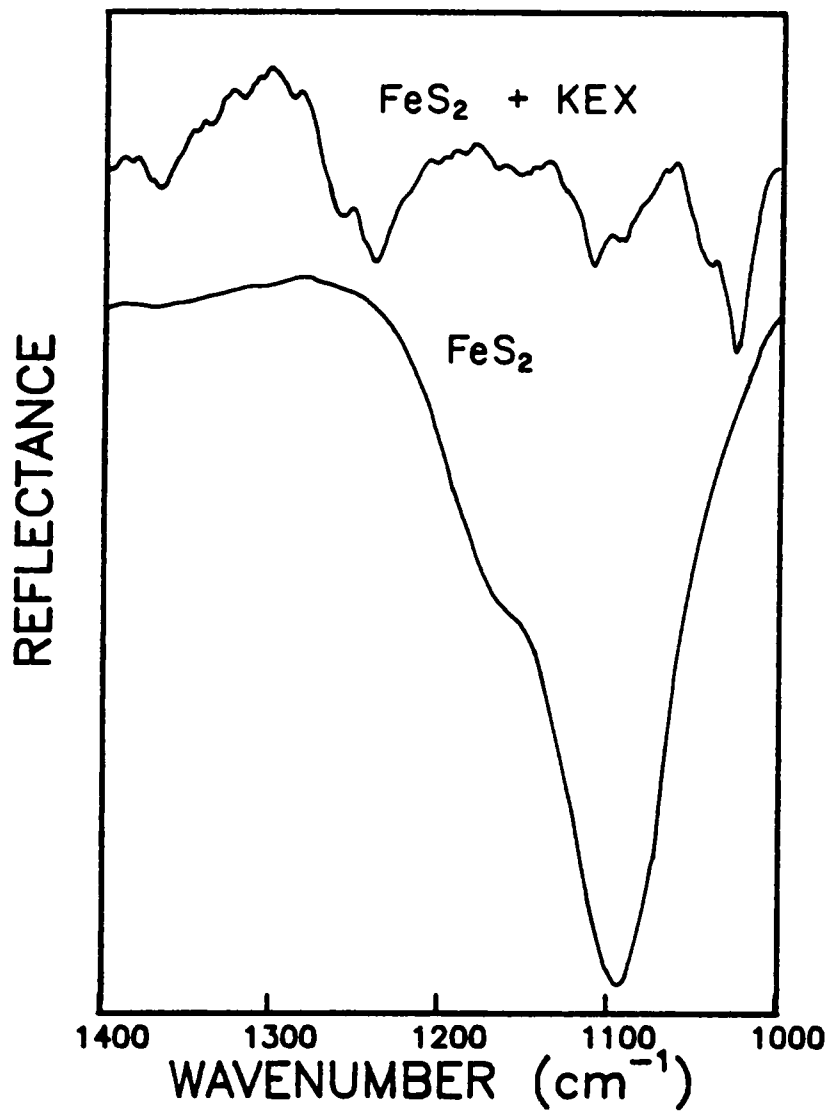

Figure 3.11. FTIR reflection spectra of IPETC adsorbed on pyrite conditioned in 0 and 5 x 10^{-4} M KEX solution at pH 6.0.

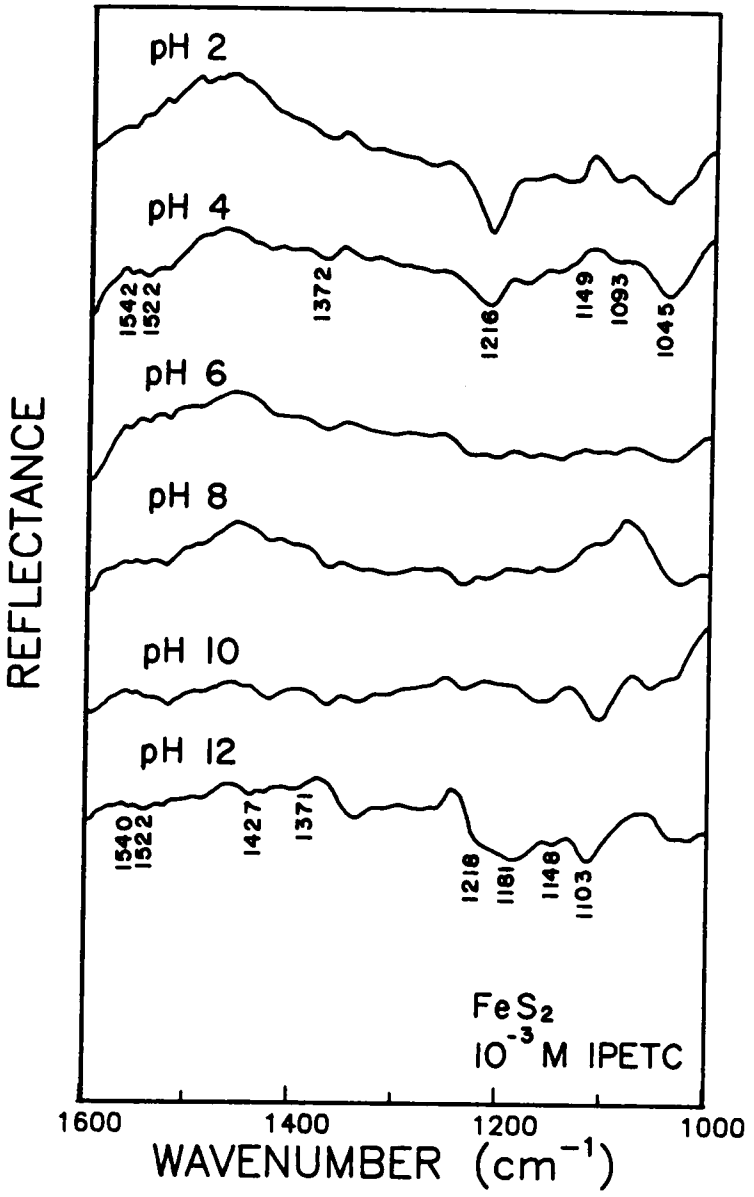

Figure 3.12. FTIR reflection spectra of IPETC adsorbed on pyrite conditioned in 10^{-3} M IPETC solution at different pH with the spectrum of pyrite in 0.01 M NaCl solution subtracted.

d. IBECTC adsorption on chalcocite

The FTIR spectra of IBECTC adsorbed on chalcocite at different pH, slightly differ from that of IBECTC (Figure 3.13). These were obtained for chalcocite treated with 10^{-3}M IBECTC solution. The C-N and C-O stretching vibrations have been shifted to 1521 cm^{-1} and 1246 cm^{-1}, respectively. The stretching band attributed to O-C=O has also been shifted to 1176 cm^{-1}. The split of the C-N vibration observed in copper-IBECTC compounds at 1543 and 1495 cm^{-1} is also seen. The peak positions characteristic of the C=O bond occur at almost the same frequencies as those of IBECTC. However, a third peak at 1728 cm^{-1} is observed close to the frequency where the C=O vibration for the copper-IBECTC compounds is found. This would indicate that the spectra is in-between the spectra of pure IBECTC and copper-IBECTC compounds and might even be a mixture of the two spectra. Based on these observations, the chemisorption of IBECTC on chalcocite probably primarily involves sulfur in its coordination with oxygen also participating in the bonding. This would form a six-membered ring compound, which agrees with the electron density calculations for alkoxycarbonyl alkyl thionocarbamates (Nagaraj et al., 1989).

Note that the degree of the shift of the C-N band due to the adsorption of the IBECTC is less than that observed with IPETC adsorption. This suggests that the bonding of the sulfur atom in IBECTC at the chalcocite surface is not as strong as with IPETC. This can be explained by the difference in the substituents involved. The substituent group in IBECTC adjacent to the C=S group is electron-withdrawing, unlike that in IPETC, which makes the electron density lower at the reactive center of IBECTC. This finding is in agreement wth Glembotskii's work (1977). However, it should be pointed out that IBECTC adsorption would still be stronger due to the formation of the chelate structure.

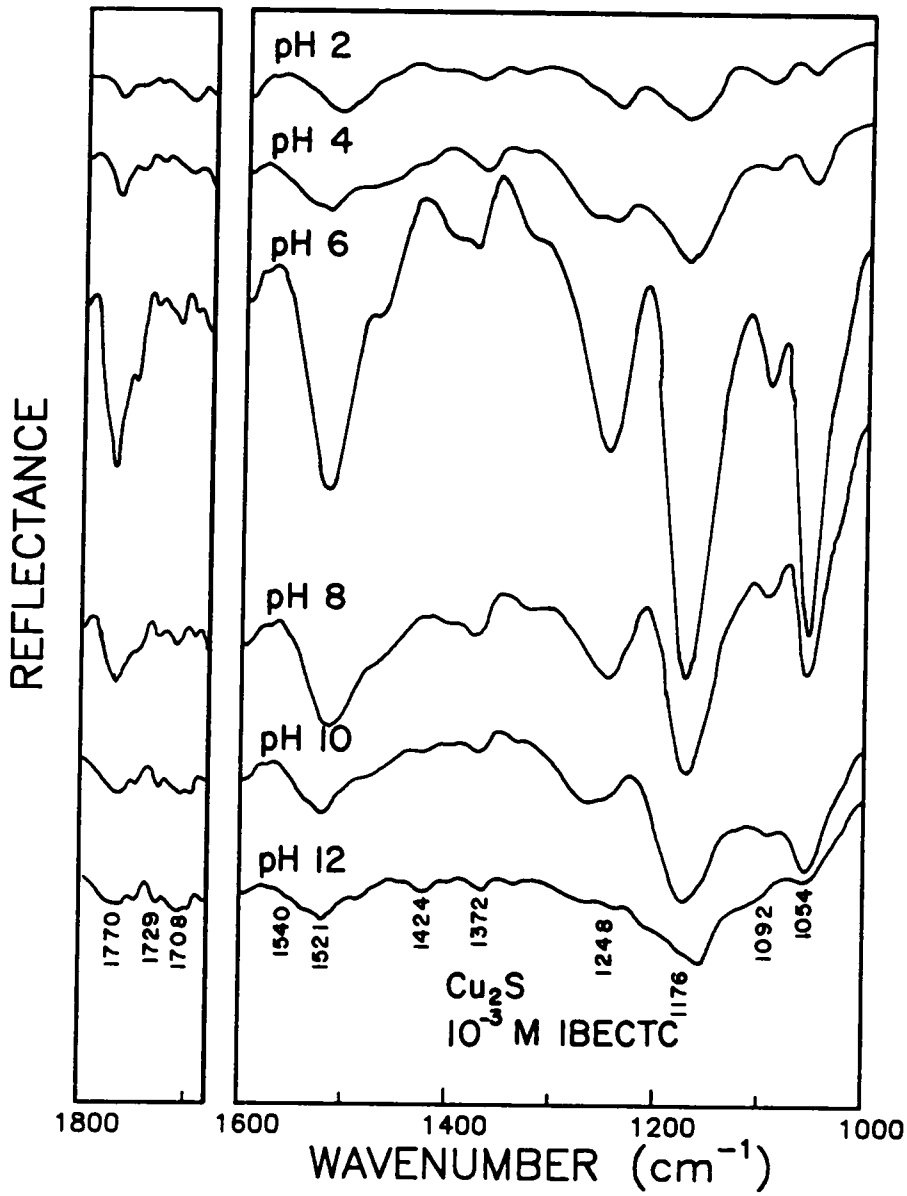

Figure 3.13. FTIR reflection spectra of IBECTC adsorbed on chalcocite conditioned in 10^{-3} M IBECTC solution at different pH.

At the higher wavenumbers (not shown) the adsorption peaks of water dominate. The bands for the N-H stretching vibrations found in this region have either disappeared or are masked by the water vibrations. Their disappearance would indicate the breaking of the N-H group in IBECTC during adsorption. The C-H stretching vibrations of the CH_3 and CH_2 groups are still present near the same frequencies where they are found in the reference compound.

The IR signal intensities for the characteristic adsorption peaks show a maximum at pH 6. This decreases continuously with increasing alkalinity. The general shape of the spectra, however, do not seem to have changed up to pH 10. At pH 12, the band at 1176 cm^{-1} has been shifted significantly. The band for the O-C=O and N-C=S group vibrations now appears at 1159 cm^{-1}. This might be due to the instability of IBECTC, which has a pKa of 10.5 (Lewellyn, 1983). At pH $\geq$ 11, the IBECTC molecule has been found to ionize into two forms according to reaction [1.5]. The other adsorption bands though, do not seem to have been affected by the ionization at pH 12.

e. IBECTC adsorption on chalcopyrite

Figure 3.14 shows the effect of pH on the adsorption of 10^{-3}M IBECTC on chalcopyrite. The FTIR spectra of IBECTC adsorbed on chalcopyrite is similar to the spectra obtained on chalcocite. Compared to the IR spectrum of IBECTC, the C-N vibrations have shifted to almost the same position as that of IBECTC adsorption on chalcocite although there is a difference in the shift of the C-O and O-C=O vibrations. The C=O bond appears at approximately the same frequencies as those of IBECTC and IBECTC on chalcocite. However, the intensities of the two major peaks at 1770 and 1752 cm^{-1} have been reversed. It can therefore be concluded that IBECTC chemisorbs on chalcopyrite in the same way as it does on chalcocite. The coordination with oxygen

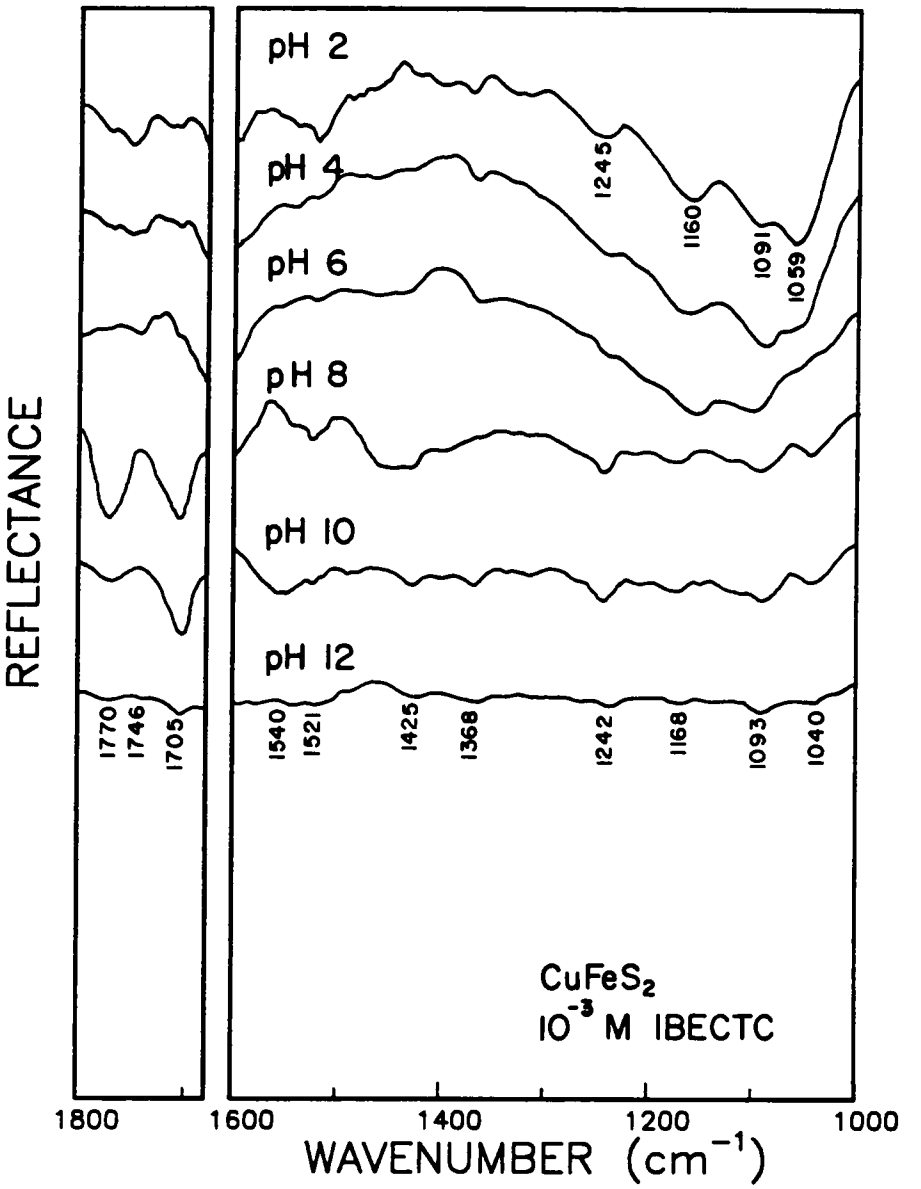

Figure 3.14. FTIR reflection spectra of IBECTC adsorbed on chalcopyrite conditioned in 10^{-3} M IBECTC solution at different pH.

would probably be stronger here compared to that found with chalcocite, as shown by the greater degree of shift of the O-C=O and change in the relative intensities of the C=O vibrations.

Based on the intensities of the IR signal, the adsorption of IBECTC on chalcopyrite is favored at acidic conditions. It indicates maximum adsorption at pH 2 which decreases continuously at higher pH. This is in good agreement with the flotation results. Changing the pH does not seem to show any significant effect on the characteristic peak positions. The ionization of IBECTC at pH 12, which was observed previously, does not seem to be evident in the IR spectrum.

f. IBECTC adsorption on pyrite

ATR measurements were carried out on pyrite in 10^{-3}M IBECTC solution, at different pH. The FTIR spectra obtained from these measurements are shown in Figure 3.15. These spectra are different from those obtained on chalcocite and chalcopyrite. The main difference is in the appearance of the band attributed to the presence of sulfoxy oxidation products on the surface of pyrite. Figure 3.16 shows that the sulfoxy oxidation products are high at acidic conditions and decreases strongly at higher pH. As has been the case with IPETC, the adsorption of IBECTC on pyrite also does not remove or prevent the formation of sulfoxy oxidation products. This may explain the improved selectivity of IBECTC against pyrite.

After subtraction of the IR spectrum of pyrite in blank solutions (without IBECTC), the resulting spectra show more clearly, the adsorption behavior of IBECTC on pyrite (Figure 3.17). It can be seen that the IR spectra has some similarity to those observed on chalcopyrite. A significant difference is in the shift of the band associated with the coordination of O-C=O and N-C=S group vibrations. On pyrite, this occurs

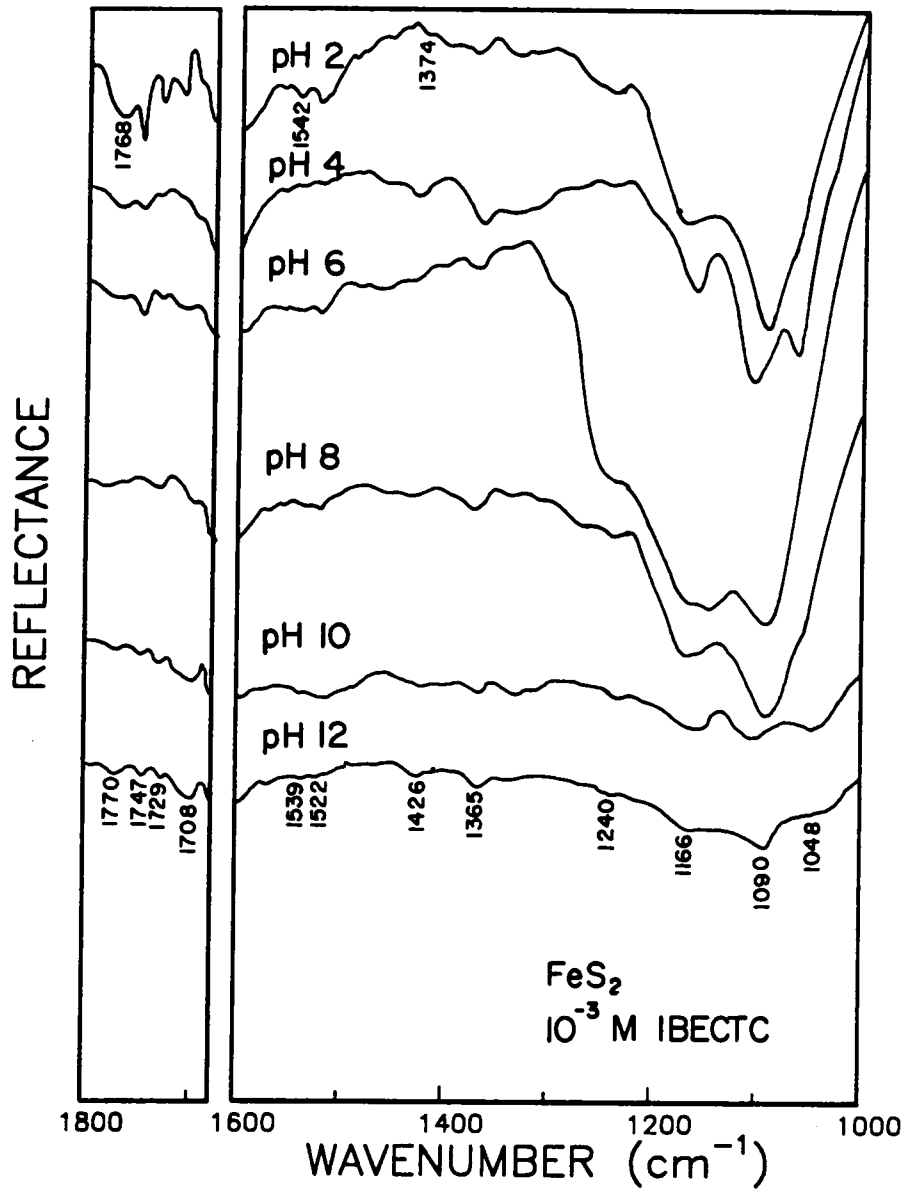

Figure 3.15. FTIR reflection spectra of IBECTC adsorbed on pyrite conditioned in 10^{-3} M IBECTC solution at different pH.

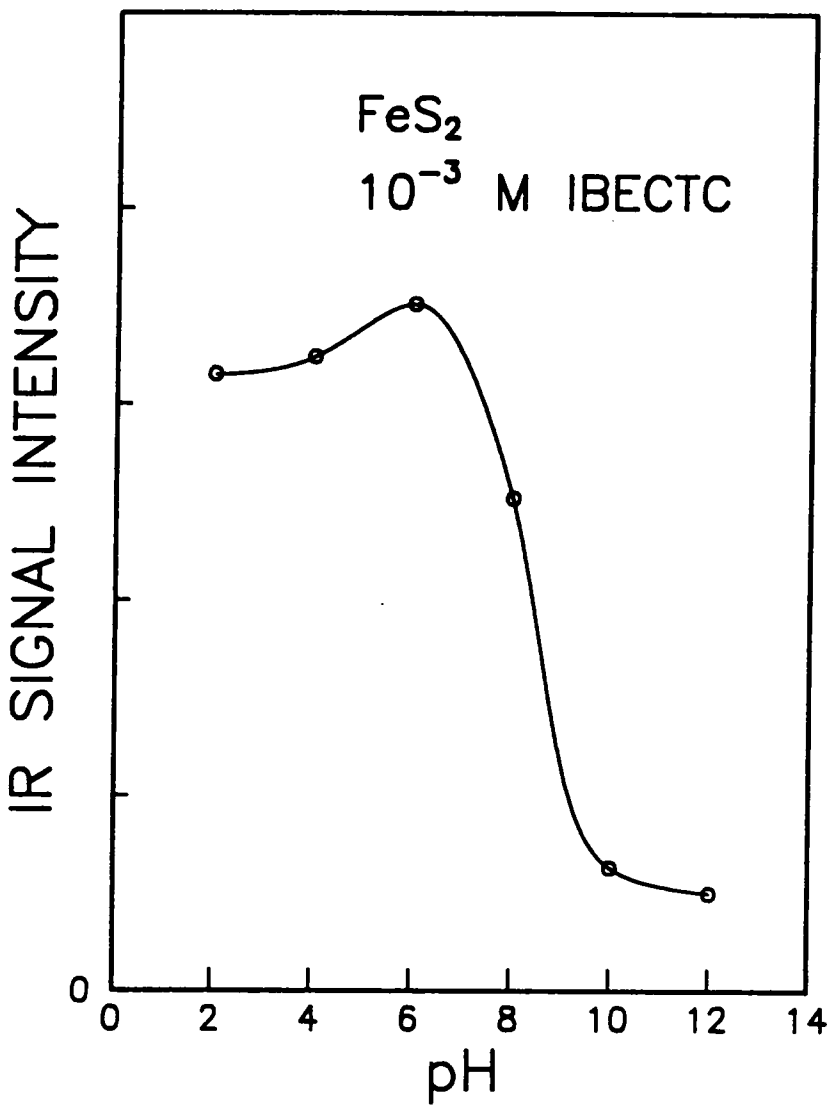

Figure 3.16. Effect of pH on the IR signal intensity of sulfoxy oxidation products detected on pyrite conditioned in 10^{-3} M IBECTC solution at different pH.

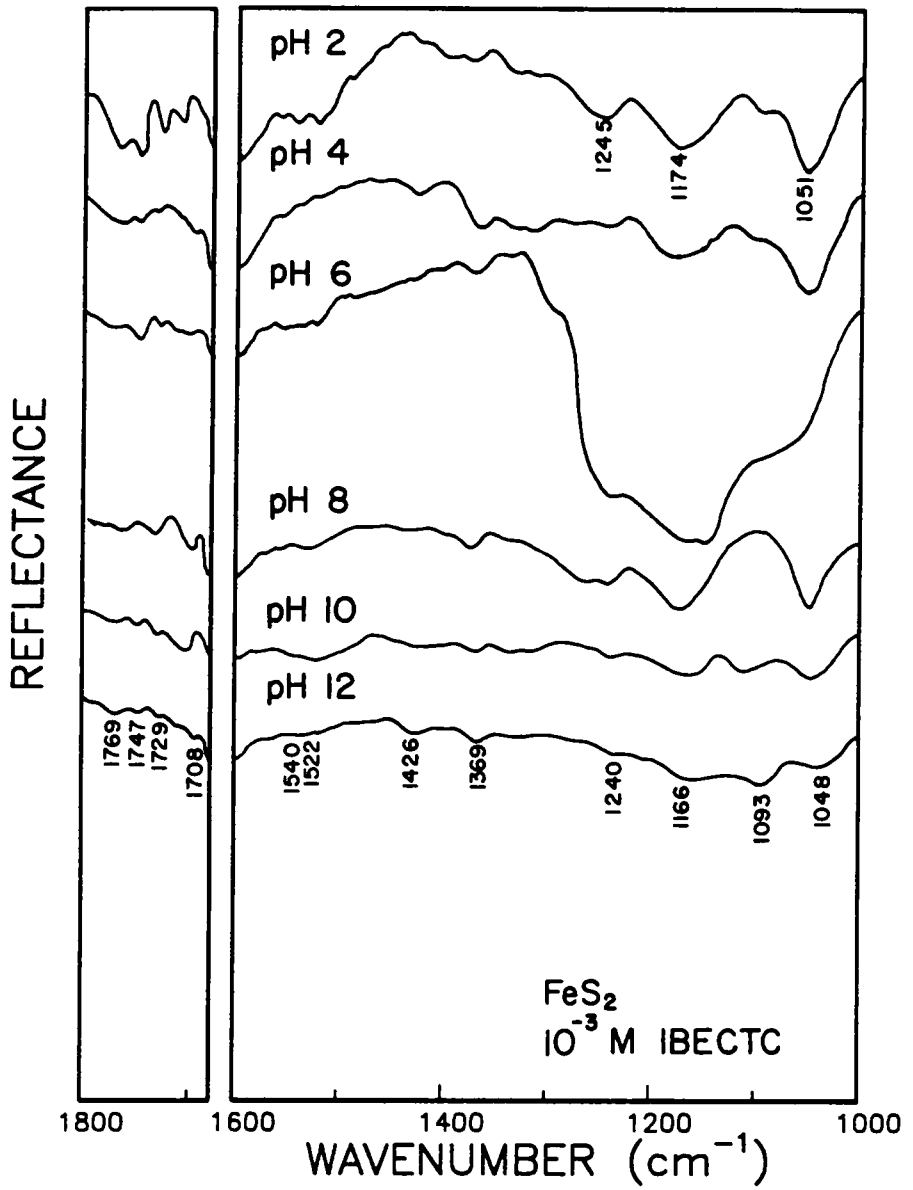

Figure 3.17. FTIR reflection spectra of IBECTC adsorbed on pyrite conditioned in 10^{-3} M IBECTC solution at different pH with the spectrum of pyrite in 0.01 M NaCl solution subtracted.

at the same frequency as that of IBECTC. The adsorption of IBECTC on pyrite, therefore, would probably be weaker. There is also the possibility that physisorption occurs on pyrite at alkaline conditions.

Except for the amount of adsorption, the pH of the solution does not seem to affect the adsorption of IBECTC. The IR signal intensities tend to decrease with increasing pH. This would probably be due to the instability of IBECTC at very alkaline conditions.

3.3.3 Effect of Concentration

In the next series of experiments, the effect of concentration on the adsorption of IPETC and IBECTC on chalcocite is investigated. The FTIR spectra obtained from chalcocite conditioned in different concentrations at pH 6 are shown in Figure 3.18. Even at a concentration as low as 10^{-5}M, IPETC adsorption is already evident in the FTIR spectrum. The bands occuring at 1500-1600 cm^{-1}, which have been attributed to mixed vibrations of the C-N stretching and N-H deformation, are present in the spectrum. This occurs at nearly the same frequencies previously found for chalcocite at acidic pH. The bands attributed to the antisymmetric and symmetric O-C=S stretching vibrations are observed at 1215 cm^{-1} and 1147 cm^{-1}, respectively. The adsorption band at 1090 cm^{-1} has contributions from C-N, C=S and C-H vibrations. Compared to the spectrum of IPETC, the slight shifts in frequencies are generally directed towards those of the bulk Cu-IPETC compound. Except for an increase in intensity, the spectra remains the same with increasing IPETC concentrations. However, at an IPETC addition of 3 x 10^{-4}M, the spectrum changes and becomes similar to that obtained at pH 6 and 10^{-3}M IPETC (Figure 3.7). The C-N stretching band now appears at 1576 cm^{-1} . The absorption band at 1215 cm^{-1} has now split into

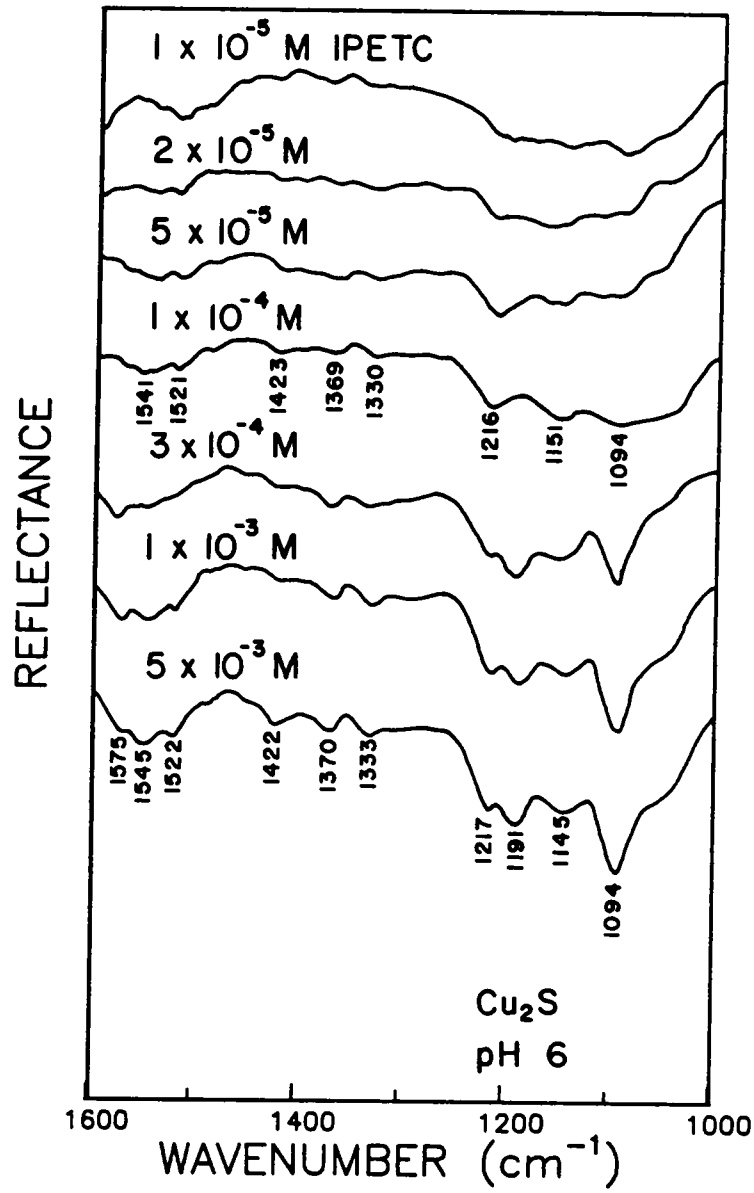

Figure 3.18. FTIR reflection spectra of IPETC adsorbed on chalcocite conditioned at different concentrations of IPETC solution at pH 6.0.

1217 and 1191 cm^{-1}. This has been attributed previously to the different resonance forms of the IPETC ligand. It is also interesting to note that the band between 1090-1100 cm^{-1} is now dominant. The spectra at higher concentrations show a slight increase in signal intensity, but do not show any new peaks or shifts in frequency.

Figure 3.19 shows the FTIR spectra of IBECTC adsorbed on chalcocite at pH 6 and different concentrations. At an IBECTC addition of 10^{-5}M, the spectrum is similar to that obtained at acidic conditions and 10^{-3}M IBECTC (Figure 3.13). The spectra do not show any shifts or appearances of new peaks up to a concentration of 5 x 10^{-5}M. Further increases in concentration show a shift of the characteristic bands toward the direction of IBECTC. The spectra obtained at this concentration appear to be a mixture of the spectra at lower concentrations and pure IBECTC. In fact, spectral subtraction of the pure IBECTC spectrum from that obtained at 10^{-3}M results in a spectrum similar to that obtained at lower concentrations. This might indicate that physical adsorption of IBECTC occurs on top of the chemisorbed layer. There is also the possibility that the physisorbed species observed at high concentrations are undissolved IBECTC molecules.

The IR signal peak intensity at the characteristic absorption bands of IPETC and IBECTC on chalcocite (1500-1550 and 1240-1250 cm^{-1}, respectively) can be used as a measure of the relative amount of collector adsorption. Figure 3.20 shows the adsorption of IPETC and IBECTC on chalcocite at pH 6 as a function of concentration. IPETC adsorption reaches a plateau with an initial concentration of 3 x 10^{-4}M, which may represent a monolayer coverage. With IBECTC, a plateau appears near 5 x 10^{-5}M, but the adsorption continues to increase at higher concentrations. As shown by the FTIR spectra, it seems that IBECTC is capable of physically adsorbing on top of the chemisorbed monolayer, while IPETC cannot. The presence of O-C=O group in this relatively large molecule may allow the physical adsorption. It is interesting to note

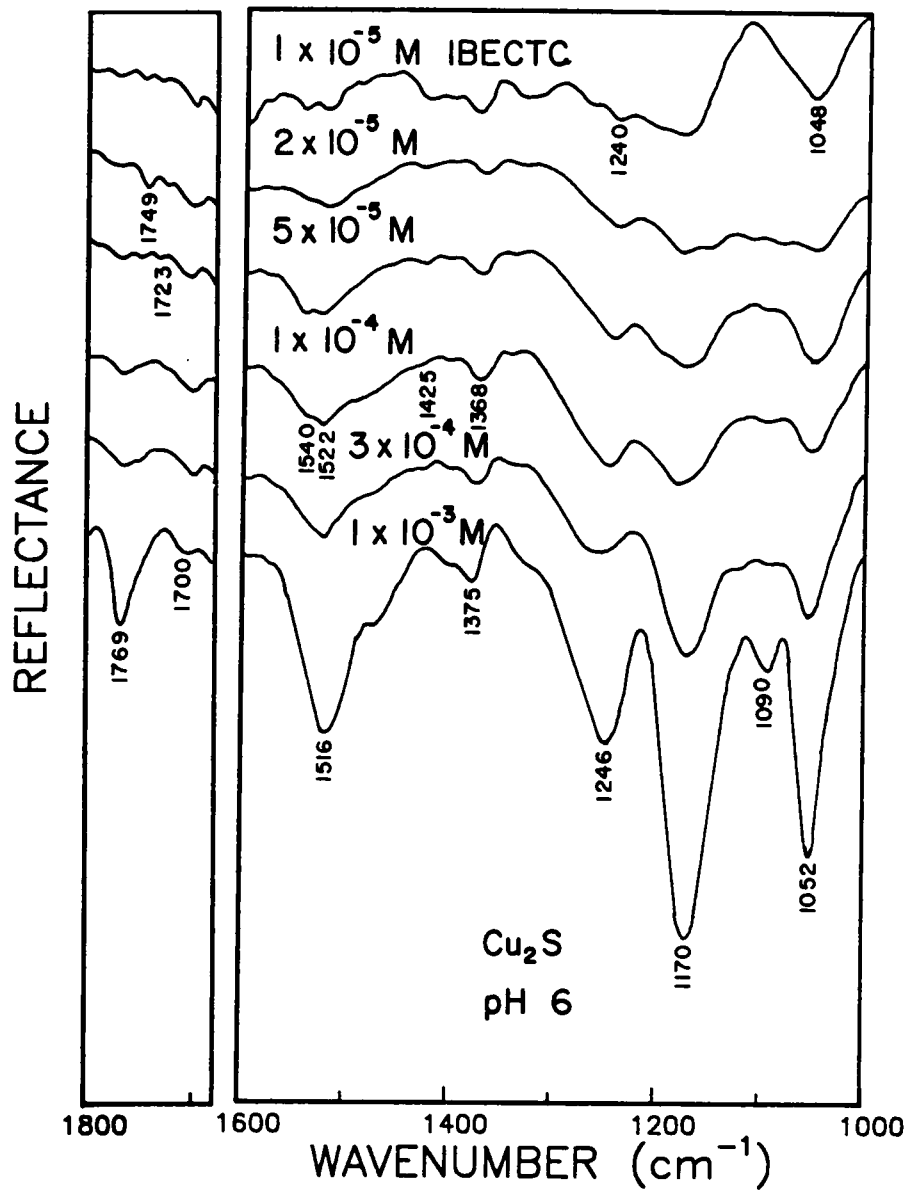

Figure 3.19. FTIR reflection spectra of IBECTC adsorbed on chalcocite conditioned at different concentrations of IBECTC solution at pH 6.0

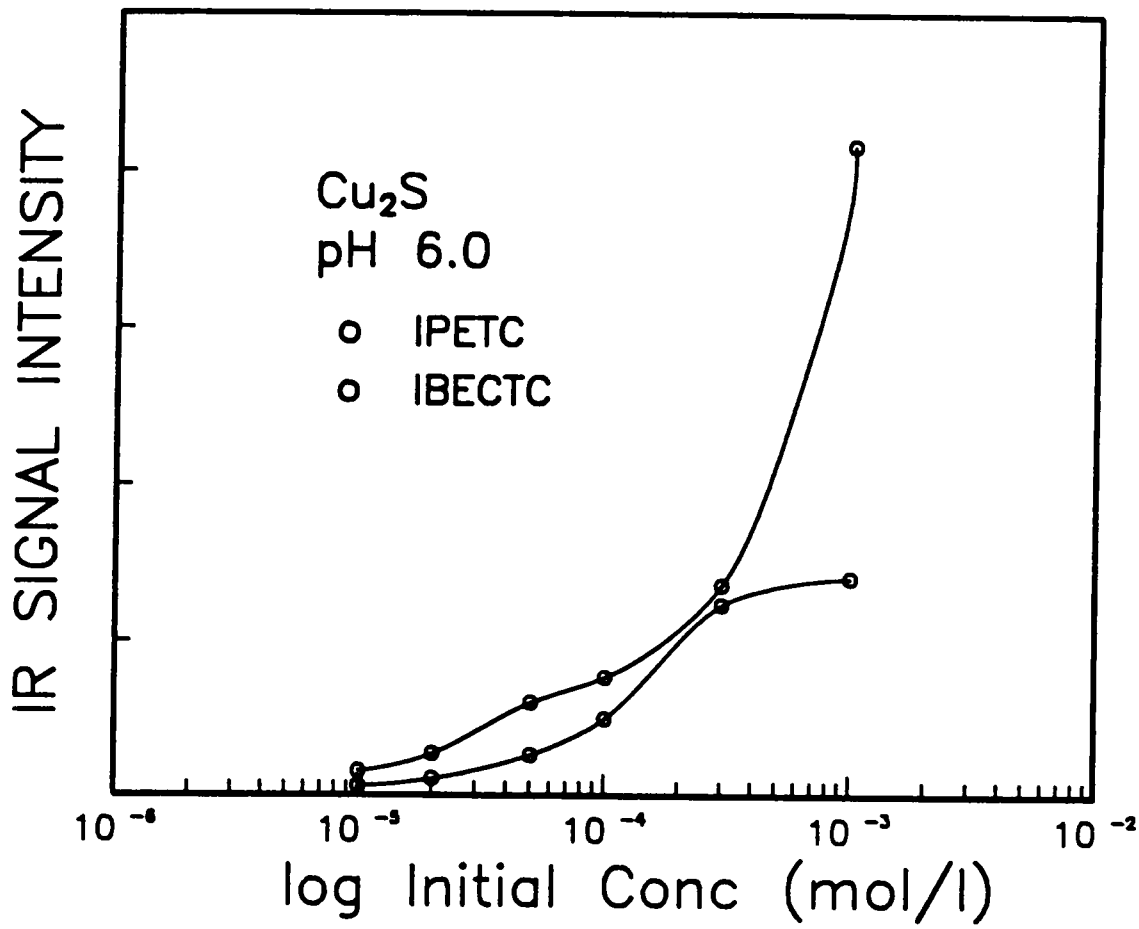

Figure 3.20. Effect of concentration on the IR signal intensity of IPETC and IBECTC adsorbed on chalcocite conditioned at pH 6.0

that the amount required for monolayer coverage of IBECTC is lower than that of IPETC.

3.3.4 Effect of Potential

Results of the voltammetric experiments showed that the thionocarbamates adsorbed on the electrode non-electrochemically. On chalcocite and copper, thionocarbamates also react electrochemically to form an adsorbed compound as the electrode is being oxidized. Consequently, a direct examination of the surface using FTIR would help verify these observations. Using an ECATR cell, in-situ FTIR investigation of IPETC and IBECTC adsorption on copper and chalcocite, under electrochemically controlled conditions, have been carried out. To check the electrochemical behavior of the cell, voltammetry has been done on a chalcocite electrode using the ECATR cell. Figure 3.21 compares the voltammogram obtained using the ECATR cell with that using a single solid mineral electrode in the standard electrochemical cell. It can be seen that the general electrochemical behavior of chalcocite is the same except for the magnitude of the current. This can be expected since the particle bed electrode has a larger surface area. The similarity of the voltammograms indicate that there is no external electrochemical effect being introduced in the ECATR cell.

a. IPETC adsorption on Cu

The reflectance spectra of the surface IPETC species on copper at different potentials and in the presence of 10^{-3}M IPETC are shown in Figure 3.22. The spectra of the IPETC adsorbed on copper are quite different from that of IPETC or the

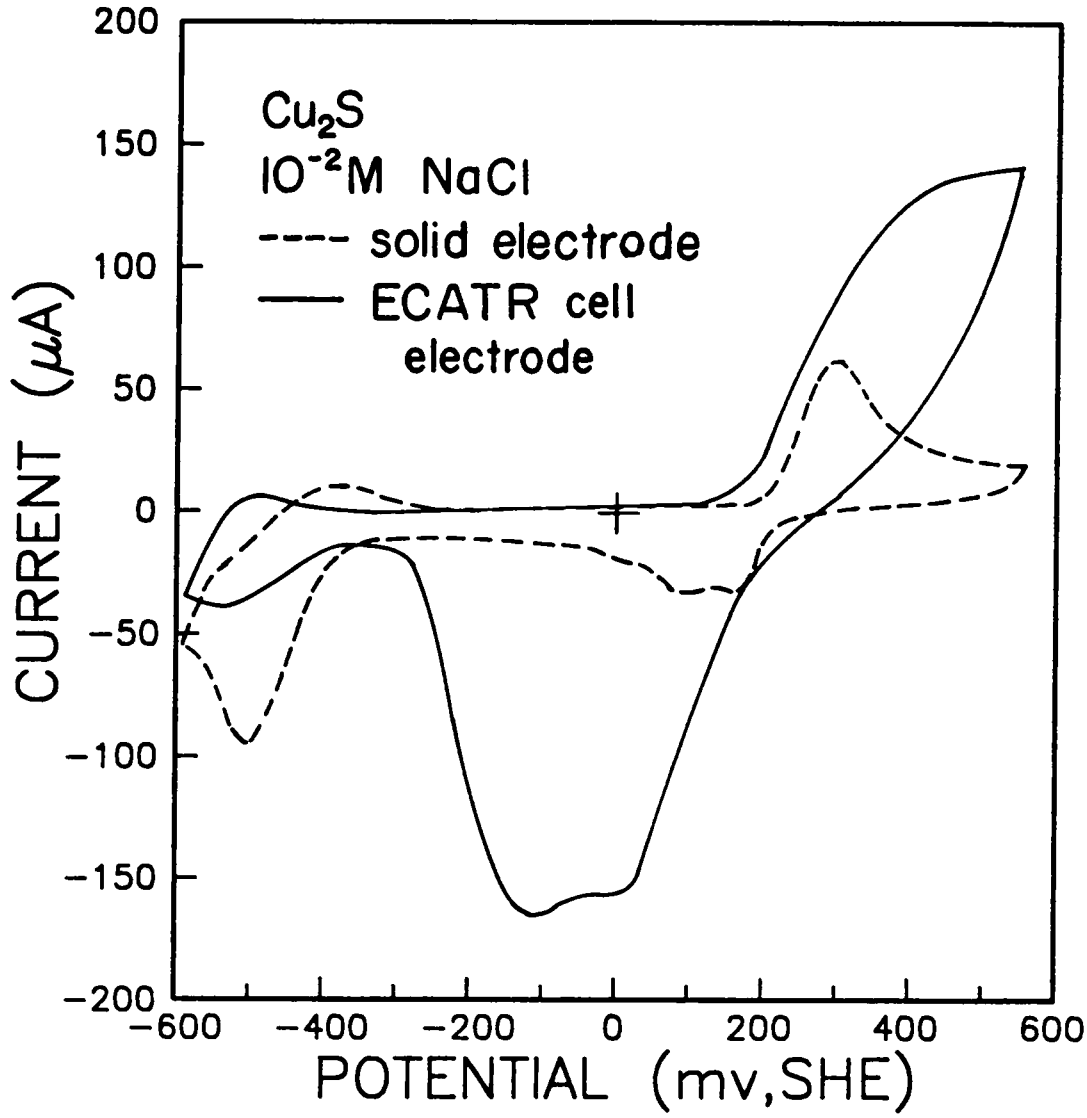

Figure 3.21. Voltammogram of chalcocite in stirred 0.01 M NaCl solution and chalcocite particle electrode in a spectroelectrochemical cell.

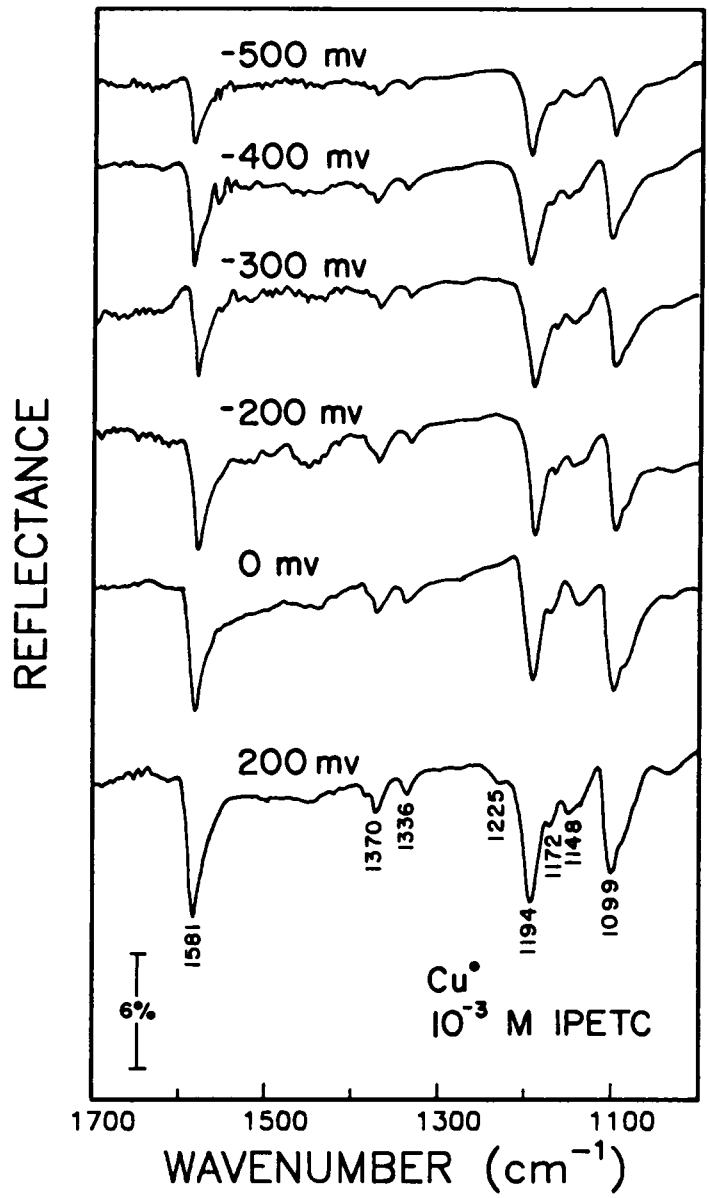

Figure 3.22. FTIR reflection spectra of IPETC adsorbed on copper conditioned in 10^{-3} M IPETC solution at pH 6.0 and different potentials.

copper-IPETC compounds. The band which has contributions from C-N stretching and N-H deformation has been shifted to 1581 cm^{-1}. Although not shown here, the band (3180-3350 cm^{-1} region) associated with the hydrogen-bonded N-H stretching vibrations has disappeared. These results suggest that the N-H bonding has been broken during the adsorption process. Also, the strong absorption band due to the antisymmetric O-C=S stretching vibration is now found at 1194 cm^{-1}. These chemical shifts would be indicative of the bonding of Cu with IPETC through the sulfur atom. This mode of bonding is similar to the one previously observed on chalcocite. However, their spectra are different presumably due to the difference in optical properties of the two surfaces.

IPETC adsorption on copper becomes significant at a potential of -500 mv. At lower potentials, there are indications of some adsorption of IPETC. However, the significance of these absorbance peaks is limited by the level of the signal to noise (S/N) ratio. Increasing the potential does not result in any distinct shift in the frequencies where the characteristic absorption bands occur. This indicates that there is only one type of adsorbed species involved in the adsorption process. Since the N-H bond is most probably broken, then IPETC adsorption of copper may be represented by a coupled chemical reaction involving reactions [2.8] and [2.10].

The anodic current attributed to the formation of a copper-IPETC compound in the voltammetry experiments is not reflected in the FTIR measurements. There is no significant shift or appearance of new peaks in the spectrum even at potentials where copper starts to oxidize. This may indicate that the IPETC interaction product observed in the voltammogram is the same as the surface species adsorbed initially at the starting potential.

Figure 3.23 shows the change in the IR signal intensity measured at 1194 cm^{-1}. Assuming this to be a direct measure of the amount of IPETC adsorbed, it can be stated

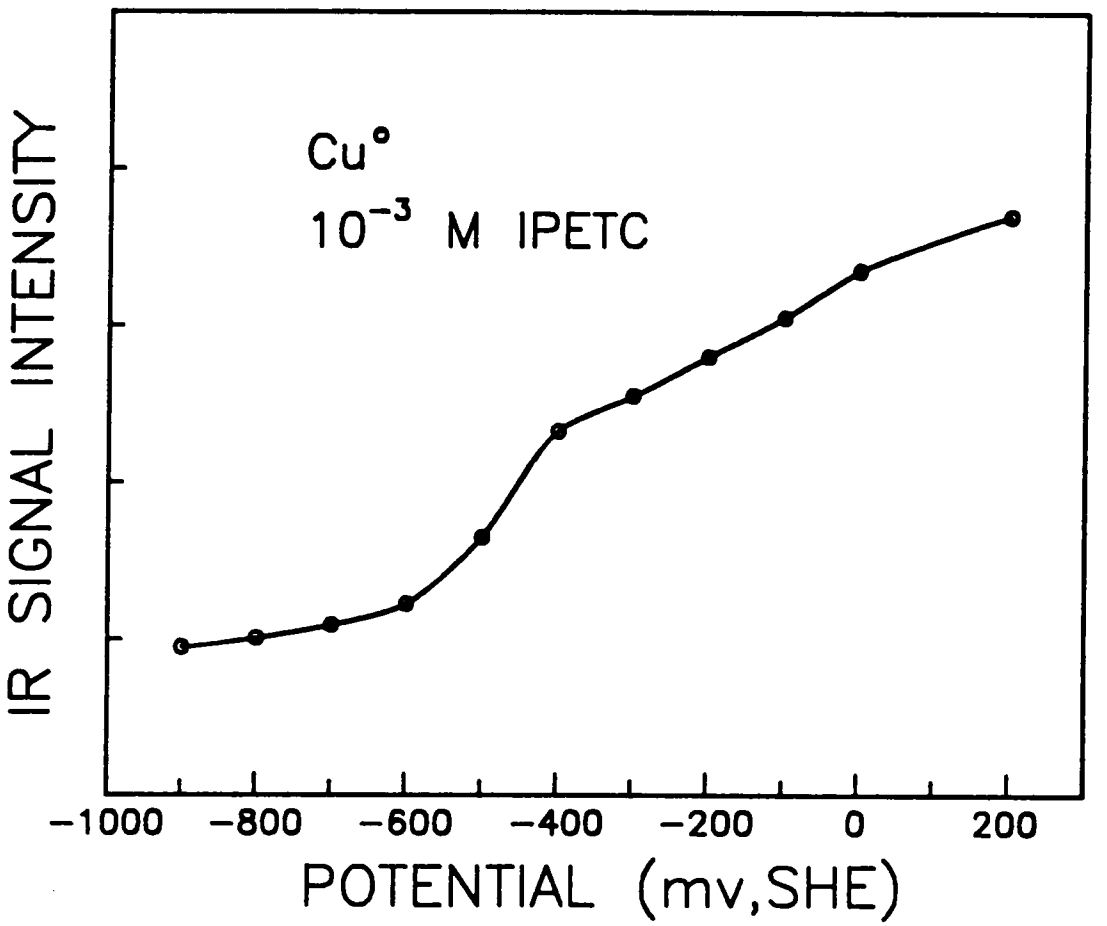

Figure 3.23. Effect of potential on the IR signal intensity of IPETC adsorbed on copper conditioned in 10^{-3} M IPETC solution at pH 6.0.

that IPETC adsorption on copper increases with increasing potential. There is some IPETC adsorption observed below -600 mv. However, as stated previously, the S/N ratio measured at these potentials limits the accuracy of the measurements. Above -600 mv, the slope of the curve changes. This might indicate that IPETC adsorption is enhanced as more Cu(I) ions become available. However, there are no indications that the products formed at these potentials are different from those adsorbed initially. It should also be noted that holding the system at a constant potential for extended periods of time resulted in a negligible change in signal intensities; therefore, the observed increase in adsorption is due to a change in potential. Thermodynamic calculations for the Cu-H_2O system have shown that Cu(I) concentration increases with increasing potential. The % $Cu(IPETC)_2Cl$ curve also increases sharply above -520 mv (Figure 2.7), which agrees with the FTIR data.

Using IRAS, the reflectance spectra of the surface IPETC species on copper at different potentials were recorded. Figure 3.24 shows that the spectra are similar to those obtained during in-situ spectroelectrochemical measurements. At the starting potential of -900 mv, IPETC is found to be slightly adsorbed. However, the signal intensity measured at this potential is not much higher than the S/N ratio. Significant IPETC adsorption is observed above -600 mv. There seems to be no apparent chemical shifts in the spectra with changing potential, an observation also made using the ECATR cell. The only significant effect of potential is on the magnitude of the signal intensities. Figure 3.25 shows the increase in signal intensity, measured at 1194 cm^{-1}, with potential. Adsorption increases sharply above -100 mv. This may be related to the copper-IPETC interaction observed at around this potential in the voltammogram (Figure 2.17). The adsorption of IPETC starts to decrease at potentials > 100 mv, which was not observed in the ATR measurements. This is probably due to the difference in the sample preparation. It should be noted that when using IRAS, the

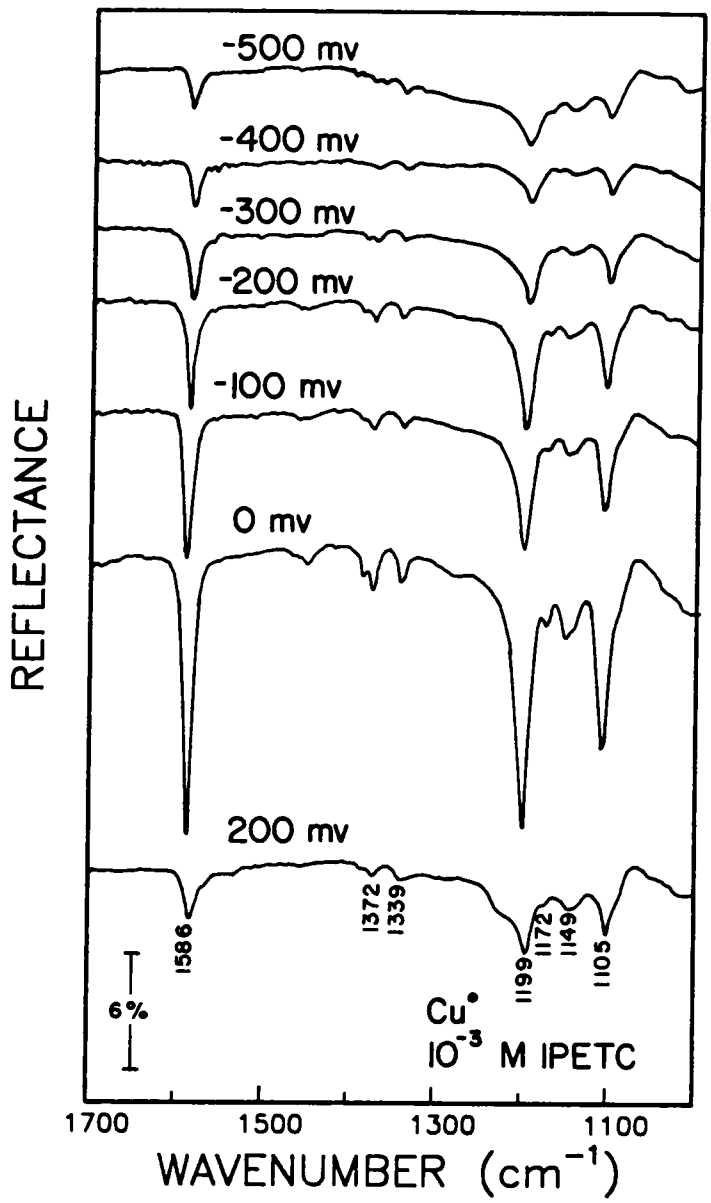

Figure 3.24. IRAS spectra of IPETC adsorbed on copper conditioned in 10^{-3} M IPETC solution at pH 6.0 and different potentials.

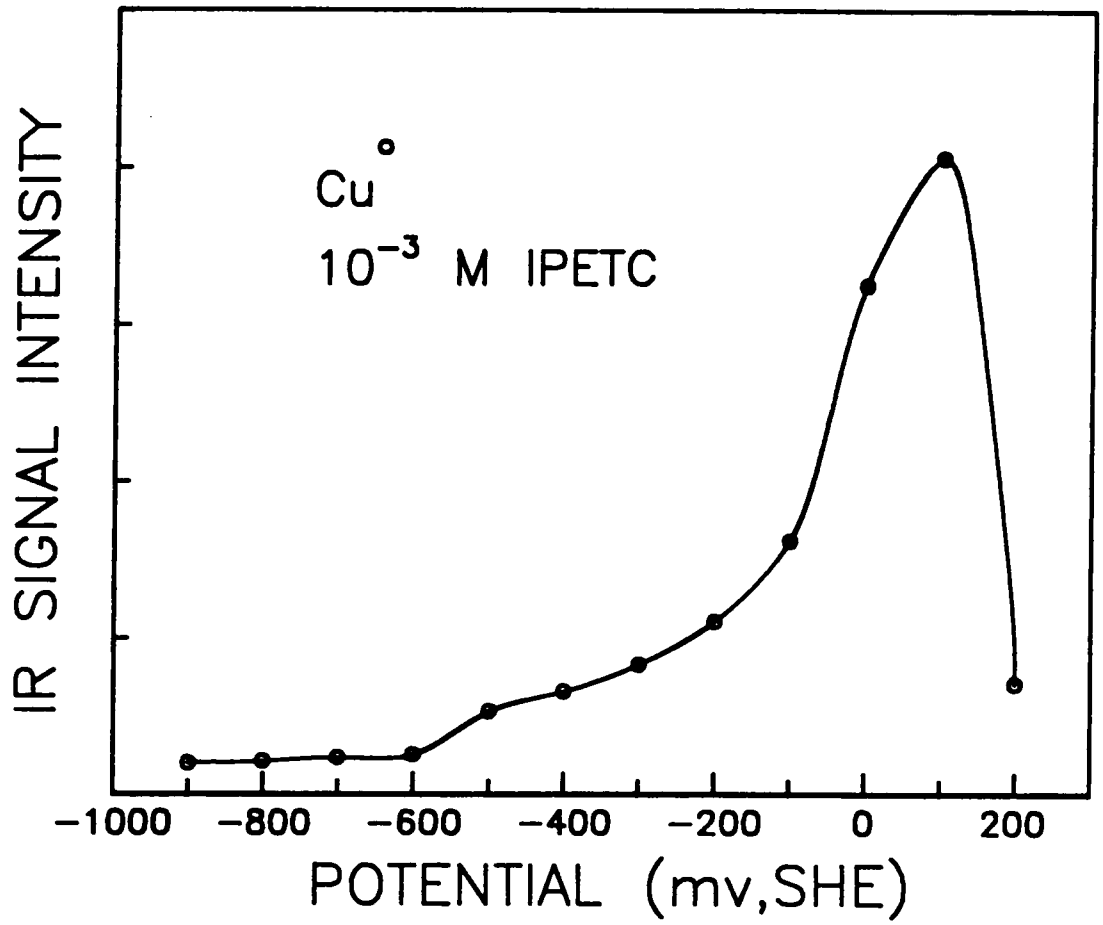

Figure 3.25. Effect of potential on the IR signal intensity of IPETC adsorbed on copper conditioned in 10^{-3} M IPETC solution at pH 6.0.

sample was freshly-cleaned prior to measurement at each potential. At higher potentials, the oxidation of the electrode to copper oxide is probably faster than IPETC adsorption. This decrease in adsorption, therefore, should not be confused with desorption.

b. IPETC adsorption on chalcocite

The ATR spectra of a chalcocite electrode surface in the presence of 10^{-3}M IPETC at different potentials are shown in Figure 3.26. The adsorption of IPETC is already observed even at a potential as low as -400 mv. An increase in potential does not seem to affect the band positions of the characteristic absorption peaks. There is also no correlation between the IR spectra and the observed anodic peak attributed to the chalcocite-IPETC interaction (Figure 2.18). The discrepancy may be an indication that the species produced by this interaction are also the same as that adsorbed initially.

The ATR spectra of the surface IPETC species on chalcocite are different from those observed on chalcocite at open-circuit potentials (Figure 3.7). Instead, they are similar to those observed on copper with the characteristic bands occuring at almost the same frequency for the two systems. This similarity may be due to the reduction of the chalcocite electrode surface to copper at the starting potential. In this experiment, cathodic curents were observed initially at the starting potential. This supports the suggestion that the chalcocite surface has been reduced to copper, which is thermodynamically favored at these conditions.

Figure 3.27 shows the effect of potential on the IR signal intensity of the characteristic absorption peak (1194 cm^{-1}). The adsorption of IPETC increases with increasing potential. Contact angle measurements (Figure 2.32) also show the same trend up to -200 mv; adsorption then remains constant at higher potentials. It should

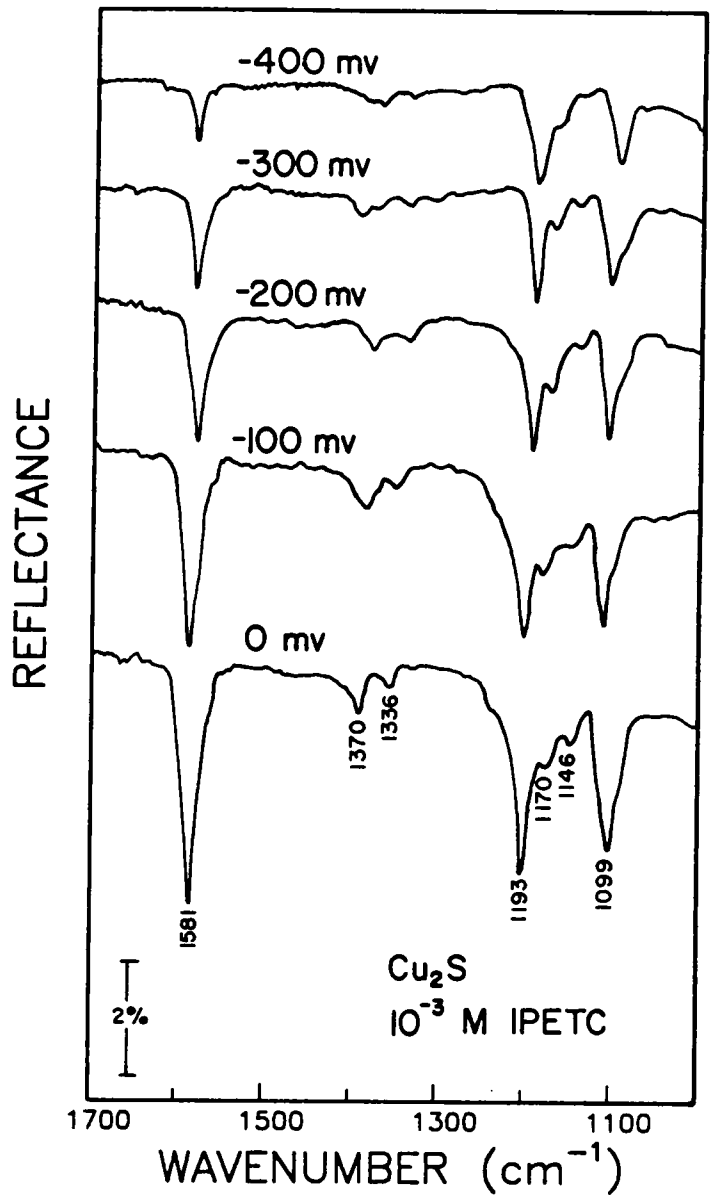

Figure 3.26. FTIR reflection spectra of IPETC adsorbed on chalcocite conditioned in 10^{-3} M IPETC solution at pH 6.0 and different potentials.

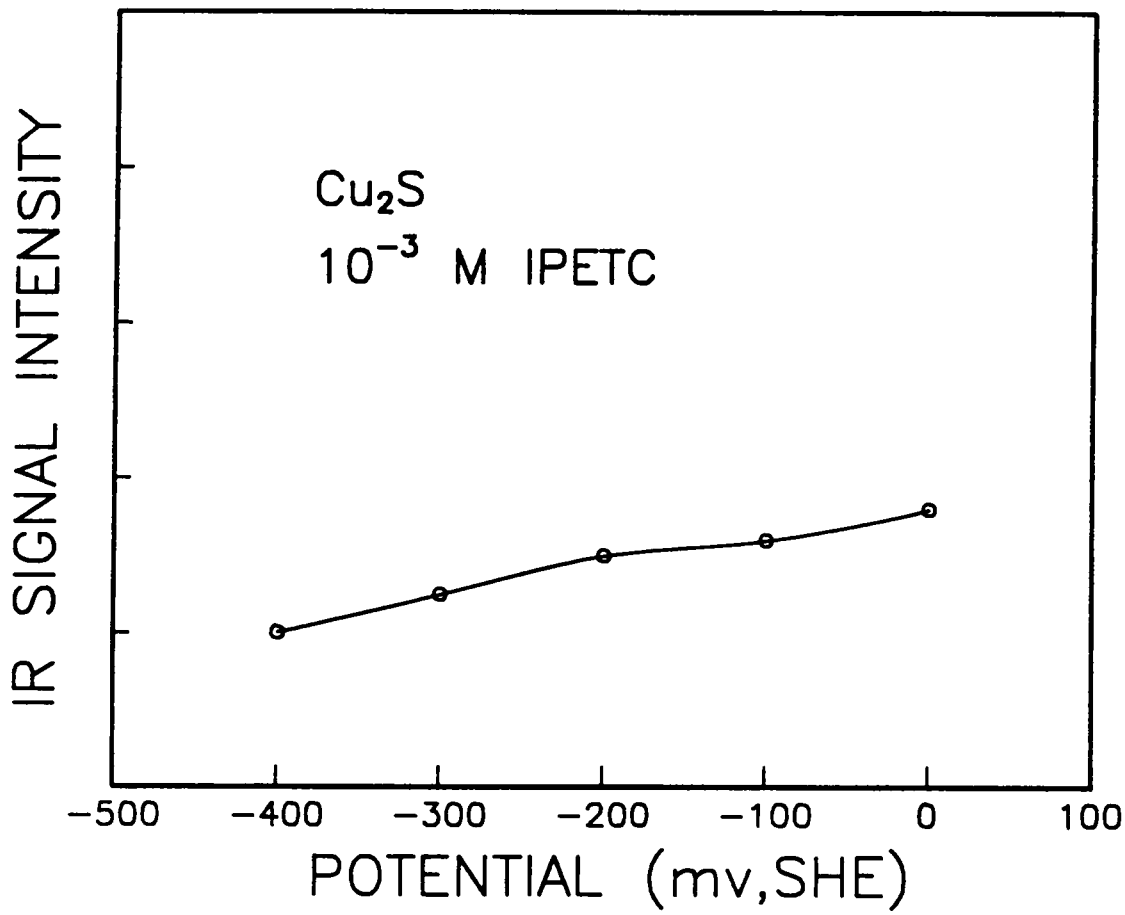

Figure 3.27. Effect of potential on the IR signal intensity of IPETC adsorbed on chalcocite conditioned in 10^{-3} M IPETC solution at pH 6.0.

be noted that the effect of holding time on the growth of the adsorption layer is negligible. The increase in adsorption may then be related to the oxidation of the chalcocite, which releases copper ions. Thermodynamic calculations show that the amount of $Cu(IPETC)_2Cl$ produced increases sharply above -520 mv and remains constant between -500 and -200 mv. Above -200 mv, % $Cu(IPETC)_2Cl$ reaches and remains maximum up to E_h > 900 mv. The calculations also show that Cu(I) concentration increases with potential for the Cu_2S-H_2O system.

c. IBECTC adsorption on Cu

The next series of FTIR measurements were carried out using 10^{-3}M IBECTC. Figure 3.28 shows some of the spectra of surface IBECTC species on copper taken from a starting potential of -900 mv up to 200 mv. The spectra observed in this experiments are different from the ATR spectra of IBECTC, but are similar to those of bulk Cu-IBECTC compounds (Figure 3.5). This suggests that IBECTC is probably chemisorbed on the copper surface.

Although not shown here, the band at a higher frequency (3255 cm^{-1} in Figure 3.5) attributed to N-H vibrations has disappeared. There is also a change in position and intensity of the band (1510-1550 cm^{-1} region) attributed to C-N and N-H vibrations. The C=O vibrations found at 1769 cm^{-1} in the IBECTC spectra are now observed at 1723 cm^{-1}. In the surface IBECTC species, the band associated with the N-C=S and O-C=O showed a significant shift of about 35 cm^{-1} from the corresponding vibration found at 1169 cm^{-1} with IBECTC.

All of these changes indicate that the S and O atoms are involved in the coordination with the Cu on the substrate surface. A six-membered chelate ring, which has also been observed for Cu-IBECTC compounds and IBECTC adsorption on

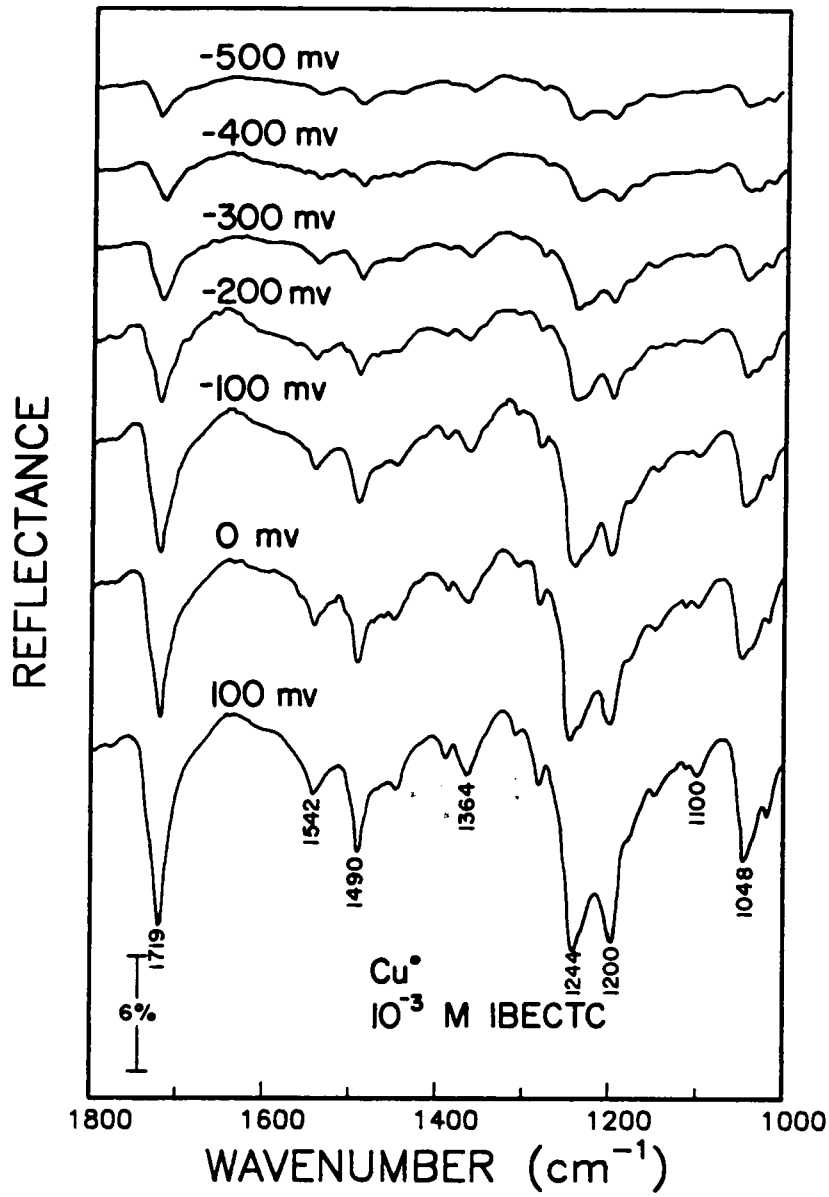

Figure 3.28. FTIR reflection spectra of IBECTC adsorbed on copper conditioned in 10^{-3} M IBECTC solution at pH 6.0 and different potentials.

chalcocite, is most probably formed during the chemisorption process. It should also be noted that the disappearance of the N-H vibrations would indicate the breaking of the hydrogen bonded N-H group. A similar observation was also made for IPETC adsorption on copper.

Similar to the findings for IPETC adsorption on copper, significant IBECTC adsorption starts above -600 mv. Increasing the potential resulted in an increase in signal intensities, but no significant chemical shifts were observed. It is also interesting to note that the anodic current associated with IBECTC interaction with copper in the voltammogram (Figure 2.22) does not result in changes in the IR spectra. The collector oxidation product observed in the voltammogram may be the same as that absorbed initially at the starting potential.

The amount of IBECTC adsorbed was monitored by measuring the change in the signal intensity of the band at 1251 cm^{-1}. Figure 3.29 shows the continued increase in adsorption with increasing potential. It should be noted that there was no significant increase in adsorption when the potential was held longer than the set conditioning time, at the starting potential. The increase in adsorption is probably due to an increase in Cu(I) concentration that results from the oxidation of the copper electrode. This was also observed for the Cu-IPETC system. Thermodynamic calculations indicate that the Cu-IBECTC compound is stable above -600 mv and a maximum amount of this compound is produced at E_h > -520 mv. This indicates reasonable agreement with the experimental data.

Using IRAS, the spectra (Figure 3.30) were similar to those obtained using the ECATR cell. Except for an increase in magnitude, there were no significant changes associated with increasing potential. Figure 3.31 shows the increase in signal intensity as a function of potential. It can be seen that this signal intensity curve is similar to that observed in the in-situ measurements except at potentials above 100 mv. The amount

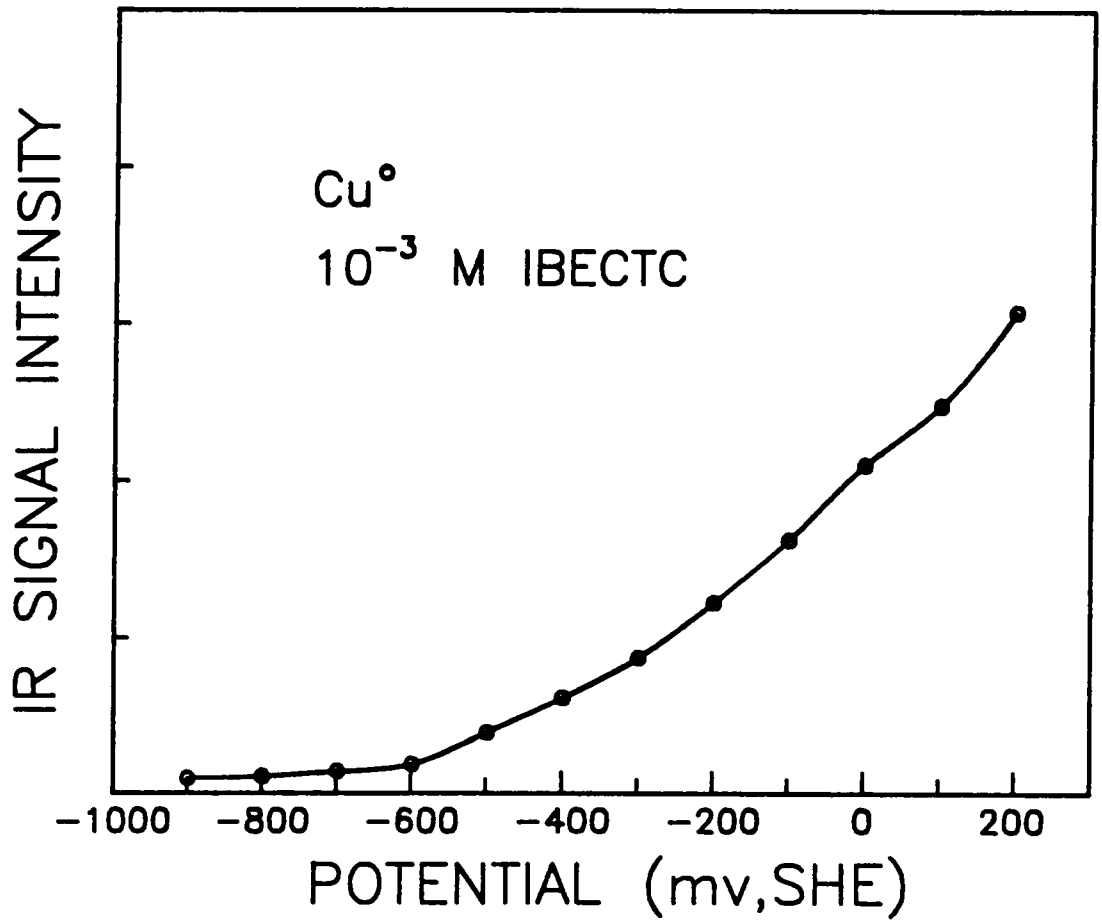

Figure 3.29. Effect of potential on the IR signal intensity of IBECTC adsorbed on copper conditioned in 10^{-3} M IBECTC solution at pH 6.0.

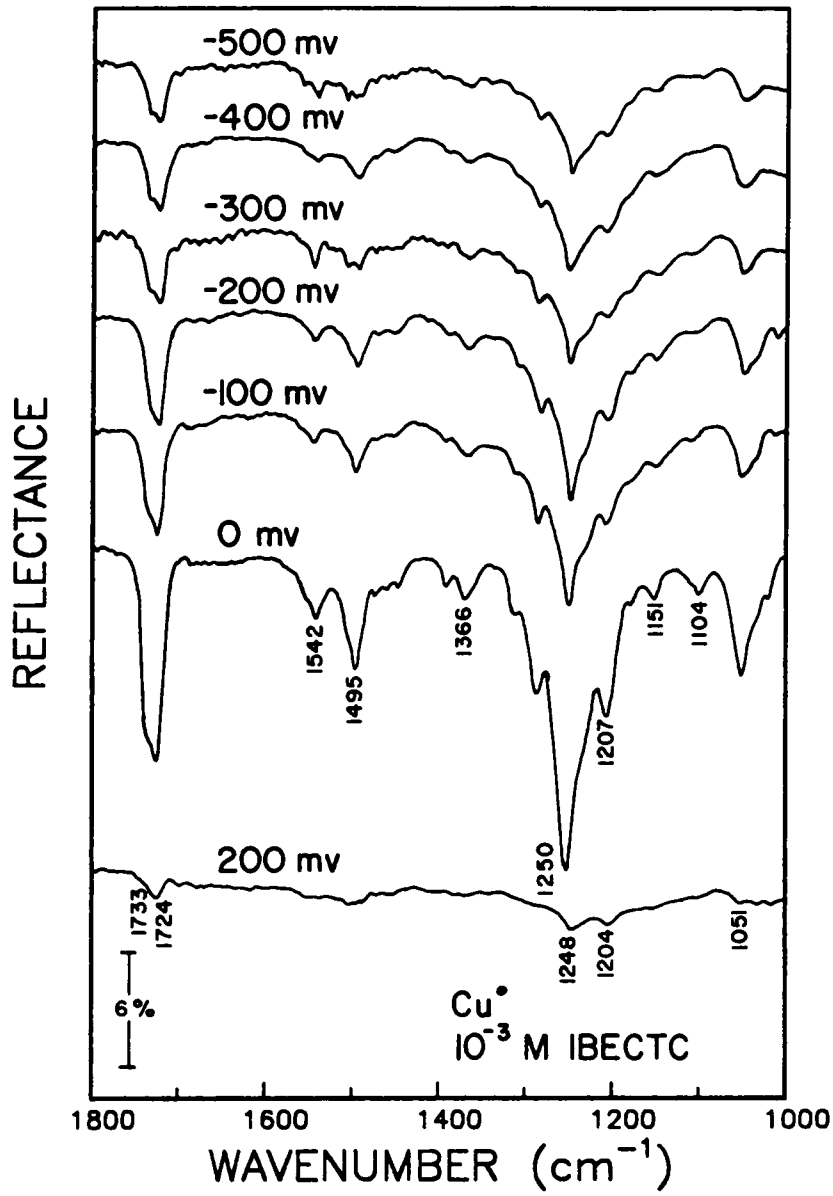

Figure 3.30. IRAS spectra of IBECTC adsorbed on copper conditioned in 10^{-3} M IBECTC solution at pH 6.0 and different potentials.

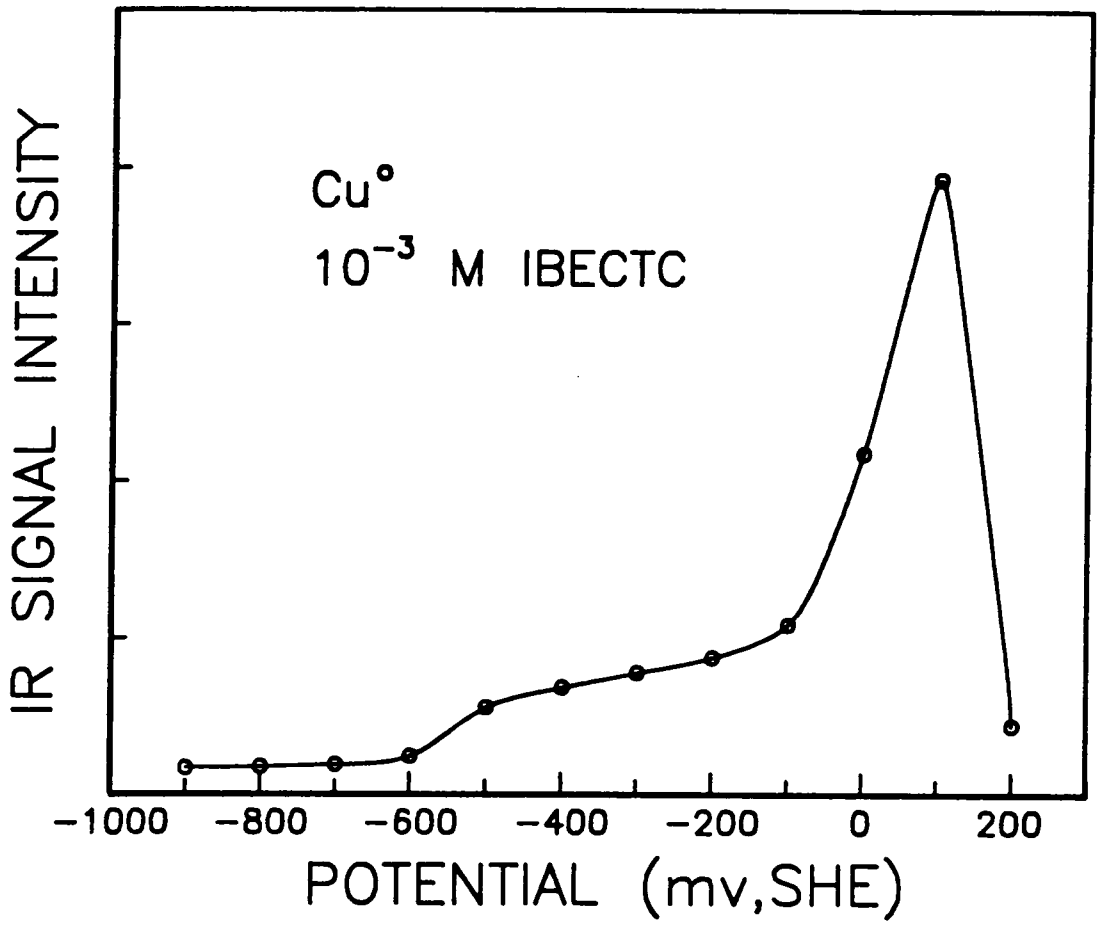

Figure 3.31. Effect of potential on the IR signal intensity of IBECTC adsorbed on copper conditioned in 10^{-3} M IBECTC solution at pH 6.0.

of IBECTC adsorbed decreases after this potential, which is different from the ATR results. A similar observation has also been found in the IRAS measurements for the Cu-IPETC system and has been explained by the difference in surface preparation techniques. This explanation is presumably also valid for the measurements made here. The decrease in adsorption should not be associated with desorption or further oxidation of the surface IBECTC species.

d. IBECTC adsorption on chalcocite

The effect of potential on the adsorption of IBECTC on chalcocite is shown in Figure 3.32. At a starting potential of -400 mv and a collector addition of 10^{-3}M, IBECTC adsorption was observed. The spectrum obtained at this potential is different from any of the previous spectra involving IBECTC. It seems that the spectrum is a mixture of surface IBECTC adsorbed on copper, and IBECTC, itself. By spectrally subtracting IBECTC, the resulting spectrum is similar to that observed on copper (not shown here). The presence of the IBECTC molecule in the IR spectrum suggests its physisorption on the electrode surface. It should be pointed out that IBECTC was found to be capable of physisorbing on top of the chemisorbed layer (as described in section 3.3.3). It is also possible that the physisorbed species are undissolved IBECTC molecules. The similarity of the spectrum to that observed on copper may indicate that chalcocite has been reduced to copper at the starting potential. This reduction was also observed in the IPETC-chalcocite system. As noted previously, chalcocite reduction to copper is thermodynamically possible at this potential and pH condition.

At -300 mv, there is no significant change in the FTIR spectrum except for a very slight increase in signal intensity. However, at potentials $\geq$ -200 mv, the spectra are different. There are no more indications of physisorbed IBECTC on the electrode

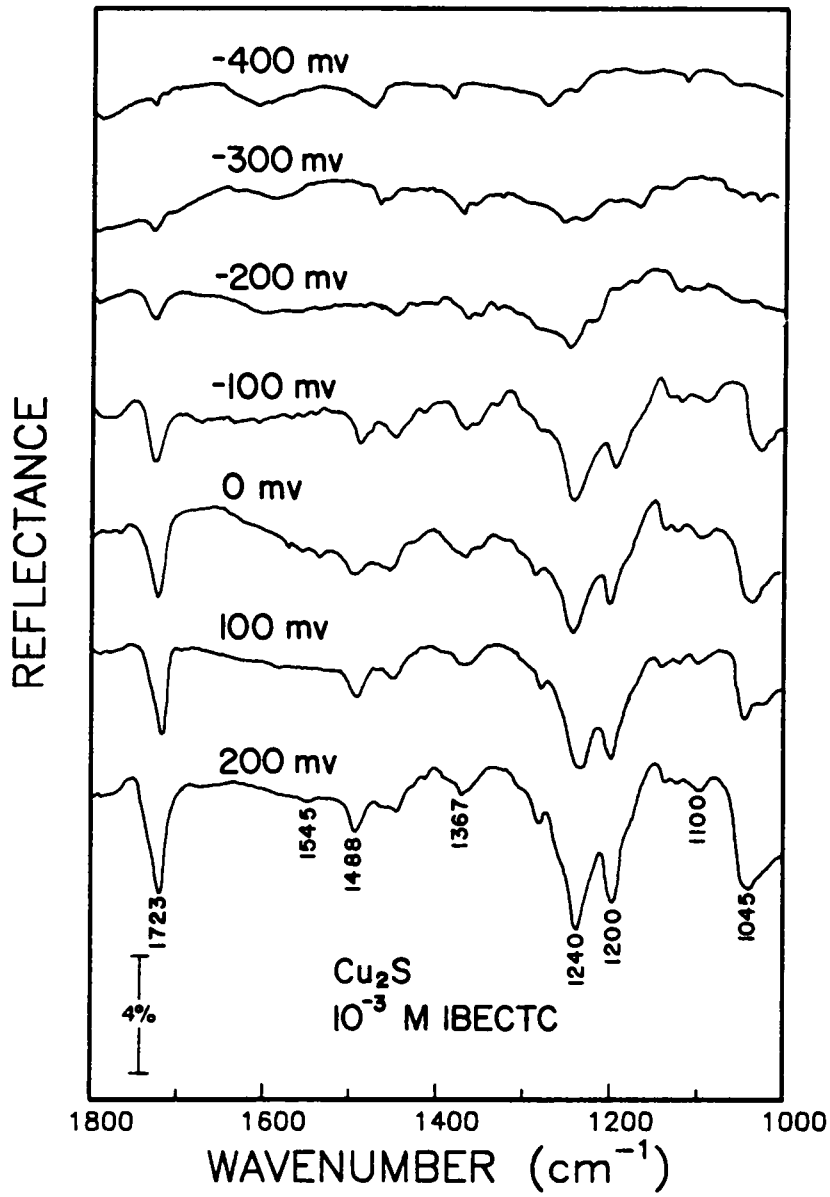

Figure 3.32. FTIR reflection spectra of IBECTC adsorbed on chalcocite conditioned in 10^{-3} M IBECTC solution at pH 6.0 and different potentials.

surface and the spectra are similar to those obtained on copper. The weakly-bound physisorbed species on the surface are probably removed by the circulating solution during the conditioning period, or by the chemisorbed species during the further oxidation of the electrode. At the potential where IBECTC interaction with chalcocite is observed in the voltammogram (Figure 2.23), there are no apparent shifts in the frequency of the characteristic absorption bands. This presumably indicates that the collector species produced at this potential are the same as those adsorbed initially at the starting potential.

The adsorption of IBECTC was also found to increase with increasing potential (Figure 3.33). The amount of adsorption was measured by the change in IR signal intensity of the peak at 1238 cm^{-1}. IBECTC adsorption is observed at the starting potential and increases sharply above -300 mv. This sharp increase probably corresponds to the disappearance of the bands due to the physisorbed IBECTC species in the FTIR spectra. At higher potentials, the signal intensity continues to increase without any apparent chemical shifts. The adsorption of IBECTC is probably enhanced by the release of copper ions into solution during chalcocite oxidation. The thermodynamic calculations from the previous chapter also indicate similar results for the Cu_2S-IBECTC system (Figure 2.8). Contact angle experiments have also shown an increase in hydrophobicity with an increase in potentials.

3.3.5 Structure and Orientation of Adsorbed Species

The IRAS technique has been used to study the adsorption of IPETC and IBECTC on copper at different degrees of coverages. The experiments were done on freshly polished copper samples conditioned in 10^{-4}M solutions of IPETC and IBECTC using

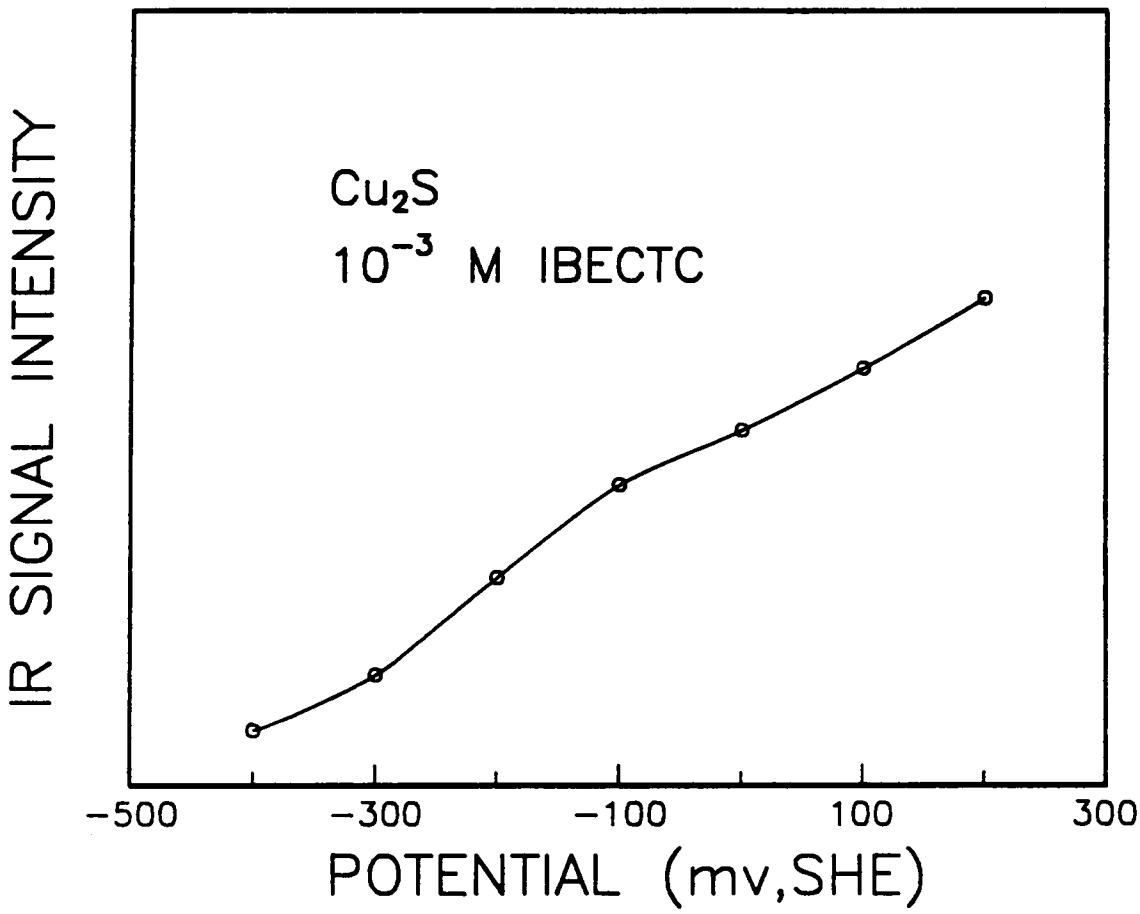

Figure 3.33. Effect of potential on the IR signal intensity of IBECTC adsorbed on chalcocite conditioned in 10^{-3} M IBECTC solution at pH 6.0.

different treatment times. The effect of pH on thionocarbamate adsorption on copper was also studied.

a. IPETC adsorption on Cu

pH 6: The IRAS spectra of IPETC adsorbed on copper at different contact times are shown in Figure 3.34. The spectra of the species adsorbed on copper are different from the ATR spectrum of IPETC. The spectra shown here, however, are similar to the IRAS spectra obtained for copper at controlled potential conditions (Figures 3.24). The adsorption of IPETC on copper was observed in the IRAS spectra even after a very short treatment time of 5 seconds. The spectra were dominated by the bands at 1586 (C-N stretching, N-H and C-H deformation), 1200 (O-C=S stretching) and 1105 cm^{-1} (C-N, C=S and C-H vibrations), as discussed in the previous sections. It is interesting to note that the band (3180-3350 cm^{-1} region) associated with the N-H stretching vibrations have disappeared. This might suggest that the N-H bonding has been broken during the adsorption of IPETC. An increase in conditioning time resulted in an increase in the intensities of the absorption bands. This indicates a growth of the adsorbed IPETC layer on the copper surface. The changes in intensities, however, were not of the same magnitude for all the bands.

Figure 3.35, which is a plot of the IR signal intensity ratio of the major characteristic bands as a function of time, shows the relative change in intensities more clearly. The C-H vibration at 2975 cm^{-1} gave the weakest signals over the entire period. At a conditioning time of less than 1 hour, the vibration due to the mixture of C-N, N-H and C-H vibrations were dominant. However, after 1 hour of treatment, the O-C=S stretching vibrations now give larger signals, which are similar to what was observed for

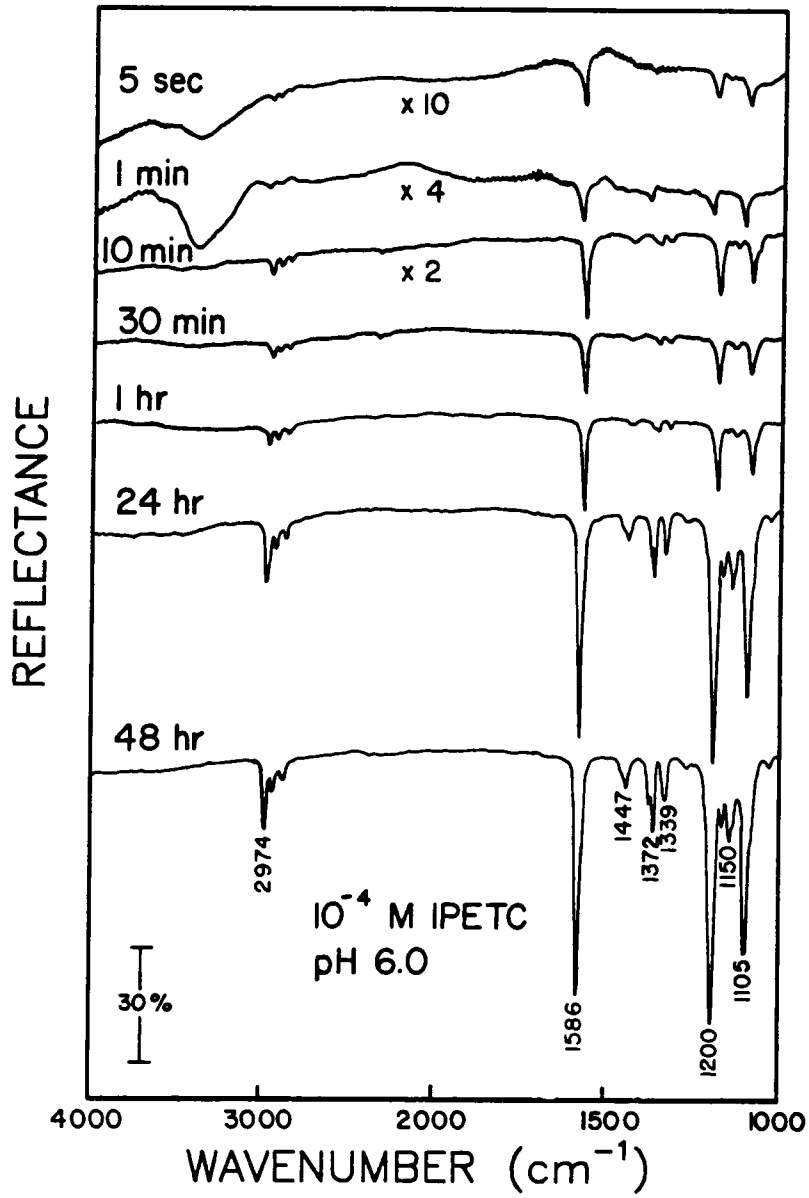

Figure 3.34. IRAS spectra of IPETC adsorbed on copper conditioned in 10^{-4} M IPETC solution at pH 6.0 and different treatment time.

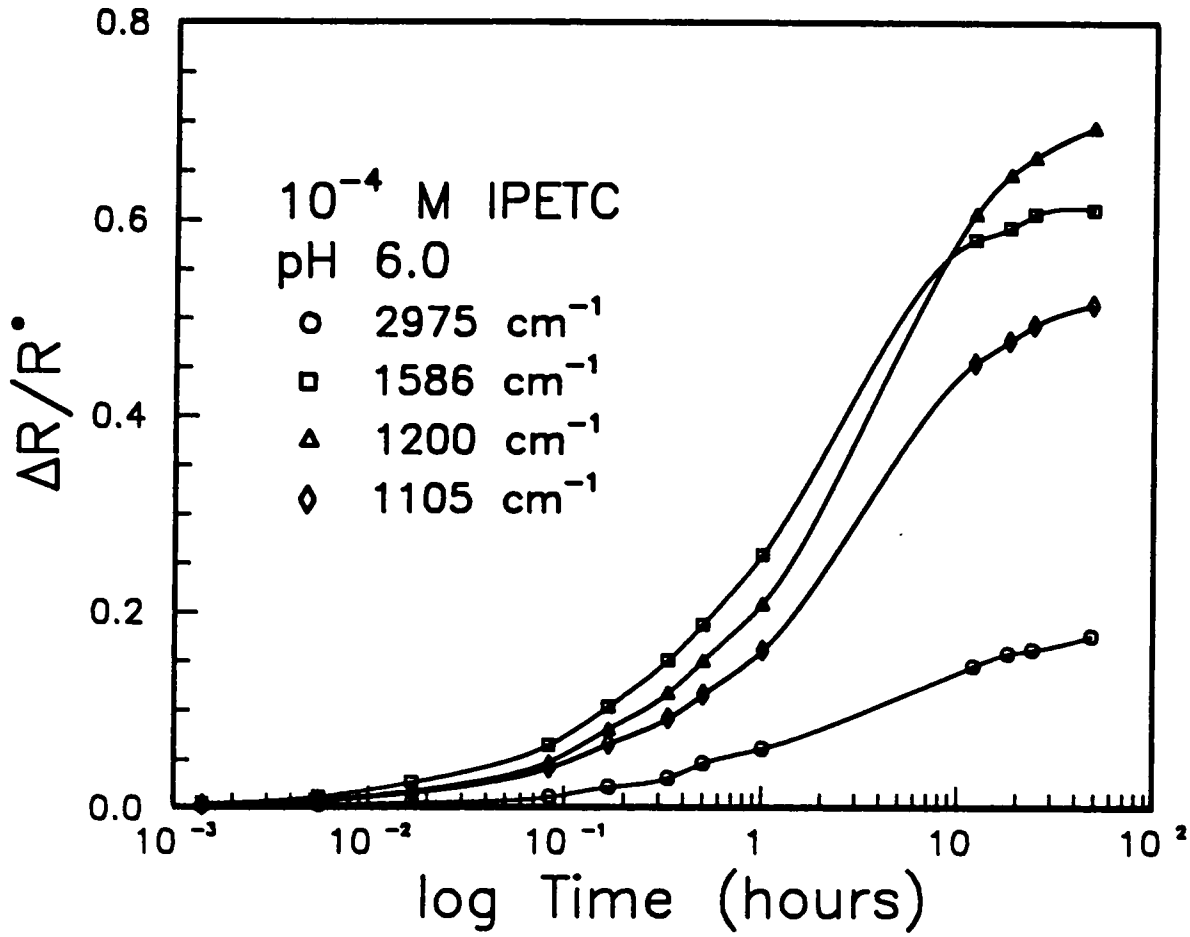

Figure 3.35. Effect of treatment time on the IR signal intensity ratio of the different characteristic bands for IPETC adsorbed on copper at pH 6.0.

bulk copper-IPETC compounds. The observed changes in the IRAS spectra associated with increasing coverage can be attributed to an orientation effect of the adsorbed molecules. This has also been found in the IRAS study of xanthate adsorption on copper (Mielczarski and Leppinen, 1987).

It is interesting to note that at conditioning times of less than 5 minutes, the O-C=S stretching vibrations appeared at 1218 and 1198 cm^{-1}. This has also been seen for IPETC adsorption on chalcocite at pH $\geq$ 6. IPETC adsorption on copper might therefore, also include the coordination of O with Cu, according to the following:

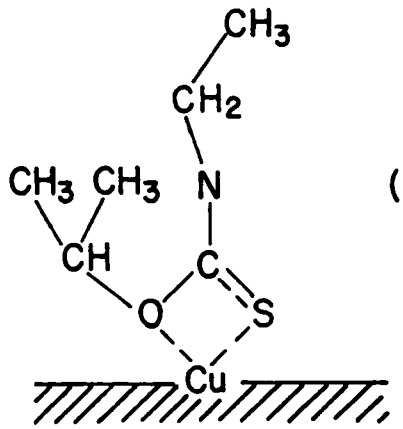

(Model I)

However, it may also be possible that the IPETC molecules are just inclined to the substrate surface. With increasing coverage, the 1218 cm^{-1} band disappeared and the coordination of IPETC was mainly through S, as shown previously.

The dominance of the C-N, O-C=S and C=S vibrations in the spectra would indicate that they have transition moments that are perpendicular to the copper surface. On the other hand, the weak signals of C-H groups would correspond to transition moments that are close to parallel to the sample surface. Therefore, the orientation of the IPETC molecule on the copper surface at close to monolayer coverage, would probably be as follows:

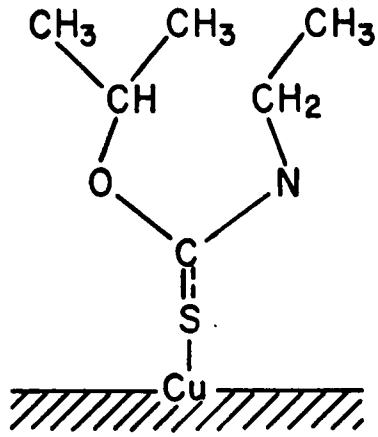

(Model II)

From the intensity ratio of the bands at 1586 cm^{-1} to those at 1200 cm^{-1}, the orientation of the adsorbed molecules can be inferred indirectly. At short treatment times, the intensity ratio was greater than 1.0, which supports Model I. This might also indicate that the adsorbed IPETC molecules were inclined to the plane of the copper surface. Although not shown clearly in Figure 3.34, this ratio was maximum after 20 minutes and then decreased continuously with time. This would probably indicate that the orientation of the molecules was going towards being close to perpendicular to the copper surface. After more than 1 hour, the ratio was similar to those found for the bulk compounds, which would indicate that the molecules were randomly oriented in the multilayer. Although there is no clear indication, the molecules were probably inverted after the monolayer level. This has been observed for xanthate and IBECTC adsorption on copper (Mielczarski and Leppinen, 1987; Mielczarski and Yoon, 1988).

pH 4: The effect of pH on the structure of the adsorbed IPETC on copper is shown in Figures 3.36 and 3.37. The IRAS spectra obtained at pH 4 were similar to those at pH 6. There were no shifts in frequency observed, but the intensity ratio of the 1586 to 1200 cm^{-1} bands are different. This would probably be due to a change in orientation. The bands attributed to the O-C=S vibrations now dominate the spectra for the entire period. The signal intensities measured for the major characteristic bands were also

lower than those observed at the higher pH. This agrees with the observations found for chalcocite, where IPETC adsorption was maximum at pH 6.

At very low coverages, (i.e., < 5 minutes treatment time), the peak at 1218 cm^{-1} was also observed and consequently, may indicate coordination through both O and S. The proposed model for this coordination was the same as that given at pH 6 (Model I). Again, it should be noted that this peak may also be due to the inclined orientation of the adsorbed molecule. At coverages close to monolayer, the interaction was now only through the S atom, as given by Model II. The spectral ratio of the 1580 to the 1200 cm^{-1} bands at submonolayer coverage was less than 1.0, suggesting that the molecules were inclined opposite to the direction observed at pH 6. This may also indicate that unlike at pH 6, the adsorbed molecules were probably randomly oriented at the submonolayer. This may be attributed to a lower adsorption density at pH 4. The degree of orientation increased until the coverage reached close to monolayer level. The molecules were probably close to perpendicular to the plane of the substrate surface at this level. The adsorbed molecules at multilayer coverage showed molecular reorientation as indicated by the similarity of their spectral ratio to the precipitates'. The adsorbed IPETC molecules are most probably randomly oriented on top of the initial layer.

b. IBECTC adsorption on Cu

pH 6: Figure 3.38 shows the IRAS spectra for IBECTC adsorbed on copper at different degrees of coverages. The ATR spectrum of IBECTC (Figure 3.6) is different from those shown here. The band assignments for the IRAS spectra are the same as those discussed for IBECTC adsorption at controlled potentials (see section 3.5.4c). IBECTC

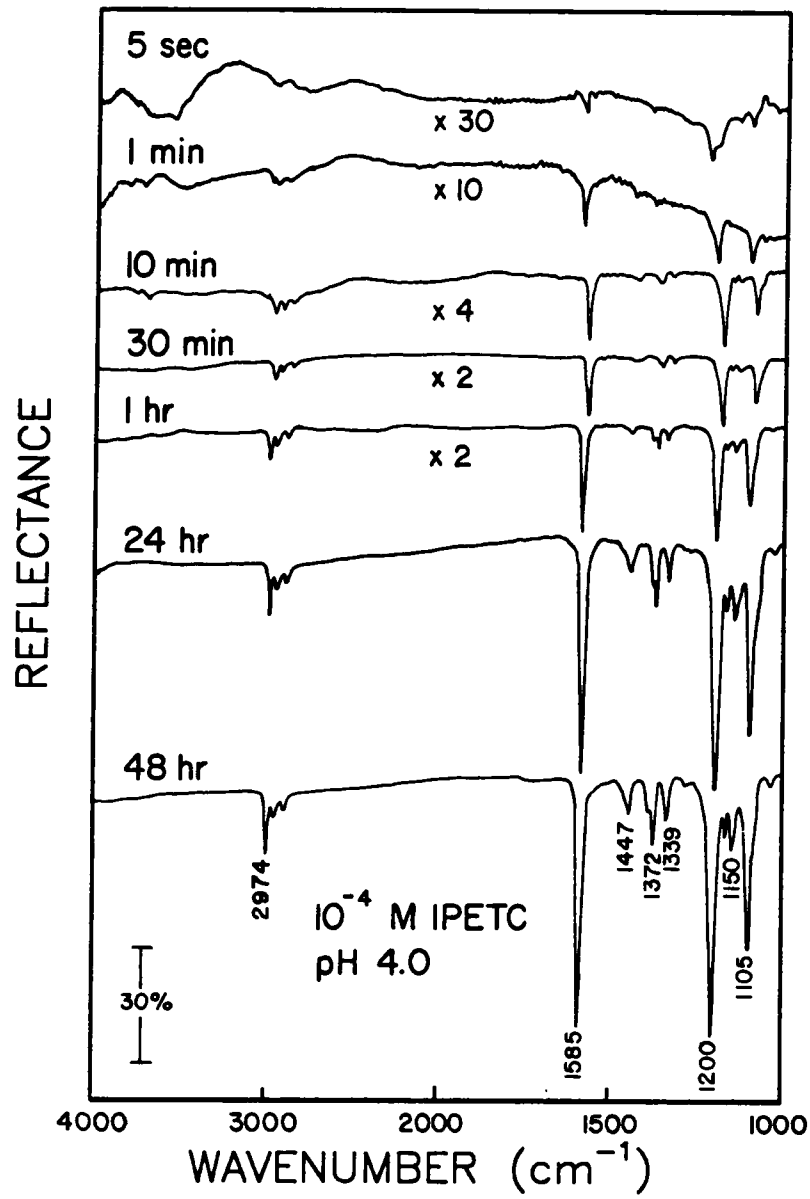

Figure 3.36. IRAS spectra of IPETC adsorbed on copper conditioned in 10^{-4} M IPETC solution at pH 4.0 and different treatment time.

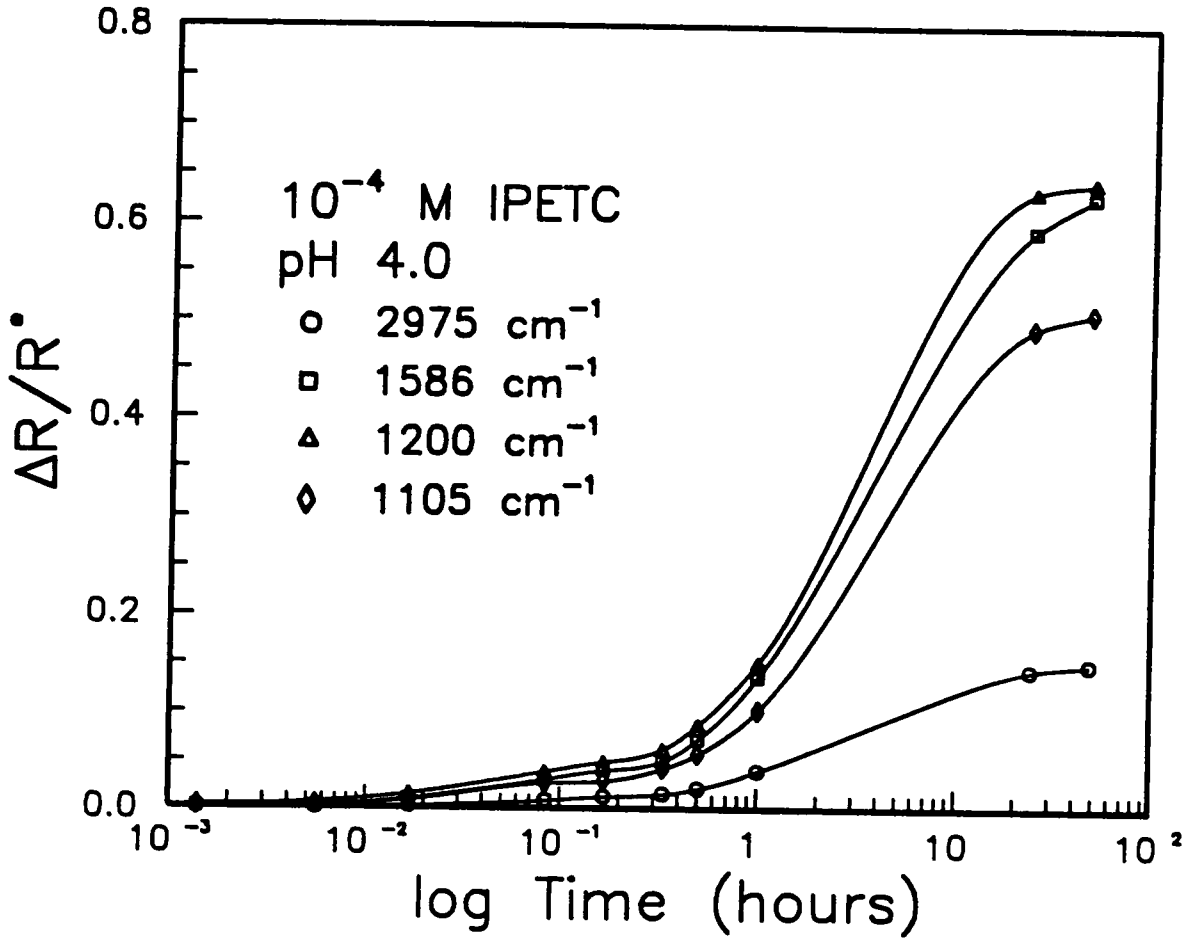

Figure 3.37. Effect of treatment time on the IR signal intensity ratio of the different characteristic bands for IPETC adsorbed on copper at pH 4.0.

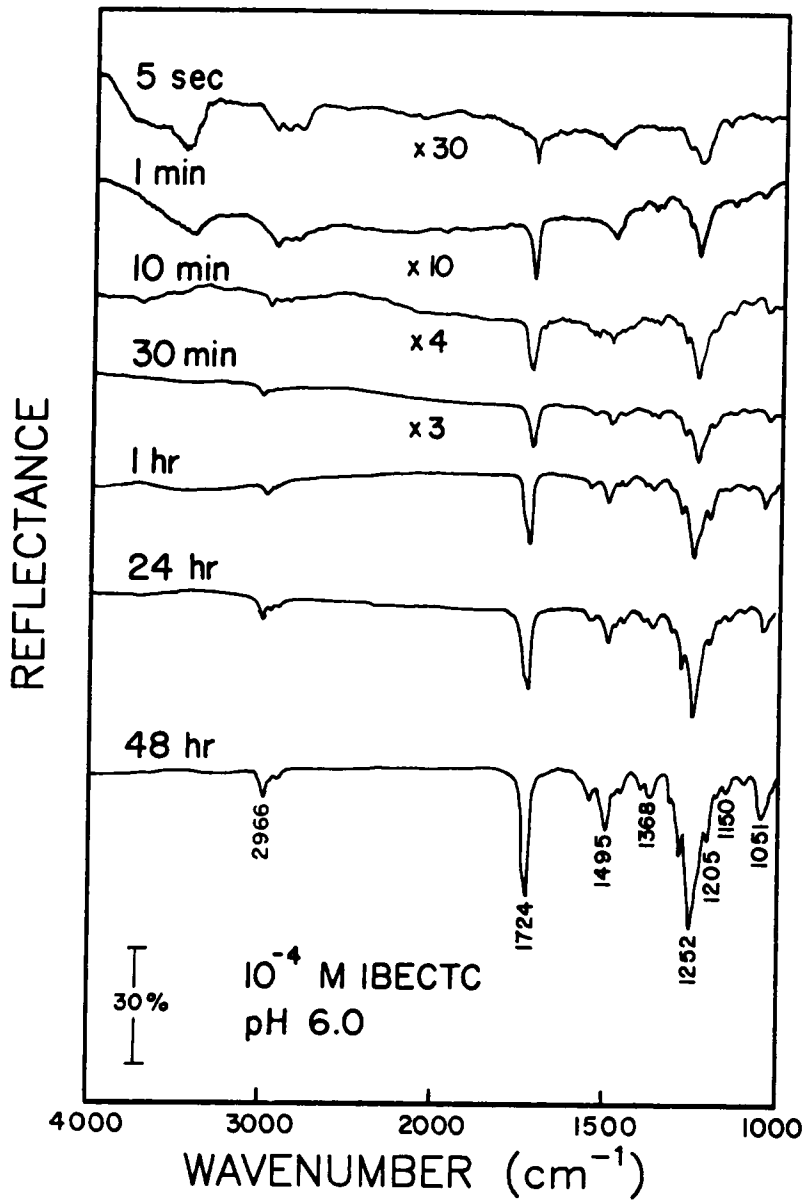

Figure 3.38. IRAS spectra of IBECTC adsorbed on copper conditioned in 10^{-4} M IBECTC solution at pH 6.0 and different treatment time.

adsorption at a very short treatment time of 5 seconds was already noticeable in the IR spectrum. The adsorption continued to grow with increasing conditioning times, as shown by the increase in signal intensities. The change in intensity was not of the same magnitude for all the bands. As discussed previously, this would indicate that the molecules were adsorbing in some type of orientation on the substrate surface.

The change in the IR signal intensity ratio of the major characteristic vibrations with conditioning time is shown in Figure 3.39. The bands which were assigned to C=O (1724 cm^{-1}), C-O and C=S (1252 cm^{-1}) vibrations dominate the spectra. At the same time, the signals due to C-H and C-N groups are relatively weaker. The adsorption of IBECTC on the copper surface at close to monolayer coverages can be inferred from this data to have the following orientation:

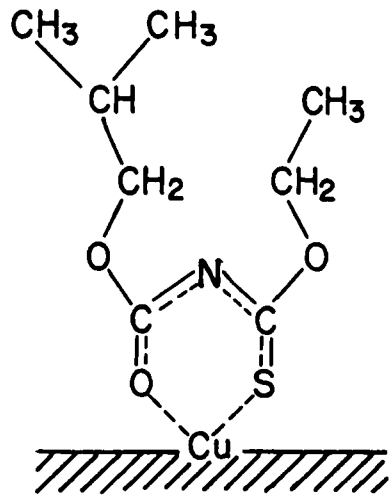

(Model III)

This is the same model of orientation proposed by Mielczarski and Yoon (1988).

Using the intensity ratio of the bands attributed to C-O and C-N vibrations, at a very short treatment time, it can be observed that the IBECTC molecules were adsorbed at an angle to the copper surface. This changed at around 20-30 minutes of conditioning, when the ratio was maximum. The molecules were now probably oriented perpendicularly to the surface. Using the equations derived by Greenler (1966) and assuming that the optical properties of xanthates and IBECTC are the same, Mielczarski

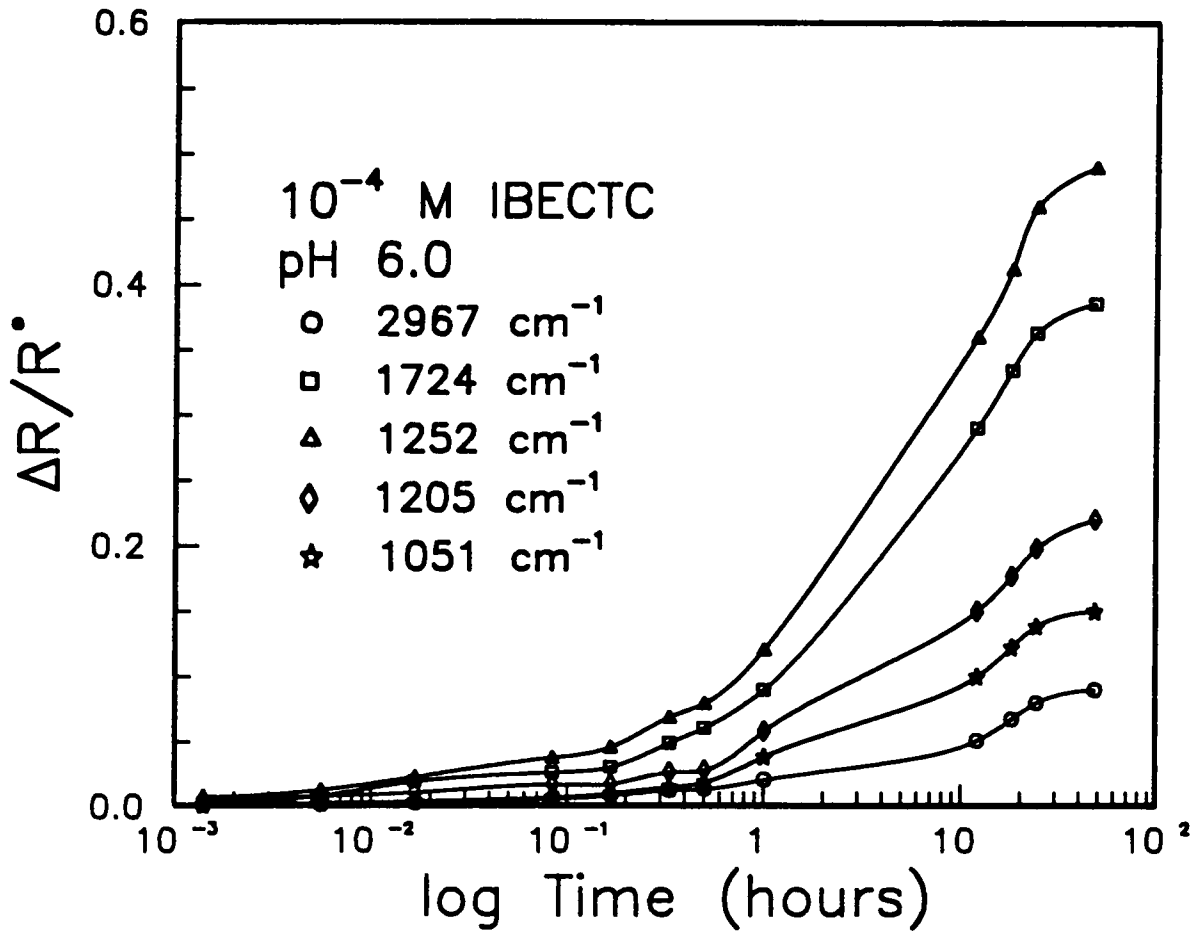

Figure 3.39. Effect of treatment time on the IR signal intensity ratio of the different characteristic bands for IBECTC adsorbed on copper at pH 6.0.

and Yoon estimated that the adsorption time required for near monolayer coverage would be about 20 minutes. The results obtained here are in agreement with their estimation.

At longer conditioning times, where second and, maybe, third layer formation was expected, the intensity ratio of all the characteristic bands changed. This indicates a reorientation of the adsorbed IBECTC on the surface, which now are probably inclined to the substrate surface. In the multilayer formation stage, the intensity ratios were similar to those found in the bulk compounds. Therefore, the molecules would probably be randomly oriented on top of the oriented first layer.

pH 4: Lowering the pH did not result in any significant change in the IRAS spectra of the adsorbed IBECTC molecule (Figure 3.40). The only noticeable change lies in the decrease in signal intensities for the samples whose conditioning time is less than or equal to 1 hour. It should be noted that in the ATR experiments, IBECTC adsorption on chalcocite was found to be maximum at pH 6. The bands due to C=O, C-O and C=S stretching vibrations still dominate the spectra, while relatively weaker signals are observed from the C-N and C-H vibrations (Figure 3.41). The molecular orientation of the adsorbed IBECTC at monolayer coverage has not changed and may be given by Model III.

At conditioning times $\leq$ 5 minutes, the ratio of the band due to C-O to that of C-N indicates that IBECTC is probably adsorbed at an angle to the plane of the substrate. However, with increasing treatment times, their ratio is maximum between 20 and 30 minutes, indicating that monolayer coverage occurs at around this time period. The molecular orientation at multilayer coverage is similar to the one observed at pH 6. This is indicated by the similar changes in the intensity ratio of the major bands attributed to adsorbed IBECTC.

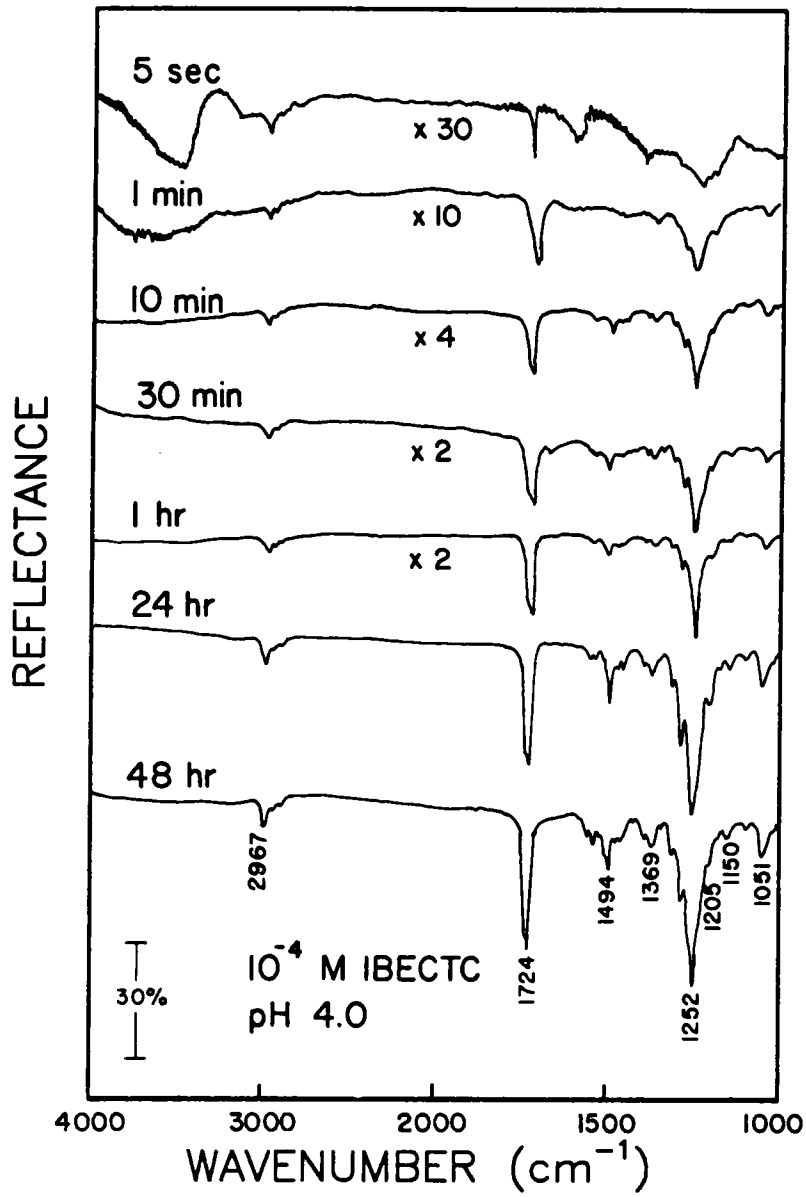

Figure 3.40. IRAS spectra of IBECTC adsorbed on copper conditioned in 10^{-4} M IBECTC solution at pH 4.0 and different treatment time.

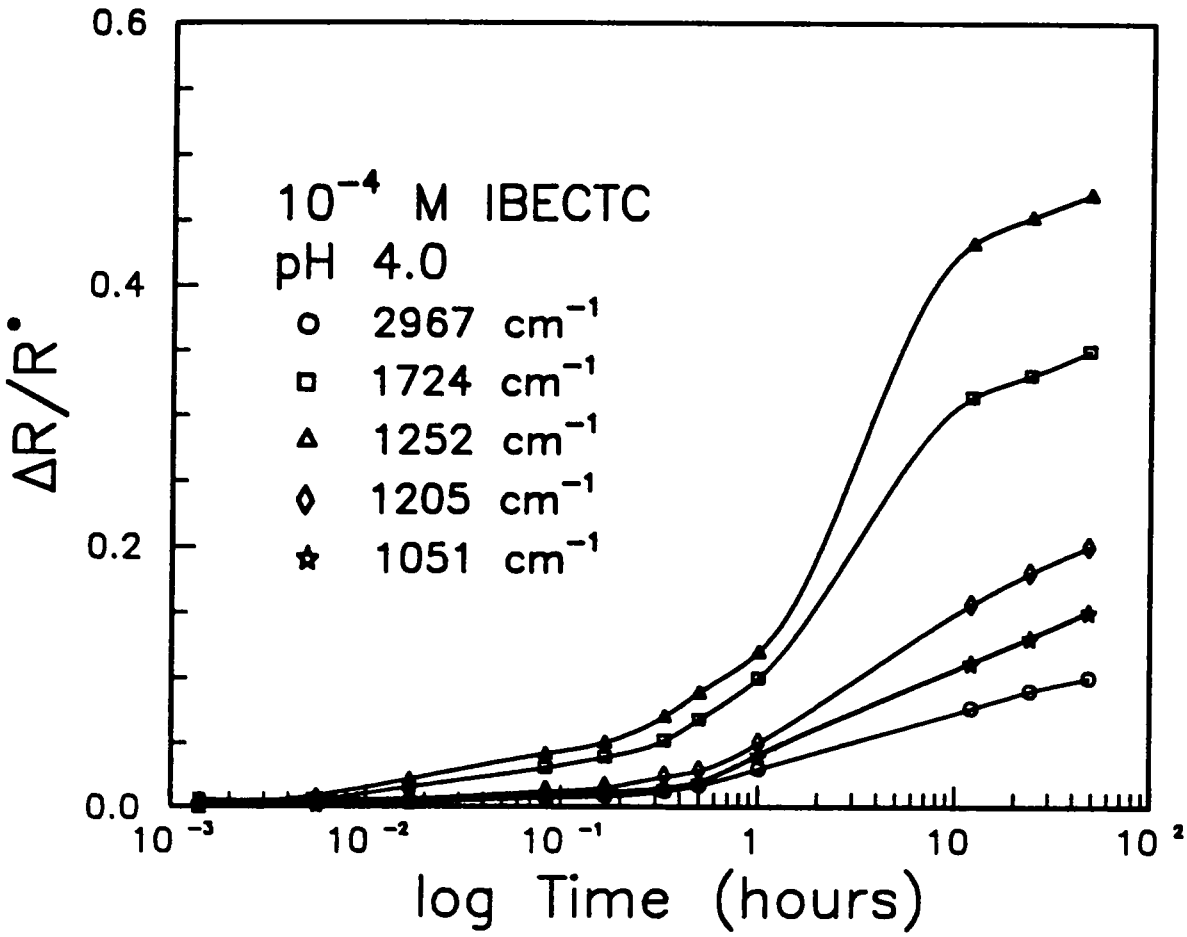

Figure 3.41. Effect of treatment time on the IR signal intensity ratio of the different characteristic bands for IBECTC adsorbed on copper at pH 4.0.

It should be pointed out that the experiments done in the absence of 10^{-2}M NaCl for these collectors gave similar results (not shown here). The signal intensities measured, however, were slightly lower than the ones shown here. Thionocarbamate adsorption may be enhanced by the presence of NaCl, although it is more likely that some other experimental factors, such as degree of polishing and cleanliness of the copper sample, may be responsible for this behavior.

3.3.6 Preferential Adsorption Studies Between Different Collectors

The reflectance spectra of IPETC and IBECTC adsorbed on copper have already been characterized in the previous section. The xanthate species adsorbed on copper has also been characterized using FTIR spectroscopy (Mielczarski and Leppinen, 1987). From the known IRAS spectra of these collectors, it would be possible to identify which species is preferentially adsorbed from solutions. Using the IRAS method, the spectra of copper treated in solutions containing different combinations of these collectors have been recorded. The resulting spectra can be used as an indirect measure of the relative strength and kinetics of the adsorption of these three collectors.

a. IPETC and KEX

Figure 3.42 shows the IRAS spectra of copper treated with a mixture of IPETC and KEX solutions (10^{-4}M, each) at pH 6.0. After 30 seconds of conditioning, the spectrum shows bands that are characteristic of surface IPETC and xanthate species. The presence of the small bands (not clearly shown here) at 1586, 1220, 1200, 1156 and 1104 cm^{-1} indicate the presence of adsorbed IPETC, as identified in the previous section. The other bands observed at 1120 and 1040 cm^{-1}, together with the peaks at 1220 and

1200 cm^{-1}, are characteristic of xanthate species adsorbed on copper (Mielczarski and Leppinen, 1987). The spectra also indicate that the xanthate film on the copper surface is oriented. Based on signal intensities (measured at 1586 and 1120 cm^{-1} for adsorbed IPETC and KEX, respectively), there is a larger amount of xanthate adsorbed compared to that of IPETC (Figure 3.43). Increasing conditioning time results in an increase in the IR signal intensities. However, the increase in the amount of xanthate adsorbed is larger.

After about 2 minutes, no more significant IPETC adsorption occurs. After 1 hour, the adsorption peaks in the IRAS spectrum are mainly due to surface xanthate species. These results indicate that xanthate is preferentially adsorbed by copper, with time. At multi-layer coverages, the adsorption of IPETC over the xanthate layer does not appear to be favored. This may be attributed to a number of factors such as strength of the interaction and the size of the collector molecule. The results agree with the conclusions from the previous section that IPETC bonding with copper is weaker compared to that for xanthate. With regards to kinetics, the adsorption of xanthate might be slightly faster when compared to that of IPETC, as suggested by the spectra at short conditioning times.

In the next series of tests, the sample was not conditioned in the mixture of the two collectors at the same time. Instead, it was alternately treated with just one collector at a time. Using 10^{-4} M IPETC and a conditioning time of 15 minutes, the spectrum of IPETC adsorbed on copper is observed (Figure 3.44). After IPETC has adsorbed on the copper sample, it is then treated in a solution containing 10^{-4}M KEX only. The resulting spectrum shows that the characteristic bands attributed to surface IPETC species are still present. The band at 1586 cm^{-1} (C-N, N-H and C-H vibrations) has not shifted but its intensity is less. The same is true for the band at 1105 cm^{-1}(C-N, C=S and C-H vibrations). However, the strong adsorption band at 1199 cm^{-1} (O-C=S

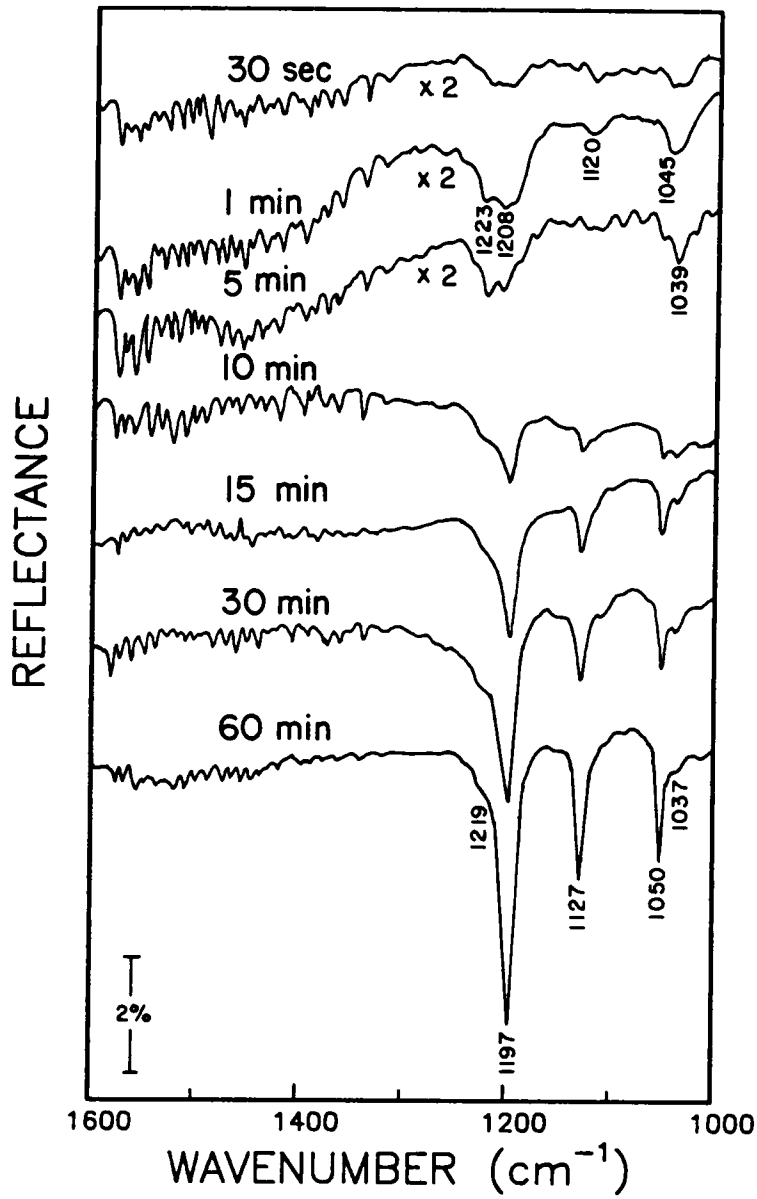

Figure 3.42. IRAS spectra of the collector adsorbed on copper conditioned in a mixture of IPETC and KEX solution (10^{-4} M, each) at pH 6.0 and different adsorption time.

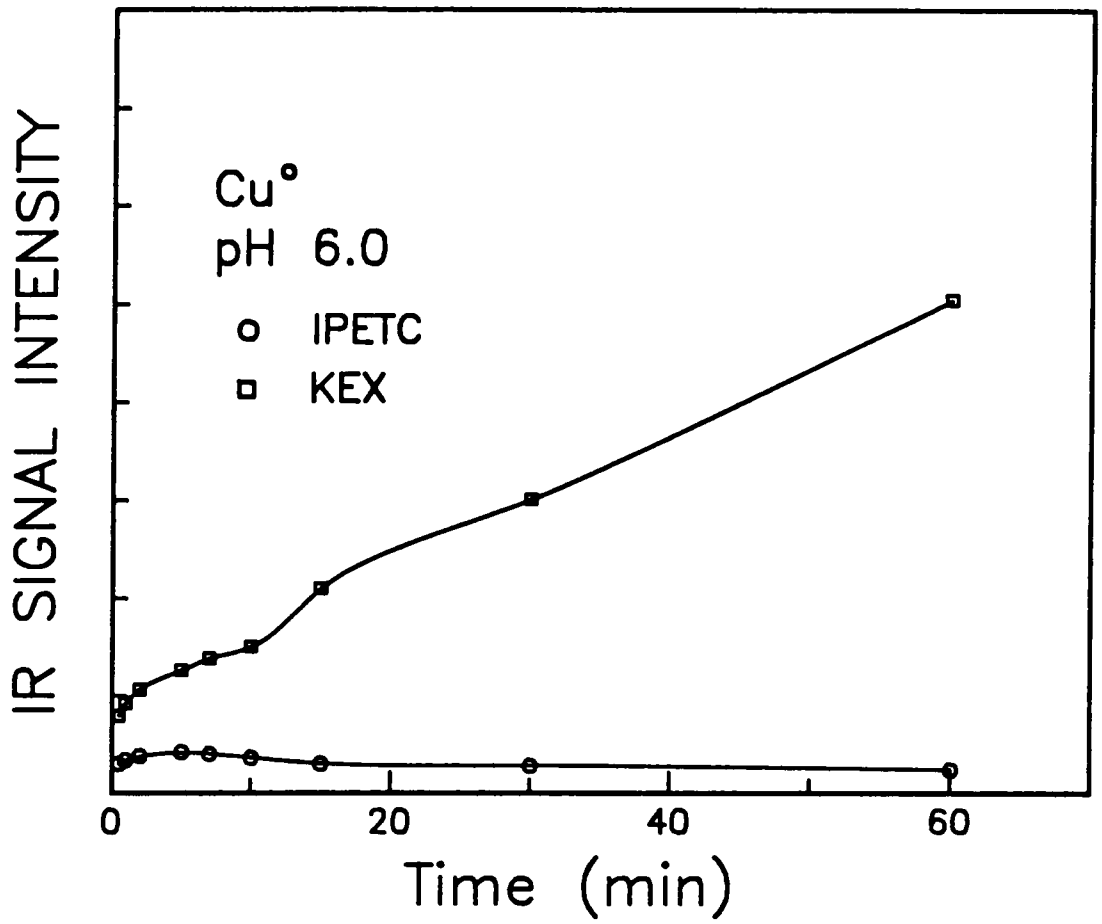

Figure 3.43. Effect of adsorption time on the IR signal intensity of the collector adsorbed on copper conditioned in a solution containing both IPETC and KEX (10^{-4} M, each) at pH 6.0.

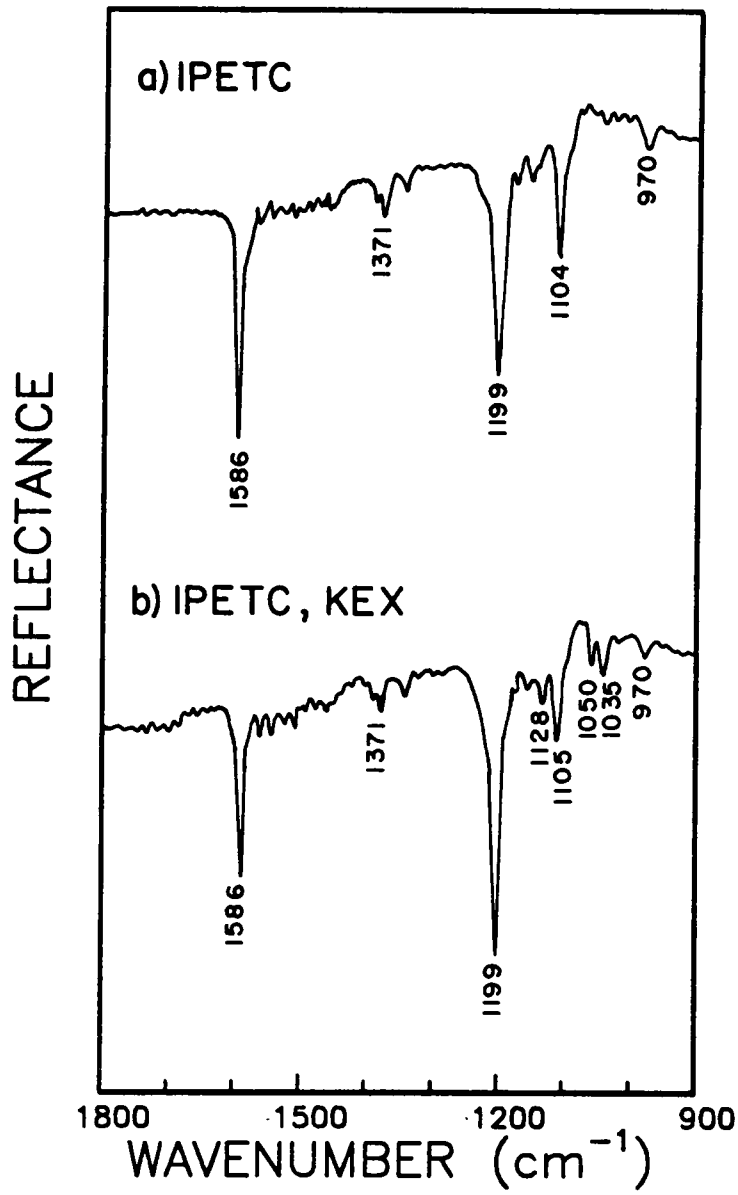

Figure 3.44. IRAS spectra of the collector adsorbed on copper conditioned in a) 10^{-4} M IPETC solution, initially and then b) 10^{-4} M KEX solution at pH 6.0.

stretching) has gained in intensity. There are also new bands observed at 1128 ($\nu_a COC$), 1050 ($\nu_a COC, \nu CC$) and 1035 cm^{-1}($\nu_a SCS$). As stated previously, these bands are due to xanthate adsorbed on copper. The decrease in the signals attributed to adsorbed IPETC may be associated with some displacement of IPETC by KEX adsorption. However, the adsorption of KEX, which has different optical properties, over the adsorbed IPETC layer probably also causes the lower signals. The similarity of the spectrum to that of the bulk compound would suggest that the adsorbed xanthate is randomly oriented on top of the oriented film of IPETC molecules on copper. This is also indicative of multi-layer coverages. Since the adsorption times for both tests were the same, the adsorption of KEX is probably faster than that of IPETC. This agrees with the conclusions made previously. However, KEX adsorption does not seem strong enough to totally displace the adsorbed IPETC.

Figure 3.45 shows the spectrum obtained when the order of the treatment is reversed. The initial spectrum indicates that the surface xanthate species are randomly oriented. This is shown by the spectrum's similarity to that of bulk copper ethyl xanthate (Mielczarski and Leppinen, 1987; Leppinen et al., 1988). The random orientation of the adsorbed xanthate molecule would mean that it has already formed multi-layers. When IPETC is introduced afterwards, no significant adsorption of IPETC can be observed. This may be due to the multi-layers of adsorbed xanthate molecules preventing further adsorption on the copper surface. The IPETC molecules probably cannot have access to surface copper after the substrate is completely covered with the other collector. In the previous case, multi-layer coverage by IPETC has probably not occurred within the conditioning time of 15 minutes. This may be the reason for the difference observed for the two cases. The strength of the bonds between copper and the collector probably plays a role here, too.

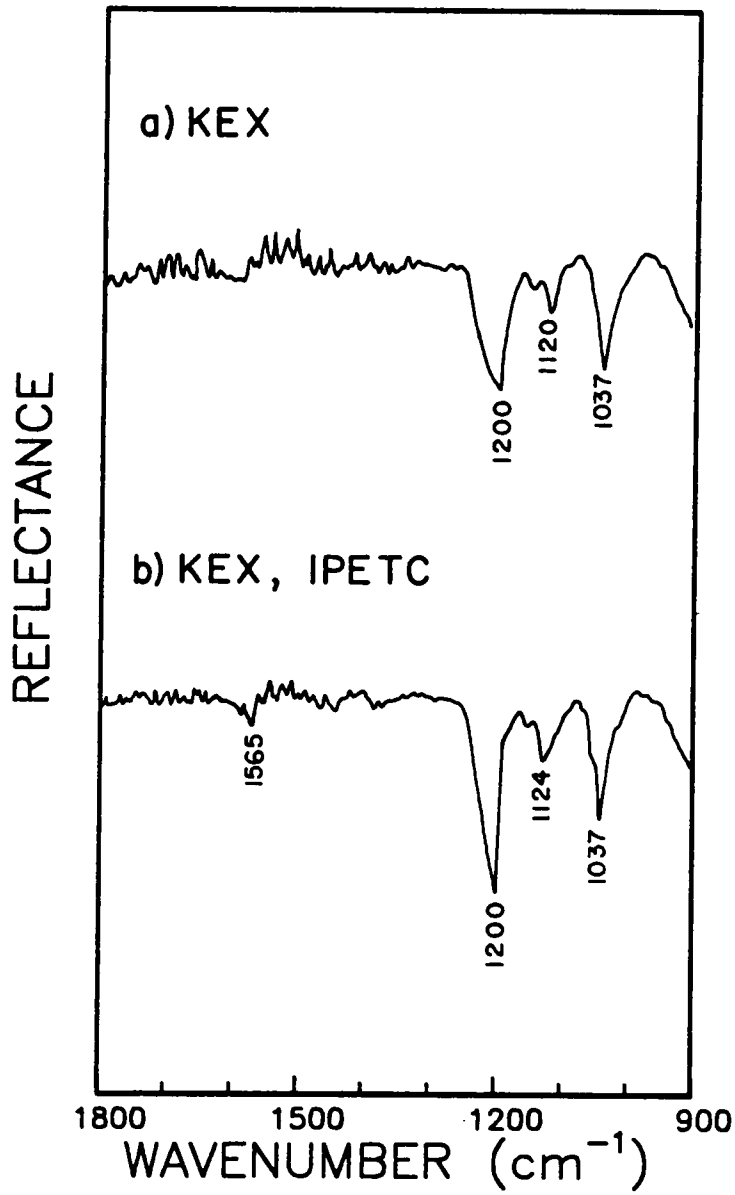

Figure 3.45. IRAS spectra of the collector adsorbed on copper conditioned in a) 10^{-4} M KEX solution, initially and then b) 10^{-4} M IPETC solution at pH 6.0.

b. IPETC and IBECTC

The next series of experiments were carried out using IPETC and IBECTC. The IRAS spectra for copper in a solution containing equal concentrations (10^{-4}M) of IPETC and IBECTC at pH 6 and different treatment times are shown in Figure 3.46. The spectra obtained at short conditioning times show that both IPETC and IBECTC are adsorbed on the copper surface. The characteristic adsorption bands attributed to surface IBECTC species are evident in the IR spectra. However, the bands corresponding to adsorbed IPETC are not too distinct and their signal intensities are relatively weaker. This would indicate that the adsorption of IBECTC is stronger and most probably, faster. It has already been stated that IBECTC is bound to copper through both the sulfur and oxygen atoms, forming a chelate ring structure. This is more stable than the binding of IPETC to copper.

At longer conditioning times, the adsorption of IBECTC increases continuously while that of IPETC seems to remain constant. The spectra indicate that IBECTC has formed more than a monolayer after 1 hour, indicating that IBECTC adsorption is indeed stronger (or capable of forming multi-layers) that IPETC adsorption. Even though IPETC has a simpler structure than IBECTC, its adsorption kinetics does not seem to be faster. Figure 3.47 shows the change in the IR signal intensity of adsorbed IPETC and IBECTC (measured at 1586 and 1724 cm^{-1}, respectively), more clearly defining the difference in the rate and amount adsorbed by the two collectors. All these results suggest that IBECTC is expected to be a better flotation collector for copper than IPETC.

The resulting IRAS spectra, when copper is conditioned initially in 10^{-4}M IPETC solution for 15 minutes, is shown in Figure 3.48. This is similar to that observed in previous experiments (Figure 3.44). After IPETC adsorption, the sample is then treated

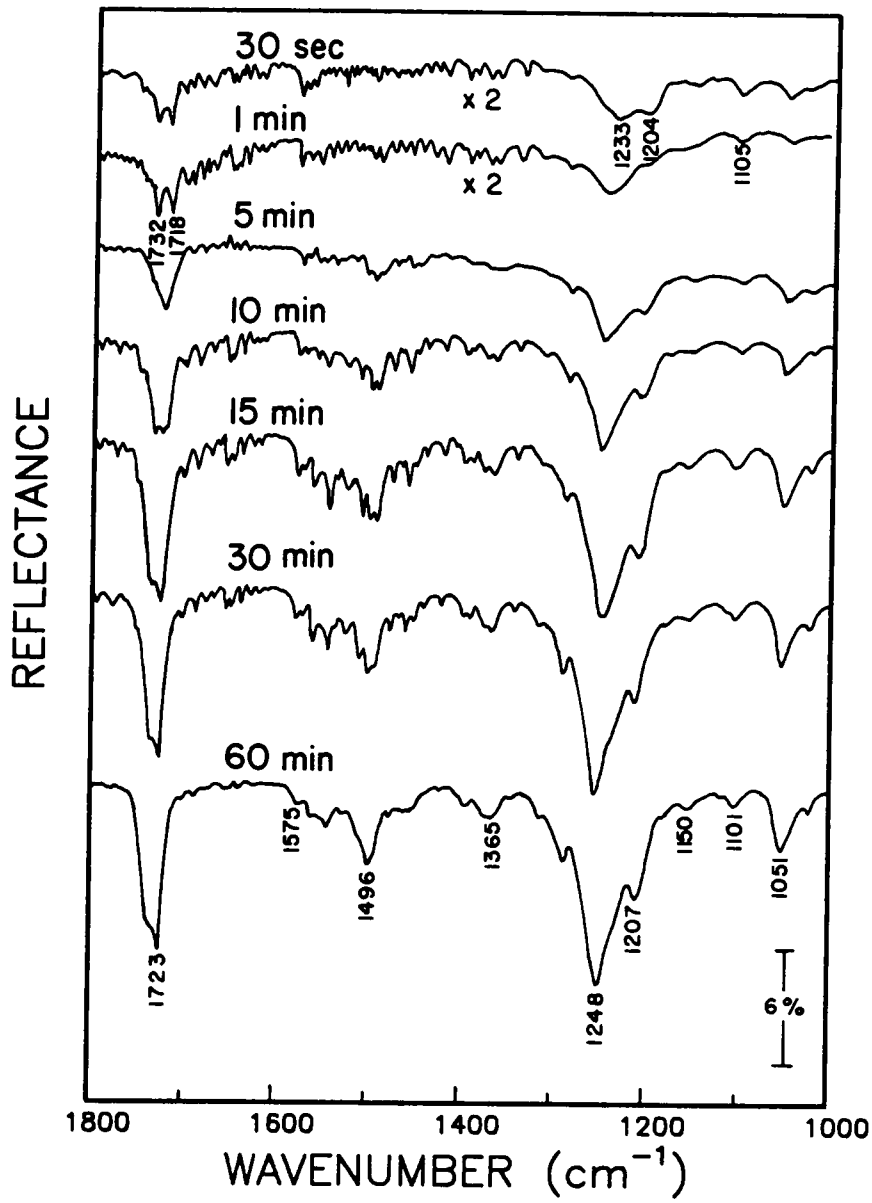

Figure 3.46. IRAS spectra of the collector adsorbed on copper conditioned in a mixture of IPETC and IBECTC solution (10^{-4} M, each) at pH 6.0 and different adsorption time.

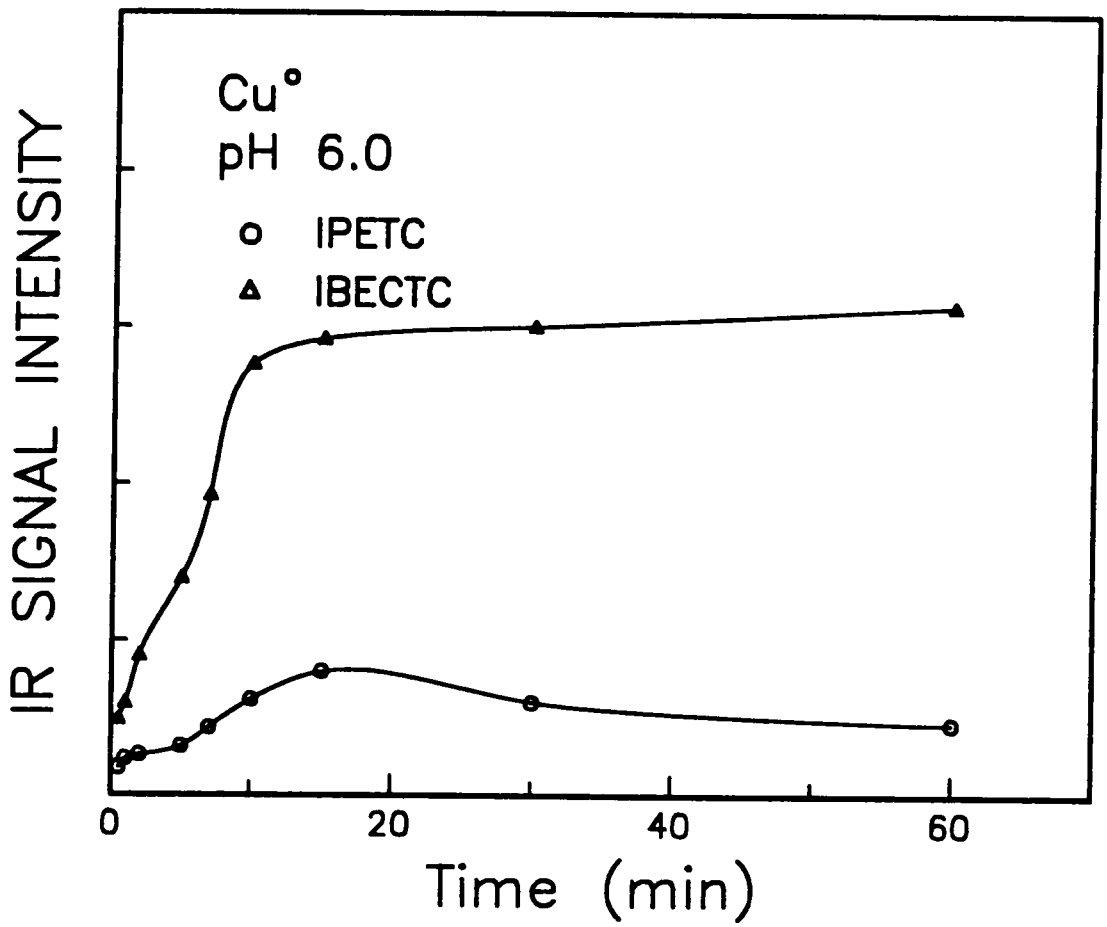

Figure 3.47. Effect of adsorption time on the IR signal intensity of the collector adsorbed on copper conditioned in a solution containing both IPETC and IBECTC (10^{-4} M, each) at pH 6

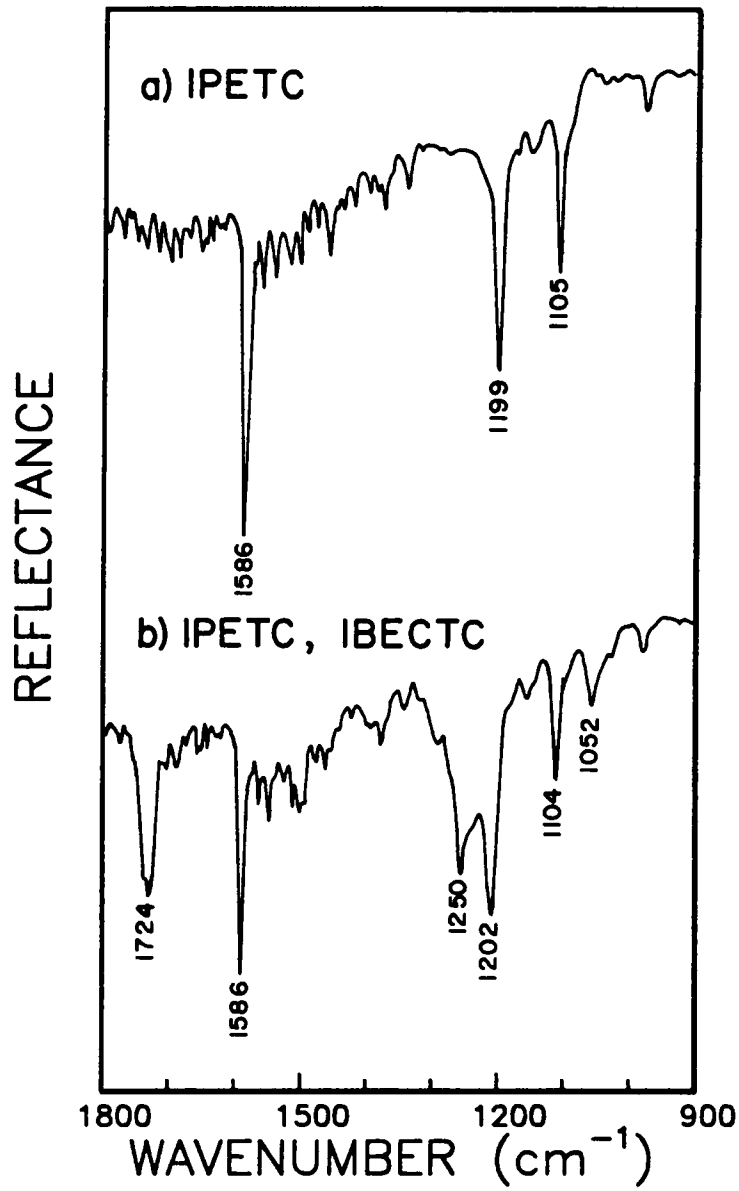

Figure 3.48. IRAS spectra of the collector adsorbed on copper conditioned in a) 10^{-4} M IPETC solution, initially and then b) 10^{-4} M IBECTC solution at pH 6.0.

in a 10^{-4}M IBECTC solution. Significant adsorption of IBECTC is observed as indicated by the presence of new bands at 1724 (C=O) 1250 (C-O and C=S) and 1052 cm^{-1}(C-O). These bands have all been attributed in the previous section to IBECTC adsorption on copper. The characteristic bands due to adsorbed IPETC are still present with no significant shift in frequency. The IR signal intensities of the IPETC adsorption bands are also observed to have slightly decreased probably due to the adsorption of IBECTC over the surface IPETC species. It should be noted, however, that the intensity ratio of the characteristic bands for adsorbed IPETC have not changed except for the band at 1200 cm^{-1}. This exception is due to the presence of vibrations at the same frequency coming from IBECTC. The results indicate that there is no total displacement of adsorbed IPETC by IBECTC. This is similar to the observations found in the preferential adsorption studies made for the IPETC-KEX system.

The results of a reverse in the order of adsorption is shown in Figure 3.49. The initial spectrum is similar to that previously observed for IBECTC on copper under similar conditions (Figure 3.40). When IPETC is introduced after IBECTC adsorption, small peaks are observed near 1583 (C-N, N-H and C-H vibrations) and 1103 cm^{-1} (C-N, C=S and C-H vibrations). The IR signal intensity of the band near 1204 cm^{-1} (O-C=S) has also increased. These changes reflect the formation of surface IPETC species on copper. However, the relative amount of IPETC adsorbed over surface IBECTC species is not as large as that seen vice-versa. This may be to the weaker adsorption of IPETC on copper. The results also show that IPETC cannot displace IBECTC as indicated by negligible change in the IR signal intensity of the adsorbed IBECTC characteristic bands. These experimental data verify the suggestion that IBECTC is a stronger collector than IPETC.

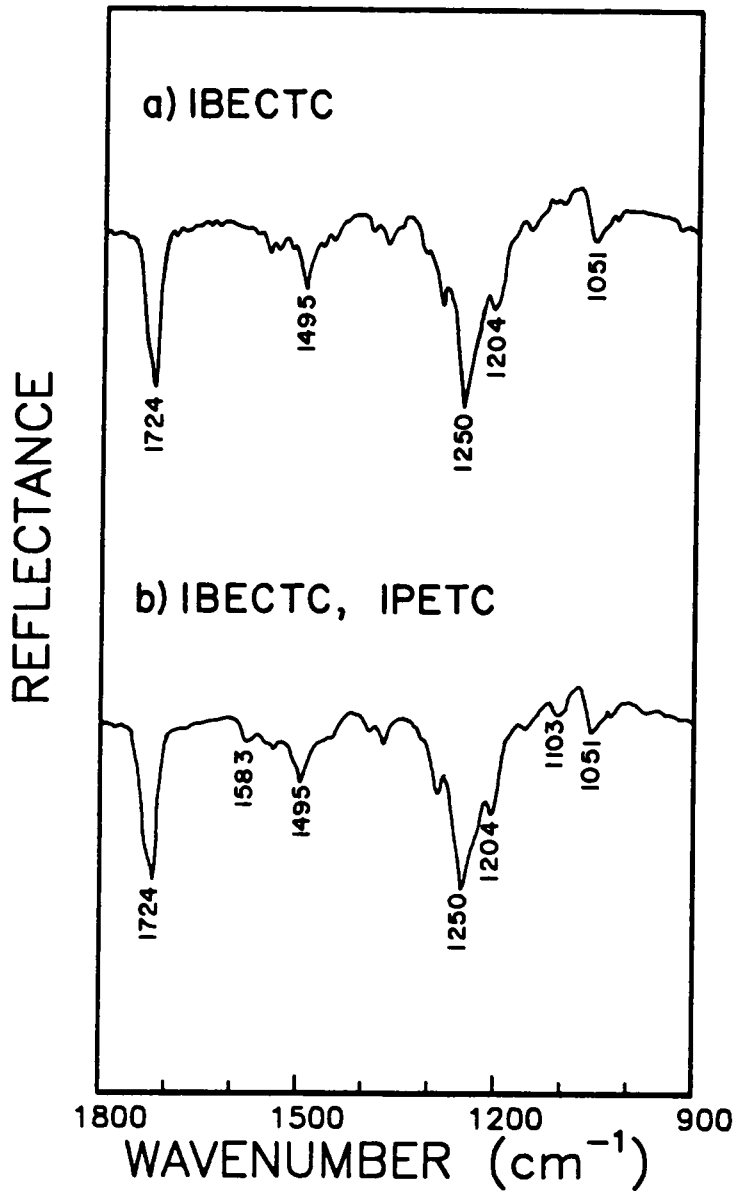

Figure 3.49. IRAS spectra of the collector adsorbed on copper conditioned in a) 10^{-4} M IBECTC solution, initially and then b) 10^{-4} M IPETC solution at pH 6.0.

c. IBECTC and KEX

The last set of collector competition studies involved IBECTC and KEX. Using solutions containing 10^{-4}M of both collectors, the spectra on the copper surface were obtained and are shown in Figure 3.50. It can be seen that both collectors are co-adsorbed on the copper surface starting from a conditioning time of 30 seconds up to 1 hour. However, at short conditioning times, the bands due to the surface xanthate species seem to dominate the spectra. As the conditioning time gets longer, the intensity of the spectra increases. The amounts of both adsorbed species continue to grow with time as is shown more clearly in Figure 3.51. Unlike the case with IPETC-KEX system, both collectors adsorb continuously. There is more xanthate adsorbed, however, over the entire period. This is shown by the larger intensities of the bands attributed to xanthate. The adsorption of xanthate is probably faster than that of IBECTC. This may be attributed to the larger molecular size of IBECTC. In terms of their strengths, there is no direct and clear evidence observed from this experiment to determine which is greater. However, since there is more xanthate adsorbed by copper, this might suggest that xanthate has a higher adsorbability. Comparison of the spectrum of surface xanthate species with that of adsorbed IBECTC indicates that copper bonds with the two sulfur atoms in xanthate while IBECTC is bound through its sulfur and oxygen atoms. The former is suggested to be a stronger bond than the latter (Mielczarski and Yoon, 1988).

Figure 3.52 compares the spectra that are obtained by conditioning copper in 10^{-4}M IBECTC solution initially and with 10^{-4}M KEX solution afterwards. After the treatment with the KEX solution, the spectrum shows the co-existence of both surface IBECTC and KEX species. The signal intensities of the characteristic absorption bands for IBECTC decreases but the intensity ratio has remained constant. The decrease in

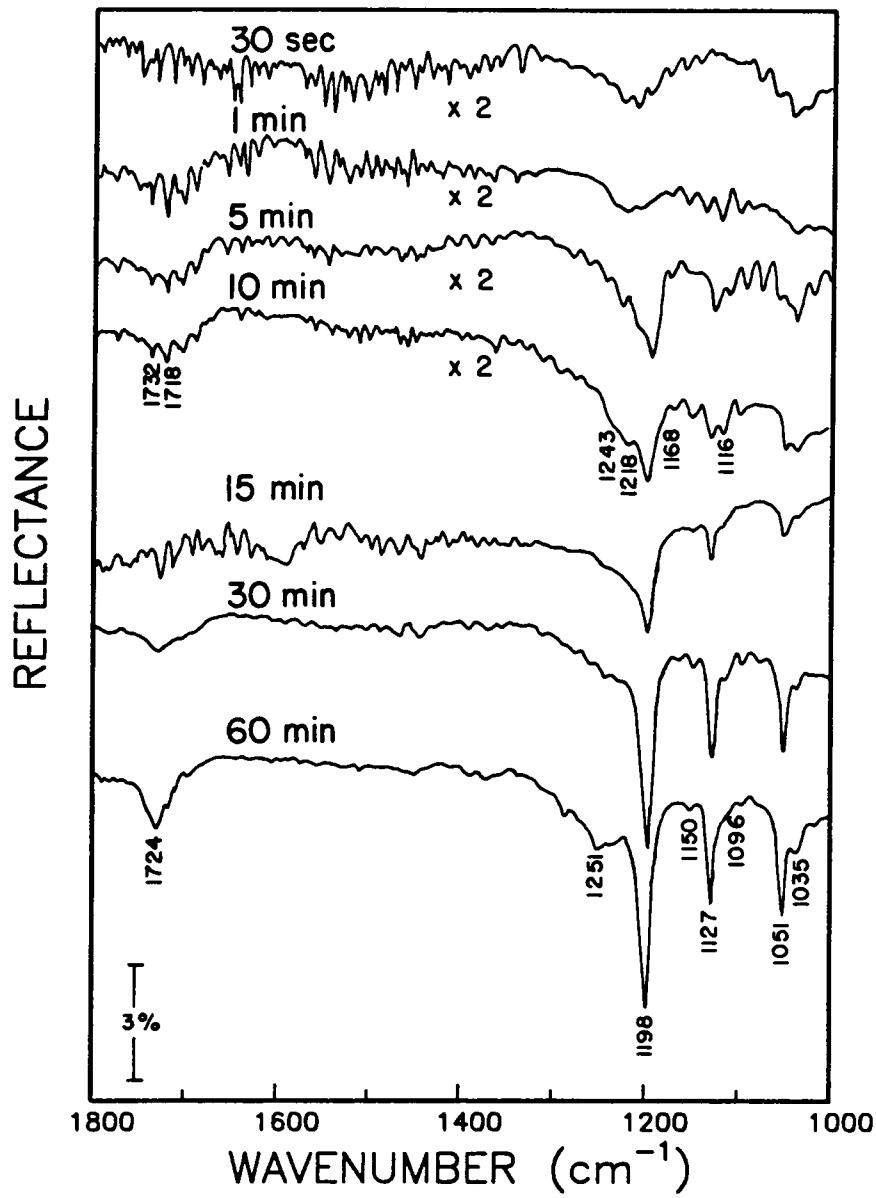

Figure 3.50. IRAS spectra of the collector adsorbed on copper conditioned in a mixture of IBECTC and KEX solution (10^{-4} M, each) at pH 6.0 and different adsorption time.

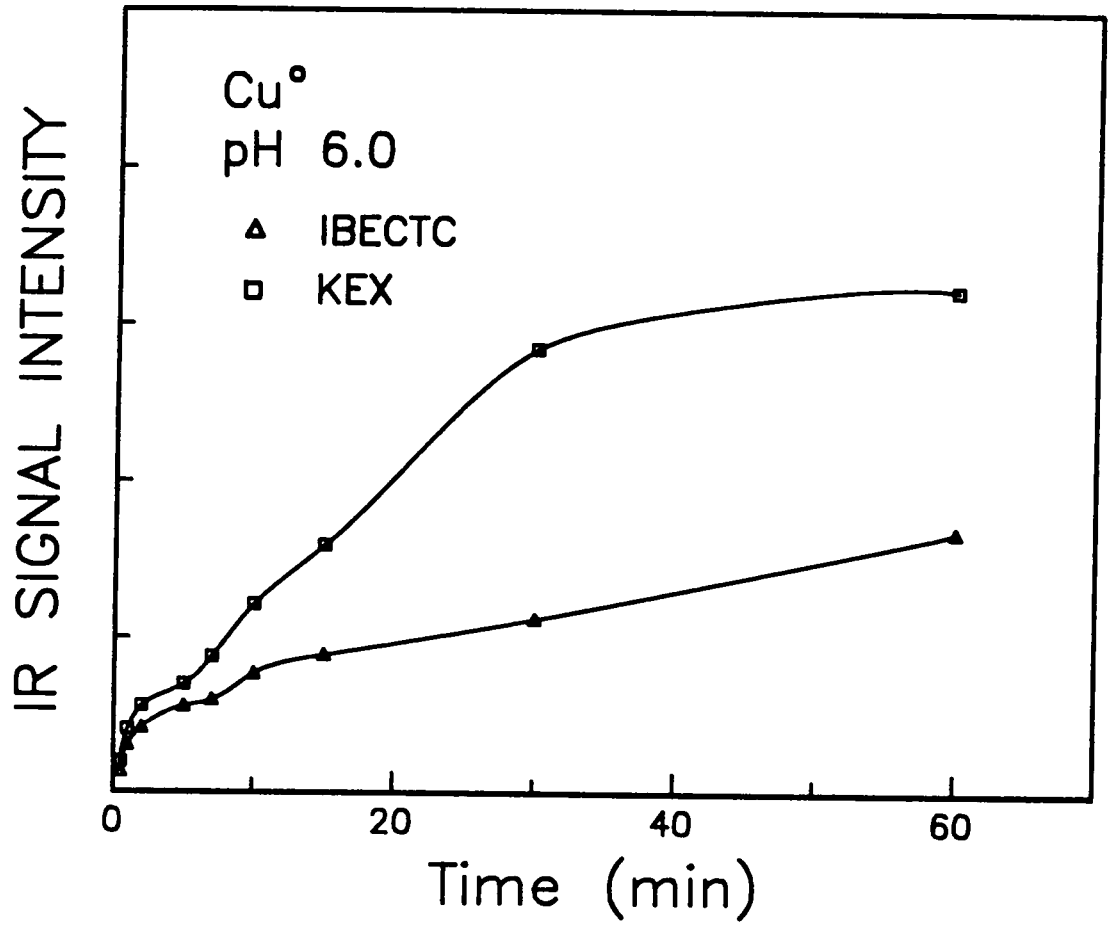

Figure 3.51. Effect of adsorption time on the IR signal intensity of the collector adsorbed on copper conditioned in a solution containing both IBECTC and KEX (10^{-4} M, each) at pH 6.0

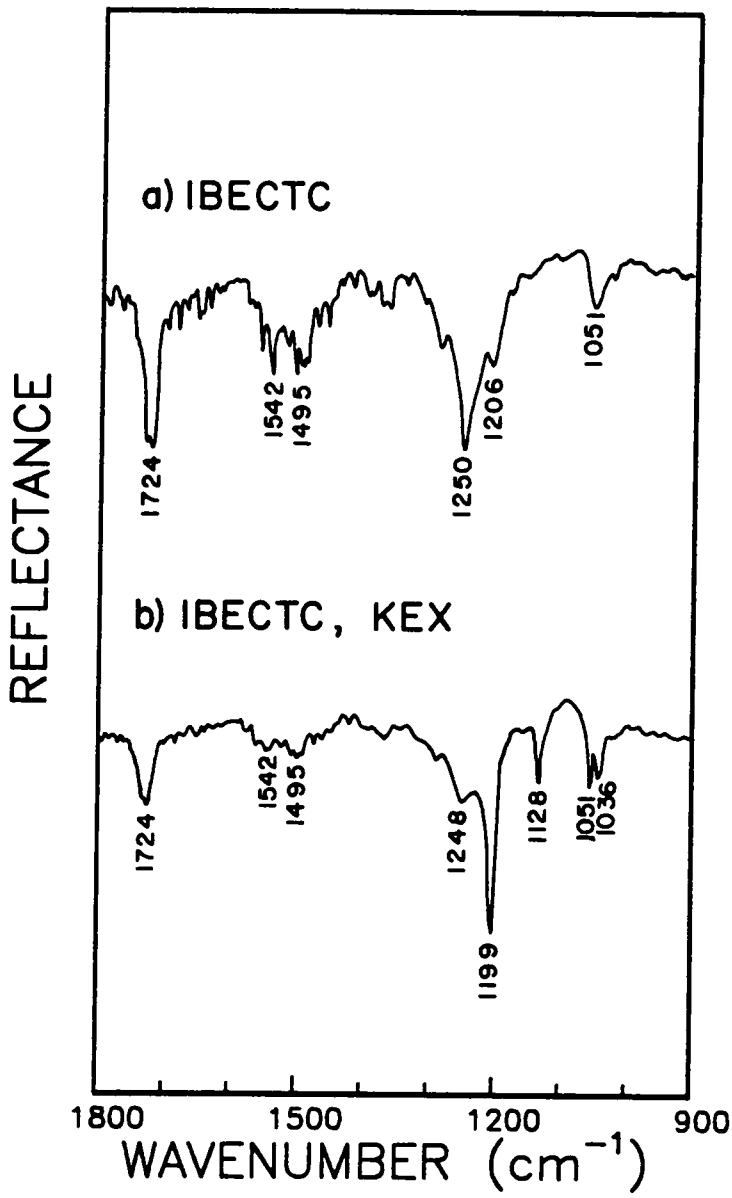

Figure 3.52. IRAS spectra of the collector adsorbed on copper conditioned in a) 10^{-4} M IBECTC solution, initially and then b) 10^{-4} M KEX solution at pH 6.0.

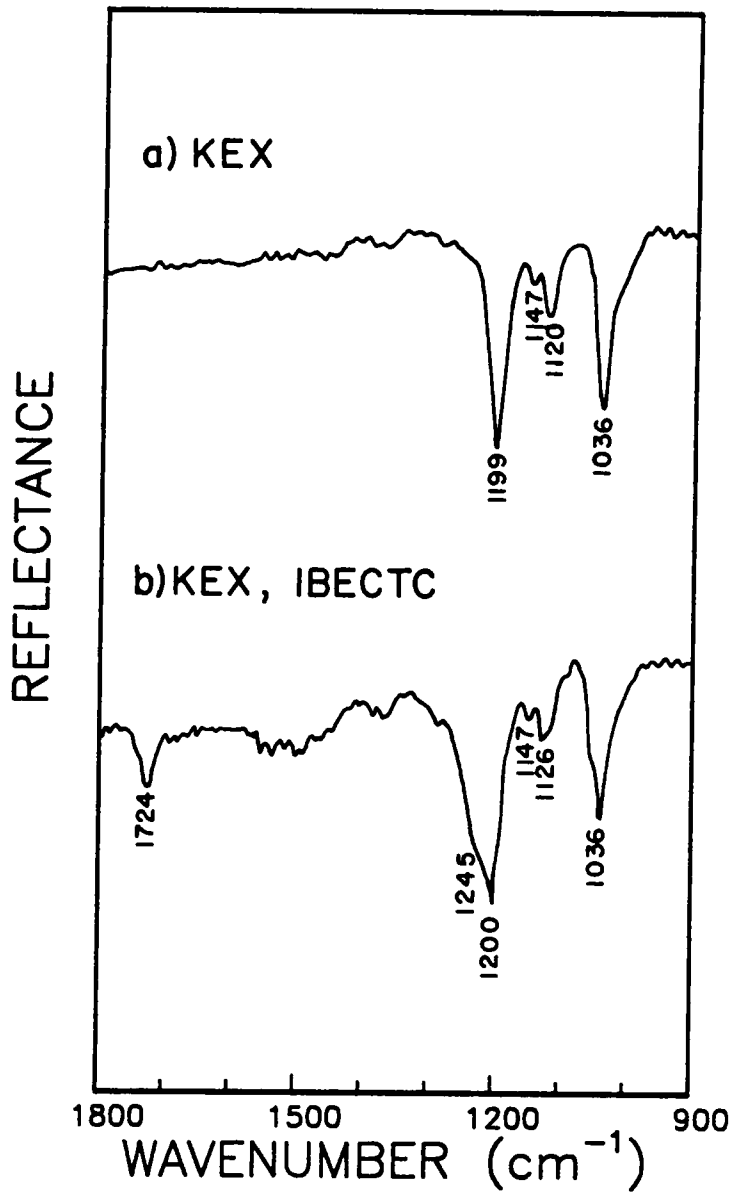

Figure 3.53. IRAS spectra of the collector adsorbed on copper conditioned in a) 10^{-4} M KEX solution, initially and then b) 10^{-4} M IBECTC solution at pH 6.0.

signal intensities of the IBECTC bands may be due to changes in optical properties of the adsorbed layers, as stated previously. However, it is possible that this decrease in intensities indicate KEX displacement of some of the adsorbed IBECTC molecules. The IR spectrum also indicate that the xanthate molecules are randomly oriented on the substrate. This may suggest that the displacement occurs in the multi-layers and probably not in the monolayer.

The spectra of the copper sample after initial adsorption of KEX followed by IBECTC (Figure 3.53) are slightly different from those with the order of adsorption reversed. The xanthate that is adsorbed initially shows random orientation, as suggested by the fact that its spectrum is similar to that of the CuX precipitates. Over the multilayers of xanthate species, IBECTC is adsorbed. This is shown by the new bands at 1724 cm^{-1} (C=O) and the shoulders at around 1245 (C-O and C=S) and 1050 cm^{-1}(C-O). As shown, IBECTC is not strong enough to displace the adsorbed xanthate species on the copper surface. The results of these different tests studying the competition between IBECTC and KEX seem to favor the conclusion that KEX is probably a stronger collector.

3.3.7 UV Spectroscopic Measurements

The adsorption of IPETC and IBECTC on sulfide minerals, particularly Cu_2S, $CuFeS_2$ and FeS_2, were studied using UV spectroscopy. These two thionocarbamates give distinct adsorption peaks at 244 and 256 nm, respectively. By analyzing the supernatant solution from the ATR experiments, the amount of thionocarbamates left in the solution can be measured. This is another method of investigating the effects of pH and concentration on thionocarbamate adsorption. The results of these

measurements can then be compared with the FTIR study. Also, using a flow-through adsorption cell, the kinetics of thionocarbamate adsorption can be determined.

a. Effect of pH on IPETC adsorption

Figure 3.54 shows the effect of pH on the adsorption of IPETC on chalcocite as analyzed by FTIR and UV spectroscopy at collector concentrations of 10^{-3} and 10^{-4}M, respectively. Also shown for comparison are the IR data obtained at an IPETC addition of 10^{-4}M. For the three sulfide minerals, the IR signal peak intensities were measured at the adsorption bands (1500-1550 cm^{-1}) characteristic of the surface IPETC species adsorbed on each mineral. From the FTIR measurements, the maximum adsorption on chalcocite occurs at pH 4 in 10^{-3}M IPETC solutions and is shifted to pH 6 when the collector concentration is reduced to 10^{-4}M. The UV analysis show, on the other hand, that the adsorption is maximum at pH 6, which is in agreement with the FTIR results obtained at same concentration. The shift of the adsorption maximum to pH 6 with the change in IPETC concentration seems to support the view that the adsorption mechanisms at pH 4 and 6 are different. This has already been suggested in light of the FTIR results obtained for IPETC adsorption on chalcocite at different pH values (Figure 3.7). The microflotation test results, done at lower concentrations, are also in excellent agreement with the spectroscopic measurements. On the other hand, thermodynamics predict an upper pH limit of around 12 (Figure 2.9).

Figure 3.55 compares the FTIR and UV results obtained with chalcopyrite at IPETC additions of 10^{-3} and 10^{-4}M, respectively. Both measurements show that IPETC adsorption decreases with increasing pH. Microflotation studies also show the same trend for chalcopyrite-IPETC systems. The amount of IPETC adsorbed on chalcopyrite is less than that on chalcocite. However, the microflotation results at low

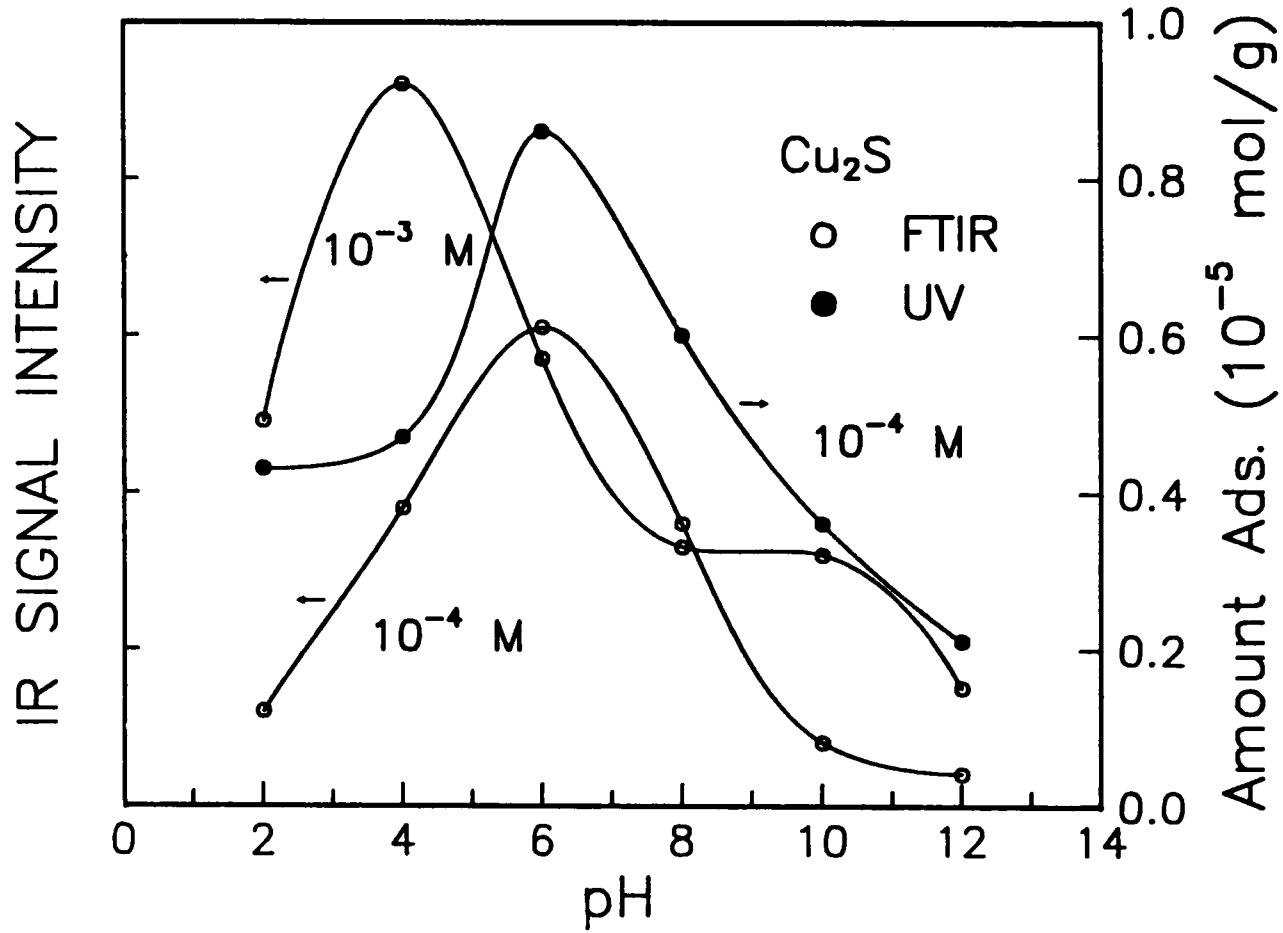

Figure 3.54. Effect of pH on the IR signal intensity and the amount of IPETC adsorbed on chalcocite at initial collector concentrations of 10^{-3} and 10^{-4} M, respectively.

IPETC concentration (Figure 2.27) show higher chalcopyrite recovery. This agrees with the conclusions made in the previous chapter that a part of the chalcopyrite floatability is probably due to collectorless flotation.

Figure 3.56 shows the results obtained for pyrite using the same initial IPETC concentrations used for the other two minerals. There is significant adsorption of IPETC on pyrite at very high pH and decreases with increasing alkalinity. However, its floatability, as shown in the previous chapter, is good only at extremely acidic conditions and high IPETC concentrations. This shows the excellent agreement between the microflotation and spectroscopic data.

Other investigators (Glembotskii et al., 1968; Bogdanov et al., 1977; Ackerman et al., 1984) have also shown that the adsorption of thionocarbamates on sulfide minerals generally decreases with increasing pH. The results of the spectroscopic measurements show that the amount of IPETC adsorbed is highest on chalcocite, followed by chalcopyrite and pyrite. Note also that there is not much difference in the amount of IPETC adsorbed on chalcopyrite and pyrite, yet the former floats much better than the latter. The inability of pyrite to float may be explained by the ATR results (Figures 3.7 to 3.9). They show that the amount of sulfoxy oxidation products present on pyrite far exceeds those on chalcocite and chalcopyrite. It was suggested that IPETC is unable to remove or prevent the formation of the sulfoxy compound from the surface of pyrite. The hydrophilicity due to the presence of this oxidation product may outweigh the hydrophobicity rendered by the IPETC adsorption. On the other hand, when using xanthate as a collector for pyrite, the oxidation product is replaced by the adsorbed dixanthogen. This may be the basis for the excellent selectivity of IPETC over xanthate observed in industrial practice and also in this work (Figures 2.20 and 2.21).

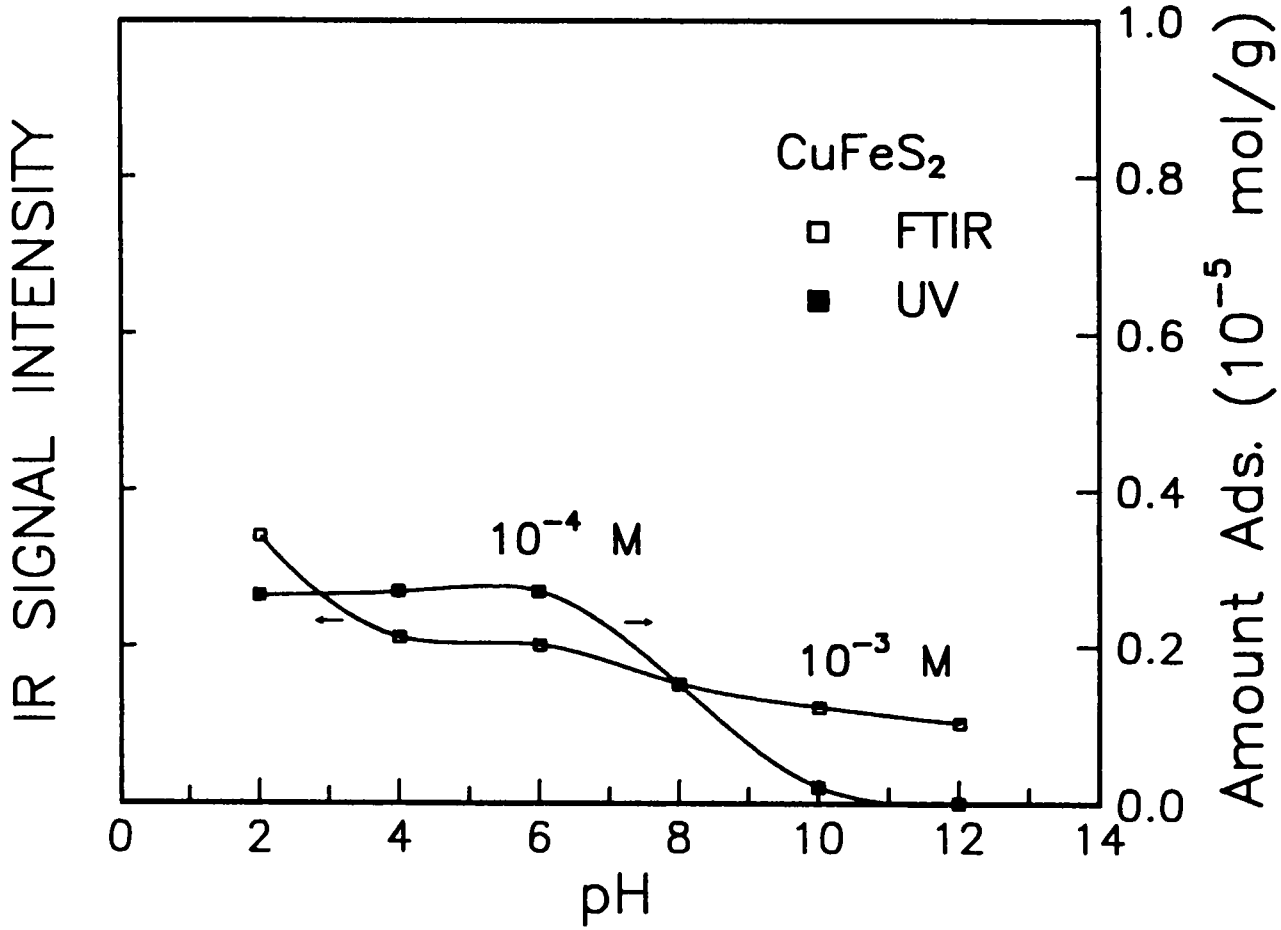

Figure 3.55. Effect of pH on the IR signal intensity and the amount of IPETC adsorbed on chalcopyrite at initial collector concentrations of 10^{-3} and 10^{-4} M, respectively.

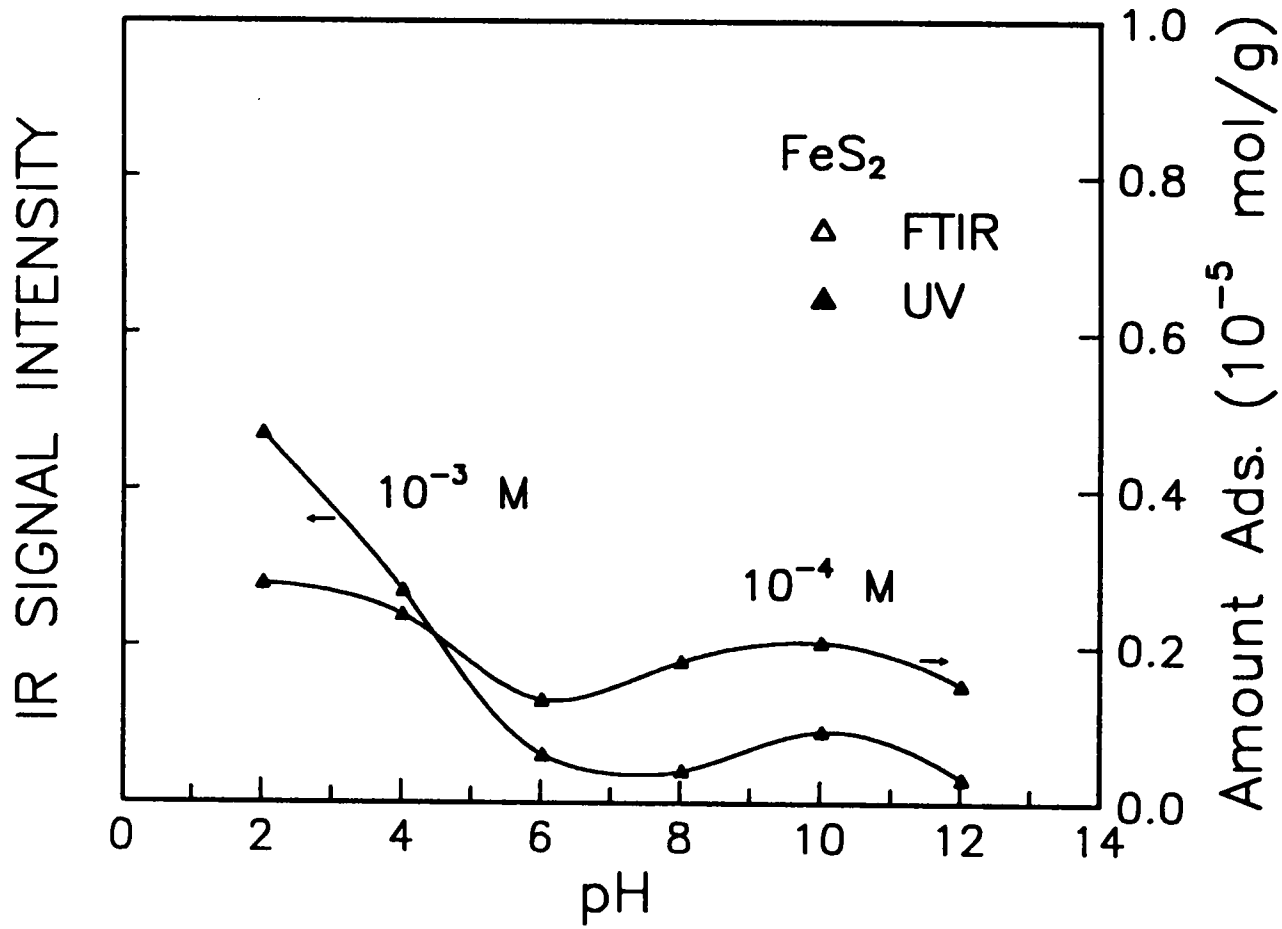

Figure 3.56. Effect of pH on the IR signal intensity and the amount of IPETC adsorbed on pyrite at initial collector concentrations of 10^{-3} and 10^{-4} M, respectively.

b. Effect of pH on IBECTC adsorption

Figure 3.57 shows the results of the adsorption measurements conducted with 10^{-4}M IBECTC using the UV adsorption technique. Also shown is the relative intensity of the characteristic absorption band (1250 cm^{-1}) of the IBECTC species adsorbed on chalcocite. Both FTIR and UV adsorption data show that IBECTC adsorption on chalcocite is effective at pH 4-10, with a maximum at pH 6. This is in excellent agreement with the results of the microflotation experiments. However, there are some discrepancy observed with the thermodynamically calculated pH range for flotation (Figure 2.10).

The effect of pH on IBECTC adsorption on chalcopyrite is shown in Figure 3.58. The signal intensity was measured at around 1250 cm^{-1} (C-O and C=S), which is one of the characteristic band for surface IBECTC species adsorbed on chalcopyrite. The adsorption of IBECTC is shown to decrease with increasing pH, which is similar to what has been observed with IPETC. The spectroscopic data correlates well with the flotation results.

Figure 3.59 shows the results obtained for pyrite in IBECTC solutions. The IR signal intensity was also measured at the same frequency as those used for the other minerals. On pyrite, the adsorption has two maxima, one at pH 8 and the other at pH 2. There is no clear explanation for this behavior. Except for this other maximum at pH 8, the UV adsorption results showed good correlation with the flotation test data over the entire pH range.

Even though IBECTC adsorption was observed on pyrite, the floatability of pyrite is good only at extremely acidic conditions and high collector concentrations. It should be noted here that, like the case with IPETC and unlike that with xanthate, the poor

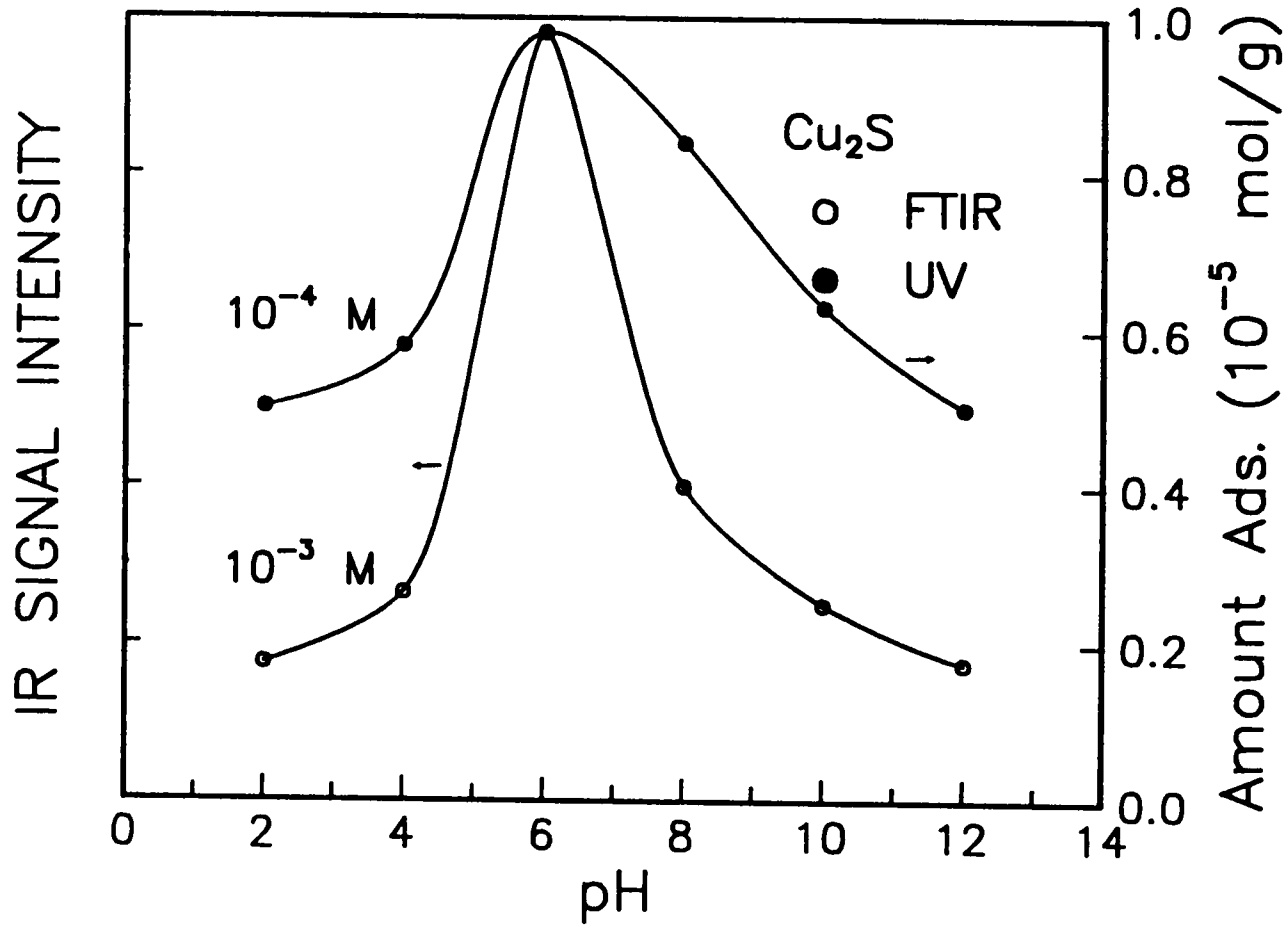

Figure 3.57. Effect of pH on the IR signal intensity and the amount of IBECTC adsorbed on chalcocite at initial collector concentrations of 10^{-3} and 10^{-4} M, respectively.

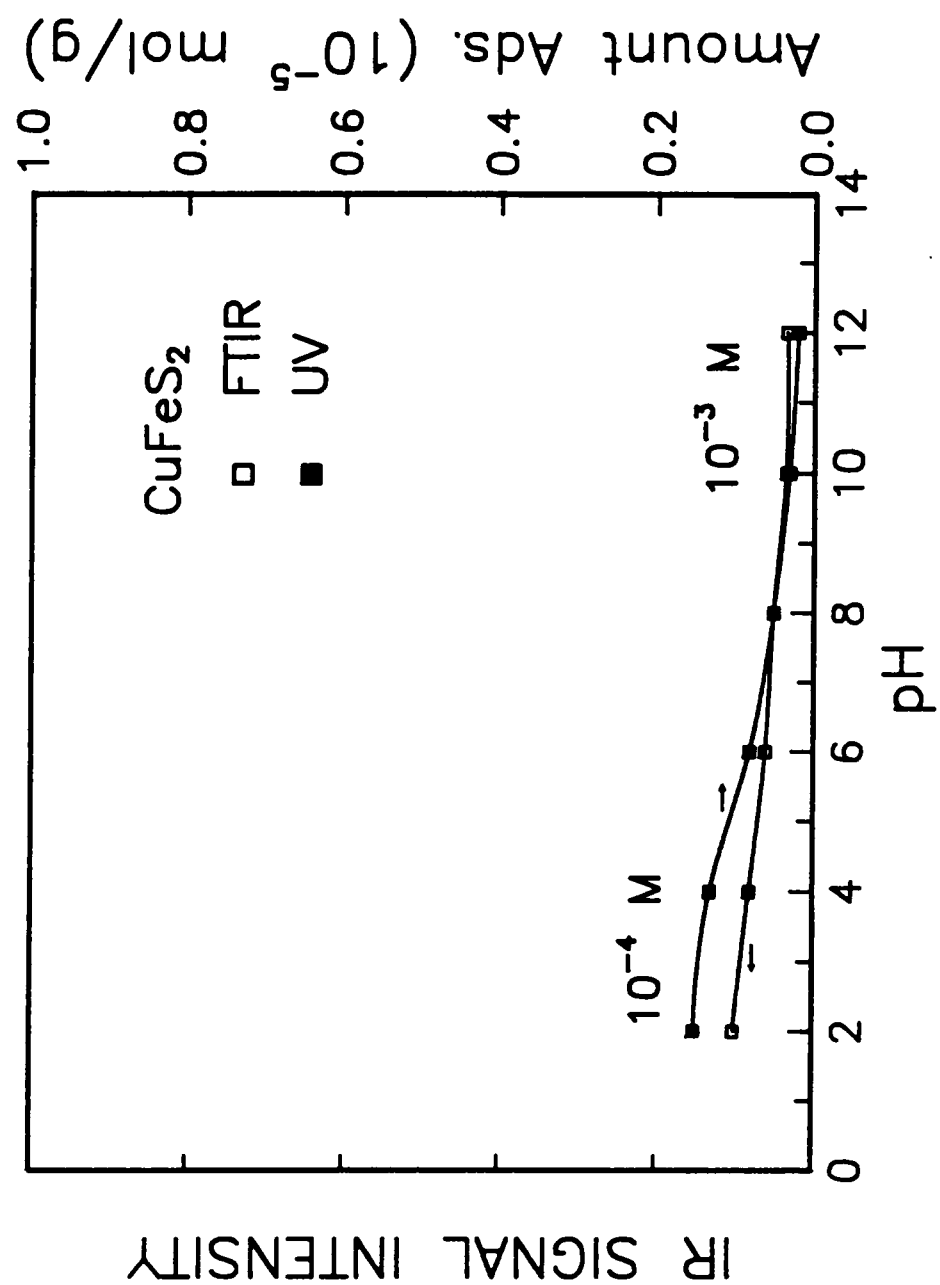

Figure 3.58. Effect of pH on the IR signal intensity and the amount of IBECTC adsorbed on chalcopyrite at initial collector concentrations of 10^{-3} and 10^{-4} M, respectively.

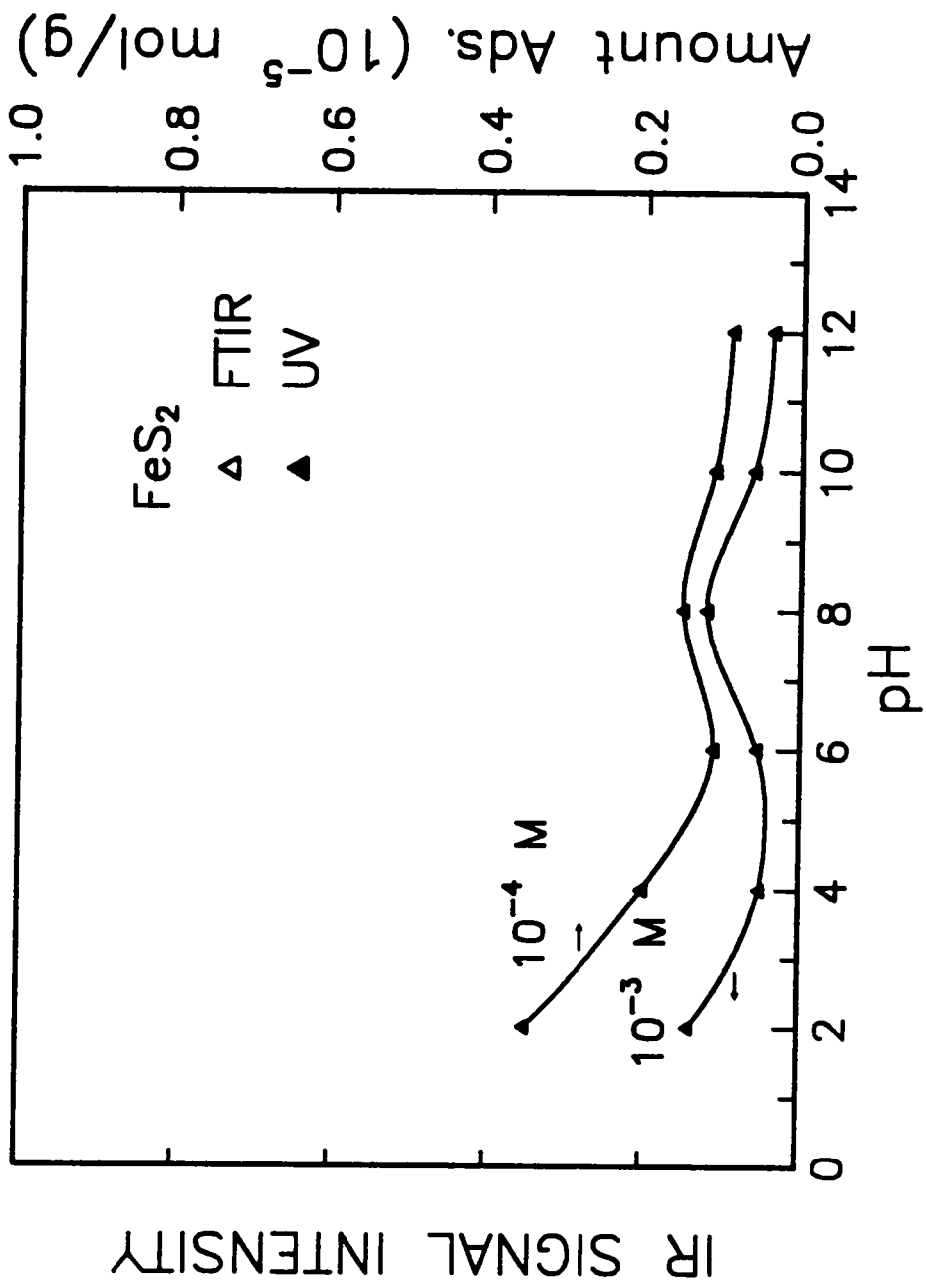

Figure 3.59. Effect of pH on the IR signal intensity and the amount of IBECTC adsorbed on pyrite at initial collector concentrations of 10^{-3} and 10^{-4} M, respectively.

floatability of pyrite may be explained by the inability of IBECTC to remove or prevent the formation of sulfoxy oxidation products.

c. Effect of Concentration

Figure 3.60 shows isotherms for the adsorption of IPETC and IBECTC on chalcocite at pH 6. The data was obtained by analyzing the supernatant solution obtained from the ATR experiments carried out at different concentrations. In the ATR experiments, all of the chalcocite samples ($< 25\ \mu m$) were conditioned for a constant time of 15 minutes. The adsorption of thionocarbamates (in mol/g) increased sharply at low concentrations and reached a plateau, Γ_{max}, at equilibrium concentrations, C_e, greater than 20×10^{-5}M. IBECTC has a higher Γ_{max} due to its capability to physisorb over the chemisorbed layer.

Based on the adsorption isotherm classification of Giles et al. (1960), the isotherms obtained here belong to the L-2 type. The L-2 type indicates a Langmuir type of isotherm with a surface saturation plateau. This is similar to the adsorption isotherm obtained for xanthate on galena (Partyka et al., 1987). At very low C_e (not clearly shown here), the shape of the isotherm for IPETC is more of an S-1 type curve. This means that it is an S-shaped curve where adsorption becomes easier as the concentration increases and saturation has not been reached. On the other hand, the isotherm for IBECTC belongs to the L-1 type, which is similar to the L-2 type except that saturation has not been reached.

Attempts to linearize the two adsorption isotherms by adapting the Langmuir model to solution adsorption are only possible at $C_e > 10^{-5}$M. The equilibrium constant, K, of the adsorption reaction can be estimated from the plot of C_e/Γ vs. C_e. This constant can be determined from the intercept of the C_e/Γ vs. C_e line,

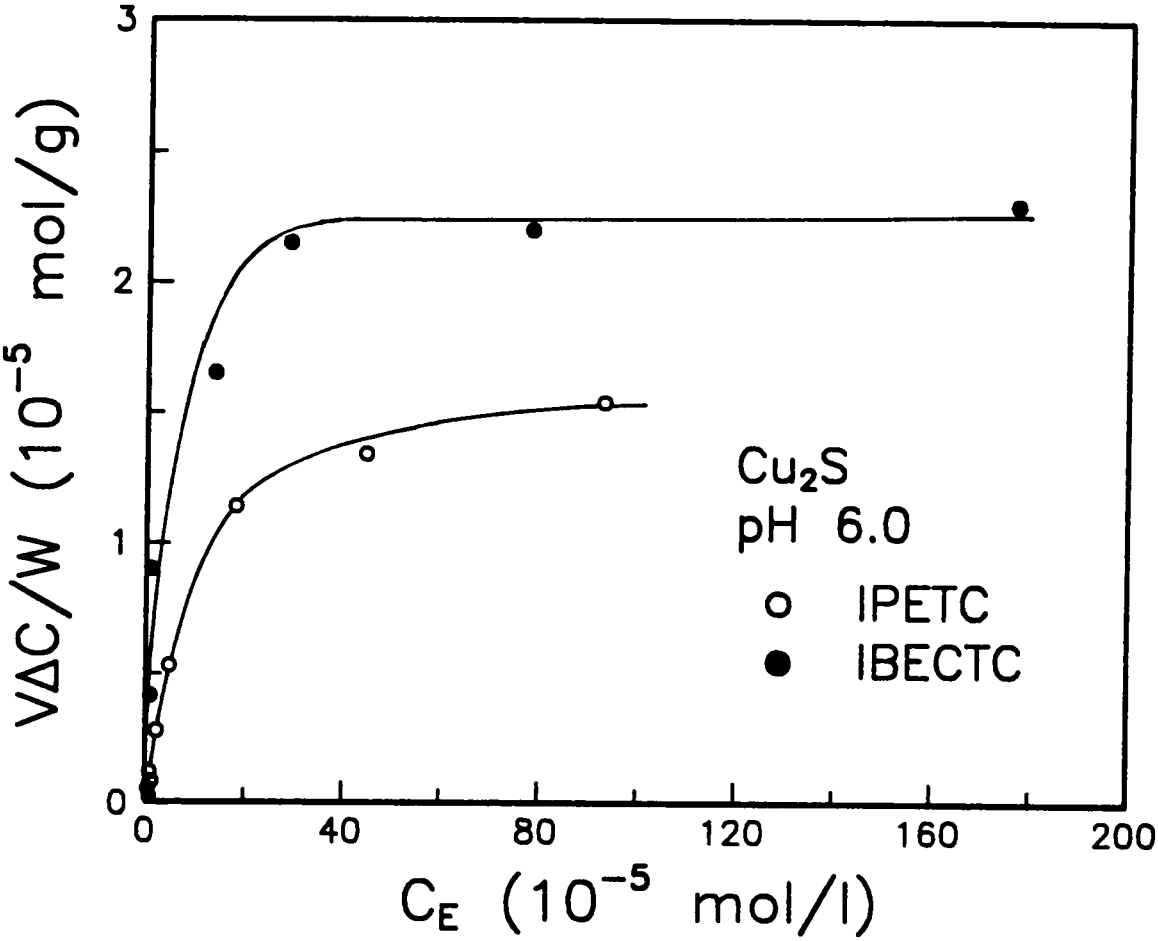

Figure 3.60. Adsorption of IPETC and IBECTC from aqueous solutions on chalcocite at pH 6.0 and 25° C.

$$\frac{1}{\Gamma_{max}K} = intercept. \qquad [3.1]$$

For IPETC and IBECTC, the values of K were estimated to be 1 x 10^4 and 2.17 x 10^4, respectively. These can be related to the thermodynamic equation,

$$\Delta G_{ads} = -RTlnK \qquad [3.2]$$

to obtain the free energy value for IPETC and IBECTC adsorption on chalcocite. The calculated ΔG_{ads} value for IPETC and IBECTC are -5.45 and -5.91 kcal/mol, respectively. These results further support the conclusion regarding the greater collecting strength of IBECTC as compared to IPETC.

It should be pointed out that extreme caution should be taken in considering these calculated thermodynamic values. Adsorption isotherms have not been obtained for other conditions, such as different pH values, temperature and treatment times. The results obtained here have also not been duplicated and more data points are needed. Because of these limitations, comparisons with other adsorption isotherms and thermodynamic values available in literature were not attempted. However, in spite of these limitations, the relative strengths of the two thionocarbamates can be inferred from the adsorption data.

d. Adsorption and kinetic studies

The amount of IPETC adsorbed on chalcocite, chalcopyrite and pyrite with time was monitored using UV spectroscopy. The experiments were done at pH 6.0 with an initial IPETC concentration of 10^{-5}M. Figure 3.61 shows the equilibrium IPETC concentration as a function of time. The greatest amount of IPETC adsorption is on

chalcocite, followed by chalcopyrite and pyrite. It can also be seen that the adsorption of IPETC on chalcocite is faster than on the the other minerals.

Figure 3.62 shows the change in equilibrium IBECTC concentration with time for chalcocite, chalcopyrite and pyrite at an initial IBECTC concentration of 10^{-5}M. Similar to the observations made for the IPETC-sulfide systems, chalcocite adsorbs the collector more than the other two minerals. The rate of the adsorption is also faster on chalcocite, as illustrated by the steeper slope.

The initial slopes of the different adsorption lines from Figures 3.61 and 3.62 were used to determine the rate of adsorption. The results are compared in Table 3.1, where the initial rate of adsorption is expressed in moles/min-g. It can be seen that the initial rate of thionocarbamate adsorption is generally higher on chalcocite, followed by chalcopyrite and pyrite. Also, the kinetics of IBECTC adsorption is faster than that of IPETC for the three minerals investigated. Pyrite adsorption of both collectors is relatively slower. This is another indication of the good selectivity of thionocarbamates against pyrite. It should be noted that the experiments were carried out at pH 6.0 where adsorption on chalcocite was more favored than on chalcopyrite or pyrite. It has previously been shown that chalcopyrite and pyrite adsorption is favored at more acidic conditions.

3.4 Summary

IPETC, IBECTC and their corresponding compounds formed with Cu(I) were characterized using ATR spectroscopy. The IR spectra of the Cu-IPETC compounds produced by using two different precipitation methods were similar. Comparison with the IR spectrum of IPETC indicated that IPETC is likely to be bonded to Cu(I) through the sulfur atom in the Cu-IPETC compounds. The spectra of the Cu-IBECTC

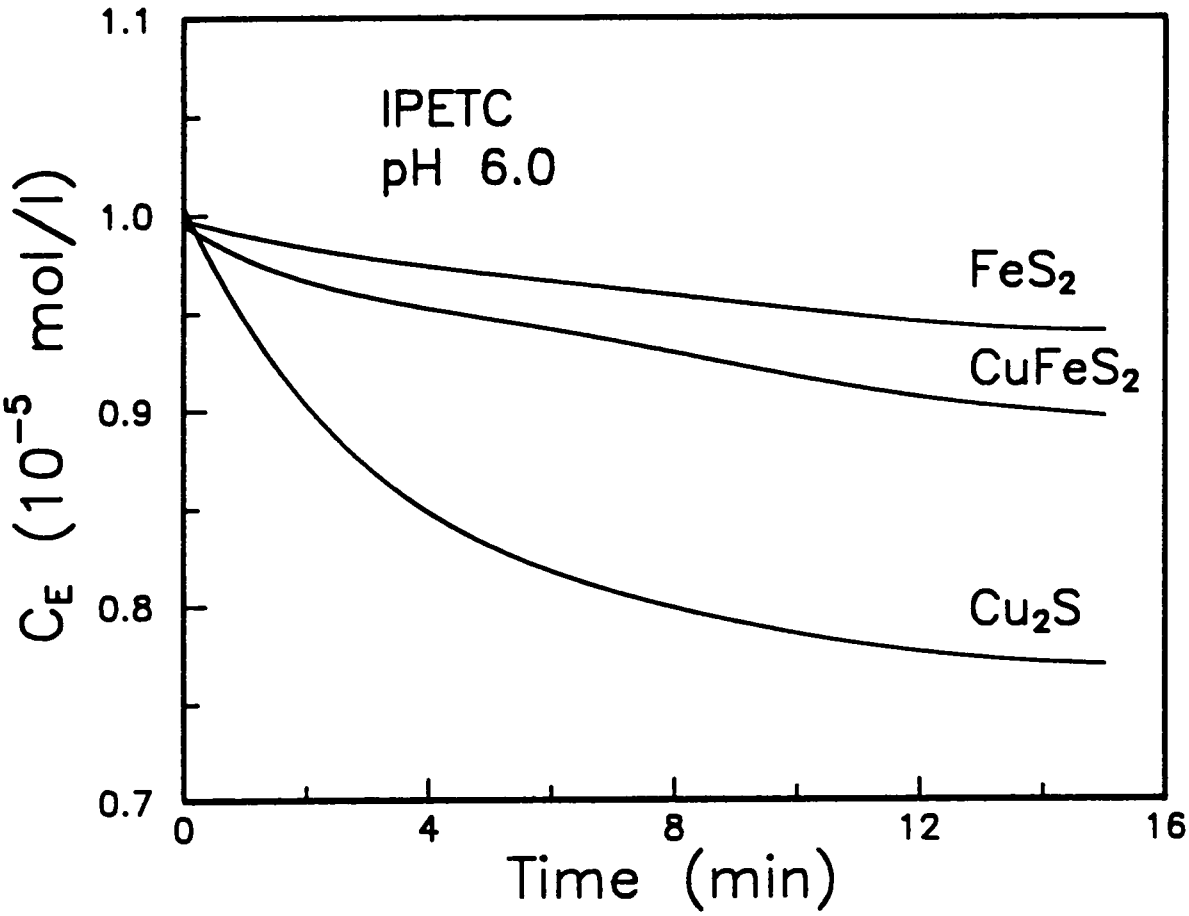

Figure 3.61. Change in the amount of IPETC adsorbed on chalcocite, chalcopyrite and pyrite with time at pH 6.0 and initial IPETC concentration of 10^{-5} M.

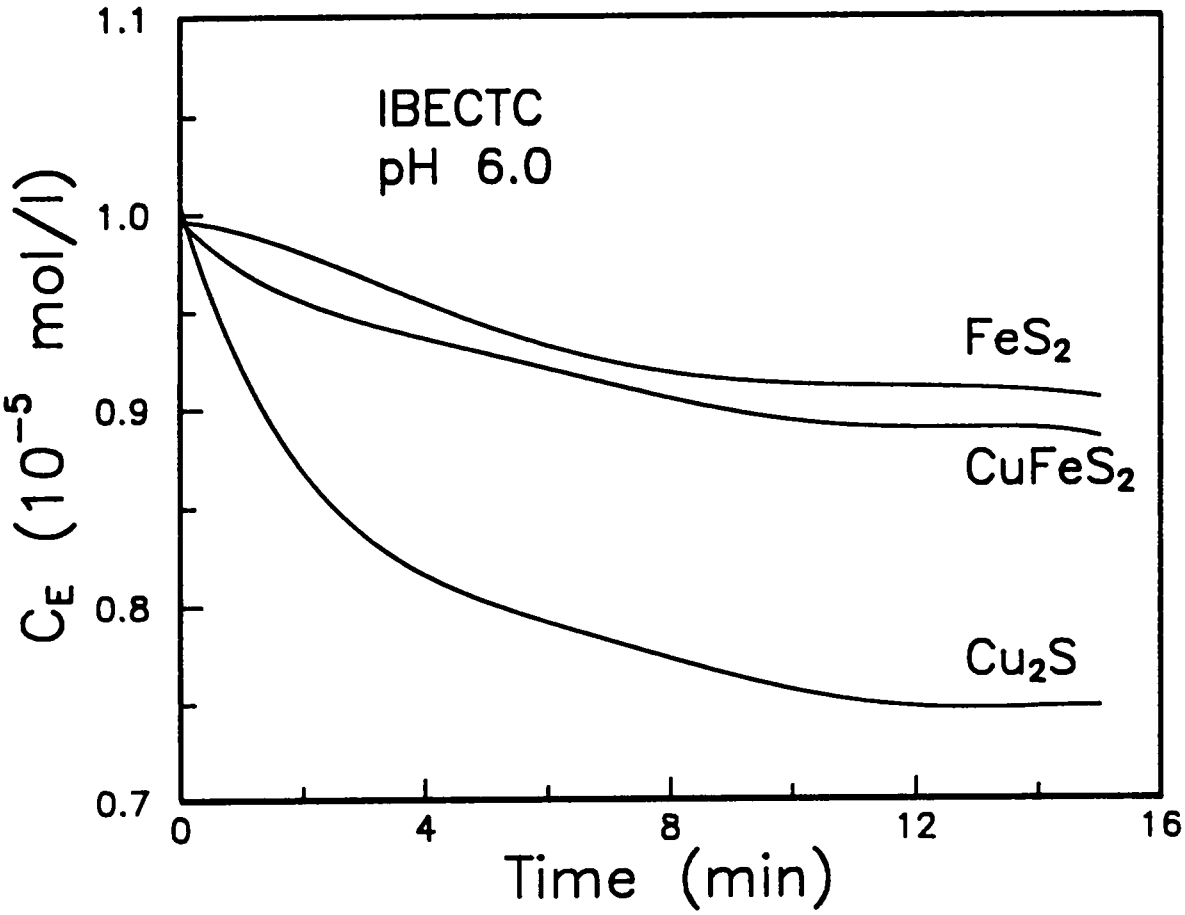

Figure 3.62. Change in the amount of IBECTC adsorbed on chalcocite, chalcopyrite and pyrite with time at pH 6.0 and initial IBECTC concentration of 10^{-5} M.

Table 3.1. The rates of thionocarbamate adsorption on sulfide minerals.

Mineral	Collector	$\Delta C/\Delta t$(moles/min-g)
Cu_2S	IPETC	5.5×10^{-8}
$CuFeS_2$		3.5×10^{-8}
FeS_2		2.0×10^{-8}
Cu_2S	IBECTC	8.5×10^{-8}
$CuFeS_2$		4.5×10^{-8}
FeS_2		1.0×10^{-8}

compounds precipitated using two different methods are also similar. The bonding of IBECTC to Cu(I) involves both sulfur and oxygen to form a six-membered chelate ring. This is expected to be more stable than the bonding found for copper-IPETC compounds. Therefore, IBECTC should be expected to be a stronger collector than IPETC.

An in-situ FTIR technique, in which the surface spectra are taken in the presence of a substantial amount of water using an ATR cell, has been used to study the adsorption of IPETC and IBECTC on chalcocite, chalcopyrite and pyrite. The results show that IPETC chemisorbed on all of these minerals, but its adsorption was most pronounced on chalcocite. The adsorption mechanism on chalcocite was observed to change with pH. Below pH 6, the coordination of IPETC with the surface copper occurs primarily through its sulfur atom, while at pH values above 6, the coordination occurs through both sulfur and oxygen. The adsorption of IPETC on chalcopyrite also involved coordination of the surface copper with sulfur and does not change with pH. The chemical shifts observed in the spectra suggest a relatively weaker chemisorption on chalcopyrite. IPETC adsorption was weaker on pyrite and it is possible that IPETC is physisorbed at alkaline conditions. The IR spectra also showed sulfoxy oxidation products present on the pyrite surface, even in the presence of IPETC. This is different from what is observed for the other minerals.

IBECTC also chemisorbed on chalcocite, but its adsorption mechanism was significantly different from that of IPETC. Due to the presence of the electron-withdrawing ethoxycarbonyl group adjacent to its C=S group, the bonding between the sulfur and the Cu(I) on the surface was weaker than in the case of IPETC. However, the existence of the O-C=O group stabilized the bonding through a chelation mechanism. The adsorption on chalcocite was maximum at pH 6. IBECTC adsorption on chalcopyrite was similar to its adsorption on chalcocite. The binding of the surface

copper in chalcopyrite was also through sulfur and oxygen. The IR spectra obtained for pyrite showed that IBECTC adsorption was weaker and that probably, physisorption occurs at alkaline conditions. There were also sulfoxy oxidation products present on the pyrite surface, which was not seen in the spectra of the other minerals.

Although both IPETC and IBECTC adsorb on pyrite, the adsorption mechanism does not involve the removal or prevention of the formation of the sulfoxy oxidation products from the surface. The hydrophilicity due to the presence of these oxidation products may outweigh the hydrophobicity rendered by thionocarbamate adsorption. The flotation of pyrite observed at pH 2 and high collector addition may be attributed to the larger amount of thionocarbamate adsorbed; thus, the surface is able to overcome the hydrophilic effect of the oxidation products. It should noted that the maximum amount of thionocarbamate adsorbed is at pH 2, while that of the sulfoxy oxidation products is at pH 4 to 6. On the other hand, the adsorption of xanthate on pyrite results in the formation of dixanthogen with no sulfoxy oxidation products. This may account for the improved flotation selectivity of IPETC and IBECTC over xanthates.

Using different concentrations of IPETC, its adsorption on chalcocite was evident in the FTIR spectra even at a concentration as low as 10^{-5}M. The bonding of IPETC was primarily through the sulfur atoms at low collector additions. However, when the IPETC addition was increased to 3 x 10^{-4}M, the IR spectrum indicated coordination through both sulfur and oxygen. It is also at this concentration where the adsorption of IPETC may correspond to monolayer coverage.

IBECTC adsorption on chalcocite was also evident at collector additions of 10^{-5}M. When the IBECTC concentration is increased to 10^{-4}M and above, the IR spectrum showed a shift toward the direction of IBECTC. It seems that IBECTC is capable of physisorbing on top of the chemisorbed monolayer, while IPETC could not. It is also possible that the physisorbed species at high collector concentration may be undissolved

IBECTC molecules. The results indicate that IBECTC has a higher adsorbability on chalcocite than IPETC.

The interaction of thionocarbamates with copper and chalcocite at different potentials have been studied in-situ using the ECATR cell. On copper, signficant IPETC adsorption is found above -500 mv. The mode of IPETC-bonding with copper is also through the sulfur atom, accompanied by the breakage of the N-H bond in IPETC. This agrees with the conclusions made from the voltammograms for copper. The adsorption is found to increase with potential and this increase has been attributed to the release of copper ions during electrode oxidation. The results from the IRAS measurements supported the conclusions made from the in-situ measurements.

The adsorption of IPETC on chalcocite has been observed at the starting potential of -400 mv. The FTIR spectra of the surface IPETC species were similar to those observed on copper. The reduction of chalcocite to copper at the starting potential may be responsible for this similarity. The adsorption of IPETC increased with increasing potential, which was also attributed to oxidation of the electrode surface that resulted in the release of copper ions. Thermodynamic calculations for the Cu^0- and Cu_2S-IPETC system were in reasonable agreement with the FTIR data.

For IBECTC adsorption on copper, the FTIR spectra indicated that a coordination of the Cu with the sulfur and oxygen to form a six-membered chelate ring was involved. This is similar to the adsorption of IBECTC on chalcocite and to its binding with Cu(I) in Cu-IBECTC compounds. The adsorption of IBECTC on copper was also found to be significant above -600 mv. At higher potentials, IBECTC adsorption is favored. The data obtained using the IRAS technique support the findings made from the in-situ study.

On chalcocite, both chemisorption and physisorption of IBECTC were observed at low potentials. The physisorption of IBECTC may probably be due to some undissolved

collector molecules present in the solution. However, at -200 mv and higher, the physisorbed species were no longer distinct in the FTIR spectra. The adsorption of IBECTC increases with increasing potential, which agrees with the contact angle measurements. The results of the thermodynamic calculations for copper and chalcocite showed a similar response of % $Cu(IBECTC)_2Cl$ to increasing potential.

The IRAS technique was used to determine the structure and orientation of the thionocarbamates adsorbed on the copper surface. IPETC adsorption was observed to grow with contact time and that close to monolayer formation can be expected after about 20 minutes. This is in general agreement with the adsorption isotherm obtained with the UV adsorption measurements. The initial adsorption layer presumably involved coordination of both sulfur and oxygen with the Cu, although it is possible that the adsorbed molecules were just inclined to the substrate surface. Near monolayer coverage, the bonding of IPETC now only involved coordination of sulfur with Cu. There were indications that the adsorbed molecules at the monolayer level were almost perpendicular to the copper surface. There is evidence that with increasing coverage, the adsorbed molecules were reoriented. At multi-layers, the ratios of the characteristic bands were similar to that of the bulk Cu-IPETC compounds indicating awere similar totion of the molecules.

At pH 4, there were no significant differences observed in the spectra, except for the lower signal intensities. The mode of adsorption was similar to that found at pH 6. In the sub-monolayer, the adsorbed IPETC molecules were probably inclined to the surface of the substrate or may even be randomly oriented. This was shown by the dominance of the bands associated with the O-C=S vibrations. At higher coverage, the orientation and structure of the adsorbed molecules were not affected by the decrease in pH.

The structure and orientation of IBECTC molecules adsorbed on copper were also studied at pH 6 and 4. The adsorption of IBECTC on copper involved the coordination

of both sulfur and oxygen with Cu. The orientation of the adsorbed IBECTC was observed to change with the amount of coverage. In the submonolayer stage, the adsorbed IBECTC molecules were suggested to be inclined to the surface. Increasing the amount of adsorbed IBECTC resulted in almost perpendicular orientation at coverages approaching a monolayer. Further adsorption of IBECTC caused a change in orientation of the adsorbed molecules. At multilayer coverage, the spectra indicated random orientation of adsorbed IBECTC. Decreasing the pH to 4 did not cause any change in the structure or orientation of the adsorbed layer. The signal intensities were lower, though, which might indicate that a longer adsorption time is needed to form the monolayer. It should be noted that IBECTC adsorption has been observed to be dependent on pH.

Using the IRAS technique, the spectra of copper treated in solutions containing mixtures of equal concentrations of different collector combinations have been recorded. The results of the preferential adsorption studies were used to compare the relative strength and kinetics of IPETC, IBECTC and KEX adsorption. In the presence of both IPETC and KEX, xanthate was preferentially adsorbed by copper. This agrees with the general observation that xanthates are stronger collectors. The sulfur bonds with copper in xanthates were found to be stronger than the corresponding coordination in IPETC. When the adsorption studies were done in sequence (i.e., one collector at a time), KEX was able to adsorb on top of the chemisorbed IPETC layer, but not vice-versa.

The IRAS spectra for copper treated in a solution containing both IPETC and IBECTC showed stronger adsorption of IBECTC than IPETC. Although both IPETC and IBECTC were co-adsorbed on copper at short conditioning times, IBECTC was preferentially adsorbed at longer contact times. When the sample was alternately treated with IPETC and IBECTC, it was found that both collectors were capable of adsorbing

on top of each other. However, IBECTC adsorption over the chemisorbed IPETC layer was more favored than the opposite situation.

The last preferential adsorption study involving IBECTC and KEX showed both collectors co-adsorbing on the copper at different treatment periods. At short conditioning times (< 1 min), xanthate adsorption was more dominant than IBECTC interaction. With increasing contact time, IBECTC adsorption increased considerably. There was more xanthate adsorbed, though, over the entire period. When adsorption was done in sequence, IBECTC adsorption on top of the xanthate layer was observed, and vice-versa.

Overall, KEX was the strongest collector among the three, followed by IBECTC and then IPETC. None of the collectors studied here was strong and adsorbs fast enough to completely displace the initially adsorbed collector layer within the set conditioning time. However, there were some indications that KEX probably was able to displace some of the initially adsorbed thionocarbamate molecules. It should be noted that the collector displacement occurred after multi-layers have already formed. The results would probably be different if the initial adsorption was limited to a submonolayer.

UV analysis of the solution obtained from the ATR measurements have also been carried out. Results from the UV adsorption studies were in good agreement with those obtained from the FTIR measurements. IPETC adsorption on chalcocite was maximum at pH 6. Chalcopyrite and pyrite showed decreasing IPETC adsorption with increasing pH. The selectivity of IPETC against pyrite was found to be best at pH 6 to 8.

The adsorption of IBECTC on chalcocite was also maximum at pH 6. The other two sulfides also showed decreasing adsorption with increasing alkalinity. The UV adsorption data showed that both IPETC and IBECTC adsorb most strongly on chalcocite, followed by chalcopyrite and pyrite. Microflotation test results from the

previous chapter were also in good agreement with the adsorption data obtained by UV spectroscopy.

Kinetic studies using UV analysis have also been done to compare the initial adsorption rates of the different sulfide minerals. The rate of IPETC adsorption was highest on chalcocite, followed by chalcopyrite and pyrite. The same trend was also observed for the adsorption of IBECTC. However, for each mineral, IBECTC adsorption was relatively faster than the adsorption of IPETC. This is indicative of the stronger collector capacity of IBECTC. Both IPETC and IBECTC also showed good selectivity against pyrite.

4.0 SURFACE ACIDITY MEASUREMENTS BY FLOW MICROCALORIMETRY

4.1 Introduction

The previous chapters have shown that thionocarbamate interactions with chalcocite and chalcopyrite are stronger than those with pyrite. This has been indicated by the selective flotation of the two copper sulfides over pyrite. Spectroscopic studies have also indicated that thionocarbamate adsorption is weaker on pyrite, does not remove the pyrite oxidation products and has slower adsorption rates. However, a more fundamental explanation of this behavior has not been clearly determined.

It has been known for many years that acid-base interactions are important in adhesion of organic substances to inorganic substrates (Fowkes et al., 1959; Fowkes, 1960; Lipatov and Sergreva, 1968; Fowkes, 1983), but adsorption has always been described as either being polar or non-polar. Recent studies, however, have found that all polar interactions, including hydrogen-bonds, can be classified as Lewis acid-base interactions (Fowkes et al., 1984; Fowkes, 1984).

The hard and soft acids and bases (HSAB) model formulated by Pearson (1963) can be applied to the flotation system. This has been attempted previously by Glembotskii

(1977) and by Somasundaran and Nagaraj (1984). However, the approaches used by these investigators were indirect. By determining the Drago E and C parameters for chalcocite and pyrite, the HSAB principle could be used directly to explain the selectivity of thionocarbamates against pyrite. The E and C parameters would indicate the electrostatic and covalent tendencies of the sulfide minerals in their interaction with collector reagents.

4.2 Acid-Base Theory

In 1923, Lewis proposed a generalized acid-base definition based upon a mechanistic approach to chemical behavior instead of structure or constitution (Lewis, 1923). A base is a substance with an available pair of electrons while an acid is any species which has a vacant orbital. In other words, a base is an electron-donor and an acid is an electron-acceptor. Subsequent developments in modern acid-base theory have been in trying to quantify acid-base strengths and reactivities (Bjerrum, 1950; Edwards, 1954; Scwarzenbach, 1956; Ahrland et al., 1958; Pearson, 1963). The strength of an acid or base was defined to be dependent on its ability to donate or accept an electron, and its polarizability. Pearson's HSAB Model classified bases into polarizable (soft) and non-polarizable (hard). Soft bases have large sizes, low oxidation states, high oxidation potentials, low electronegativity and are easily distorted. Hard bases have the opposite properties. The acids were also divided into these two categories. Any Lewis acid with properties that lead to low polarizability (i.e., small size, high positive charge, etc.) was considered hard. On the other hand, soft acids have properties contributing to high polarizability. Pearson also stated the general principle that hard acids prefer to bond with hard bases and soft bases prefer to bond with soft acids.

Drago devised an alternate approach to reactivity and proposed a four-parameter equation for correlating enthalpies of acid-base interaction (Drago and Wayland, 1965; Drago, 1967; Drago et al., 1971):

$$-\Delta H_{ads} = E_A E_B + C_A C_B. \qquad [4.1]$$

The parameters E_A and E_B were interpreted as the susceptibility of the acid and base, respectively, to undergo electrostatic interaction. C_A and C_B were defined as the susceptibility of the acid and base, respectively, to form covalent bonds. It can be inferred from equation [4.1] that acid-base interactions are particularly good in cases where both acid and base have large susceptibilities to the same kind of interaction. This is parallel to Pearson's rule.

Pearson (1966) and Klopman (1968) suggested that softness and hardness can be correlated with C and E, respectively. Acids and bases with large ratios of C/E can be regarded as soft, while those with small ratios are hard. However, some caution should be taken in handling C/E values since the significance of the individual E and C values is sometimes lost when they are combined in a ratio.

4.3 Application of the E and C Model

The components of the flotation system can be categorized using Pearson's HSAB model. In general, anions in solution, water and flotation reagents capable of providing an electron pair can be classified as bases. Hard bases include those reagents with active oxygen and nitrogen atoms such as carboxylate and amines. On the other hand, soft bases are those reagents whose reactive atoms are sulfur and phosphorus. This will include some of the thiol collectors. Metal and hydrogen ions, as well as metal atoms

on a metallic surface, are considered as acids. Minerals can also be considered as acids. The classification of metal ions into hard and soft acids, as defined by Pearson (1963), is given in Table 4.1. There is no definite classification, however, for minerals.

The HSAB model has been applied qualitatively to flotation systems in earlier work (Seryakova et al., 1975; Glembotskii, 1977). IPETC is considered a soft base due to its sulfur atom being the active atom. It is interesting to note that IPETC has O, S and N atoms. Based on electron density and steric accessibility, sulfur has the greatest reactive capacity of this three atoms in IPETC. Studies involving extraction of metal ions by IPETC showed that only soft metal ions (i.e., Cu(I), Ag(I), Hg(II)) were effectively extracted by IPETC. It should be emphasized that Fe, Zn, Co, and Ni were not extracted under any of the experimental conditions studied. This would indicate, therefore, that thionocarbamates (soft bases) would be good collectors for copper sulfides and precious metals (soft acids). Actual flotation data from this study and the literature (Glembotskii and Livshits, 1967; Livshits et al., 1974; Ackerman et al., 1968; Nagaraj et al., 1986; 1988) show this to be true. This is a good example of the application of Pearson's principle.

The hardness or softness of minerals has been based indirectly by the investigators mentioned earlier, on the original class (a) or (b) classification (Ahrland et al., 1958) for metal ions. There is no direct evidence of the validity of this assumption. However, using Drago's E and C parameters, the minerals can be classified directly. Determination of these parameters is done by utilizing the E-C equation. The E and C values for other compounds were determined by using over 280 enthalpies of adduct formation available in the literature and application of Drago's linear transfiguration matrix to equation [4.1] (Drago et al., 1971). To obtain the E and C parameters for sulfide minerals using Drago's matrix method, enthalpy data of the interaction of all these compounds with sulfide minerals is required. However, such information is not

Table 4.1. Classification of metal ions as Lewis acids.

Hard [class (a)]	Soft [class (b)]
Li^+, Na^+, K^+, Be^{2+}, Mg^{2+}	Cu^+, Ag^+, Au^+, Tl^+, Hg^+
Ca^{2+}, Sr^{2+}, Mn^{2+}, Zn^{2+}, Al^{3+}	Pd^{2+}, Cd^{2+}, Pt^{2+}, Hg^{2+}
Sc^{3+}, Ca^{3+}, In^{3+}, La^{3+}, Ce^{3+}	Te^{3+}, Au^{3+}
Cr^{3+}, Co^{3+}, Fe^{3+}, Si^{4+}, Ti^{4+}	Pt^{4+}, Te^{4+}
Zr^{4+}, Th^{4+}, Po^{4+}, Ge^{4+}, Sn^{4+}	
Borderline	
Fe^{2+}, Co^{2+}, Cu^{2+}, Zn^{2+}, Pb^{2+}, Bi^{3+}, Sb^{3+}, Sn^{2+}	

available and is well beyond the scope of this work. Instead, the work will be limited to using three organic bases in the determination of the E and C constants for chalcocite and pyrite.

Drago's E-C equation can be rearranged to a linear form:

$$E_A = \frac{-\Delta H_{ads}}{E_B} - C_A(\frac{C_B}{E_B}) \qquad [4.2]$$

where

$$\frac{-\Delta H_{ads}}{E_B} = intercept \qquad [4.3]$$

and

$$-(\frac{C_B}{E_B}) = slope. \qquad [4.4]$$

By measuring enthalpies of interaction of the acid (sulfide mineral) with bases whose E_B and C_B values are known, E_A and C_A are the only unknowns in equation [4.2]. Selecting different values of C_A, the corresponding value of E_A can be calculated. These would produce a line similar to those given in Figures 4.5 and 4.6. If data obtained with other bases are plotted, then the intersection of these lines will give the E_A and C_A for the acid. Another method of estimating these parameters is to put equation [4.1] into a standard form for multiple regression:

$$-\Delta H_{ads} = \beta_0 + X_1 E_A + X_2 C_A. \qquad [4.5]$$

where X_1 and X_2 are the E and C values, respectively, for the different bases. In this case, the value of β_0 is assumed to be zero. The values of E_A and C_A can then be

obtained by multiple regression analysis. The benefit of this approach is that it is a more rigorous statistical method that shows the fit of the model to the data.

4.4 Experimental

4.4.1 Materials

The experiments were done using chalcocite and pyrite samples, which were obtained from the same source as those stated in Chapter 2.0. The solvent used for these studies was HPLC grade cyclohexane from Fisher Scientific. This was dried, prior to each test, with 8-12 mesh Davison 3 - Å molecular sieves (activated for at least 1 hour under vacuum at 250° C) and stored under nitrogen. All the glassware were oven-dried for at least 24 hours at 50° C immediately prior to use. Solutions were made fresh daily.

The organic bases used for the calorimetry were: ethyl acetate (HPLC grade from Fisher Scientific), triethylamine (99+ mol% from Aldrich Chemical) and methylpyrrole (99 mol% from Aldrich Chemical). The solvent used for cleaning the syringe and the teflon tubing lines of the microcalorimeter was HPLC grade acetone from Fisher Scientific.

4.4.2 Flow Microcalorimetry

A Microscal Flow Microcalorimeter (FMC) Model 3V was used in the determination of the heat of adsorption. The FMC has a teflon cell fitted in a metal block that is insulated with mineral wool (Figure 4.1). There are inlet and outlet tubes connected to the cell. The thermistor bridge comprises of two glass-encapsulated

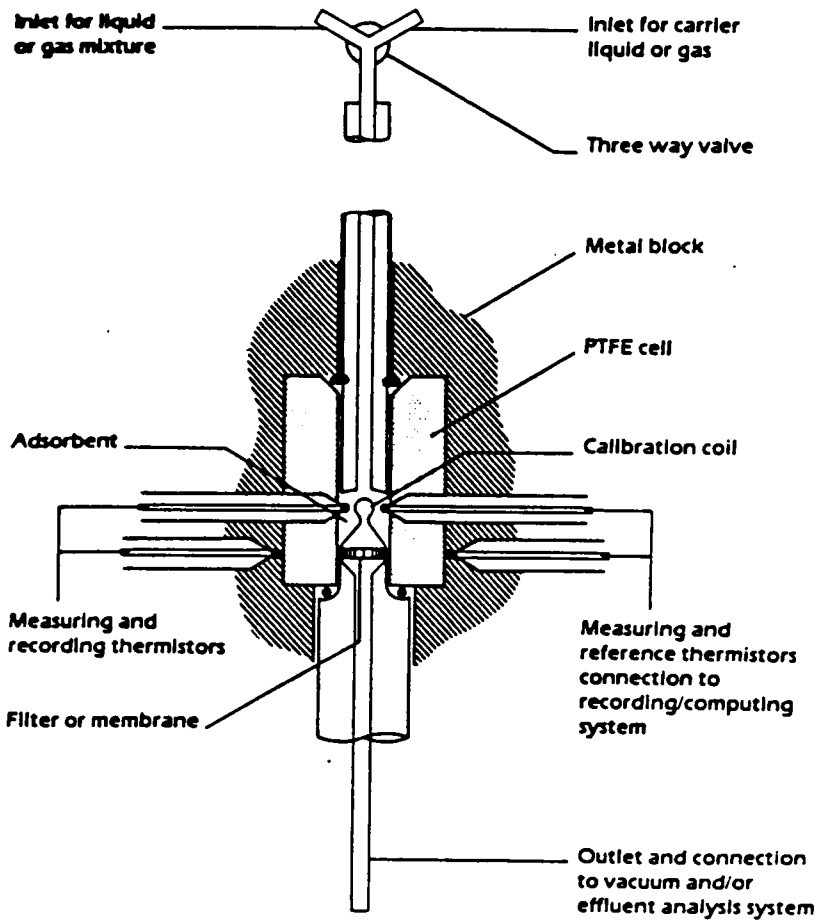

Figure 4.1. Schematic representation of the flow microcalorimeter for adsorption studies.

thermistors which detect the temperature of the cell content, and two reference thermistors located in the cell wall. Calibration of the unit is done through the use of a calibration coil of fine wire placed in the adsorption bed. Known amounts of electrical energy are passed through the coil in the packed bed while the solvent is being pumped through the bed. The entire unit is housed in a draft-proof enclosure to reduce the effect of environmental fluctuations.

The measurements were carried out by filling the adsorption bed with 0.42 gm of the freshly-ground mineral (53-75 μm). It was found, by trial and error, that this amount of solids resulted in a well-packed bed. This is important because the efficiency of the calorimeter depends on the degree of filling. The calorimeter was then evacuated and the solvent introduced afterwards. The solvent is introduced into the system at a steady rate of 3.3 ml/hr by a syringe micropump and two Valco Instrument changeover valves for switching between solvent and solution (Figure 4.2). After the unit has attained equilibrium, as indicated by a constant slope (or flatness) of the measured volts vs. time curve, the solution line was switched over to the solvent containing the adsorbate. The solution that flowed through the bed, at a steady rate of 3.3 ml/hr, is then collected and the amount of remaining adsorbate is determined by UV spectroscopy.

The vacuum system for evacuation of the bed consists of an Edwards rotary vacuum pump and a liquid nitrogen vapor trap and line attached through the bed outlet. A pressure gauge attached between the vapor trap and the bed was used to monitor the pressure during bed-evacuation. During the pump-down of the mineral bed, an endotherm, resulting from the evaporative cooling of the bed as traces of adsorbed water evaporate, is recorded by the FMC (Figure 4.3). It can be seen that after 10-15 minutes, the thermistors have returned to equilibrium.

Since the amount of moisture in the system affects the resulting heats of interaction between the mineral and the base, the following procedure was used to ensure

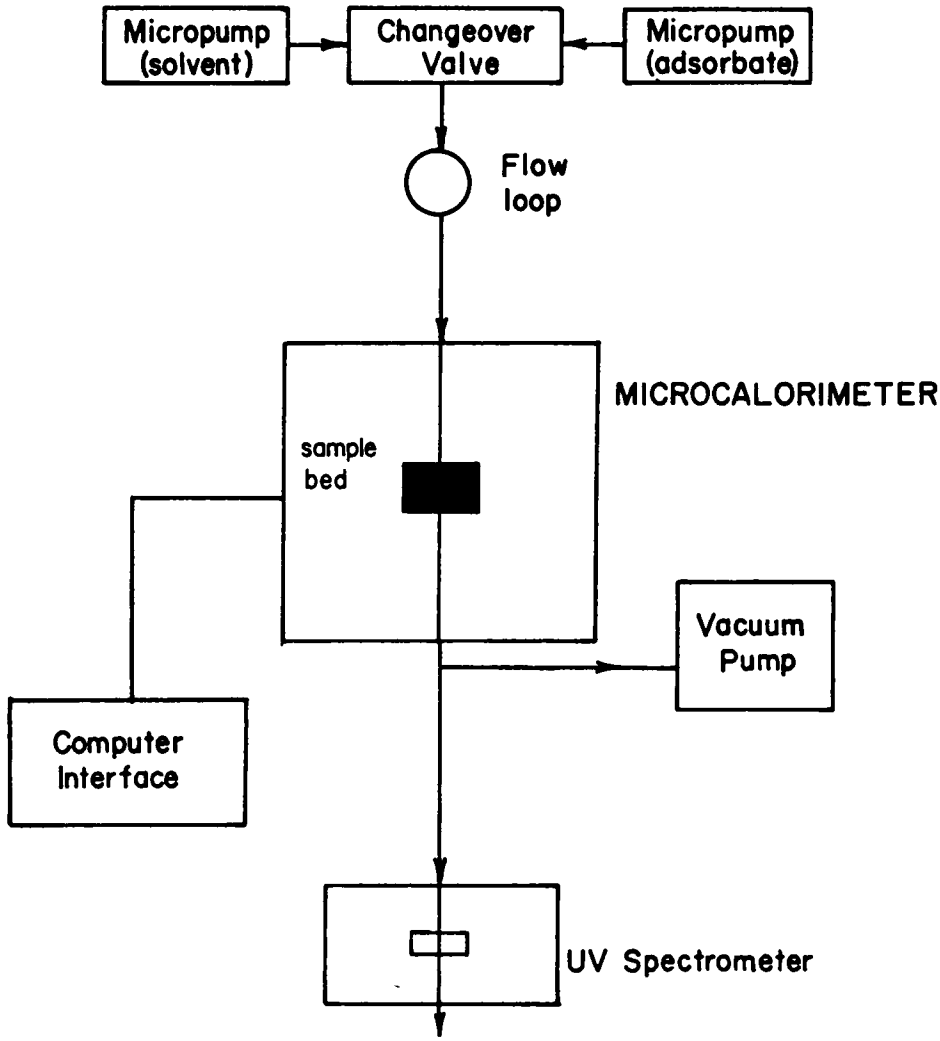

Figure 4.2. Schematic diagram of the flow microcalorimetric experimental arrangement.

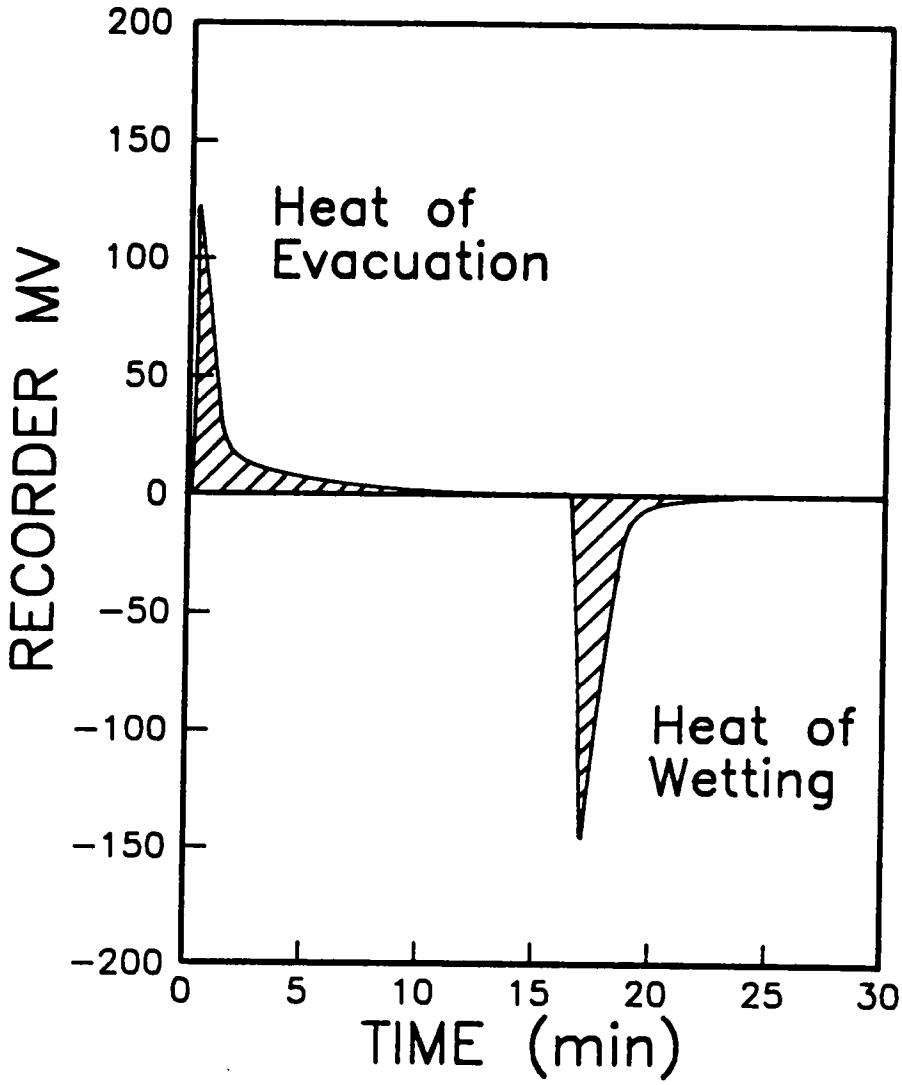

Figure 4.3. Evaporative cooling in the microcalorimeter bed during vacuum pump-down, and subsequent heat of wetting of chalcocite by cyclohexane.

reproducibly-dry samples. The freshly-ground mineral was dry-loaded into the bed and evacuated for 15 minutes (with a final pressure gauge reading of < 5 mbar). The solvent, dried to the required degree of water saturation (usually < 10%), was then pumped through the bed for 2 hours at a flow rate of 6.6 ml/hr. This is the same procedure used by Joslin and Fowkes (1985) to ensure that the sample had a controlled degree of water saturation.

The experimental data was recorded and analyzed using the Microscal Calorimeter Digital Output-processing System (CALDOS). This system enables the analysis of the calibration and experimental data and converts the results into heats of interaction (expressed in mJ).

To check the accuracy of the technique, the flow microcalorimetry experiments that were done for α-ferric oxide (Joslin and Fowkes, 1985) were repeated. Using the same sample (α-ferric oxide, R-1299, from Charles Pfizer, Inc.) and solutions, the results showed reproducible heats of adsorption which agreed with their reported values.

4.4.3 UV spectroscopy

The amount of the organic base remaining in solution after interaction with the solids were determined using a Perkin Elmer Lambda Array 3840 UV/VIS Spectrophotometer. On-line analysis of the solution was abandoned after it was observed that the change in concentration of the base solutions with time was too small for the solution flow rate involved. This is due to the small surface area of the mineral samples (0.1-0.2 m^2/g). However, over the entire period of the interaction, the change in concentration can be detected with more accuracy and precision because of the larger volume of the solution involved. The collection of the absorbate solution was limited to the period between the start of the absorbate solution flowing to the bed and the end

of the interaction. The former was determined prior to the experiment while the latter is indicated by the FMC recorder trace.

A 1-cm pathlength quartz cell was used for the measurements. The calibration curves were constructed using similar procedures discussed in Chapter 3.0. Cyclohexane was used as the solvent and reference solution. To ensure that the measured changes in the UV absorbance were due to the interactions between the organic base and the mineral only, blank tests were done. Cyclohexane (without any organic base) was passed through the sample bed with the same experimental conditions used for the actual tests and the solution collected afterwards. There was no apparent UV adsorbing species produced by the solvent with the sulfide minerals.

4.5 Results and Discussions

The flow microcalorimetry data was utilized for the determination of the E and C constants of chalcocite and pyrite. The heats of interaction between chalcocite and the following bases: triethylamine ($(C_2H_5)_3N$), ethyl acetate ($CH_3COOC_2H_5$) and methylpyrrole (C_5H_7N), were measured experimentally because no data has been reported in literature. The heats of interaction of pyrite with the same three organic bases were also determined. The initial concentration of the organic bases used for all the experiments was 10^{-3}M.

4.5.1 Flow Microcalorimetric Measurements

A typical adsorption exotherm recorded by the FMC system is shown in Figure 4.4. This particular experiment is for the adsorption of triethylamine in cyclohexane on a

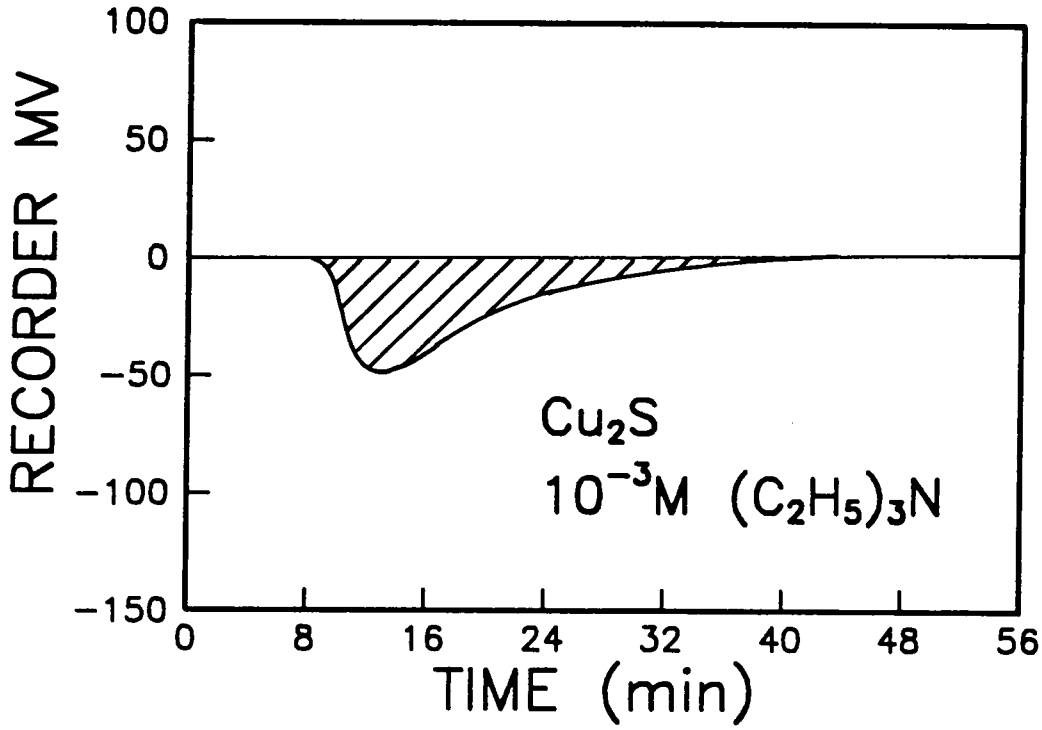

Figure 4.4. Typical flow microcalorimetric adsorption exotherm for a 10^{-3}M solution of triethylamine in cyclohexane flowing through a bed of chalcocite.

chalcocite bed. As shown, the shaded area represents the heat of adsorption resulting from the acid-base interaction. All of the adsorption experiments were conducted at 25°C.

Table 4.2 shows the measured heats of interaction between different acid-base systems. All the reported heats of adsorption are the average of at least 5 replications. Also listed are the known E_B and C_B constants for the organic bases as reported by Drago (1980). The heats associated with pyrite interaction are higher compared to that with chalcocite interaction. Also, triethylamine-sulfide systems show the highest heats of adsorption when compared to the other systems. It is interesting to note that the order of the bases in terms of the magnitude of the heat measured and their C/E ratio are the same. This is indicative of the relative degree of interactions between acid and base.

4.5.2 Estimation of the E and C Parameters

In this study, three organic bases of appreciably different C/E ratios were used so that the E_A and C_A constants of the sulfide minerals could be accurately determined. This is shown by the significant difference of the slopes of the C_A vs. E_A plot for each base (Figure 4.5). This plot is obtained by using equation [4.2] and substituting different C_A values into the equation to get the corresponding value of E_A . If the data perfectly fit the model, the three lines should intersect at a unique point. However, this is hardly attainable due to experimental limitations. The corresponding intersection occurs in a small region, instead. Table 4.3 lists the different intersection points. The average C_A value for chalcocite was 0.78 ± 0.08 $(kcal/mol)^{1/2}$. This value is lower than those observed for silica ($C_A = 1.16 \pm 0.02$), rutile ($C_A = 1.02 \pm 0.03$) and α-ferric oxide ($C_A = 0.80 \pm 0.2$). The average value of E_A for chalcocite was 0.81 ± 0.42 $(kcal/mol)^{1/2}$. Again, this

Table 4.2. Acid-base results from flow microcalorimetry.

Acid	Base	ΔH (kcal/mol)	C_B	E_B	C/E
Cu_2S	Triethylamine	-9.10 ± 0.02	11.09	0.99	11.20
	Methylpyrrole	-6.19 ± 0.22	6.47	1.26	5.13
	Ethyl acetate	-1.97 ± 0.10	1.74	0.97	1.79
FeS_2	Triethylamine	-13.44 ± 0.39	11.09	0.99	11.20
	Methylpyrrole	-9.41 ± 0.26	6.47	1.26	5.13
	Ethyl acetate	-3.60 ± 0.15	1.74	0.97	1.79

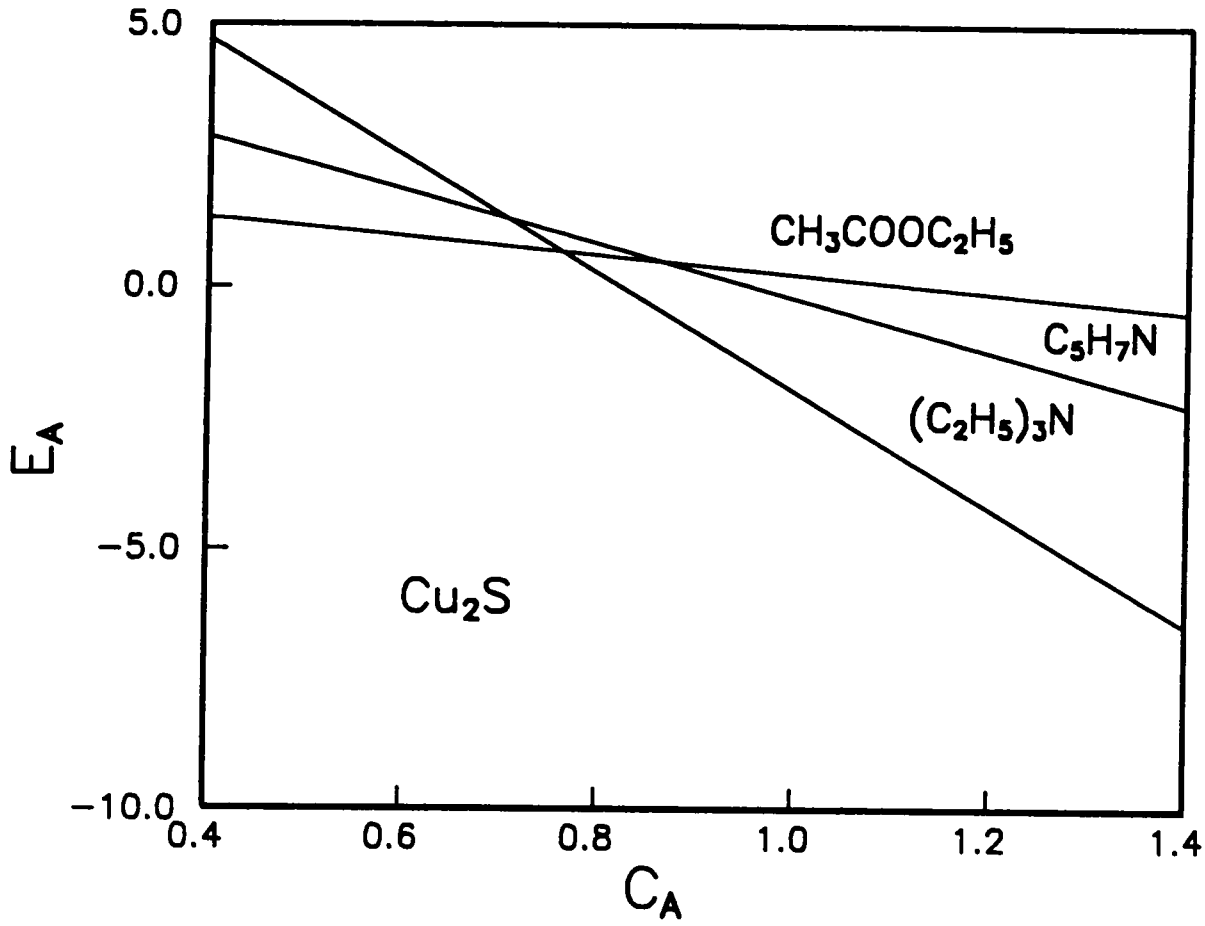

Figure 4.5. Graphical determination of the E and C parameters for chalcocite using equation [4.2].

Table 4.3. Graphical estimation of C and E parameters for chalcocite.

INTERSECTION POINT	C_A $(kcal/mol)^{1/2}$	E_A $(kcal/mol)^{1/2}$
Triethylamine/Ethyl acetate	0.76	0.66
Triethylamine/Methylpyrrole	0.71	1.28
Ethyl acetate/Methylpyrrole	0.86	0.48
Average values	0.78 ± 0.08	0.81 ± 0.42

C/E ratio for chalcocite = 0.96

is much lower than those for silica (E_A = 4.3 ± 0.1), rutile (E_A = 5.7 ± 0.2) and α-ferric oxide (E_A = 4.5 ± 1.1). Based on the graphically determined E_A and C_A values, the C/E ratio for chalcocite is 0.96. This is much higher than the C/E values for the silica (0.27), rutile (0.18) and α-ferric oxide (0.17). Clearly, chalcocite is a much softer acid than the three oxides. It should be pointed out that the metal ions of these oxides belong to the class (a) or hard acids (see Table 4.1).

The result of fitting the Drago model to the data obtained using Equation [4.4] is listed in Table 4.4. This was obtained by utilizing the General Linear Models Procedure of the Statistical Anaylsis System (SAS) program. The predicted values of the C_A and E_A constants were 0.75 ± 0.05 and 0.87 ± 0.32 $(kcal/mol)^{1/2}$, respectively. The C/E ratio of chalcocite, calculated from these values was 0.86. These values are in good agreement with that obtained from the graphical method. The statistical report shows the accuracy of the estimated values for the Drago parameters.

The graphical estimation of the C_A and E_A parameters for pyrite using equation [4.1] is shown in Figure 4.6. The significant difference of the slopes indicates that the resulting parameters will be properly defined (Drago, 1973). The intersections of the lines occur at a small region and are listed in Table 4.5. The average value of C_A observed for pyrite was 1.06 ± 0.06 $(kcal/mol)^{1/2}$. Compared to the other oxides with known C and E constants, pyrite has a lower C_A than silica, but not rutile and α-ferric oxide. Pyrite would then have a relatively higher covalent interaction tendency than rutile or α-ferric oxide. The average E_A value for pyrite was calculated to be 1.93 ± 0.31 $(kcal/mol)^{1/2}$. This is significantly lower than those determined for the three oxides. The C/E ratio for pyrite as determined graphically, was 0.55. Based on this C/E ratio, pyrite is a softer acid compared to the three oxides mentioned above. It should be noted that based on HSAB principle, metal ions bonded to hard bases would make them harder

Table 4.4. Statistical report from the regression of equation [4.4].

Variable	Estimate	DF	Std. Error	t for H_0 = 0 (variable = 0)	Prob > /T/
C_A	0.75	1	0.05	16.29	0.04
E_A	0.87	1	0.32	2.73	0.22

C/E ratio for chalcocite = 0.86

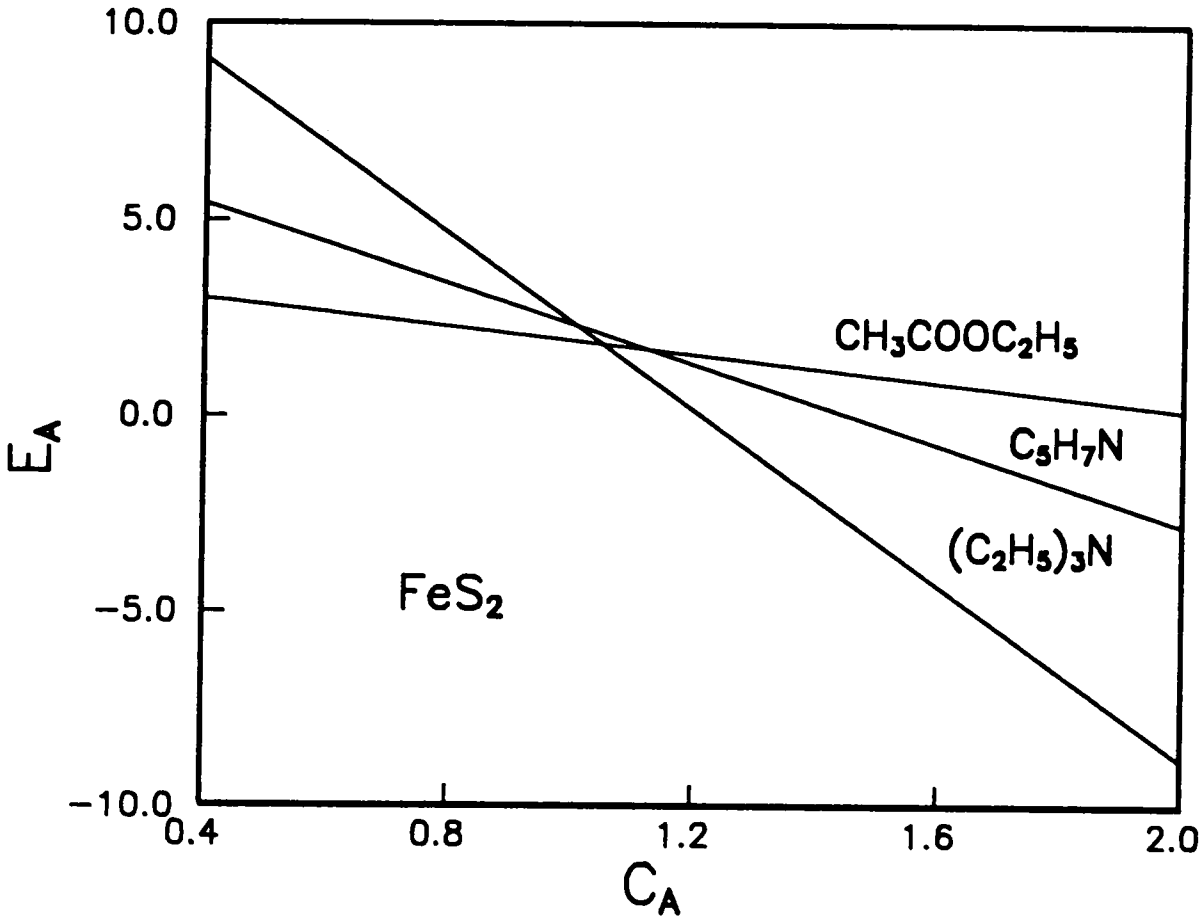

Figure 4.6. Graphical determination of the E and C parameters for pyrite using equation [4.2].

Table 4.5. Graphical estimation of C and E parameters for pyrite.

INTERSECTION POINT	C_A $(kcal/mol)^{1/2}$	E_A $(kcal/mol)^{1/2}$
Triethylamine/Ethyl acetate	1.05	1.82
Triethylamine/Methylpyrrole	1.01	2.29
Ethyl acetate/Methylpyrrole	1.12	1.69
Average values	1.06 ± 0.06	1.93 ± 0.31

C/E ratio for pyrite = 0.55

acids. This would suggest that oxides are harder acids than sulfides; thus, the above conclusion is in agreement with the HSAB model.

Table 4.6 shows the statistical fitting of equation[4.4] to the observed data. This was obtained by utilizing the same multiple regression technique. The estimates of the parameters were given as $C_A = 1.04 \pm 0.03$ and $E_A = 1.98 \pm 0.24$ $(kcal/mol)^{1/2}$. These values agree with the ones determined graphically. Based on the E_A and C_A values, pyrite has a larger susceptibility to undergo both electrostatic and covalent interactions than chalcocite. However, this difference is greater with regards to the electrostatic interactions. It would therefore be expected that pyrite would tend to react better with bases of high E_B than chalcocite would.

In terms of acidity, the greater susceptibility of pyrite to undergo electrostatic interactions may be interpreted to mean that pyrite has a harder character. Comparisons of the C/E ratio indicate this to be true. Even though Fe^{2+} is a borderline acid, the C and E parameters categorize pyrite as being a hard acid. It should be noted that the oxidation of pyrite produces Fe^{3+} (hard acid) on its surface. It is intersting to note that from the list of compounds that have known E and C values (Drago, 1980), bases with active sulfur atoms (i.e., $(CH_3)_2S$) tend to have lower E values than those with active oxygen or nitrogen atoms (i.e., $(CH_2)_4O$, NH_3). These factors may then explain the preference of IPETC (soft base) to chalcocite (soft acid) over pyrite (hard acid).

In the case of IBECTC, a second reactive center, oxygen, is present in the molecule. Since oxygen is the hardest base, its presence would change the acidic character of the reagent. According to the HSAB model, IBECTC should also then be able to interact with pyrite. This ability to interact with pyrite, although relatively weak, has been experimentally shown in this study. The presence of both a soft and a hard base in IBECTC may also be used to explain the adsorption behavior of IBECTC with

Table 4.6. Statistical report from the regression of equation [4.4].

Variable	Estimate	DF	Std. Error	t for $H_0 = 0$ (variable = 0)	Prob > /T/
C_A	1.04	1	0.03	29.84	0.02
E_A	1.98	1	0.24	8.22	0.08

C/E ratio for pyrite = 0.52

chalcocite. As shown previously in the ATR measurements, the bonding of the sulfur atom in IBECTC with Cu is weaker than in the case involving IPETC. This is in agreement with the HSAB principle. However, the total strength of the bonding with IBECTC is not weakened since a chelate ring structure is formed. This is a stable bond which is stronger than the binding of sulfur in IPETC with Cu.

Application of the HSAB theory can also be extended to other flotation systems. The selectivity of some other reagents against pyrite can be explained by the difference in the C/E ratios between pyrite and chalcocite. Dithiophosphate, according to Glembotskii (1977), is a softer base than xanthate, due to the influence of the phosphorous on the electron density of the sulfur atom. This would explain the selectivity of DTP against pyrite (hard acid), but not on chalcocite (soft acid). In the case involving oxide minerals, the C/E ratios of silica, rutile and ferric oxide indicate them to be hard acids. Based on the HSAB model, their interaction with collectors that have active atoms of oxygen and nitrogen, such as carboxylates and amines, would be favored. This is exactly what has been observed for oxide flotation (Leja, 1982).

4.6 Summary

The HSAB principle states that hard acids prefer to react with hard bases and soft acids with soft bases. This has been used to explain and predict processes such as displacement reactions, complex stability, solvation and others (Pearson, 1963; 1965; 1967; 1968). In this study, the HSAB principle has also been used to explain the selectivity of the thionocarbamate collectors against pyrite.

The IPETC molecule is considered to be a soft base since its reactive donor atom is sulfur. Consequently, the interaction of IPETC with soft acids should be favored . Based on Pearson's classification of metal ions, Fe is a hard acid while Cu is soft. This

might, therefore, explain the selectivity of IPETC collectors for copper sulfides. However, the classification of sulfides is an indirect one and has no experimental basis. The E-C model of Drago has been used for the classification of the sulfide minerals in terms of their covalent and elecrostatic interaction tendencies. This can then be related to the hardness or softness of the acid.

Flow microcalorimetry was used to determine the heats of interaction of three organic bases (triethylamine, methylpyrrole and ethyl acetate) with chalcocite and pyrite. Using these heat values and Drago's equation, the E and C parameters of chalcocite and pyrite were determined. The calculated values of C_A and E_A for chalcocite were 0.75 $\pm$ 0.05 and 0.87 $\pm$ 0.32 $(kcal/mol)^{1/2}$, respectively, and the C/E ratio was 0.86. For pyrite, C_A and E_A were estimated to be 1.04 $\pm$ 0.03 and 1.98 $\pm$ 0.24 $(kcal/mol)^{1/2}$, respectively, with a C/E ratio of 0.52. The E and C parameters indicate that pyrite has a larger tendency to undergo electrostatic interaction than chalcocite. Pyrite also has a lower C/E ratio. All these lead to a conclusion that pyrite is indeed, a harder acid than chalcocite, and that the selectivity of thionocarbamates against pyrite is in accordance with the HSAB principle.

The reactive atoms of IBECTC molecule are S (soft base) and O (hard base). It can be inferred that IBECTC would have a slightly better interaction than IPETC would, for hard acids (like pyrite), a behavior which has been shown in the previous chapters. However, IBECTC, owing to its strong collecting properties due to the presence of the two reactive centers, has not lost its selectivity against pyrite.

5.0 SUMMARY AND CONCLUSIONS

5.1 Adsorption Behavior of IPETC on Sulfides

The E_h-pH diagrams constructed from the thermodynamic calculations for the Cu^0- and Cu_2S-IPETC systems show a large region where $Cu(IPETC)_2Cl$ is stable. Assuming this specie is responsible for making the metallic copper or chalcocite surface hydrophobic, flotation is anticipated in these E_h-pH regions. The calculations indicate that the floatability of metallic copper and chalcocite is dependent on potential and pH.

The electrochemical data on metallic copper show an anodic peak which may be attributed to IPETC interaction. This interaction may be represented by the coupled chemical reaction of the EC type involving an initial electron-transfer:

$$Cu^0 \rightarrow Cu^+ + e^- \qquad [5.1]$$

followed immediately by a chemical reaction,

$$Cu^+ + IPETC \rightarrow Cu(IPETC)' + H^+ \qquad [5.2]$$

where $(IPETC)' = (C_3H_7\text{-}OCSN^-\text{-}C_2H_5)$.

A similar interaction with IPETC is seen on chalcocite. However, instead of reaction [5.1], the electron-transfer step of the interaction is,

$$Cu_2S \rightarrow xCu^+ + Cu_{2-x}S + xe^-. \qquad [5.3]$$

The Cu(I) then reacts with IPETC according to reaction [5.2]. For both copper and chalcocite, the anodic peaks associated with the IPETC interactions are shifted to higher potentials with the decrease in pH. This supports the suggested pH-dependent reactions given above. However, the anodic peaks are observed at potentials higher than where the initial formation of the Cu-IPETC compound is predicted in the E_h -pH diagrams.

There are no IPETC interaction peaks observed on platinum, chalcopyrite and pyrite. The absence of any IPETC interaction peak may be attributed to a lack of metallic ions coming from the electrode that may react with IPETC. However, there are indications that adsorption of IPETC occurs at the starting potential. This is indicated by the passivation of the electrode surfaces.

The flotation recoveries of chalcocite, chalcopyrite and pyrite with IPETC are dependent on pH. Microflotation data obtained with 10^{-7}M IPETC solutions indicate good flotation of chalcocite and chalcopyrite below pH 8, while pyrite flotation is negligible for the entire pH range. Chalcopyrite recovery is higher than that of chalcocite, which is presumably due to the natural floatability of chalcopyrite. Thermodynamic predictions are in reasonable agreement with the chalcocite flotation test data.

IPETC adsorption on all three sulfide minerals is observed in the in-situ FTIR measurements. Its adsorption is strongest on chalcocite followed by chalcopyrite and pyrite. The adsorption mechanism on chalcocite presumably changes with pH. Below pH 6, the coordination of IPETC with Cu occurs primarily through its sulfur. At higher pH values, the coordination occurs through both sulfur and oxygen to form a four-

membered chelate ring. There are no indications of coordination with nitrogen, which is not sterically accessible to form a bond.

The adsorption of IPETC on chalcopyrite involves coordination of the surface copper with sulfur only. This coordination does not change with pH. The chemical shifts of the characteristic bands in the spectra for chalcopyrite suggest relatively weaker chemisorption than that observed on chalcocite.

On pyrite, IPETC chemisorption is much weaker as indicated by the shift of the characteristic peaks toward the direction of pure IPETC. At higher pH values, the amount of collector adsorbed decreases and the spectral shift towards IPETC becomes more significant, suggesting IPETC physisorption on pyrite. The selectivity of IPETC against pyrite may be explained by its inability to remove or prevent the formation of sulfoxy oxidation products on the pyrite surface. This is not observed on chalcocite and chalcopyrite, nor in xanthate adsorption on pyrite.

At a higher IPETC concentration, pyrite flotation becomes significant below pH 4. This may be attributed to the larger amount of IPETC adsorbed, which presumably causes the surface to overcome the presence of the hydrophilic oxidation products and become hydrophobic. However, it should be noted that effective separation of chalcocite and chalcopyrite from pyrite is still possible at pH $\geq$ 6. This demonstrates the selectivity of IPETC against pyrite flotation, even at higher collector addition.

The contact angle measurements show increasing hydrophobicity of chalcocite, chalcopyrite and pyrite with the addition of 10^{-4}M IPETC over the entire potential range. On chalcocite, the contact angle increases continously from the starting potential until it becomes maximum and remains constant above -200 mv. This indicates IPETC adsorption below the potential where its interaction with chalcocite was observed in the voltammogram. The effect of E_h on % $Cu(IPETC)_2Cl$, as calculated for the Cu_2S-IPETC system, shows a sharp increase above the same potential. The

hydrophobicity of chalcopyrite also shows a similar response to an increase in potential. On the other hand, pyrite shows constant contact angle values, which are not high enough to indicate good floatability, for the entire potential range.

A spectroelectrochemical ATR cell has been constructed for in-situ FTIR measurements of thionocarbamate adsorption on copper and chalcocite at different potentials. The adsorption of IPETC on chalcocite is also observed at potentials lower than where it is observed in the voltammograms. This agrees with the results of the contact angle measurements and the thermodynamic calculations. The mode of IPETC bonding with copper is through the sulfur atom accompanied by the breakage of the N-H group in IPETC. This supports the reactions suggested for the IPETC interaction observed in the voltammetric investigation. There are no changes observed in the IR spectra at the potential where the IPETC interaction peaks are observed in the voltammograms for copper and chalcocite. The interaction product may presumably be similar to the initial adsorbed species.

Using the IRAS technique, IPETC adsorption at pH 6 is found to grow with adsorption time. The initial adsorbed layers probably involves coordination of both sulfur and oxygen with the surface copper. At near monolayer coverage, the bonding of IPETC now involves coordination through sulfur only. At this stage, the adsorbed molecules are presumably perpendicular to the copper surface and may be represented by the following:

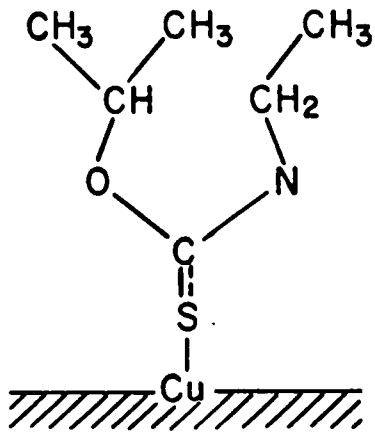

At higher coverages, there is a reorientation of the adsorbed molecules with the spectra approaching that of the bulk Cu-IPETC compounds. There is no significant difference observed at pH 4 except for the lower signal intensities.

The preferential adsorption studies show that between IPETC and KEX, xanthate is preferentially adsorbed by copper. This agrees with the observations made here and by other investigators that xanthates are stronger collectors. The bonding between copper and sulfur is stronger in xanthate than in IPETC. KEX is capable of adsorbing on top of the chemisorbed IPETC layer, but not vice-versa. Compared to IBECTC, IPETC is also a weaker collector. However, both thionocarbamate collectors are capable of adsorbing on top of each other. IBECTC adsorption over chemisorbed IPETC, though, is more favored than the opposite situation.

UV analysis of the solution from the ATR measurements agree with the quantitative analysis of the corresponding FTIR data. IPETC adsorption on chalcocite is maximum at pH 6. Chalcopyrite and pyrite shows decreasing IPETC adsorption with increasing pH. The amount of IPETC adsorbed decreases in the following order : chalcocite > chalcopyrite > pyrite. The selectivity of IPETC against pyrite is best between pH 6 and 8. Kinetic studies using UV spectroscopy indicate that the rate of IPETC adsorption follows the same trend.

5.2 Adsorption Behavior of IBECTC on Sulfides

Thermodynamic calculations have also been carried to construct E_h -pH diagrams for the Cu^0- and Cu_2S-IBECTC systems. The stability region of $Cu(IBECTC)_2Cl$ is found to be larger than that for $Cu(IPETC)_2Cl$. Thus, the flotation of Cu^0 or Cu_2S with IBECTC is expected over a broader range of E_h -pH conditions. The floatability of Cu^0 and Cu_2S in the presence of IBECTC is also shown to be dependent on E_h and pH.

Anodic oxidation of IBECTC does not occur in any of the electrodes. Electrochemical interaction of the collector is observed, however, on the copper and chalcocite electrodes. The mechanism of IBECTC interaction with copper may be represented by the coupled chemical reaction of the EC type involving reaction [5.1] followed by the chemical reaction with IBECTC,

$$Cu^{+} + IBECTC \rightarrow Cu(IBECTC)' + H^{+} \qquad [5.4]$$

where (IBECTC)' = (C_4H_9-OCSN$^-$OCO-C_2H_5).

Chalcocite interaction with IBECTC observed above 0 mv at pH 4.6 may also be attributed to a coupled chemical reaction. The initial electron-transfer step involves reaction [5.3] followed immediately by reaction [5.4].

Electrochemical interactions of IBECTC with the other three electrodes are not observed in their respective voltammograms. These electrodes are passivated, though, by the adsorption of IBECTC on the electrode surfaces.

The flotation recovery of the three sulfide minerals with IBECTC are dependent on pH. The floatability of chalcocite and chalcopyrite is good below pH 8 with 10^{-7} M IBECTC. The results of the thermodynamic calculations for the Cu_2S-IBECTC system are in agreement with the chalcocite flotation data. Pyrite flotation is negligible over the entire pH range, demonstrating the collector's selectivity. Increasing the IBECTC concentration results in better floatability of chalcocite and chalcopyrite and significant pyrite recovery at pH < 4.

The FTIR measurement show that IBECTC chemisorbs on chalcocite with its adsorption mechanism being significantly different from that of IPETC. Due to the presence of the electron-withdrawing ethoxycarbonyl group adjacent to its C=S group, the bonding between the sulfur and the surface copper atom is weaker than in the case of IPETC. However, the introduction of the O-C=O group in IBECTC stabilizes the

bonding through a chelation mechanism. This reagent exhibits the strongest adsorbability on chalcocite, with its maximum occurring at pH 6. This is followed by chalcopyrite and pyrite.

On chalcopyrite, the adsorption mechanism is similar to the one for chalcocite. However, IBECTC adsorption on chalcopyrite decreases with increasing pH. IBECTC also adsorbs on pyrite, but its adsorption does not remove or prevent the formation of the sulfoxy oxidation products from the surface. At high IBECTC additions and acidic pH, however, the larger amount of collector adsorbed presumably makes the surface overcome the hydrophilic effect of the oxidation products on the surface. The results here and those for IPETC may account for the improved selectivity of thionocarbamate collectors over xanthates.

Contact angle measurements show an increase in hydrophobicity of chalcocite, chalcopyrite and pyrite at all E_h conditions with the addition of 10^{-4}M IBECTC. The response of the sulfide minerals to potential is the same as that observed with IPETC. The only significant difference is in the higher contact angles measured in IBECTC solutions. The contact angles measured on pyrite, though, are also not high enough to indicate good floatability.

The in-situ spectroelectrochemical measurements also show that IBECTC adsorption on copper and chalcocite increases with potential. However, the collector adsorption is observed on both electrodes at potentials lower than where the IBECTC interaction peaks occurs in the voltammograms. The mechanism of IBECTC adsorption on copper involves a coordination of the sulfur and oxygen atoms with the surface copper to form a six-membered chelate ring. This is exactly the same mechanism suggested for IBECTC adsorption on chalcocite.

The adsorption of IBECTC is more favorable at higher potentials due to the release of more Cu ions during the oxidation of the electrode. The electrochemical interaction

of IBECTC with copper and chalcocite observed in the voltammogram does not cause any changes in the IR spectra. This indicates that the adsorbed species adsorbed initially are the same as that produced by the interaction process.

The structure and orientation of IBECTC molecules adsorbed on copper at pH 4 and 6 have been determined through the IRAS technique. The adsorption of IBECTC on copper has been described earlier. At monolayer coverage, the IBECTC molecule that is adsorbed on the copper surface may be shown as:

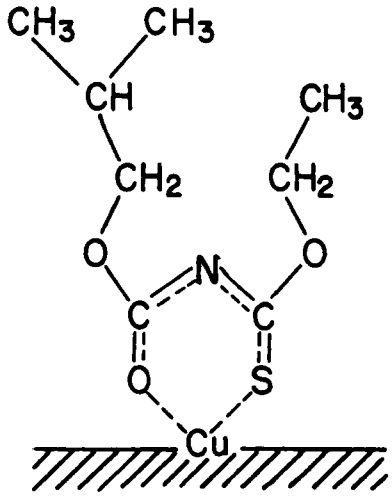

The orientation of the adsorbed molecules changes with the amount of coverage. Initially, the molecules are presumably inclined in relation to the substrate surface and become perpendicular when the coverage is about a monolayer. Further adsorption causes a reorientation of the molecules. The pH does not seem to cause any significant change in the structure and orientation of the adsorbed molecules.

In the presence of both IBECTC and IPETC, the former is found to be adsorbed more favorably than IPETC. Between IBECTC and KEX, both collectors co-adsorb on the copper surface at different treatment periods. However, xanthate adsorption is slightly more prevalent. If the collector adsorption is done one at a time, IBECTC can adsorb over the xanthate layer and vice-versa. Overall, the order of relative adsorbability and kinetics of adsorption is as follows: KEX > IBECTC > IPETC.

None of the three collectors, however, is strong enough to completely displace the initially adsorbed collector layer.

The results of the quantitative analysis of the ATR data are in excellent agreement with the UV spectroscopic measurements. The adsorption of IBECTC on chalcocite is maximum at pH 6 and decreases with increasing pH on the other two sulfides. The UV adsorption data show that IBECTC adsorbs most strongly on chalcocite, followed by chalcopyrite and pyrite. Microflotation tests results are in good agreement with the spectroscopic data.

The rate of IBECTC adsorption follows the same order, i.e., chalcocite, chalcopyrite and pyrite. Also, for each sulfide mineral, IBECTC adsorption is relatively faster than the adsorption of IPETC. This is an indication of the higher collecting power of IBECTC than that of IPETC.

5.3 Application of the HSAB Concept

The interactions of thionocarbamates with chalcocite and chalcopyrite have been proven to be more favored than with pyrite. The HSAB concept by Pearson can be applied to explain this observation.

The IPETC molecule (pKa > 12) is considered to be a soft base because its reactive donor atom, i.e., sulfur, is a soft base. For the IBECTC molecule, the presence of ethoxycarbonyl results in two reactive centers, i.e., sulfur (soft base) and oxygen (hard base). This would make the reagent a harder base than IPETC. However, the overall softness of the reagent, which should be characterized by the C/E ratio, did not seem to have been affected much, as shown by only a small decrease in pKa (= 10.5). Consequently, the interaction of IPETC and IBECTC with soft acids, such as chalcocite and chalcopyrite, should be favored according to the HSAB concept.

Using the microcalorimetry data and Drago's E - C model, the acidity of chalcocite and pyrite have been determined. The calculated values of C_A and E_A for chalcocite are 0.75 ± 0.05 and 0.87 ± 0.32 $(kcal/mol)^{½}$, respectively, which gives a C/E ratio of 0.86. For pyrite, C_A and E_A have been determined to be 1.98 ± 0.24 and 1.04 ± 0.03 $(kcal/mol)^{½}$, respectively, which gives a C/E ratio of 0.52. Based on the C and E parameters, pyrite is a harder acid than chalcocite. This provides additional explanation for the observed selectivity of both IPETC and IBECTC against pyrite.

6.0 RECOMMENDATIONS FOR FUTURE RESEARCH

Further electrochemical studies should be carried out, particularly on copper and chalcocite electrodes. The anodic peaks attributed to thionocarbamate interactions with the surface copper need to be investigated more extensively to verify the proposed coupled chemical reaction. The EC mechanism can be verified by the following diagnostic tests (Southhampton Electrochemistry Group, 1985): i) the anodic peak current (I_p^A) to cathodic peak current (I_p^C) ratio is less than one as the scan rate (v) is increased; ii) $I_p^C / v^{1/2}$ decreases slightly with increasing v; iii) the cathodic peak potential (E_p^C) is positive for the reversible case; iv) E_p^C shifts negatively with increasing v, and in the pure kinetic region, shifts by 30/n mv per 10 times increase in v.

Galvanic effects between different sulfide minerals have been known to affect floatability. Flotation tests using artificial mixtures of copper sulfides and iron sulfides with thionocarbamates will indicate if there is any effect. The concentrates can be analyzed using image analysis to determine the amount of each sulfide mineral recovered.

Flotation tests with other collectors should be carried out to determine the relative strength of thionocarbamates. Besides measuring the recovery, the flotation rate should also be determined. Flotation rate is also important in evaluating different collectors (Ackerman et al., 1984). The rate criterion, together with the ultimate recovery, helps

in discerning the superior reagent between different collectors showing similar recovery of a mineral. Knowledge of the flotation rate will give a clearer view of how the new collectors compare against the standard flotation reagents. The flotation tests can also be done at different collector concentrations to determine the minimum amount of collector required for good recovery (i.e., 80%).

The flotation characterization of the sulfide minerals with thionocarbamates have all been done in the presence of oxygen. Since oxygen is known to play a part in the adsorption of thiol collectors, microflotation experiments should be done in controlled atmospheric conditions.

The structure and orientation of thionocarbamates adsorbed on chalcocite, chalcopyrite and pyrite need to be determined. Other investigators have used the IRAS technique on polished solid sulfide minerals (Mielczarski and Yoon, 1988a; 1988b). Although there is some skepticism about this technique being ex-situ, this would be helpful in clarifying the in-situ ATR results obtained for these minerals. The IRAS measurements can be complemented by other surface analysis techniques such as X-ray photoelectron spectroscopy, Auger spectroscopy and mass spectroscopy.

Using the IRAS technique, the preferential adsorption studies should be extended to sulfide minerals. The competition between different collectors' adsorption on copper sulfides, as well as on iron sulfides, should be studied. The results will show the relative strength of the different collectors. The selectivity of thionocarbamates against pyrite can also be further understood with this study. The preferential adsorption measurements can also be carried out for other collectors. The use of three different collectors in solution may give some interesting information.

Kinetic studies are important in understanding the flotation chemistry of different reagents. The kinetics of adsorption of other collectors on sulfide minerals should also be determined. Together with the flotation rate constants, the effectiveness of different

collectors can be clearly measured. Also, by conducting the experiments at several different temperatures, the actual energy for the adsorption process can be determined. These results can be compared with the heat of adsorption determined using a microcalorimeter.

The application of Pearson's HSAB principle to flotation systems is becoming more significant, especially in the design of new collector reagents. It has been shown in this study that it is useful in explaining the selectivity of thionocarbamates. This type of study can be applied to other sulfide minerals. Information on the relative softness or hardness of different sulfide minerals and collectors will be useful in understanding the adsorption mechanism of collectors. These data will provide explanations on why some collectors are applicable only to particular minerals. All of these will help in synthesizing new reagents for specific applications.

Lastly, the electronic structure is very important in the determination of the reactivity and the selectivity of different collectors. Using ab initio molecular orbital calculations, the effects of different substituents on the electronic structure of the collector molecules can be studied. From the calculations, the collector molecule with the most promise can be investigated by applying similar techniques used in this study.

BIBLIOGRAPHY

Ackerman, P.K., Harris, G.H., Klimpel, R.R. and Aplan, F.F., 1984. Effect of alkyl substituents on performance of thionocarbamates as copper sulfide and pyrite collectors. In: M.P. Jones and R. Oblatt (Editors), *Reagents in the Minerals Industry*. Inst. Min. Metall., London, 251-264.

Ackerman, P.K., Harris, G.H., Klimpel, R.R. and Aplan, F.F., 1986. Importance of reagent purity in the evaluation of flotation collectors. *Trans. Inst. Min. Metall.*, 95:C165-168.

Ackerman, P.K., Harris, G.H., Klimpel, R.R. and Aplan, F.F., 1987. Evaluation of flotation collectors for copper sulfides and pyrite. I. Common sulfhydryl collectors. *Inst. J. Miner. Process.*, 21:105-127.

Ahrland, S., Chatt, J. and Davies, N.R., 1958. The relative affinities of ligand atoms for acceptor molecules. *Quart. Revs. Chem. Soc.*, 12:265-276.

Albery, W.J. and Hitchman, M.L., 1971. *Ring-disc Electrodes*. Clarendon Press, New York, 1971.

Basilio, C.I., 1985. *Thermodynamics and Electrochemistry of the Chalcocite-Potassium Ethyl Xanthate System*. M.Sc. Thesis, Virginia Polytechnic Institute & State University, Blacksburg, Virginia.

Basilio, C.I., Pritzker, M.D. and Yoon, R.H., 1985. Thermodynamics, electrochemistry and flotation of the chalcocite-potassium ethyl xanthate system. SME-AIME Annual Meeting, New York, New York. *Preprint 85-86*.

Basilio, C.I., Leppinen, J.O. and Yoon, R.H., 1988. Flotation and adsorption study of modified thionocarbamates on sulfide minerals. SME-AIME Annual Meeting, Denver, Colorado, *Preprint 88-156*.

Bellamy, L.J., 1975. *The Infrared Spectra of Complex Molecules*. Chapman and Hall, London, Chapters 12 and 22.

Bjerrum, J., 1950. The tendency of metal ions toward complex formation. *J. Chem. Rev.*, 46:381-401.

Bogdanov, O.S., Vainshenker, I.A., Podnek, A.K., Ryaboi, V.I. and Yanis, N.A., 1976. Trends in the search for effective collectors. *Tsvet. Metal.*, 49(4):72-80.

Bogdanov, O.S., Podnek, A.K., Ryaboi, V.I. and Yanis, N.A., 1977. Reagents chemisorption on minerals as a process of formation of surface compounds with a coordination bond. In: *Proceedings of the XIIth International Mineral Processing Congress*. Sao Paulo, Brazil, Paper 2.

Bold, W. and Breiter, M.W., 1961. Untersuchung des anodischen aufbauo und der kathodischen reduktion der sauerstoff-belegungan glatten Pt-elektroden. *Electrochim Acta*, 5:145-160.

Bolth, F.A., Crozier, R.D. and Strow, L.E., 1975. U.S. Patent 3,907,854.

Breiter, M.W., 1963. Voltammetric study of halide ion adsorption on platinum in perchloric acid solutions. *Electrochim. Acta*, 8:925-936.

Celik, M., 1988. Unpublished results.

Celik, M., 1989. Private communication.

Chander, S. and Fuerstenau, D.W., 1974. The effect of potassium diethyl dithiophosphate on the electrochemical properties of platinum, copper and copper sulfide in aqueous solutions. *J. Electroanal. Chem. Inter. Electrochem.*, 56:217-247.

Cotton, F. and Wilkinson, G., 1980. *Advanced Inorganic Chemistry*. Wiley-Interscience Publications, New York.

Crozier, R.D., 1984. Plant reagents. Part 1: Changing patterns in the supply of flotation reagents. *Mining Mag.*, September, 202-219.

Dow Chemical Company, 1968. *Flotation Fundamentals and Mining Chemicals*. The Dow Chemical Company, Midland, Michigan.

Drago, R.S., 1967. Donor-acceptor interactions. *Chem. Brit.*, 3:516-520.

Drago, R.S., 1973. Quantitative evaluation and prediction of donor-acceptor interactions. *Struct. Bonding (Berlin)*, 15:73-139.

Drago, R.S., 1980. The interpretation of reactivity in chemical and biological systems with the E and C model. *Coord. Chem. Rev.*, 33:251-277.

Drago, R.S. and Wayland, B.B., 1965. A double-scale equation for correlating enthalpies of Lewis acid-base interactions. *J. Amer. Chem. Soc.*, 87:3571-3577.

Drago, R.S., Vogel, G.C. and Needham, T.E., 1871. A four-parameter equation for predicting enthalpies of adduct formation. *J. Amer. Chem. Soc.*, 93:6014-6026.

Edwards, J.O., 1954. Correlation of relative rates and equilibria with a double basicity scale. *J. Amer. Chem. Soc.*, 76:1540-1547.

Eriksson, G.A., 1979. An algorithm for the computation of aqueous multicomponent, multiphase equilibria. *Anal. Chim. Acta*, 112:375-383.

Fahrenfort, J., 1961. Attenuated total reflection: a new principle for the production of useful infra-red reflection spectra of organic compounds. *Spectrochim. Acta*, 17:698-709.

Forssberg, K.S.E., Antti, B. and Palsson, B.I., 1984. Computer-assisted calculations of thermodynamic equilibria in the chalcopyrite-ethyl xanthate system. In: *Reagents in the Mineral Industry*. IMM, London, 251-264.

Fowkes, F.M., 1960. Orientation potentials of monolayers adsorbed at the metal-ion interface. *J. Phys. Chem.*, 64:726-728.

Fowkes, F.M., 1983. Acid-base interactions in polymer adhesion. In: K.L. Mittal (Editor), *Physicochemical Aspects of Polymer Surfaces, Vol. 2*. Plenum Press, New York, 583-603.

Fowkes, F.M., 1984. Spectral and calorimetric determinations of the intermolecular interaction of solvents. *Polym. Mater. Sci. Eng.*, 51:522-527.

Fowkes. F.M., Ronay, G.S. and Schick, M.J., 1959. Monolayers in equilibrium with lenses of oil on water. II. Dependence of equilibrium pressure on the pH and on the concentration of surfactant. *J. Phys. Chem.*, 63:1684-1686.

Fowkes, F.M., Tischler, D.O., Wolfe, J.A., Lannigan, L.A., Ademu-John, C.M. and Halliwell, M.J., 1984. Acid-base complexes of polymers. *J. Polym. Sci. Polym. Chem. Ed.*, 22:547-566.

Frumkin, A.N., 1963. Hydrogen overvoltage and adsorption phenomena. In: P. Delahay (Editor), *Advances in Electrochemistry and Electrochemical Engineering*. Interscience Publishers, New York, Vol. 3, 287-391.

Fu, Y.L. and Wang, S.S., 1987a. U.S. Patent 4,657,688.

Fu, Y.L. and Strydom, P.J., 1987b. U.S Patent 4,659,853.

Fuerstenau, D.W., 1988. Flotation science and engineering advances and challenges. In: E. Forssberg (Editor), *XVI International Mineral Processing Congress*. Stockholm, Sweden, 63-79.

Gardner, J.R. and Woods, R., 1979. An electrochemical investigation of the natural floatability of chalcopyrite. *Int. J. Miner. Process.*, 6:1-16.

Giles, C.H., MacEwan, T.H., Nakhwa, S.N. and Smith, D., 1960. Studies in adsorption. *J. Chem. Soc.*, 3973.

Glembotskii, A.V., 1970. Investigating and constructing new flotation reagents with specific properties. *Tsvet. Metal.*, 43(5):90-92.

Glembotskii, A.V., 1977. Theoretical principles of forecasting and modifying collector properties. *Tsvet. Metal.*, 50(4):61-65.

Glembotskii, A.V. and Frolov, Y.G., 1978. Mechanisms of collector attachment to mineral surfaces during flotation. *Tsvet. Metal.*, 51(4):111-115.

Glembotskii, A.V. and Livshits, A.K., 1967. *Tsvetraya Metalurgiya (Bull. Inst. Tsvetmetamformatsiya)*, 19:19-23.

Glembotskii, A.V. and Livshits, A.K., 1969. On the stability of dialkylthionocarbamate attachment to certain sulfides. *Tsvet. Metal.*, 42(4):37-38.

Glembotskii, A.V., Shubov, L.Ya. and Livshits, A.K., 1968. Selectivity of dialkylthionocarbamate action during sulfide flotation. *Tsvet. Metal.*, 47(7):8-11.

Glembotskii, A.V., Orlov, A.M. and Yelutin, A.M., 1984. An efficient collector for flotation of ores of non-ferrous and noble metals. *Tsvet. Metal.*, 57(5):109-111.

Glembotskii, A.V., Podvishensky, N.S. and Ivanov, S.E., 1986. Chemisorption of MIG-4E on the minerals of sulfide ores. *Tsvet. Metal.*, 59(10):87-90.

Glembotskii, A.V., Desiatov, A.M., Kondratieva, L.V., Ryaboi, V.I., Petrova, L.N., Ustinov, I.D., Pomazov, V.D. and Krasnukhina, A.V., 1988. New flotation reagents for sulfide and non-sulfide ores in the USSR. In: E. Forssberg (Editor), *XVI International Mineral Processing Congress.* Stockholm, Sweden, 81-91.

Golden, W.G., 1985. Fourier transform infrared refelction-absorption spectroscopy. In: J.R. Ferraro and L.J. Basile (Editors), *Fourier Transform Infrared Spectroscopy, Applications to Chemical Systems, Vol. 4.* Academic Press, Orlando, Florida, Chapter 8.

Golden, W.G., Dunn, D.S. and Overend, J., 1981. A method for measuring infrared reflection-absorption spectra of molecules adsorbed on low-area surfaces at monolayer and submonolayer concentration. *J. Catal.*, 71:395-404.

Golden, W.G., Saperstein, O.D., Severson, M.W. and Overend, J., 1984. Infrared reflection-absorption spectroscopy of surface species: a comparison of fourier transform and dispersive methods. *J. Phy. Chem.*, 88(3):574-580.

Goold, L.A. and Finkelstein, N.P., 1972. The reaction of sulphide minerals with thiol compounds. National Institute for Metallurgy, Johannesburg, South Africa, *Report No. 1439.*

Greenler, R.G., 1966. Infrared study of adsorbed molecules on metal surfaces by reflection techniques. *J. Chem. Phys.*, 44:310-315.

Greenler, R.G., Rahn, R.R. and Schwartz, J.P., 1971. The effect of index of refraction on the position, shape and intensity of infrared bands in reflection-absorption spectra. *J. Catal.*, 23:42-48.

Griffiths, P.R. and de Haseth, J.A., 1986. *Fourier Transform Infrared Spectrometry.* Wiley-Interscience Publication, New York.

Hamilton, I.C. and Woods, R., 1981. An investigation of surface oxidation of pyrite and pyrrhotite by linear potential sweep voltammetry. *J. Electroanal. Chem.*, 118:327-343.

Handley, T.H. and Dean, J.A., 1960. Trialkyl thiophosphates: selective extractants for silver and mercury. *Anal. Chem.*, 32:1878-1883.

Harrick, N.J., 1963. Total internal reflection and its application to surface studies. *Ann. N. Y. Acad. Sci.*, 101:928-938.

Harrick, N.J., 1965. Electric field strengths at totally reflecting interfaces. *J. Opt. Soc. Am.*, 55:851-862.

Harrick, N.J., 1967. *Internal Reflection Spectroscopy.* Harrick Scientific Corp., New York.

Harris, G.H. and Fishback, B.C., 1954. U.S. Patent 2,691,635.

Heyes, G.W. and Trahar, W.J., 1979. Oxidation-reduction effects in the flotation of chalcocite and cuprite. *Int. J. Miner. Process.*, 6:229-252.

Janetski, N.D., Woodburn, S.I. and Woods, R., 1977. An electrochemical investigation of pyrite flotation and depression. *Int. J. Miner. Process.*, 4:227-239.

Jones, M.H. and Woodcock, J.T., 1969. Spectrophotometric determination of Z-200 (isopropyl etylthionocarbamate) in flotation liquors. *Proc. Aust. Inst. Min. Met.*, 231:11-18.

Joslin, S.T. and Fowkes, F.M., 1985. Surface acidity of ferric oxides studied by flow microcalorimetry. *Ind. Eng. Chem. Prod. Res. Dev.*, 24(3):369-375.

Keller, C.H., 1925. U.S. Patent 1,554,216.

Kitchener, J. A., 1984. The froth flotation process: past, present and future - in brief. In: K.J. Ives (Editor), *The Scientific Basis of Flotation.* NATO ASI series, No. 75(E).

Klimpel, R.R., 1988. The industrial practice of sulfide mineral collectors. In: P. Somasundaran and B.M. Moudgil (Editors), *Reagents in Mineral Technology.* Marcel Dekker, Inc., New York.

Klimpel, R.R. Hansen, R.D. and Fee, B.S., 1988. Recent advances in new frother and collector chemistry for sulfide mineral flotation. In: E. Forssberg (Editor), *XVI International Mineral Processing Congress.* Stockholm, Sweden, 1173-1184.

Klopman, G., 1968. Chemical reactivity and the concept of charge- and frontier controlled reactions. *J. Amer. Chem. Soc.*, 90:223-234.

Leja, J., 1982. *Surface Chemistry of Froth Flotation.* Plenum Press, New York.

Leppinen, J.O., 1987. Unpublished results.

Leppinen, J.O., Basilio, C.I. and Yoon, R.H., 1988. Spectroelectrochemical study of ethyl xanthate adsorption on sulfide minerals. In: P.E. Richardson and R. Woods (Editors), *Electrochemistry in Mineral and Metal Processing II.* The Electrochemical Society, Pennington, New Jersey, 49-65.

Lewellyn, M.E., 1983. Cyanamid Internal Reports.

Lewellyn, M.E. and Wang, S.S., 1985. O-alkyl-N-allyl thionocarbamates: new oily collectors for sulfide ores. SME-AIME Annual Meeting, New York, New York, *Preprint 85-31.*

Lewis, G.N., 1923. *Valence and the Structure of Atoms and Molecules.* Chemical Catalog Co., New York.

Lipatov, Y.S. and Segeeva, L.M., 1974. *Adsorption of Polymers.* Halsted, New York.

Livshits, A.K., Bazanova, N.M. and Akimova, N.P., 1974. *Tsvetraya Metallurgiya (Bull. Inst. Tsvetmetinformasiya),* 19:32-34.

Mielczarski, J. and Leppinen, J., 1987. Infrared reflection absorption spectroscopic study of adsorption of xanthates on copper. *Surface Sci.,* 187:526-538.

Mielczarski, J. and Yoon, R.H., 1988a. Spectroscopic studies of the structure of the adsorption layer of thionocarbamate. I. on copper and activated zinc sulfide. submitted to *J. Coll. Interf. Sci..*

Mielczarski, J. and Yoon, R.H., 1988b. FTIR external reflection study of molecular orientation in spontaneously adsorbed layers on low-adsorption subtstrates. submitted to *J. Phys. Chem..*

Miller, F.A. and Wilkins, C.H., 1952. Infrared spectra and characteristic frequencies of inorganic ions. *Anal. Chem.,* 24(8):1253-1275.

Mingione, P.A., 1984. Use of dialkyl dithiophosphate promoters as mineral flotation agents. In: M.J. Jones and R. Oblatt (Editors), *Reagents in the Mineral Industry.* Inst. Min. Metall., London, 19-24.

Mirabella, F.M., 1985. Internal reflection spectroscopy. *Appl. Spectro. Rev.,* 21:45-178.

Nagaraj, D.R. and Wang, S.S., 1986. U.S. Patent 4,587,013.

Nagaraj, D.R. and Wang, S.S., 1987. U.S. Patent 4,661,278.

Nagaraj, D.R., Basilio, C.I. and Yoon, R.H., 1989. The chemistry and structure-activity relationships for new sulfide collectors. SME-AIME Annual Meeting, Las Vegas, Nevada.

Nagaraj, D.R., Fu, Y.L. and Wang, S.S., 1985. U.S. Patent 4,556,482 and 4,556,483.

Nagaraj, D.R., Fu, Y.L. and Wang, S.S., 1986. U.S. Patent 4,584,097 and 4,595,493.

Nagaraj, D.R., Wang, S.S. and Frattaroli, D.R., 1986. Flotation of copper sulfide minerals and pyrite with new and existing sulfur-containing collectors. In: L.E. Fielding and A.R. Gordon (Editors), *Proceedings 13th CMMI Congress - Metallurgy*. Singapore, CMMI and Aust. Inst. Min. Met., 49-57.

Nagaraj, D.R., Lewellyn, M.E., Wang, S.S., Mingione, P.A. and Scanlon, M.J., 1988. New sulfide and precious metals collectors: for acid, neutral and mildly alkaline circuits. In: E. Forssberg (Editor), *XVI International Mineral Processing Congress*. Stockholm, Sweden, 121-1232.

Palsson, B.I. and Forssberg, K.S.E., 1988. Computer-assisted calculations of thermodynamic equilibria in the galena-ethyl xanthate system. *Int. J. Miner. Process.*, 23:93-121.

Partyka, S., Arnaud, M. and Lindheimer, M., 1987. Adsorption of ethylxanthate onto galena at low surface coverages. *Coll. and Surf.* , 26:141-153.

Pearson, R.G., 1963. Hard and soft acids and bases. *J. Amer. Chem. Soc.*, 85:3533-3539.

Pearson, R.G., 1965. Acids and bases. *Science*, 151:172-177.

Pearson, R.G., 1967. Hard and soft acids and bases. *Chem. Brit.*, 3:103-107.

Pearson, R.G., 1968. Hard and soft acids and bases (HSAB). I. fundamental principles. *J. Chem. Educ.*, 45:581-587.

Pritzker, M.D. and Yoon, R.H., 1984a. Thermodynamic calculations on sulfide flotation systems. I. Galena-ethyl xanthate system in the absence and presence of metastable species. *Int. J Miner. Process.*, 12:95-125.

Pritzker, M.D. and Yoon, R.H., 1984b. Thermodynamic calculations and electrochemical studies on the galena-ethyl xanthate system. In: P.E. Richardson, S. Srinivasan and R. Woods (Editors), *Proceedings of the International Symposium on Electrochemistry in Mineral and Metal Processing*. The Electrochemical Society, Pennington, NJ, 84-10:26-53.

Pritzker, M.D., Yoon, R.H., Basilio, C.I. and Choi, W.Z., 1985. Solution and flotation chemistry of sulfide minerals. *Can. Metall. Quarterly*, 24:27-38.

Rao, C.N.R., Verkataraghavan, R. and Kasturi, T.R., 1964. Contribution to the infrared system of organosulphur compounds. *Can. J. Chem.*, 42:36-42.

Richardson, P.E. and Walker, G.W., 1985. The flotation of chalcocite, bornite, chalcopyrite and pyrite in an electrochemical flotation cell. In: *XV International Mineral Processing Congress*. Cannes, Vol. 2, 198-210.

Rickard, T.A., 1932. *A History of American Mining*. AIME Series, McGraw-Hill Book Co., New York.

Schwarzenbach, G., 1956. Organic complex-forming compounds. *Experientia,* Suppl. No. 5, 162-192.

Seryakova, I.V., Vorobiova, G.A., Glembotskii, A.V. and Zolotov, Yu.A., 1975. Extraction of metals by neutral sulfur-containing extractants. Part I. O-isopropyl-N-ethylthionocarbamate. *Anal. Chim. Acta,* 77:183-190.

Shcherbakov, V.A. and Perepechin, V.I., 1983. Testing collectors for the flotation of copper-nickel ores. *Tsvet. Metal.,* 56(7):96-98.

Silverstein, R.M., Bassler, G.C. and Morill, T.C., 1980. *Spectrometric Identification of Organic Compounds.* John Wiley and Sons, New York.

Solozhenkin, D.M., Shvengler, F.A. Kopitsya, N.I., Ivanov, A.V., Semenov, E.V. and Komaarov, Yu.I., 1982. Synthesis and study of complexes of copper with O-butyl-N-methyl thionocarabamte. *Dokl. Akad. Nauk SSSR,* 264:896-900.

Somasundaran, P. and Nagaraj, D.R., 1984. chemistry and applications of chelating agents in flotation and flocculation. In: M.J. Jones and R. Oblatt (Ediotrs), *Reagents in the Mineral Industry.* Inst. Min. Metall., London, 209-220.

Southampton Electrochemistry Group, 1985. *Instrumental Methods in Electrochemistry.* Halsted Press, New York.

Strojek, J.W. and Mielczarski, J., 1983. Spectroscopic investigation of the solid-liquid interface by the ATR technique. *Adv. Coll. Interf. Sci.,* 19:309-327.

Sutherland, K.L. and Wark, I.W., 1955. *Principles of Flotation* Aust. Inst. Min. Metal., Melbourne, Australia.

Swalen, J.O. and Rabolt, J.F., 1985. Characteristics of orientation and lateral order in thin films by fourier transform infrared spectroscopy. In: J.R. Ferraro and L.J. Basile (Editors), *Fourier Transform Infrared Spectroscopy, Applications to Chemical Systems. Vol. 4.* Academy Press, Orlando, Florida, Chapter 8.

Tarantelli, T. and Furlani, C., 1971. Palladium (II) and platinum (II) complexes of thiocarbamic esters. *J. Chem. Soc.* A, 1216-1217.

Tompkins, H.G., 1975. Infrared reflection-absorption spectroscopy. In: A.W. Czanderina (Editor), *Method of Surface Analysis.* Elsevier Scientific Publishing Co., New York, Chapter 10.

U.S. Bureau of Mines, 1987. *Minerals Yearbook, 1985.* U.S. Government Printing Office, Washington, D.C., Vol. 1.

Vassos, B.H. and Ewing, G.W., 1983. *Electronalytical Chemistry.* John Wiley and Sons, New York.

Walker, G.W., Stout, J.V. and Richardson, P.E., 1984. Electrochemical flotation of sulfides: reaction of chalcocite in aqueous solution. *Int. J. Min. Process.,* 12:55-72.

Whitworth, F.T., 1926. Australian Patent 2404.

Woods, R., 1971. The oxidation of ethyl xanthate on platinum, gold, copper and galena electrodes. Relation to the mechanism of mineral flotation. *J. Phys. Chem.*, 75:354-362.

Woods, R., 1987. Private communication.

Woods, R., Yoon, R.H. and Young, C.A., 1987. Eh-pH diagrams for stable and metastable phases in the copper-sulfur-water system. *Int. J. Miner Process.*, 20:109-120.

Young, C.A., 1987. *Nonstoichiometry of Chalcocite in water-Xanthate Systems.* M.Sc. Thesis, Virginia Polytechnic Institute and State University, Blacksburg, Virginia.

Young, C.A., Woods, R. and Yoon, R.H., 1988. A voltammetric study of chalcocite oxidation to metastable copper sulfides. In: P.E. Richardson and R. Woods (Editors), *Electrochemistry in Mineral and Metal Processing II.* The Electrochemical Society, Pennington, New Jersey.

Zeisse, W.C., 1822. Vorlenfige anzeige einer neven klasse von schwefelverbindugen. *J. Chem. Phys.* 35:173-176.

The vita has been removed from the scanned document